The roles of the novel RNA-binding protein ANKHD1 in shear stress-mediated endothelial dependent-vasoprotection

By: Areej Omar Alahmadi

A thesis submitted in partial fulfilment of the requirements for the degree of Doctor of Philosophy

The University of Sheffield

Faculty of Medicine, Dentistry & Health

Department of Infection, Immunity and Cardiovascular Disease

October 2022

Acknowledgment

It is a humbling experience to thank those people who have helped me along the journey of my PhD. I would like to express my deepest appreciation to my primary supervisor Dr. Maria Fragiadaki for her support during my PhD studies. Her guidance and timely advice helped me all the time in the lab and during writing this thesis.

My deepest gratitude also extends to my second supervisor Prof Paul Evans and my third supervisor Prof Sheila Francis for their encouragement, comments and continuous help.

Many thanks to Prof Dorian Haskard and Courtney Chatterton-Bartley at the National Heart and Lung institution, Imperial College of London, for the training opportunity provided on the biotinylated 3'UTR *in vitro* pulldown experiment.

Special thanks to my sponsor, King Abdulaziz University, for this great opportunity to get my higher education at a world-top-ranked university, the university of Sheffield.

I am extremely grateful to my mother Fauziah Almehmadi and my father Omar Alahmadi for their love, encouragement and supporting my dreams. They are usually there whenever I need them. I would like to extend my thanks to my brothers (Ahmed, Marwan, Hassan and Shakir) and my sister Maria for the good times in my life.

Award and conferences

Award

1st BSCR poster prize: British Society for Cardiovascular Research, Bristol,

September 2021.

Title: The novel RNA-binding protein ANKHD1 is required for vascular health via

stabilisation of eNOS and PTGIS

Conferences

oral presentations

Young investigator award, British Atherosclerosis society meeting, September 2021.

Title: The novel RNA-binding protein ANKHD1 is required for vascular health via

stabilisation of eNOS and PTGIS

17th International symposium on Biomechanics in Vascular Biology and

Cardiovascular Disease, in Rotterdam, the Netherlands, February 2022.

Title: Laminar flow enhances vasoprotective eNOS and PTGIS via the RNA-binding

Protein ANKHD1

Posters

The Joint BAS / BSCR meeting at the BCS conference in Manchester, June 2022.

Title: The novel RNA-binding protein ANKHD1 provides vasoprotection via

enhancing eNOS and PTGIS

Abstract

Rationale and Hypothesis: Cardiovascular disease is the top cause of death worldwide. Atherosclerosis is a chronic cardiovascular disease, caused by the accumulation of lipids in large and medium arteries. Plaques develop preferentially at arterial branches and bends. This asymmetric distribution of plaque is controlled by shear stress, a force exerted throughout the vascular beds, at different magnitudes, by flowing blood. High-magnitude uniform shear stress promotes vascular integrity and is thus atheroprotective. Protective high shear stress (HSS) promotes a number of well-known cytoprotective genes, including endothelial nitric oxide synthase (*eNOS*), prostacyclin synthase (*PTGIS*) and kruppel-like factors 2 (*KLF2*) while suppressing inflammation. On the contrary low shear stress (LSS) promotes the development of inflammation and plaque growth. Our laboratory has recently revealed that ankyrin repeats and single KH domain 1 (ANKHD1), which is highly expressed in endothelial cells, is an RNA-binding protein. Yet the role of ANKHD1 in controlling vascular function remains largely unknown. <u>I hypothesize that ANKHD1 may have a major vascular role, via controlling a number of cytoprotective molecules.</u>

Methodology: To identify ANKHD1 functions, loss-of-function of ANKHD1 was performed using *ANKHD1*-specific siRNA via lipotransfection in HSS-stimulated human coronary artery endothelial cells (HCAECs) followed by RNA-sequencing. The effect of different shear stress conditions on ANKHD1 expression was examined both *in vivo*, in the mouse aortic arch, and *in vitro* in primary human endothelial cells. Primary human umbilical vein endothelial cells (HUVECs) and HCAECs were exposed to either protective (~13 dyne/cm^2) or athero-promoting (~4 dyne/cm^2) shear stress using an orbital shaker for 72 hours. ANKHD1 levels were quantified by RT-qPCR, immunoblotting and immunofluorescence staining. The molecular mechanism of ANKHD1 in regulating the cytoprotective molecules was studied using RNA immunoprecipitation (RIP) assays. Effects on message stability were examined by

RNA stability assay and by *in vitro* synthesis of biotinylated RNA followed by RNA pulldown. To examine the potential role of ANKHD1 in the control of vascular integrity *in vivo*, ANKHD1-deficient and wild-type aortas were subjected to macroscopic and microscopic (*en-face* staining) inspection to study size and vessel morphology and any alteration in the expression of cytoprotective genes. To examine the potential systemic factors influencing atherosclerosis development in *Ankhd1* mouse models, blood glucose and cholesterol levels, blood pressure, heart rate and body weight were measured. The influence of ANKHD1 on atherosclerosis was assessed in PSCK9 mice with *Ankhd1*$^{+/+}$, *Ankhd1*$^{+/-}$, or *Ankhd1*$^{-/-}$.

Findings: RNA-sequencing of human endothelial cells coupled with gene ontology analysis showed that lowering the expression of *ANKHD1* changes the expression of a number of genes that are involved in shear stress responses and atherosclerosis. With a series of *in vivo* and *in vitro* experiments, I demonstrated that ANKHD1 is under the control of atheroprotective shear stress, assessed by increased levels of *ANKHD1* mRNA in HCAECs and HUVECs (HCAECs p= 0.0475, N= 5; HUVECs: p= 0.0043, N= 4) and ANKHD1 protein in HCAECs (p= 0.0137, N= 5) stimulated with shear stress by the orbital shaker. In mouse aortas, ANKHD1 protein was increased in areas of the mouse aorta exposed to HSS (p= 0.0266, N= 6). To further delineate the function of ANKHD1, I focused on three atheroprotective molecules that are regulated by shear stress, namely *eNOS*, *PTGIS* and *KLF2*. *ANKHD1* silencing in HSS-induced HCAECs (N= 6) led to a significant reduction in *eNOS* mRNA (*ANKHD1*siRNA-1: adjusted p= 0.0247; *ANKHD1*siRNA-2: adjusted p= 0.0209), *PTGIS* mRNA (*ANKHD1*siRNA-1: adjusted p= 0.0227; *ANKHD1*siRNA-2: adjusted p= 0.0271) and *KLF2* mRNA (*ANKHD1*siRNA-1: adjusted p= 0.0133; *ANKHD1*siRNA-2: adjusted p= 0.0130). Mechanistically, ANKHD1 binds to *eNOS*, *PTGIS* and *KLF2* mRNAs. It enhances *eNOS* mRNA stability and binds directly to the 3'UTR of *eNOS*, near a region of natural instability, known as the AU-rich Element (AUR). Comparison of *Ankhd1*$^{+/+}$ and *Ankhd1*$^{-/-}$ mice revealed

that ANKHD1 positively regulated eNOS (N= 8-11, p= 0.0425) and PTGIS (N= 6-13, p= 0.0045) as well as vessel diameter (0.8343 mm in $Ankhd1^{-/-}$ vs 0.9318 mm in $Ankhd1^{+/+}$ (20-weeks of age). $Ankhd1$ genetic deletion does not affect glucose levels, cholesterol levels, body weight or heart rate. However, $Ankhd1^{-/-}$ mice exhibited increased inflammation as observed by expression of E-selectin (CD62E), increased thrombosis and accelerated atherosclerosis.

Conclusions: This study has discovered ANKHD1 as a novel cytoprotective molecule that maintains vascular health and attenuates atherogenesis by controlling critical processes in inflammation, vasorelaxation and thrombosis.

Table of contents

List of figures

List of tables

Abbreviations

3'UTR: 3'untranslated region

Ach: acetylcholine

ACs: Adenylyl cyclase

ActD: actinomycin D

ADM: adrenomedullin

Akt: Protein kinase B/ serine/threonine kinase

ANKHD1: Ankyrin repeats single KH domain 1

AP-1: Activator protein 1

AT1R: angiotensin II type 1 receptor

ATP: Adenosine triphosphate

AUR: AU-rich element

BH4: cofactors tetrahydrobiopterin

c-Src: proto-oncogene tyrosine-protein kinase

cAMP: Cyclic adenosine monophosphate

CD62E: E-selectin

cGMP: Cyclic guanosine 5′-monophosphate

ChIP-Seq: Chromatin immunoprecipitation and deep sequencing

COX-2: Cyclooxygenase-2

CRC: colorectal cancer

CTNNB1/beta-cateinin: catenin beta 1

DUSP1: dual specificity phosphatase 1

EGFL7: epidermal growth factor–like domain 7

eNOS: Endothelial nitric oxide synthase

EPCRs: endothelial protein C receptors

ERK5: extracellular-signal-regulated kinase 5

ET-1: endothelin 1

F3: Tissue factor

FPKM: fragments per kilobase of transcript sequence per million base pairs sequenced

Gab1: Grb2-associated binder 1

GCs: Guanylyl cyclase

GM-CSF: Granulocyte-macrophage colony-stimulating factor

GPC1: glypican 1

GSTO-1: glutathione S-transferase omega 1

GSTP-1: glutathione S-transferase pi 1

GTPCH: GTP cyclohydrolase I

HCAECs: human coronary artery endothelial cells

hnRNP E1: Heterogeneous nuclear ribonucleoprotein E1

HO-1: heme oxygenase-1

HPRT: hypoxanthine phosphoribosyltransferase

HSS: high shear stress

HUVECs: human umbilical vein endothelial cells

ICAM-1: Intercellular adhesion molecule 1

IκB: I kappa B

IKBKB/ IKKβ: inhibitor of nuclear factor kappa B kinase subunit beta

IL1R1: interleukin 1 receptor type 1

IL1β: interleukin 1 beta

iNOS: inducible NOS

IPs: prostacyclin receptors

JUN: Jun proto-oncogene, AP-1 transcription factor subunit

KDR/VEGFR2: kinase insert domain receptor

KEGG: Kyoto Encyclopedia of Genes and Genomes

KLF2: Kruppel-like factor 2

KLF4: Kruppel-like factor 4

LDL: low density lipoprotein

LDLR: low-density lipoprotein receptor

lncRNA: long noncoding RNA

LSS: low shear stress

MAPK11: mitogen-activated protein kinase 11

MAPK12: mitogen-activated protein kinase 12

MAPK7/ERK5: mitogen-activated protein kinase 7

MAT2A: methionine adenosyltransferase 2A

MCP1: monocyte chemoattractant protein 1

MEF2: Myocyte enhancer factor-2

MEK5: Mitogen-activated protein kinase 5

MLCK: Myosin light-chain kinase

NES: nuclear export sequence

NFκB: nuclear factor kappa B

NLS: nuclear localisation signal

nNOS: neuronal NOS

NO: Nitric oxide

NOS: Nitric oxide synthase

NOX1: NADPH oxidase 1

NOX2: NADPH oxidase 2

NOXO1: NADPH oxidase organizer 1

NR2F2: nuclear receptor subfamily 2 group F member 2

NRF2: nuclear factor erythroid 2–related factor 2/NFE2 like bZIP transcription factor 2

OSS: oscillatory shear stress

oxLDL: Oxidised LDL

PAI-1: plasminogen activator inhibitor 1

PCSK9: Proprotein convertase subtilisin/kexin type 9

PECAM-1/CD31: Platelet and endothelial cell adhesion molecule 1

PGH2: Prostaglandin H2

PGI$_2$: Prostacyclin

PI3K: Phosphoinositide 3-kinase

PKA: Protein kinase A

PKG: Protein kinase G

PLCγ: phospholipase C gamma

PTGIS: Prostacyclin synthase

QKI: Quaking

qPCR: quantitative polymerase chain reaction

RAC2: Rac family small GTPase 2

RAC3: Rac family small GTPase 3

RIP: RNA immunoprecipitation

ROBO4: Roundabout 4

ROS: reactive oxygen radicals

RPL13AP25: ribosomal protein L13a pseudogene 25

RT: reverse transcription

RT-PCR: reverse-transcriptase PCR

SH2: Src homology 2

SMCs: Smooth muscle cells

SQSTM1: sequestosome 1

t-PAs: plasminogen activators

TFPI-b: tissue factor pathway inhibitor b

TM: thrombomodulin

TNF-a: tumour necrosis factor alpha

TTP: tristetraprolin

TXA$_2$: thromboxane A$_2$

UTP: uridine-5'-triphosphate

VCAM-1: vascular cell adhesion molecule 1

VE-cadherin/ CDH5: Vascular endothelial cadherin/ cadherin 5

VEGF: vascular endothelial growth factor

VEGFR2: vascular endothelial growth factor receptor 2

VWF: von Willebrand factor

Chapter 1: Introduction: Endothelial-dependent vasoprotection

Endothelial cells occupy the innermost blood vessel layer facing the flowing blood. Throughout the vasculature, endothelial cells do not always show homogenous behaviour. Endothelial phenotype can be affected by its location within the arterial pattern (straight vessels versus bends and branches). The arterial pattern has a large impact on determining the haemodynamic force of the blood flow, which is exerted on endothelial cells (Friedman et al., 1983; Suo et al., 2007). Endothelial cells lining straight vessels are exposed to unidirectional and protective blood flow with high shear stress (HSS), also called laminar shear stress. Cells residing in arterial curvatures and branches experience disturbed blood flow and low shear stress (LSS) (Suo et al., 2007; Winter et al., 2019).

1.1. Shear stress is a localised modifier of atherosclerosis progression via regulating endothelial cell functions

Atherosclerosis is a multifactorial cardiovascular disease, a known cause of myocardial and cerebral infarction and a leading cause of mortality worldwide (WHO, 2019). Its development has been linked with (i) systemic factors, which are hypercholesterolemia, diabetes mellitus and hypertension (ArmstrongWarner and Connor, 1970; Sowers et al., 1993). (ii) localised factors, which are arterial geometry, shear stress, mass transport and focal endothelial injury (CaroFitz-Gerald and Schroter, 1969; Moore, 1979; Friedman et al., 1983; Tarbell, 2003; Suo et al., 2007) and (iii) other factors, which include the effects of aging, genetic causes and lifestyle choices, poor diet, lack of exercise, obesity and smoking (Howard et al., 1998; McGill et al., 2002; Mahe et al., 2011; Khera et al., 2016). Looking at the localised factors, atherosclerosis initially develops as a progressive inflammatory process in the sub-endothelium of arterial branch points and bends, eventually leading to established plaque development that can result in plaque rupture and subsequent thrombosis causing myocardial

infarction and stroke (Figure 1.1). A mechanism as to why wall shear stress affects plaque development is that these different conditions (i.e., HSS and LSS) directly affect the function of the endothelium layer via controlling the release of either vasoprotective molecules, such as nitric oxide (NO) (CaroFitz-Gerald and Schroter, 1969; Pedersen et al., 1999; Virmani et al., 2000; Dekker et al., 2005; Parmar et al., 2006; Suo et al., 2007) or disease-causing molecules such as E-selectin/CD62E (Collins et al., 2000; Bertani et al., 2021).

Atherosclerosis Development

Myocardial infarction

| Initial Thickening (Type I lesion) | Fatty streak (Type II lesion) | Intermediate lesion (Type III lesion) | Fibrous Plaque (Type IV lesion) | Thin-cap fibroatheroma (Type V lesion) | Plaque rupture |

Accumulation of SMCs and MQs in intima

Foam cell formation

- Acellular lipid core
- Higher levels of MQs and SMCs

Fibrous cap covering necrotic core

Expanded lipid and necrotic core covered with thin fibrous cap

- High levels of stenosis
- Thin fibrous cap
- Largest necrotic core

Figure 1.1. Atherosclerotic plaque progression and classification according to American Heart Association (AHA). Atherosclerosis develops as chronic inflammatory lesions. They pass through several progressive stages of inflammatory cell accumulation, macromolecule infiltration (e.g., LDL), foam cell formation (lipid-laden macrophages), necrotic core (apoptotic debris) and fibrous cap generation, stenosis and finally plaque rupture and thrombosis. Abbreviations: Macrophage (MQ); Smooth muscle cells (SMCs).

Shear stress is the tangential force applied by the flowing blood on the inner layers of vascular beds, which are lined by endothelial cells, multi-functional cells with specialised roles within the vasculature. In 1969, Caro et al. observed the link between the shear stress magnitude and plaque distribution throughout the arterial tree, and as such, he is considered one of the fathers of the field. Low arterial wall shear stress is associated with early and accelerated atherosclerotic plaque development. In contrast, high arterial wall shear stress is associated with atheroprotection.

In straight blood vessels, the shear stress magnitude is estimated by this Poiseuille's equation:

$$\tau \text{ (Shear stress level)} = \frac{4 \times [\mu \text{ (blood viscosity)} \times Q \text{ (blood flow)}]}{\pi \text{ (circle circumference to inner diameter)} \times r^3 \text{ (radius of the circle)}}$$

This equation highlights the importance of the blood viscosity (μ), which can be determined by the composition of blood (e.g., red blood cell numbers), blood flow rate (Q), which is dependent on the vessel architecture, as well as the vessel diameter, together determining the force experienced by endothelial cells. Altering any of these parameters will result in altered shear stress (τ) with possibly adverse or positive consequences in cell physiology (MalekAlper and Izumo, 1999).

Studies using hyperlipidaemic mouse models, such as *ApoE*$^{-/-}$ and PCSK9 mice, enhanced our knowledge of atherosclerotic plaque development. Apolipoprotein E (ApoE) is a lipoprotein receptor ligand that enhances lipoprotein clearance. Therefore, deletion of the *ApoE* gene (*ApoE*$^{-/-}$) coupled with a high-fat diet also leads to hypercholesterolemia and plaque development (Zhang et al., 1992). Proprotein convertase subtilisin/kexin type 9 (PCSK9) is a ubiquitously expressed protein that binds and enhances lysosomal degradation of low-density lipoprotein receptor (LDLR). The LDLR is responsible for lipid clearance, including cholesterol. Lower LDLR levels lead to a decrease in low-density lipoprotein (LDL)

metabolism and hypercholesterolemia. PCSK9 viral delivery into mice, induces an increase of PCSK9 levels and activity, in turn leading to hypercholesterolemia when animals are fed a high-fat diet. The combination of those events leads to the development of plaques and atherosclerosis (Bjørklund et al., 2014). Both of these models (*ApoE*$^{-/-}$ and PCSK9) are used to model human disease, as the inner curvature of the primary aortic arch is exposed to LSS, and thus, is more prone to atherosclerosis development whereas the outer curvature exposed to HSS is usually protected from atherosclerosis (Suo et al., 2007; Hanna et al., 2012; Bjørklund et al., 2014; Winter et al., 2019), (Figure 1.2).

A *ApoE$^{-/-}$* **mouse aorta**

Atherosclerotic plaques

(Hanna et al., 2012)

B PCSK9 mouse aorta

(Bjørklund et al., 2014)

C Wall shear stress computational measurement

WSS [N/m^2]
3.5 HSS
1.75
0 LSS

(Winter et al., 2019)
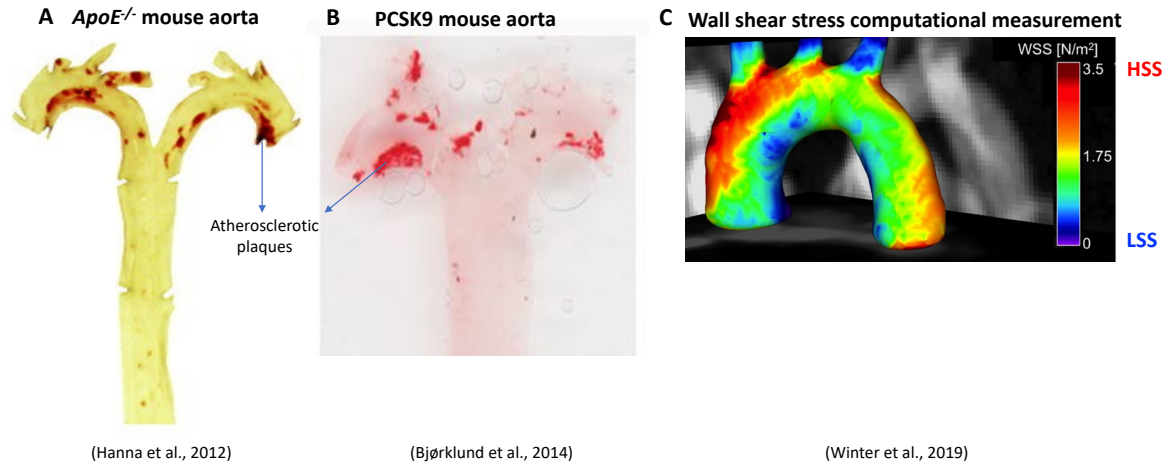
Figure 1.2. Atherosclerosis plaque distribution in the LSS areas of murine aortas. (A and B) Aortas of mice with atherosclerosis were stained with oil red O, which is used to stain lipids. Plaques are mainly localised in the inner curvature of the primary (ascending) aortic arch. (C) Wall shear stress measurement of mouse aortic arch showing the wall shear stress magnitudes. LSS of the flowing blood acts on the inner curvature while HSS acts on the outer curvature.

Applying partial carotid ligation or perivascular cast on the mouse carotid artery modifies the shear stress pattern and allows the study of the subsequent vascular wall changes (Cheng et al., 2006; Nam et al., 2009), (Figure 1.3). Cheng et al. (2006) findings confirm that the high wall shear stress prevented plaque development whereas LSS and oscillatory shear stress (OSS) accelerated atherosclerotic plaque development in *ApoE*$^{-/-}$ mice with a high-fat diet. In carotid artery partial ligation, LSS activated endothelial cells leading to proatherogenic gene upregulation and accelerated atherosclerosis development (Nam et al., 2009). These two models together highlight the importance of shear stress in mediating atherogenesis.

To overcome issues of accumulation of molecules and lipids in constricted areas, specific and controlled shear stress can also be applied on cultured primary endothelial cells with various assays. The 6-well orbital plate method is one of the most commonly used to study endothelial cell responses in a physiological microenvironment (Warboys et al., 2014). The computational quantification of the shear stress generated by the orbital shaker system showed that the rotational frequency achieved at 200-220 rpm in the periphery of a 6-well plate is similar to shear stress forces in straight portions of arteries. Endothelial cells in the periphery of each well show an atheroprotective phenotype. However, the endothelial cells in the centre of the plate are exposed to LSS and show a pro-atherogenic phenotype (Dardik et al., 2005; Warboys et al., 2014; Meng, 2022). This simple *in vitro* model confirms the validity of using the orbital shaker system to assess whether a gene or a cluster of genes is atheroprotective/atheroprone. This *in vitro* system also provides evidence for the direct link of shear stress in controlling endothelial cell behaviour and atherogenesis. The disadvantage of this system is that endothelial cells grown on plastic plates do not come into contact with physiological extracellular matrix or blood components and cells, which limits the conclusions that can be drawn by using the *in vitro* system in isolation. Combining *in vitro* reductionist

experiments (plate system) with *in vivo* experiments and human studies offers a more comprehensive means to study the role of genes in atherosclerosis.
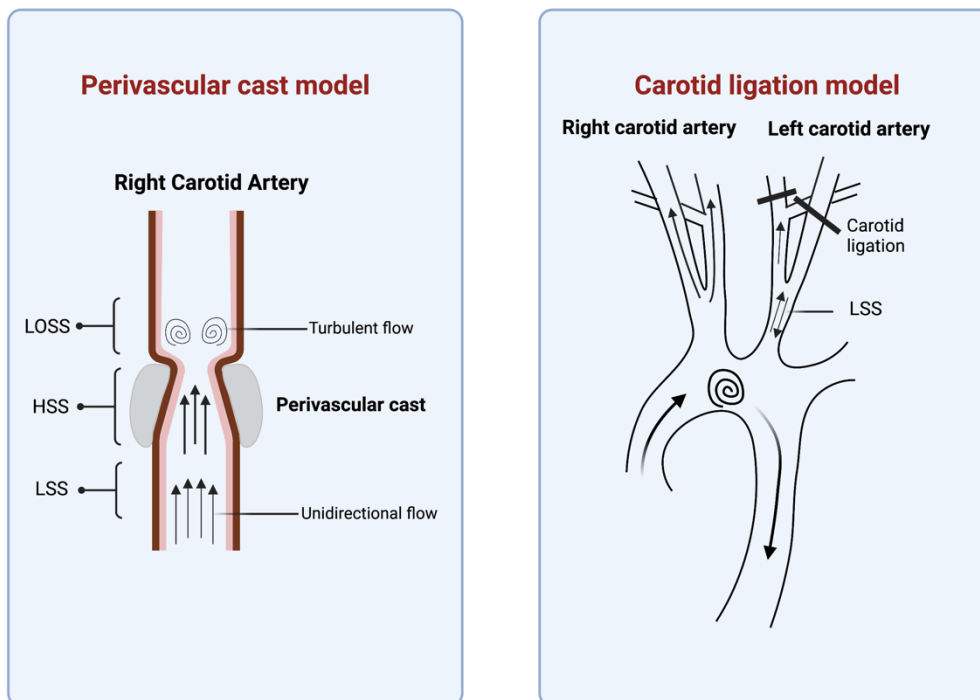
Figure 1.3. In vivo shear stress models. Shear stress was modified in hyperlipidaemic (*ApoE^{-/-}*) mice via either a perivascular cast or aortic ligation of carotid arteries. Perivascular cast (left diagram) generates unidirectional flow with LSS upstream, HSS in the stenosis area and low oscillatory shear stress (LOSS) downstream. Left carotid ligation (right diagram) generates LSS in hyperlipidaemic mice.

Studies have been conducted to determine the importance of endothelial function in different vascular beds. Endothelial cells are able to sense and respond to a number of cues including mechanics. They have mechanosensors, such as the glycocalyx, junctional complexes including the platelet and endothelial cell adhesion molecule 1 (PECAM-1 [CD31]), vascular endothelial cadherin (VE-cadherin [CD144]) and vascular endothelial growth factor receptor 2 (VEGFR2), ion channels (e.g., Piezo), G protein-coupled receptors, caveola, primary cilia and integrins (Figure 1.4). These mechanosensors translate the different shear stress stimuli into intra-cellular signals that affect endothelial cell behaviour (Tzima et al., 2005; Ranade et al., 2014; Wang et al., 2015; Iring et al., 2019; Bartosch et al., 2021; Li et al., 2022).
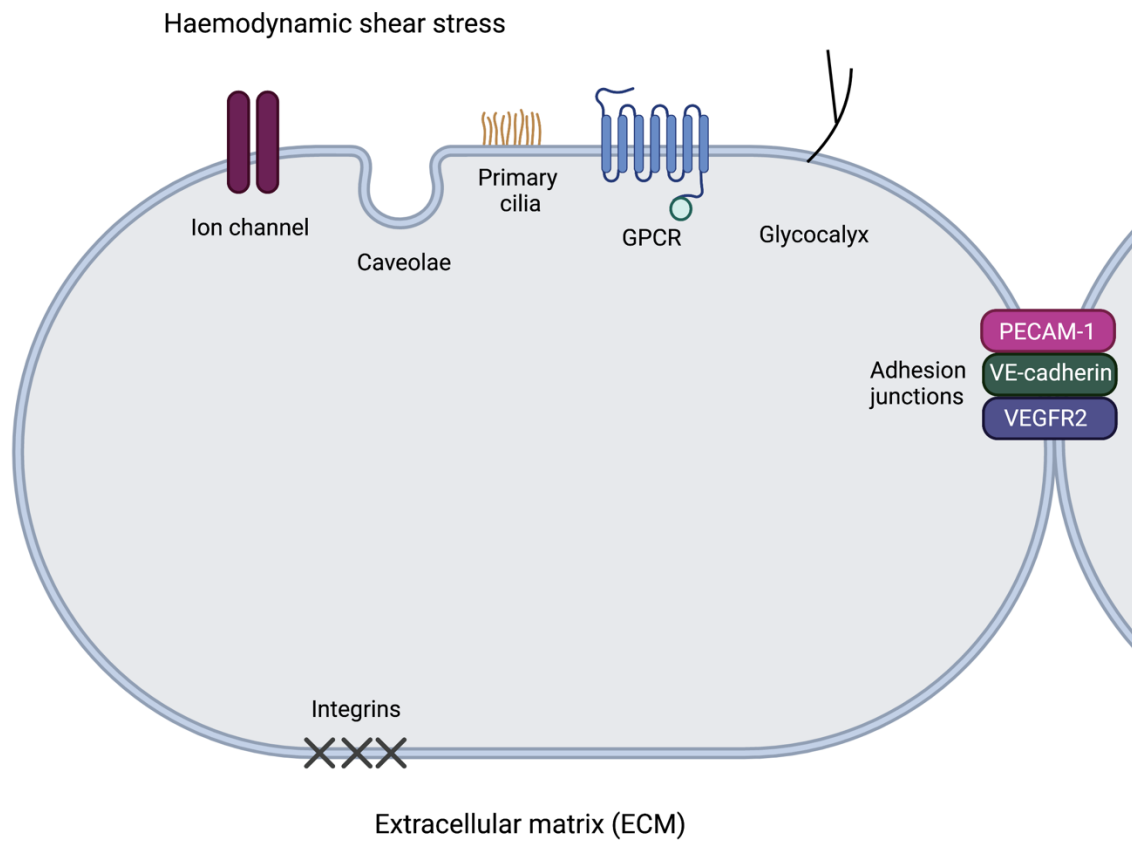
Figure 1.4. Endothelial cell mechanosensors. Mechanosensors are distributed on the apical surface of the endothelial cell facing the flowing blood (ion channel, caveola, primary cilia, G protein-coupled receptors (GPCR) and glycocalyx), inter-endothelial cell junctions (PECAM-1, VE-cadherin and VEGFR2) and basal surface of the endothelium (integrins) which interacts with ECM components.

Endothelial cells under HSS are elongated and aligned unidirectionally with the blood flow (Reidy and Langille, 1980). They are selectively permeable to circulating macromolecules, such as LDL (HerrmannMalinauskas and Truskey, 1994; Weber et al., 2014; de Bruin et al., 2016). They are anti-adhesive and anti-inflammatory (SenBanerjee et al., 2004; Suo et al., 2007; Lu et al., 2019). They also maintain whole-vessel tone (Ignarro et al., 1987; Russell-Puleri et al., 2017; Iring et al., 2019), control levels of oxidative stress (SiuGao and Cai, 2016; Psefteli et al., 2021), and prevent thrombus formation (Parmar et al., 2006; Zhou et al., 2012). As a result, endothelial cells are anti-atherogenic, anti-inflammatory and anti-thrombogenic when their function is not compromised. Areas of arteries with this healthy endothelium are generally protected from the development of early atherosclerosis.

On the other hand, endothelial cells under LSS are shorter, more rounded, and misaligned (Reidy and Langille, 1980). Phenotypically, they are more permeable to macromolecules including LDL (HerrmannMalinauskas and Truskey, 1994; Weber et al., 2014), have higher levels of oxidative stress (SiuGao and Cai, 2016; Psefteli et al., 2021), become adhesive, proinflammatory (SenBanerjee et al., 2004; Suo et al., 2007; Harry et al., 2008), and prothrombotic (Parmar et al., 2006; Zhou et al., 2012). As a result, the focal nature of LSS generates micro-conditioning in turn leading to an area of endothelial dysfunction, 'marking' this area for accelerated atherosclerosis.

1.1.1. *Shear stress regulates endothelial cell permeability*

The inter-endothelial gap (space between two endothelial cells) of the branches and bends is normally 30–450 nm whereas the gap of the unbranched regions is normally 10–25 nm (Kao et al., 1995). The differences in the vessel wall permeability have been attributed to mass transport mechanisms and haemodynamic shear stress (CaroFitz-Gerald and Schroter, 1969; Tarbell, 2003). According to the mass transport theory, additional mechanisms promote atherosclerosis, for example, insufficient oxygen transport (hypoxia) through the endothelial cells and enhancing the transportation of circulating inflammatory cells and macromolecules, such as LDL, into leaky endothelial junctions in the inner curvature and branches (Tarbell, 2003). It has been shown that LSS promotes endothelial cell apoptosis via increasing reactive oxygen species (ROS) levels and mitosis which in turn generate leaky junctions (Dardik et al., 2005; Zhang et al., 2013). These results indicate that shear stress can also influence the mass transport mechanism.

The haemodynamic effect of the unidirectional flow maintains the inter-endothelial barrier by controlling endothelial contractile and junctional forces (ConklinVito and Chen, 2007; Weber et al., 2014; de Bruin et al., 2016). Myosin light-chain kinase (MYLK) and RhoA positively regulate myosin light-chain phosphorylation, which results in F-actin stress fibre formation, leading to endothelial contraction and elongation, and thus, controlling inter-endothelial permeability (van Nieuw Amerongen et al., 2000). Regions under unidirectional flow exposed to HSS inhibit both MYLK and RhoA, resulting in a more resistant endothelium. LSS regions, on the other hand, have increased MYLK and RhoA expression leading to LSS-induced endothelium permeability (Weber et al., 2014). MYLK pathway has been also activated in inflammation when tumour necrosis factor alpha (TNF-a) activates CD62E, generating intercellular gaps and inflammatory cell infiltration (Kiely et al., 2003).

Apart from endothelial contractility, the inter-junctional forces of endothelial cells are facilitated by tight junction proteins (e.g., occludin) and adherins (e.g., catenin beta 1 [beta-catenin] and VE-cadherin) (ConklinVito and Chen, 2007; de Bruin et al., 2016; Yang, F. et al., 2020). Conklin et al. (2007) and Yang et al. (2020) identified that LSS and OSS lead to the dysfunction of cell-cell junctions. LSS and OSS downregulate occludin mRNA and protein expression in the endothelium of mouse and porcine vessels and primary human endothelial cells, resulting in high inter-endothelial permeability (Conklin et al., 2007; Yang et al., 2020). On the other hand, healthy endothelium exposed to HSS maintains its tight junction protein (occludin) and adherins (VE-cadherin and beta-catenin) expression and function, resulting in a more resistant endothelium. It has been shown that HSS induces the RNA-binding protein Quaking (QKI), which enhances VE-cadherin and beta-catenin expression and activity, resulting in highly resistant endothelium (ConklinVito and Chen, 2007; de Bruin et al., 2016; Yang, F. et al., 2020).

Arterial bifurcations and bends show high levels of permeability to macromolecules, such as LDL, compared with unbranched arteries (Kao et al., 1995; ConklinVito and Chen, 2007; van den BergSpaan and Vink, 2009). Increased permeability to lipids is a pathogenic process. Mice and rats that were administered high-fat diet had increased accumulation of LDL in bends and bifurcations of the arterial tree (Kao et al., 1995; van den BergSpaan and Vink, 2009). Taken together, this demonstrates that cell-cell contacts are important for intact endothelial function and shear stress is a significant modulator of how endothelial cell interacts with their neighbours and regulates permeability.

1.1.2. Shear stress regulates endothelial-dependent vasoactivity

Functional endothelial cells promote efficient vasorelaxation. However, endothelial denudation impairs vascular relaxation in mice, rats, and humans (MalmsjöEdvinsson and Erlinge, 1998; Wihlborg et al., 2003; Guns et al., 2005; ChengVanhoutte and Leung, 2018). Under HSS, endothelial cells upregulate vasorelaxant mediators, such as NO and prostacyclin (PGI_2), and downregulate vasoconstrictive mediators, such as endothelin 1 (ET-1) (McCormick et al., 2001; Yamamoto et al., 2003; Yamamoto et al., 2006; Russell-Puleri et al., 2017). When functional endothelial cells are exposed to HSS, they produce high levels of vasorelaxant agonists, such as adenosine triphosphate (ATP), uridine-5'-triphosphate (UTP), acetylcholine (Ach) and substance P (Milner et al., 1990; Saiag et al., 2009). These vasorelaxant agonists can interact with P2X and P2Y receptors on endothelial cells to activate Ca^{+2} influx; in turn enhancing NO generation from endothelial eNOS and PGI_2 from PTGIS (Wihlborg et al., 2003; Yamamoto et al., 2003; Yamamoto et al., 2006; Wang et al., 2015; ChengVanhoutte and Leung, 2018; PiaoHong and Son, 2018).

Endothelial NO, subsequently, diffuses into the smooth muscle cell (SMC) layers to activate guanylyl cyclase (GCs), which elevates cyclic guanosine 5′-monophosphate (cGMP). cGMP then activates protein kinase G (PKG), which in turn activates SMC relaxation (Coletta et al., 2012; ChengVanhoutte and Leung, 2018). Apart from NO, PGI_2 is a vasodilator also produced by endothelial cells (ChengVanhoutte and Leung, 2018). PGI_2 released from endothelial cells that have been exposed to HSS (Russell-Puleri et al., 2017) binds to prostacyclin receptors (IPs) and G-protein-coupled receptors decorating the surface of SMCs. This causes adenylyl cyclase (AC) to generate high levels of cyclic adenosine monophosphate (cAMP), which in turn activates protein kinase alpha (PKA) and results in SMC relaxation (Russell-Puleri et al., 2017; ChengVanhoutte and Leung, 2018).

1.1.3. Shear stress regulates the thrombotic phenotype of endothelial cells

Endothelial cells maintain blood in a normal fluid state by preventing unnecessary clotting. During injury, however, endothelial cells protect the region of the blood vessel affected by promoting clot formation at the site of an injury. Hence endothelial cells can play either an anti-thrombotic or pro-thrombotic role depending on the specific tissue needs. In normal healthy vessels, endothelial cells prevent platelet adhesion and aggregation (primary haemostasis) as well as the coagulation cascade (secondary haemostasis), and promote fibrinolysis, which is the process of thrombus degradation (Kisiel et al., 1977; TatesonMoncada and Vane, 1977; Vehar and Davie, 1980; Mellion et al., 1981; Owen and Esmon, 1981; IchinoseKisiel and Fujikawa, 1984; RadomskiPalmer and Moncada, 1987; Stearns-Kurosawa et al., 1996; Maroney et al., 2013). See Figure 1.5.

To prevent primary haemostasis, healthy endothelial cells produce NO and PGI_2 to prevent platelet adhesion and aggregation which can lead to the formation of a platelet plug (TatesonMoncada and Vane, 1977; Mellion et al., 1981; RadomskiPalmer and Moncada, 1987). NO and PGI_2 enhance the expression of cGMP to inhibit platelet adhesion (RadomskiPalmer and Moncada, 1987). Both PGI_2 and NO not only inhibit platelet adhesion but also prevent platelet aggregation by increasing platelet cAMP and cGMP levels, respectively (TatesonMoncada and Vane, 1977; Mellion et al., 1981). As mentioned, HSS enhances the production of NO and PGI_2 (Yamamoto et al., 2006; Russell-Puleri et al., 2017), and as such, maintains the anti-thrombotic phenotype of the endothelium.

To promote primary haemostasis, endothelial cells secrete von Willebrand factor (VWF) via exocytosis, which promotes platelet adhesion, platelet aggregation, and factor-VIII stabilisation in plasma (Weiss et al., 1974; WeissSussman and Hoyer, 1977; Galbusera et al., 1997). In endothelial injury, platelet tethering to the subendothelial collagens is facilitated by the platelet glycoprotein Ibα on the platelet surface that binds to soluble VWF. VWF binds to

collagen via its domain A3 binding (Nieuwenhuis et al., 1985; SavageSixma and Ruggeri, 2002). In mice with atherosclerosis, endothelial VWF showed to enhance platelet and leukocyte adhesion and accelerate atherosclerosis in LSS regions (Doddapattar et al., 2018).

To prevent secondary haemostasis, healthy endothelial cells express thrombomodulin (TM), endothelial protein C receptors (EPCRs), and tissue factor pathway inhibitor b (TFPI-b) to maintain the endothelial cells' anticoagulant properties. TM inhibits fibrin formation and also platelet accumulation (Cadroy et al., 1997). EPCRs bind to and prime protein C to be activated by the thrombomodulin-thrombin complex, and the activated protein C inhibits factor Va and factor VIIIa (Kisiel et al., 1977; Vehar and Davie, 1980; Owen and Esmon, 1981; Stearns-Kurosawa et al., 1996). TFPI-b is the most potent TFPI isoform that attenuates VIIa/Tissue factor (VIIa/F3) and factor Xa activities, as opposed to the platelet isoform (TFPI-a) (Maroney et al., 2013). All of these endothelial anticoagulant modulators eventually inhibit excessive thrombin generation.

To promote fibrinolysis, functional endothelial cells express tissue plasminogen activators (t-PAs) in response to thrombin, factor Xa, and tissue kallikrein (IchinoseKisiel and Fujikawa, 1984). The binding of t-PAs and plasminogen to clot fibrin mesh enhances t-PA activity in converting plasminogen to plasmin, which in turn degrades fibrin (ZamarronLijnen and Collen, 1984). Endothelial cells also release plasminogen activator inhibitor 1 (PAI-1) to inhibit excessive t-PA activity (Thorsen and Philips, 1984). HSS enhances the antithrombotic transcription factor KLF2 (Dekker et al., 2006). KLF2 regulates primary and secondary homeostasis and fibrinolysis to maintain blood in a fluid state and prevent bleeding. KLF2 promotes the production of NO, PGI_2, TM and VWF and inhibits PAI-1 and F3 from endothelial cells (Lin et al., 2005; Dekker et al., 2005; Dekker et al., 2006).
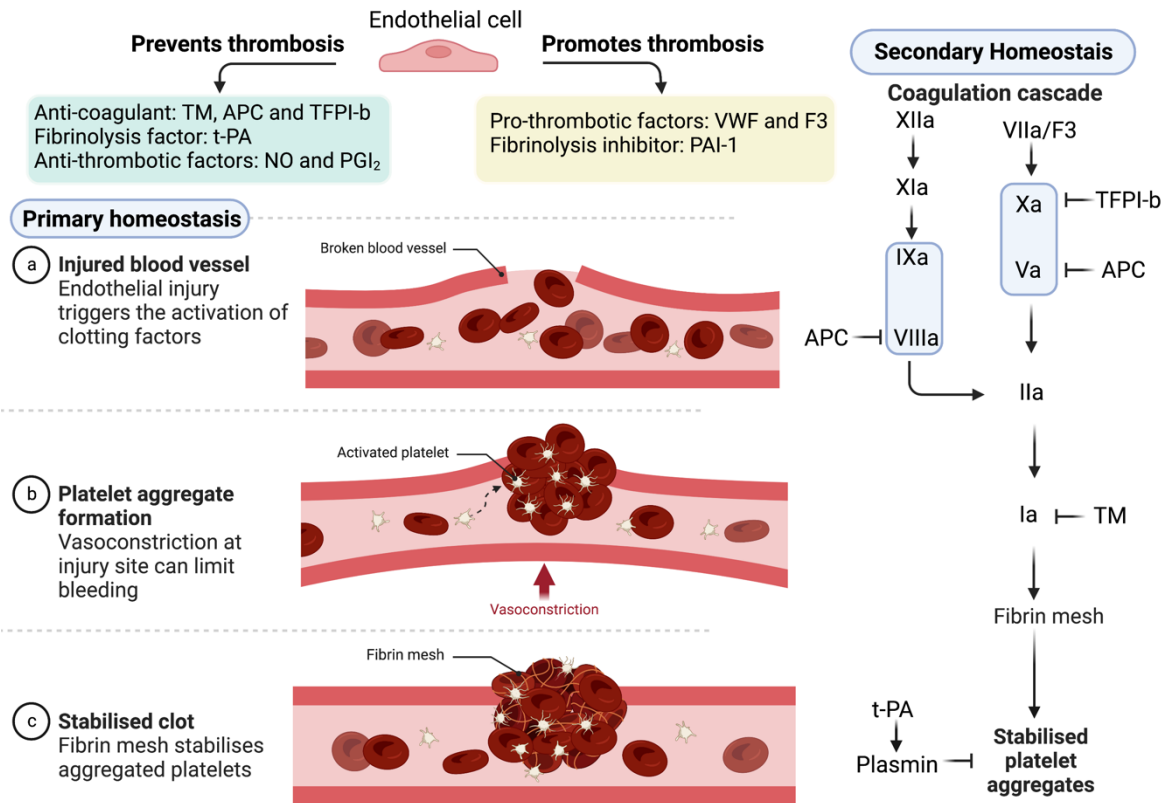
Figure 1.5. Endothelial cells maintain a balanced antithrombotic/prothrombotic system. They release inhibitors that attenuate platelet adhesion and aggregation (primary homeostasis), subsequent coagulation cascade (secondary homeostasis) initiation on the surface of activated platelets and fibrinolysis. These result in localising the clot at the site of injury and prevent excessive clot formation. In addition, endothelial cells produce vasoconstrictors (e.g., ET-1) to prevent excessive bleeding during injury. Abbreviations: activated coagulation factors: Ia, IIa, Va, VII/TF (VII/F3), VIIIa, IXa, Xa, XIa, XIIa.

1.1.4. Shear stress regulates inflammation

HSS helps endothelial cells remain anti-adhesive and non-chemotactic toward immune cells, such as monocytes and lymphocytes. This is because, endothelial cells have low levels of adhesive glycoprotein molecules, such as intercellular adhesion molecule 1 (ICAM-1) and vascular cell adhesion molecule 1 (VCAM-1), and of the chemokines, such as monocyte chemoattractant protein 1 (MCP1) that induce monocyte recruitment to the sub-endothelium to promote atherogenesis (McCormick et al., 2001; Yu et al., 2002; Suo et al., 2007; Harry et al., 2008; Lu et al., 2019). In contrast, disturbed blood flow having LSS enhances proinflammatory endothelial cell phenotype via the activation of proinflammatory pathways, which are JNK pathway and nuclear factor kappa B (NFκB) pathway (MohanMohan and Sprague, 1997; Nagel et al., 1999; Gareus et al., 2008). Jun pathway activation in LSS regions results in the transcription factor AP-1 activation and AP-1 translocation into the nucleus, which subsequently promotes inflammatory gene expression, such as MCP1 (Martin et al., 1997; Nagel et al., 1999). NFκB activation occurs when inflammatory cytokines (e.g., IL1-β) in athero-indusive conditions enhance NFκB activation which results in the expression of different adhesion molecules and cytokines by endothelial cells, which actively contribute to inflammation, such as ICAM-1, VCAM-1, CD62E, P-selectin and IL1-β (Hiscott et al., 1993; MohanMohan and Sprague, 1997; Nagel et al., 1999; Ghosh and Hayden, 2008; Libby, 2017), (Figure 1.6).

In atherosclerosis, ICAM-1 and VCAM-1 are highly expressed in atheroprone arterial regions (Nakashima et al., 1998). Oxidised LDL (oxLDL) enhances the endothelial expression of ICAM-1, VCAM-1, and P-selectin but not CD62E (Gebuhrer et al., 1995; Khan et al., 1995; Patel et al., 2019). Mice lacking ICAM-1, CD62E, P-selectin or activated NFκB developed smaller atherosclerosis lesions compared with the control group (Collins et al., 2000; Gareus

et al., 2008). Based on these *in vivo* findings, increased and persistent expression of adhesion

molecules in areas of endothelial dysfunction promotes atherogenesis.
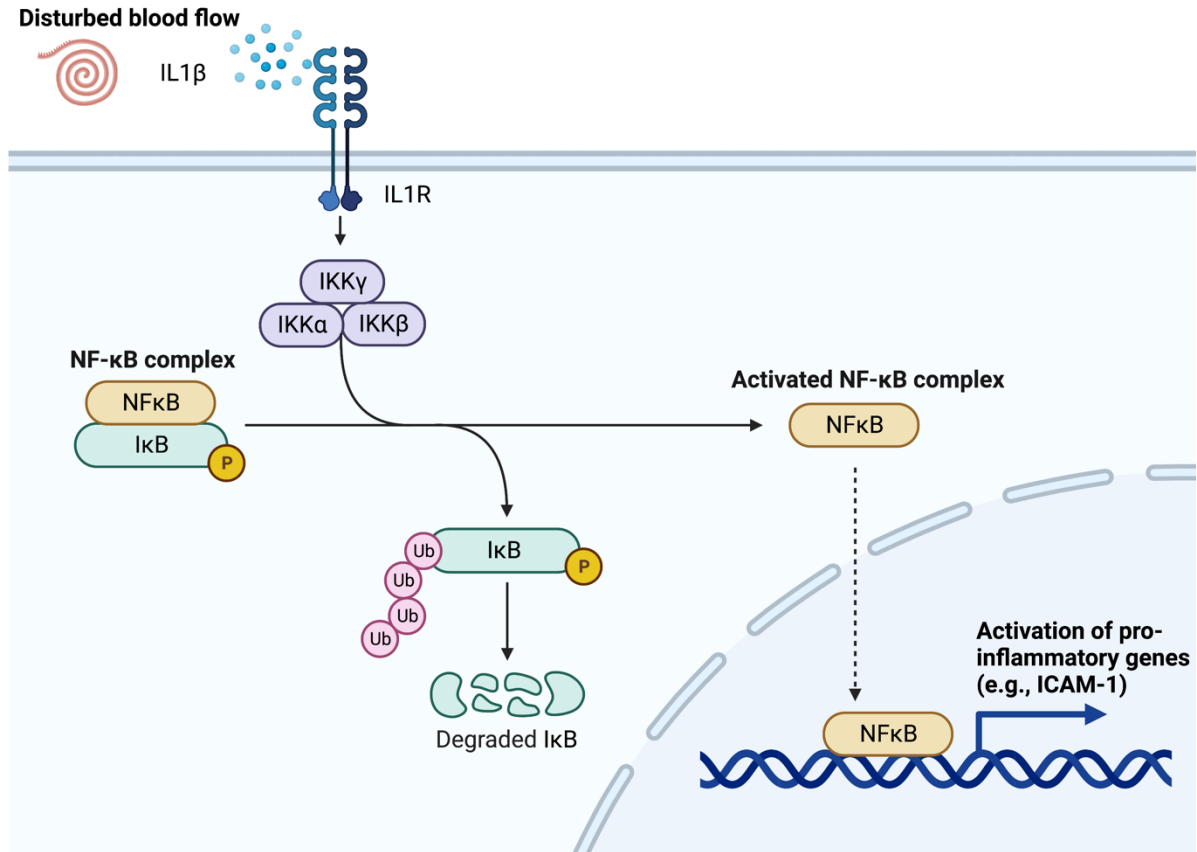
Figure 1.6. Atheroprone areas have activated pro-inflammatory NFκB signalling. IL1β can activates IkappaB kinase complex (IKK$a/\beta/\gamma$) which in turn induce ubiquitination and degradation of the inhibitor of NFκB (I kappa B, IκB). This results in NFκB activation, NFκB nuclear translocation and transcription of pro-inflammatory target genes, such as ICAM-1.

1.1.5. Shear stress regulates the endothelial redox system

In atheroprotective areas of mouse aortas, which are exposed to HSS, endothelial cells produce lower levels of the oxidant ROS, particularly superoxide, and high levels of the antioxidant nuclear factor erythroid 2–related factor 2 (NRF2); thus, maintaining balanced redox system (Zakkar et al., 2009; Luo et al., 2022). ROS inhibition occurs when HSS promotes the regulatory p47phox protein to make a complex with NADPH oxidase 2 (NOX2) to produce high levels of NO and low levels of superoxide; thus, minimising the levels of oxidative stress (SiuGao and Cai, 2016). Furthermore, unidirectional HSS upregulates and activates NRF2 via phosphorylation at serine40 and nuclear translocation. This results in the upregulation of the expression of antioxidant genes, such as heme oxygenase-1 (HO-1) (Psefteli et al., 2021). On the contrary, in atheroprone areas of mouse aortas, which are exposed to low and oscillatory shear stress, endothelial cells produce high levels of the oxidant ROS and low levels of the antioxidant NRF2, resulting in elevated oxidative stress (Zakkar et al., 2009; Luo et al., 2022). LSS-exposed human endothelial cells elevate oxidative stress by inhibiting NRF2 activity and NO production and enhancing ROS formation (SiuGao and Cai, 2016; Psefteli et al., 2021). NADPH oxidase organizer 1 associated with NADPH oxidase 1 (NOXO1-NOX1 complex) in endothelial cells generates high superoxide levels under LSS conditions (SiuGao and Cai, 2016). LSS via superoxide also elevates the oxidation modification of LDL (Hwang et al., 2003). Elevated oxidative stress affects endothelial permeability, endothelial-induced vasorelaxation, endothelial antithrombotic status, and anti-inflammatory status (Drake et al., 1991; Gebuhrer et al., 1995; Khan et al., 1995; Yan et al., 2005; DeMaio et al., 2006; ChengVanhoutte and Leung, 2018; Patel et al., 2019). Modified LDL attenuates tight endothelial cell junctions, increases intercellular permeability, and decreases the expression of tight junction proteins, such as occludin (Yan et al., 2005; DeMaio et al., 2006). In atherosclerosis, high superoxide levels resulted in reduced vasorelaxation (ChengVanhoutte

and Leung, 2018). Dysfunctional endothelial cells exposed to oxidative stress upregulate the prothrombotic tissue factor (F3) (Drake et al., 1991), thus enhancing thrombin synthesis, leading to thrombosis. As has been mentioned, oxLDL promotes inflammation by upregulating endothelial ICAM-1, VCAM-1, and P-selectin but not CD62E (Gebuhrer et al., 1995; Khan et al., 1995; Patel et al., 2019). These results highlight the effect of LSS on oxidative stress that affects the macromolecule transportation system and promotes vasoconstriction, thrombosis and inflammation, and as such, results in dysfunctional endothelium and atherogenesis.

1.2. Key regulatory molecules contributing to vasoprotection

1.2.1. Kruppel-like factors: KLF2 and KLF4

In response to HSS, the transcription factors *KLF2* and *KLF4* are upregulated in endothelial cells (SenBanerjee et al., 2004; Parmar et al., 2006; Clark et al., 2011; Lu et al., 2019). HSS enhances *KLF2* via the successive phosphorylation of mitogen-activated protein kinase 5 (MEK5), extracellular-signal-regulated kinase 5 (ERK5), and myocyte enhancer factor-2 (MEF2), resulting in *KLF2* expression (Parmar et al., 2006). *KLF4* expression is also enhanced by HSS-induced MEK5 and ERK5 (Clark et al., 2011).

Stabilised *KLF2* and *KLF4* expression is promoted by *AF131217.1*, a shear-sensitive long noncoding RNA (lncRNA), in response to flow. This occurs when *AF131217.1* inhibits *miR-128-3p*, the miRNA that inhibits *KLF2* and *KLF4* expression (Lu et al., 2019).

Functionally, KLF2 and KLF4 via upregulating vasoprotective molecules can inhibit thrombosis and inflammation and enhance vascular relaxation (SenBanerjee et al., 2004; Lin et al., 2005; Parmar et al., 2006; Kumar et al., 2011; Zhou et al., 2012; Lu et al., 2019). Their involvement in *eNOS* induction (SenBanerjee et al., 2004; Clark et al., 2011) highlights their role in platelet inactivation, anti-inflammation, and vascular relaxation.

KLF2, in particular, is produced in large amounts in atheroprotective regions (Parmar et al., 2006) and plays a major role in helping endothelial cells maintain antithrombotic and anticoagulant phenotypes. KLF2 in healthy endothelial cells upregulates anti-thrombotic molecules *eNOS*, *TM* and *t-PA* and downregulates pro-thrombotic molecules *F3*, *VWF* and *PAI-1* (Lin et al., 2005; Parmar et al., 2006; Kumar et al., 2013). Overexpression of KLF2 in human endothelial cells resulted in prolonged whole blood clotting time (Lin et al., 2005; Kumar et al., 2013). Human endothelial cells with low levels of KLF2 were shown to be capable of promoting shorter clotting times. The possible causes of the shorter clotting times are attributed to diminished major antithrombotic elements and upregulated pro-thrombotic elements in human cells with low KLF2 levels (Lin et al., 2005).

LDL downregulates *KLF2* expression by attenuating *KLF2* promoter activity via enhancing DNA-methyltransferase 1 (DNMT1)-mediated DNA methylation in human endothelial cells and affects the expression of KLF2 downstream components (Kumar et al., 2013). KLF2 and KLF4 exert their anti-inflammatory function by inhibiting *VCAM-1* and *ICAM-1* (SenBanerjee et al., 2004; Lu et al., 2019). Additionally, KLF2 inhibits adhesion molecules (e.g., *CD62E*), chemokines (e.g., *MCP1*), and growth factors (e.g., Granulocyte-macrophage colony-stimulating factor [*GM-CSF*]) (SenBanerjee et al., 2004; Lin et al., 2005; Parmar et al., 2006). *Klf2*$^{+/-}$ Mice (with one copy deletion of *Klf2*) with atherosclerosis have larger plaque sizes and higher levels of lipid accumulation when compared to the control group (*Klf2*$^{+/+}$ *ApoE*$^{-/-}$ mice) (Atkins et al., 2008). These data show the vasoprotective roles of endothelial KLF2 and KLF4 by controlling several key genes, suggesting their involvement in HSS-mediated vasoprotection.

1.2.2. Endothelial nitric oxide synthase

Nitric oxide synthase (NOS) has three isoforms: inducible NOS (iNOS), endothelial NOS (eNOS) and neuronal NOS (nNOS). KLF2 and KLF4 induce the transcription activity of *NOS3*—the gene that produces *eNOS* mRNA. *eNOS* mRNA is stable, under high shear conditions, but the mechanism underlying its stabilisation has not yet been explored. The activation of eNOS protein requires phosphorylation of serine-1177 and serine-632 (Dimmeler et al., 1999; SenBanerjee et al., 2004; Dixit et al., 2005; Dekker et al., 2005; Dekker et al., 2006; Parmar et al., 2006; Villarreal et al., 2010; Clark et al., 2011; Wang et al., 2015; SiuGao and Cai, 2016; Iring et al., 2019; Lu et al., 2019); see Figure 1.7. eNOS activity also requires high levels of the cofactors tetrahydrobiopterin (BH4) and L-arginine. Activated eNOS exists as a dimer (known as coupled eNOS) and coupled eNOS is atheroprotective as it increases NO bioavailability and decreases superoxide. This occurs when coupled eNOS synthesises NO and L-citrulline from oxygen and L-arginine. Low levels of cofactors result in oxygen reduction, and thus, generating superoxide (Ozaki et al., 2002; Kuzkaya et al., 2003; SiuGao and Cai, 2016; Chao et al., 2018; Douglas et al., 2018).

In terms of *NOS3* transcription, previous studies showed that it is under the transcriptional control of KLF2 and KLF4, which themselves are upregulated by protective laminar flow. HSS enhances the successive phosphorylation of MEK5, ERK5 and MEF2, resulting in *KLF2* and *KLF4* mRNA transcription. KLF2 and KLF4 induce a transcription induction of *NOS3* mRNA (SenBanerjee et al., 2004; Parmar et al., 2006; Villarreal et al., 2010; Clark et al., 2011; Lu et al., 2019).

The mRNA of *eNOS* is relatively stable with a reported half-life of more than 18 hours under laminar shear stress (Davis et al., 2001; Weber et al., 2005). mRNA stability is regulated by specific nucleotide sequences typically located in the 3' untranslated region (3'UTR). These 'cis-acting' sequences form the scaffold for the binding of 'trans-acting' factors, typically

proteins with RNA-binding domains that bind the stem-loop RNA structures to facilitate regulation. Evidence that *eNOS* mRNA may be under the control of RNA-binding proteins came from original observations that *eNOS* mRNA stability is increased drastically (by 4-fold) in growing cells when compared to nongrowing cells and this requires a 3'UTR sequence (Searles et al., 1999). Moreover, treatment of cells with the pro-inflammatory cytokine TNF-a causes a reduction in *eNOS* mRNA stability, due to an increase of the translation elongation factor 1-alpha 1, which binds the 3'UTR of *eNOS* to reduce *eNOS* mRNA half-life (Yan, G. et al., 2008). Laminar shear stress has been shown to increase the polyadenylation of the 3'UTR of *eNOS*; thus, promoting its mRNA stability (Weber et al., 2005), but the trans-acting factors responsible for this effect are currently unknown. Ho et al. (2013) found that the 3' UTR of *eNOS* plays a critical role in *eNOS* mRNA fate. Specifically, the 3'UTR of *eNOS* has highly conserved CU-rich elements, which are sequences rich in cytosine (C) and uracil (U) nucleotides (e.g., UUUCCC). CU-rich elements are targets for several RNA and DNA binding proteins and are critical sites for mRNA stability regulation. In the case of *eNOS*, heterogeneous nuclear ribonucleoprotein E1 (hnRNP E1) was shown to bind to *eNOS* CU-rich element and enhance *eNOS* mRNA stability (Ho et al., 2013) in static conditions. Whether this binding is altered under differing conditions of shear stress is currently unknown. Taken together, laminar shear stress causes an increase in *eNOS* transcription maintained by a prolonged increase in *eNOS* mRNA stability, which is under the control of a number of processes and proteins many of which are currently unknown.

The eNOS protein that is subsequently produced can be activated in a Ca^{2+}-dependent manner, which promotes short-term eNOS activation, or via ser1177 and ser632 phosphorylation, which promotes long-term eNOS activation. In terms of short-term eNOS activation, HSS-induced acetylcholine can increase intracellular calcium, thus enhancing NO release (Coletta et al., 2012). For long-term eNOS activation, HSS-induced ATP release can

induce ser1177 and ser632 phosphorylation (Figure 1.7). To phosphorylate eNOS ser1177, ATP interacts with an endothelial P2Y receptor, resulting in activating PECAM-1(CD31)/VE-cadherin/VEGFR2 complex, which subsequently enhances proto-oncogene tyrosine-protein kinase (c-Src), phosphoinositide 3-kinase (PI3K) and Grb2-associated binder 1 (Gab1)/protein kinase B (Akt). The Gab1/Akt pathway enhances eNOS-ser1177 phosphorylation via activated Akt (Dimmeler et al., 1999; Jin et al., 2005; Tzima et al., 2005; Wang et al., 2015; SiuGao and Cai, 2016; Chao et al., 2018; Iring et al., 2019). c-Src not only activated eNOS protein but also enhanced *eNOS* mRNA expression under the HSS condition (Davis et al., 2001).

Glypican 1 is a core proteoglycan component of the mechanosensor glycocalyx, which has also been shown to activate PECAM-1 via phosphorylation at tyr686; thus, activating the c-Src pathway (Tzima et al., 2005; Bartosch et al., 2021). Glypican 1 inhibition attenuates eNOS phosphorylation and NO production (Ebong et al., 2014; Zeng and Liu, 2016; Bartosch et al., 2021). Mice lacking glypican 1 have been shown to have impaired eNOS protein function (Bartosch et al., 2021; Mahmoud et al., 2021).

eNOS ser632 phosphorylation occurs by AKT and requires HSS-induced ATP, which is facilitated by the mechanosensitive cation channel PIEZO1. In HSS, activated c-Src enhances not only eNOS ser1177 but also eNOS ser632 phosphorylation. This occurs when c-Src activates PI3K, enhancing the Gab1/Src homology 2 (SH2) pathway, and the Gab1/SH2 pathway via activated PKA and resulting in phosphorylating eNOS at ser632. PIEZO1 can also facilitate the phosphorylation of eNOS at ser632 by enhancing endothelial cells to generate and release adrenomedullin (ADM). Autocrine and paracrine binding of ADM to the endothelial CALCRL/PAMP2 receptor can activate G protein (G_s); this induces adenylyl cyclase (ACs) to convert AMP to cAMP, which activates PKA, resulting in eNOS ser632 phosphorylation (Dimmeler et al., 1999; Dixit et al., 2005; Wang et al., 2015; SiuGao and Cai, 2016; Chao et al., 2018; Iring et al., 2019). As a consequence of eNOS ser1177 and ser632 phosphorylation,

eNOS becomes activated and dimerised, which increases NO bioavailability and decreases superoxide generation (Wang et al., 2015; SiuGao and Cai, 2016; Iring et al., 2019).
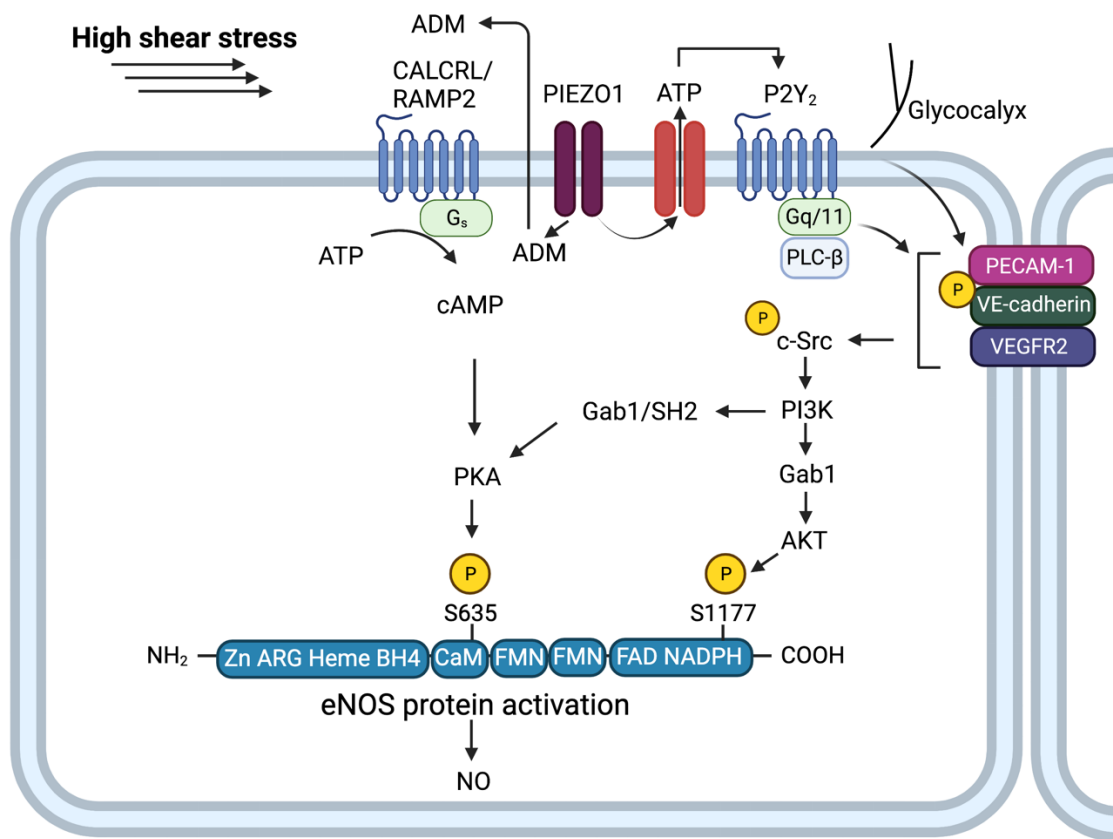
Figure 1.7. Endothelial-dependent vasoprotection via NO production. This diagram summarises HSS-induced eNOS protein activity and NO release.

eNOS in atherosclerosis

In a report by Knowles et al. (2000), mice with atherosclerosis yet lacking *enos* (*ApoE*
-/-/ enos -/-) had more plaques than the control group. Ponnuswamy et al. (2012) observed high
levels of mononuclear–endothelial cell interaction and subsequent leukocyte infiltration into
the subendothelium in *ApoE -/-/ enos -/-*. Despite high levels of leukocyte recruitment,
superoxide was significantly decreased in this mouse group. In a study by Ozaki et al. (2002),
overexpression of *enos* in *ApoE -/-* mice increased plaque size and superoxide production, which
then were diminished after endothelial denudation. These studies indicate that eNOS
contributes to oxidative stress by generating elevated superoxide levels in atherosclerosis.
Interestingly, Douglas et al. (2018) showed that reduced *enos* levels in mice with
atherosclerosis did not significantly change the plaque sizes. They also studied the effect of the
presence of sufficient BH4, an essential cofactor for NO production and activity, by studying
the inhibition of GTP cyclohydrolase I (*GTPCH*) in endothelial cells of mice. GTPCH catalyses
BH4 production. Mice that lacked endothelial GTPCH had reduced NO bioavailability,
accelerated atherogenesis, induced vasoconstriction, and elevated superoxide levels and
VCAM-1 (Ozaki et al., 2002; Douglas et al., 2018). Therefore, eNOS requires BH4 to provide
atheroprotection, vasorelaxation and anti-oxidative stress and anti-inflammatory
microenvironment.

Apart from cofactor bioavailability, LSS attenuates the levels of eNOS expression and
activity (Hwang et al., 2003; SiuGao and Cai, 2016; Chao et al., 2018). In terms of *eNOS*
expression, it is unknown whether LSS prevents *de novo eNOS* synthesis or reduces *eNOS*
mRNA stability. In terms of eNOS activity, LSS enhances eNOS uncoupling via the
NOXO1/NOX1 complex and angiotensin II type 1 receptor (AT1R), resulting in elevated
superoxide levels, decreased NO bioavailability, and, therefore, high oxidative stress levels
(SiuGao and Cai, 2016; Chao et al., 2018). High levels of oxidative stress generate more

oxLDL. OxLDL reduces *eNOS* expression and activity, NO production, and consequently, endothelial-dependent vasorelaxation (da Silva et al., 2022). On the ground of these studies, high levels of oxidative stress generated by athero-inducive shear stress impair eNOS function which accelerates atherogenesis.

1.2.3. Prostacyclin

PGI_2 is a member of the prostaglandin lipid family; it is produced by endothelial cells (Moncada et al., 1976) and enhances endothelial-dependent vasorelaxation (ChengVanhoutte and Leung, 2018). Mice that lack PGI_2 develop hypertension (Yokoyama et al., 2002). It is thus important to maintain the levels of prostacyclin for vasoprotection. HSS is essential for PGI_2 production by endothelial cells (Russell-Puleri et al., 2017). HSS-induced ATP release also enhances PGI_2 production, and this occurs when ATP binds to an endothelial P2Y receptor (Wihlborg et al., 2003). Russell-Puleri et al. (2017) found that HSS induces glypican1 which results in activating PECAM-1 (CD31)—an endothelial adhesion molecule that successively activates PI3K, integrin-a5b1 and p38 phosphorylation—which results in both transcription and translation induction of cyclooxygenase-2 (COX-2), which in turn can oxidise arachidonic acid to form prostaglandin H2 (PGH2). Then, prostacyclin synthase (PTGIS) can convert PGH2 to $PGI_{2,}$ generating prostacyclin to keep the vasculature healthy (Moncada et al., 1976; Russell-Puleri et al., 2017; Bartosch et al., 2021); see figure 1.8.

There is little known about *PTGIS* production. While a study has revealed a shear stress–responsive sequence (GAGACC) in the promoter of *PTGIS* (Yokoyama et al., 1996), whether *PTGIS* expression is shear responsive has not yet been examined. Dekker et al. (2006) found that KLF2 can control vasorelaxation not only via *eNOS* expression but also via transcriptionally upregulating *PTGIS*, in turn leading to elevated prostacyclin production, suggesting that *PTGIS* is shear responsive as it is regulated by KLF2.
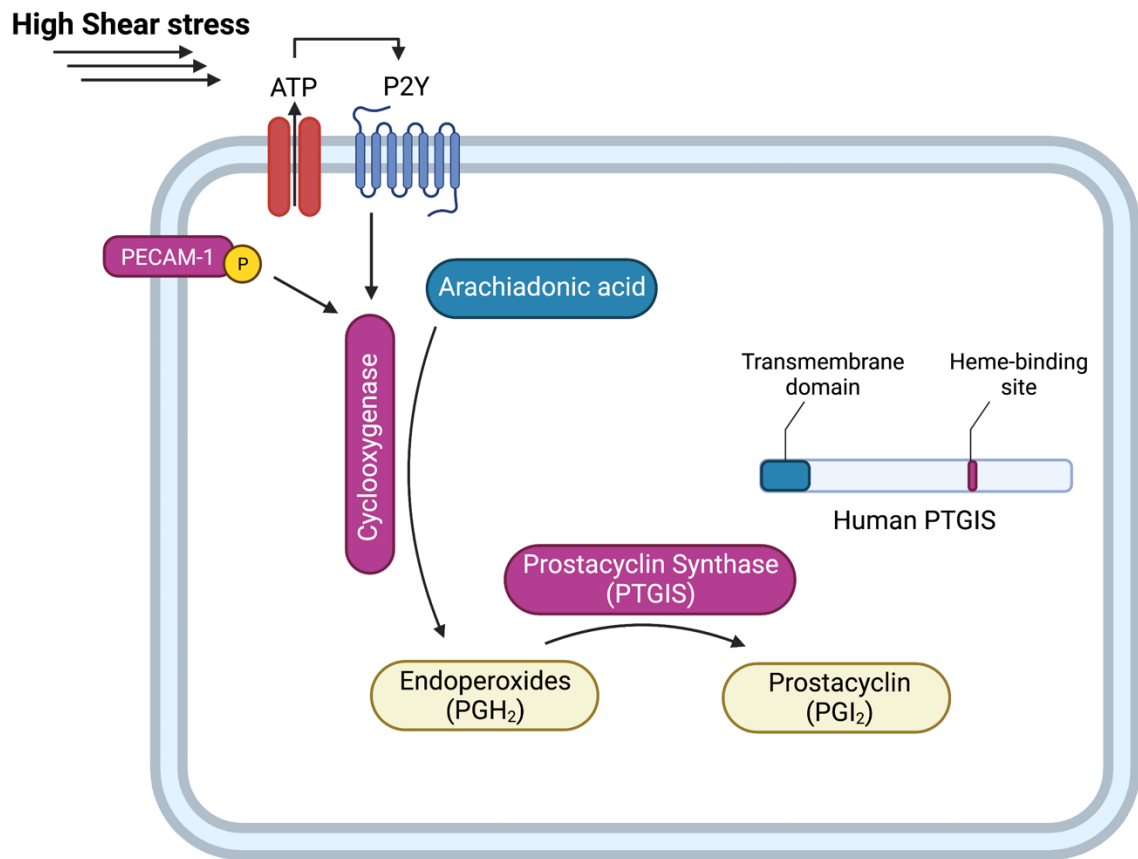
Figure 1.8. Endothelial-dependent vasoprotection via PGI₂ production. This diagram summarises HSS-induced PGI₂ generation via arachidonic acid metabolism.

PGI$_2$ in atherosclerosis

PGI$_2$ is a vasorelaxant, antithrombotic, anti-inflammatory, and antiatherogenic molecule (Moncada et al., 1976; TatesonMoncada and Vane, 1977; Murata et al., 1997; Kobayashi et al., 2004). In rabbits and mice with atherosclerosis, PGI$_2$ levels decreased after four months of administering a high-fat diet (Gryglewski et al., 1978; CyrusDing and Praticò, 2010). Mice with atherosclerosis yet lacking PGI$_2$ receptors (*ApoE$^{-/-}$, IP$^{-/-}$*) developed more plaque, higher platelet reactivity, elevated ICAM-1 expression, and massive leukocyte infiltration compared to control groups (*ApoE$^{-/-}$, IP$^{+/+}$*) (Kobayashi et al., 2004). Mice lacking PGI$_2$ receptors (*IP$^{-/-}$*) also developed occlusive thrombi (Murata et al., 1997). In addition, mice with genetic deletion of *Ptgis*, which encodes the enzyme PTGIS that produces PGI$_2$, had accelerated atherosclerosis progression (Yokoyama et al., 2002). A study of 138 human individuals who developed stroke showed a massive reduction in PGI$_2$ and NO and elevated oxLDL levels when compared with 34 healthy individuals (Tao et al., 2022). Taken together these results support that PGI$_2$ and NO can provide atheroprotection/vasoprotection in animal models and humans.

1.2.4. Ankyrin repeat single KH domain 1

Ankyrin repeats and single KH domain 1 (ANKHD1) is an RNA-binding protein that is highly conserved between humans and mice (93% similarity). Structurally, ANKHD1 is composed of two distinct ankyrin repeats that are known to mediate protein-protein interactions and a single and highly conserved KH RNA-binding domain (Figure 1.9). ANKHD1 is a large protein (2542 amino acids) with a predicted size of 269kDa. ANKHD1 also contains a number of low complexity sequences and three coiled-coils domains, its predicted alpha fold structure can be seen in figure 1.9: B. ANKHD1 is made up of 21 transcripts. miRTarBase analysis suggests that ANKHD1 may be under the control of a number of microRNAs, namely miR-17-5p, miR-26a-5p, miR-424-5p, miR-320a and miR-185-5p (Huang et al., 2022).

A

Human ANKHD1

2542 aa

	Ankyrin repeats
	KH domain
	NES
	NLS

B

KH domain
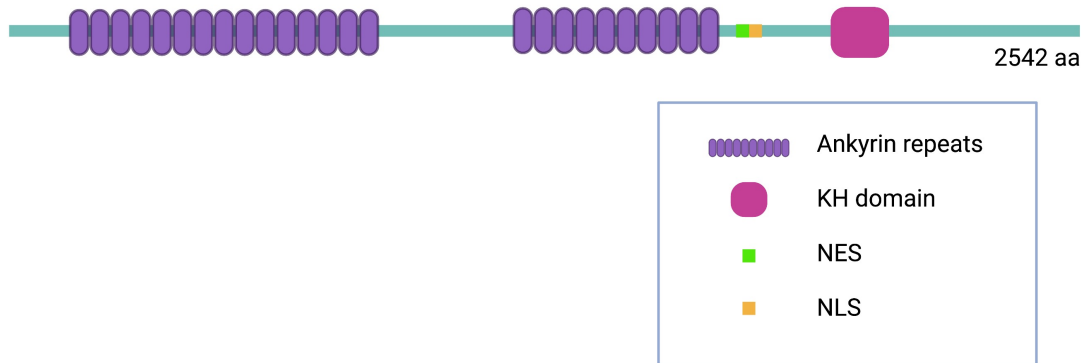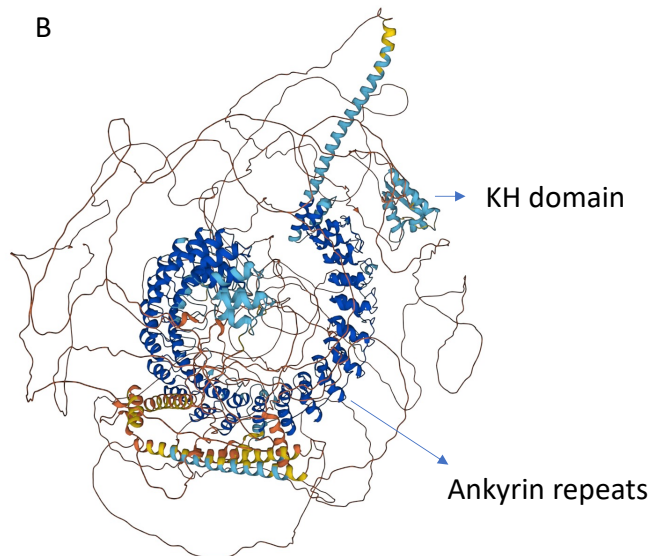
Ankyrin repeats

Figure 1.9. Diagrams showing ANKHD1 conserved domains. ANKHD1 protein domains (A) are multiple ankyrin repeats, which regulate protein-protein binding, KH domain, which binds to a single-stranded nucleic acid sequence, and nuclear localisation signal (NLS) and nuclear export sequence (NES), which transports molecules between the nucleus and cytoplasm. Alpha fold predicted model of ANKHD1 full-length (ANKHD1-203) (B).

ANKHD1 was first identified as a JAK/STAT positive regulator in a genome-wide RNA intereference study in *Drosophila Melanogaster* (Müller et al., 2005). It was subsequently shown to also regulate the Hippo pathway, which means it regulates cellular growth and survival (SidorBrain and Thompson, 2013). The molecular mechanisms in promoting JAK/STAT pathway activity were not studied. Therefore, Fisher et al. (2018) identified ANKHD1 as a positive regulator of the JAK/STAT pathway via regulating cytokine receptor stability and dimerization (Dome-receptors in *Drosophila* and Erythropoietin receptors in human cells). ANKHD1 via its ankyrin repeats can physically form a protein-protein interaction with Dome-receptor to enhance Dome-receptor stability, which results in direct activation of the JAK/STAT pathway.

It was also unknown how ANKHD1 regulates the Hippo pathway mechanistically. Therefore, Sidor et al. (2019) showed that the second ankyrin repeat of ANKHD1 has a non-canonical NLS which has been found to be critical for translocating the transcription coactivator YAP1 into the nucleus via protein-protein interaction. In *ANKHD1* silenced cells, YAP1 failed to move into the nucleus, and as such, the hippo pathway was aberrantly regulated.

Both the Hippo and JAK/STAT signalling pathways are essential for tissue growth. Therefore, ANKHD1 was studied in cancer where it has been shown to be upregulated in several cancers, such as renal cell carcinoma, glioma and colorectal carcinoma. Fragiadaki and Zeidler (2018) identified for the first time that ANKHD1, which contains an evolutionarily conserved RNA-binding KH domain, can bind RNA and exert its function through RNA binding. Specifically, it was shown that ANKHD1 binds to miRNA29a-3p and this interaction positively regulates clear cell renal cell carcinoma cell proliferation. Yang et al. (2020) also provided further evidence that ANKHD1 is an RNA-binding protein. They found that ANKHD1 can bind and stabilise the lncRNA *LINC00346* in glioma endothelial cells, eventually enhancing glioma angiogenesis via upregulation of the critical angiogenic

regulators epidermal growth factor–like domain 7 (EGFL7) and Roundabout 4 (ROBO4). Whether ANKHD1 can bind to these microRNAs and lncRNAs in endothelial cells of people without cancer remains unknown.

Additional evidence for the RNA binding ability of ANKHD1 was demonstrated more recently. ANKHD1 together with the lncRNA *MALAT1* can enhance YAP1 transcription and activity leading to PI3K/AKT pathway activation in colorectal cancer (CRC) cells. This results in protection from apoptosis and DNA damage by reducing ROS formation and promoting proliferation and survival; thus, enhancing radio-resistance in CRC cells (Yao et al., 2022). Additionally, *MALAT1* enhances angiogenesis and epithelial-to-mesenchymal transition in CRC cells via YAP1 (Sun et al., 2019). Whether ANKHD1 promotes angiogenesis via *MALAT1*-YAP1 has not yet been studied. It would be of interest to examine if these interactions of ANKHD1 with lncRNAs are cancer-specific.

As mentioned above, activated PI3K/AKT in the healthy endothelium can enhance NO bioavailability (Dimmeler et al., 1999; Dixit et al., 2005; Jin et al., 2005). Yet the role of ANKHD1 in healthy vasculature and the context of atherosclerosis is completely unexplored. Single-cell RNA sequencing of the heart muscle shows the highest levels of ANKHD1 were in endothelial cells compared to all other cells (Cell type atlas - ANKHD1 - The Genotype-Tissue Expression (Gtexportal, 2021); Figure 1.10). Whether ANKHD1 regulates key molecules involved in major endothelial cell functions is currently unknown—little is known about ANKHD1, and its role in vasculature has not yet been studied.

Figure 1.10. Single-cell expression of ANKHD1 mRNA in heart tissue. ANKHD1 showed

to be highly expressed in endothelial cells of heart tissue (blue box) (Gtexportal, 2021).

1.3. Conclusion and knowledge gap

Studies on functional endothelial activity have illustrated effective vasoactive modulators that provide optimal functions in regulating vasorelaxation, inflammation, thrombosis, oxidative stress and atheroprotection. The molecular mechanisms that control endothelial cells, especially at the mRNA level, have not yet been explored; for example, it is unclear how NO/PGI$_2$ bioavailability is sustained under HSS. It is also unclear whether ANKHD1 is involved in regulating ROS by potentially controlling the expression and activity of the major genes, such as eNOS/PTGIS at the mRNA and/or protein levels.

1.4. Hypothesis and aims

I hypothesise that ANKHD1, which is highly expressed in arteries, drives cytoprotective pathways, the disruption of which is expected to promote atherosclerosis.

Aims:

1. Determine ANKHD1 functions in primary human endothelial cells.

2. Establish whether ANKHD1 is controlled by shear stress using both human cells and mouse aortas.

3. Determine the role of ANKHD1 in the vasculature by characterising the first *Ankhd1* knockout animals.

4. Investigate the potential role of ANKHD1 in protecting against the development of atherosclerosis in the PCSK-9 mouse model and cellular models.

Chapter 2: Materials and Methods

2.1. Materials

2.1.1. Mouse models

Mouse models were used to quantify aortic diameters, assess systemic risk factors and apply *en-face* staining:

We used 17 *Ankhd1* wild-type (*Ankhd1$^{+/+}$*), 4 *Ankhd1* heterozygous (*Ankhd1$^{+/-}$*) and 14 *Ankhd1* knockout (*Ankhd1$^{-/-}$*) mouse models. They are listed below in Table 2.1.

Animal Number	Genotype	Gender	Age
230551	*Ankhd1$^{-/-}$*	Female	5 weeks
230552	*Ankhd1$^{+/-}$*	Female	5 weeks
235148	*Ankhd1$^{+/-}$*	Male	4 weeks
235152	*Ankhd1$^{+/-}$*	Female	4 weeks
238493	*Ankhd1$^{+/-}$*	Male	4 weeks
238498	*Ankhd1$^{+/+}$*	Male	4 weeks
238500	*Ankhd1$^{+/+}$*	Female	4 weeks
240462	*Ankhd1$^{+/+}$*	Female	5.5 weeks
240877	*Ankhd1$^{+/+}$*	Male	5 weeks
240878	*Ankhd1$^{+/+}$*	Male	5 weeks
240881	*Ankhd1$^{+/+}$*	Female	5 weeks
242161	*Ankhd1$^{+/+}$*	Male	4 weeks
242163	*Ankhd1$^{-/-}$*	Female	4 weeks
242166	*Ankhd1$^{-/-}$*	Female	4 weeks
264593	*Ankhd1$^{+/+}$*	Male	5 months
264594	*Ankhd1$^{-/-}$*	Male	5 months
264595	*Ankhd1$^{+/+}$*	Male	5 months
264596	*Ankhd1$^{-/-}$*	Male	5 months
264597	*Ankhd1$^{+/+}$*	Male	5 months
264598	*Ankhd1$^{-/-}$*	Female	5 months
264599	*Ankhd1$^{+/+}$*	Female	5 months
270988	*Ankhd1$^{+/+}$*	Male	5 months
270989	*Ankhd1$^{+/+}$*	Male	5 months
270991	*Ankhd1$^{+/+}$*	Male	5 months
270993	*Ankhd1$^{-/-}$*	Male	5 months
270994	*Ankhd1$^{-/-}$*	Male	5 months
271939	*Ankhd1$^{-/-}$*	Male	5 months
271942	*Ankhd1$^{-/-}$*	Female	5 months
272687	*Ankhd1$^{-/-}$*	Male	5 months

272688	*Ankhd1$^{-/-}$*	Female	5 months
272691	*Ankhd1$^{+/+}$*	Female	5 months
310596	*Ankhd1$^{-/-}$*	Male	5 months
310598	*Ankhd1$^{-/-}$*	Male	5 months
310601	*Ankhd1$^{+/+}$*	Female	5 months
310602	*Ankhd1$^{+/+}$*	Female	5 months
Table 2.1. List of mouse models.			

2.1.2. Atherosclerosis mouse models

Ankhd1$^{+/+}$(N= 6), *Ankhd1*$^{-/+}$ (N= 7) and *Ankhd1*$^{-/-}$ (N= 7) mouse models were virally transduced with a single tail-vain injection of 50 μl of PCSK9-AAV followed by changing into a high fat diet for 12 weeks to induce atherosclerosis. All mice that developed atherosclerosis are listed in table 2.2.

Mouse ID	Genotype	Gender	Age
247839	*Ankhd1*$^{+/-}$	Male	5 months
247840	*Ankhd1*$^{+/-}$	Male	5 months
247842	*Ankhd1*$^{+/+}$	Male	5 months
247844	*Ankhd1*$^{+/+}$	Male	5 months
247845	*Ankhd1*$^{+/-}$	Male	5 months
217281	***Ankhd1*$^{-/-}$**	**Male**	**6.5 months**
217283	*Ankhd1*$^{+/-}$	Female	6.5 months
217284	***Ankhd1*$^{-/-}$**	**Female**	**6.5 months**
217285	*Ankhd1*$^{+/-}$	Female	6.5 months
214931	***Ankhd1*$^{-/-}$**	**Male**	**7.5 months**
214932	***Ankhd1*$^{-/-}$**	**Male**	**7.5 months**
283111	*Ankhd1*$^{+/-}$	Female	5 months
283113	*Ankhd1*$^{+/-}$	Female	5 months
287421	***Ankhd1*$^{-/-}$**	**Male**	**5 months**
287422	*Ankhd1*$^{+/+}$	Male	5 months
287425	*Ankhd1*$^{+/+}$	Female	5 months
287426	*Ankhd1*$^{+/+}$	Female	5 months
287427	***Ankhd1*$^{-/-}$**	**Female**	**5 months**
287879	***Ankhd1*$^{-/-}$**	**Female**	**5 months**
Table 2.2. PSCK9 mouse models used for atherosclerotic plaque size quantification.			

2.1.3. Primary cells

The primary cells used for culture, shear stress treatment, ANKHD1 silencing, immunofluorescence staining, RNA immunoprecipitation (RIP) and RNA stability were human coronary artery endothelial cells (HCAECs) and/or human umbilical vein endothelial cells (HUVECs). See Table 2.3.

HCAECs	Passage
Donor K	3
Donor L	3
Donor C	3
Donor D	3
Donor H	3
Donor E	3
HUVECs	Passage
Donor 6	3
Donor 4	3
Donor 7	3
Donor 5	3
Donor C	3
Table 2.3. List of donors of primary endothelial cells.	

2.1.4. Antibodies

The antibodies used for *en-face* staining, immunofluorescence staining, western

blotting and RIP are listed in Table 2.4.

Antibodies	Lot number (catalogue number)	Source	Stock concentration (dilution)	Experiments
488 anti-mouse CD31	B211217 (102514)	BioLegend	0.5 mg/mL (diluted 1:50 in 3% BSA with 1% TBST)	Endothelial cell-specific marker used for *en-face* staining
568 gout anti-rabbit IgG	2045347 (A11036)	Thermo Fisher	2 mg/mL (diluted 1:150 in 3% BSA with 1% TBST)	Secondary antibody used for *en-face* staining
Rabbit anti-ANKHD1	A40193 (HPA008718)	Atlas Antibodies	0.2 mg/mL (diluted 1:100 in 3% BSA with 1% TBST)	Primary antibody used for *en-face* staining, western blotting and RIP assay
Rabbit (DA1E) mAb IgG XP (R) isotype control 3900S	3900S	Cell signalling	0.25 mg/mL (diluted 1:1000 in 3% BSA with 1% TBST)	Negative control used for *en-face* staining
Polyclonal gout anti-rabbit immunoglobulins/HRP	41372205 (P0448)	Dako	0.30 g/L (5 μL diluted in 5% milk in 1%TBST)	Secondary antibody used for western blotting
Polyclonal gout anti-mouse immunoglobulins/HRP	20078279 (P0447)	Dako	1 g/L (5 μL diluted in 5% milk in 1%TBST)	Secondary antibody used for western blotting
Rb pAb to PTGIS/PGIS	GR298379-8 (AB23668)	Abcam	0.100 mg/mL (diluted 1:200 in 3% BSA with 1% TBST)	Primary antibody used for *en-face* staining and western blotting

Polyclonal rabbit anti-eNOS/NOS type III	25707 (610229)	BD Biosciences	0.250 mg/mL (diluted 1:100 in 3% BSA with 1% TBST)	Primary antibody used for *en-face* staining and western blotting
Purified Mouse Anti-Human CD144 (VE-cadherin)	(555661)	BD Pharmingen	0.5 mg/ml (Diluted 1:100 in 3% BSA with 1% TBST)	Primary antibody used for immunofluorescence staining
Anti-mouse IgG Alexa Fluor 488	(4408S)	Cell Signalling	0.25 mg/mL (Diluted 1:100 in 3% BSA with 1% TBST)	Secondary antibody used for immunofluorescence staining
Rabbit polyclonal CD62E (E-selectin)	GR3244531-8 (AB18981)	Abcam	0.5 mg/mL (Diluted 1:100 in 3% BSA with 1% TBST)	Primary antibody used for *en-face* staining
Rabbit polyclonal CD62E (E-selectin)	(NBP1-45545)	Novus	0.5 mg/mL (Diluted 1:100 in 3% BSA with 1% TBST)	Primary antibody used for *en-face* staining
Mouse Monoclonal B-actin	GR3398637-1 (AB8224)	Abcam	1 mg/mL (Diluted 1:1000 in 3% BSA with 1% TBST)	Primary antibody used for western blotting
Rabbit polyclonal HPRT	GR3327070-2 (AB10479)	Abcam	1 mg/mL (Diluted 1:1000 in 3% BSA with 1% TBST)	Primary antibody used for western blotting
B-tubulin	(2146S)	Cell Signalling	(Diluted 1:1000 in 3% BSA with 1% TBST)	Primary antibody used for western blotting

Table 2.4. List of antibodies used for staining, western blotting and immunoprecipitation.

Abbreviations: bovine serum albumin (BSA); tris-buffered saline and tween 20 (TBST);

hypoxanthine phosphoribosyltransferase (HPRT); horseradish peroxidase (HRP); nitric oxide synthase III (NOS III). 65

2.1.5. Primers

The primers used for quantitative polymerase chain reaction (qPCR) are listed in Table 2.5.

Primers	Sequence	Application (Transcript length)
Hs *HPRT*	**Forward (20 bp)** 5'TTGGTCAGGCAGTATAATCC3' **Reverse (20 bp)** 5'GGGCATATCCTACAACAAAC3'	Internal loading control (housekeeping gene, 133 bp)
Hs *B-actin*	**Forward (20 bp)** 5'ATCATTGCTCCTCCTGAGCG3' **Reverse (18 bp)** 5'GACAGCGAGGCCAGGATG3'	Internal loading control (housekeeping gene, 65 bp)
Hs *ANKHD1* (transcript variants: *ANKHD1-203 ANKHD1-204 ANKHD1-205*)	**Forward (20 bp)** 5'ATGTCAACTCCCAGTCTGCA3' **Reverse (20 bp)** 5'CTTCCACATGACCTGCACTG3'	Target gene (168 bp)
Hs *ANKHD1-203* **(Full length)**	**Forward (20 bp)** 5'CAGTGCTTGGACACTTGGAA3' **Reverse (20 bp)** 5'AAAAACTTGCCAGAGGAGCA3'	Target gene [159 bp]
Hs *KLF2*	**Forward (19 bp)** 5'GCATCTGAAGGCGCATCTG3' **Reverse (18 bp)** 5'TTCGGTAGTGGCGCGTGA3'	Target gene
Hs *KLF4*	**Forward (23 bp)** 5'GCAAAACCTACACAAAGAGTTCC3' **Reverse (18 bp)** 5'GGTGCCCCGTGTGTTTAC3'	High-shear regulated gene (Zhou et al., 2012) used for quality control. [103 bp]
Hs *eNOS*	**Forward (20 bp)** 5'AGAACTCTTCCTTCTGCCCC3' **Reverse (18 bp)** 5'ATGTTGGACACTGCCGGG3'	High-shear regulated gene (Zhang et al., 2016) used for quality control in assessing ANKHD1 expression in non-transfected cells. In cells lipotransfected with siRNAs, eNOS is the target gene. [117 bp]
Hs *MCP1*	**Forward (20 bp)** 5'GCAGAAGTGGGTTCAGGATT3'	Low-shear regulated gene (McCormick et

	Reverse (20 bp) 5'TGGGTTGTGGAGTGAGTGTT3'	al., 2001) used for quality control. [83 bp]
Hs *F3*	**Forward (20 bp)** 5'GAGTACAGACAGCCCGGTAG3' **Reverse (20 bp)** 5'CCCACTCCTGCCTTTCTACA3'	Target gene [150 bp]
Hs *GPC1*	**Forward (20 bp)** 5'GCTGGTCTACTGTGCTCACT3' **Reverse (20 bp)** 5'CCCGATGTACCCCAGAACTT3'	Target gene [171 bp]
Hs *IL1β*	**Forward (20 bp)** 5'GGAGAATGACCTGAGCACCT3' **Reverse (20 bp)** 5'TGATCGTACAGGTGCATCGT3'	Target gene [106 bp]
Hs *ICAM-1*	**Forward (20 bp)** 5'CCGGCCAGCTTATACACAAG3' **Reverse (20 bp)** 5'ACATTGGAGTCTGCTGGGAA3'	Target gene [123 bp]
Hs *GSTP-1*	**Forward (20 bp)** 5'CCGCTGCAAATACATCTCCC3' **Reverse (20 bp)** 5' GCAGGTTGTAGTCAGCGAAG3'	Target gene [170 bp]
Hs *GSTO-1*	**Forward (20 bp)** 5'CCCCTATGAGAAAGCTTGCC3' **Reverse (21 bp)** 5'CAGAACCTCCTCTAGCTTGGT3'	Target gene [154 bp]
Hs *PTGIS*	**Forward (20 bp)** 5'TTCCACATTACAGCCCCAGT3' **Reverse (19 bp)** 5'CAGCACTGCATGGAGGTTG3'	Target gene [110 bp]

Table 2.5. Primer pairs used for qPCR. Abbreviations: glutathione S-transferase pi 1 (*GSTP-1*); glutathione S-transferase omega 1 (*GSTO-1*); glypican 1 (*GPC1*); Interleukin 1 beta (*IL1β*).

2.1.6. The small interfering RNAs (siRNAs)

The three aliquots of siRNAs used in this study are non-target siRNA,

*ANKHD1*siRNA-1 and *ANKHD1*siRNA-2. See table 2.6.

siRNA	Catalogue number	Supplier
Non-target siRNA (NT-siRNA; control siRNA)	D-001206-13-20	Dharmacon
*ANKHD1*siRNA-1	M-014405-00-0010,	Dharmacon
*ANKHD1*siRNA-2	D-014405-01	Dharmacon
Table 2.6. siRNAs used for ANKHD1 silencing in primary human endothelial cells.		

2.1.7. Reagents, solutes, gels and kits

The reagents, solutes, gels and kits used are listed in Table 2.7.

Reagent/solutes/kits	Lot number (catalogue/ reference number)	Source	Experiments
0.05% Trypsin, 0.53 mM EDTA, 1x sodium bicarbonate	27121013 (25-052-CV)	Corning	Primary cell culture
2-Propanol (isopropanol)	BCBV7093	SIGMA	RNA extraction
5x iScript Reaction Mix iScript Reverse Transcriptase	(1708890) (1708891)	BIO-RAD	RT-PCR
100% Ethanol	16K024017	VWR Chemicals	RNA extraction
Amersham™ ECL Select™ Western Blotting Detection Reagent	(RPN2235)	Cytiva	Western blotting
Actinomycin D	0457563-4 (11421)	Cayman Chemical	RNA stability
Benzonase	(E1014)	Sigma	Biotinylated 3'UTR pulldown
Biotin RNA Labeling Mix	(11685597910)	Roche	Biotinylated 3'UTR transcription
Distilled water DNase/RNase Free	1762915 (10977035)	Gibco	qPCR
Dynabeads M-280 Streptavidin	(11205D)	Invitrogen	Biotinylated 3'UTR pulldown
Lipofectamine RNAiMAX Reagent	2067471 (13778-075)	Thermo Fisher	RNA silencing
Magna RIP Kit	(17-700)	Millipore	RIP assay
Methanol	1910599 (M/4000/17)	Fisher Chemical	Cell fixation for immunofluorescence staining
Mini-Protean TGX Gels	(4561025)	BIO-RAD	Western blotting
miRNeasy Micro Kit	(217084)	Qiagen	RNA extraction
Nuclease-Free Water	0000257361 (P119A)	Promega	RNA extraction and RT-PCR
OPTI-MEM I (1X) Reduced Serum Medium	1616013 (31985062)	Gibco	RNA silencing
Precision Plus Protein™	(161-0373)	BIO-RAD	Western blotting
ProLong™ Diamond Antifade Mountant	2086315 (P36970)	Thermo Fisher	Mounting media for *en-face* and

			immunofluorescence staining
Protease inhibitor cocktail tablets	(11836153001)	Roche	Protein extraction
Skim milk	BCBT8091 (70166500G)	Sigma	Western blotting
Sodium Acetate (3 M), pH 5.5, RNase-free	(AM9740)	Invitrogen	Biotinylated 3'UTR pulldown
SP6/T7 Transcription Kit	(10999644001)	Roche	Biotinylated 3'UTR transcription
SsoAdvanced™ Universal SYBR Green Supermix	(L001894 A)	Bio-Rad	qPCR
SUPERaseIn (RNase inhibitor)	(AM2694)	Invitrogen	Biotinylated 3'UTR pulldown
TO-PRO™ -3 iodide (642/661)	1976612 (T3605)	Thermo Fisher	*en-face* staining
Trans-Blot Turbo transfer pack	64446217 (1704158)	BIO-RAD	Western blotting (Transfer system)
Table 2.7. List of reagents, solutes, gels and kits. Abbreviations: ethylenediaminetetraacetic acid (EDTA); reverse-transcriptase PCR (RT-PCR); deoxyribonuclease (DNase); ribonuclease (RNase).			

2.1.8. Buffers, media and stains

The buffers, media and stains used in this study are listed in Table 2.8.

Buffer/media/stains	Content	Supplier	Application
1% Gelatine	1 g gelatine 100 mL distilled water	In-house	Cell culture
1% TBS with Tween 20 (1% TBST)	25 mL of 20x TBS pH 7.4 (distilled water, NaCl, KCl, Tris Base) 500 mL distilled water 500 μL Tween 20	In-house	Western blotting and *en-face* staining
1% Tris-buffered saline (1% TBS)	25 mL of 20x TBS pH 7.4 (distilled water, NaCl, KCl, Tris Base) 500 mL distilled water	In-house	Cell extraction
3% Blocking buffer BSA	0.6 g bovine serum albumin 20 mL of 1% TBST	In-house	*en-face* staining
5% milk buffer	2.5 g skim milk 50 mL 1% TBST	In-house	Western blotting
10x Running buffer	30.3 g Tris-base 10 g SDS (50 mL 20% SDS) 144.2 g Glycine up to 1000 mL distilled water	In-house	Western blotting
DMEM media	100 mL of DMEM media 10 mL of foetal bovine serum 10 mL of newborn calf serum 200 μL of endothelial cell–specific growth factor 100 μL of heparin	In-house	HUVECs culture
Endothelial cell growth medium MV	0.05 mL/mL Fetal calf serum 0.004 mL/mL Endothelial cell growth supplement 10 ng/mL Epidermal growth factor 90 μg/mL Heparin 1 μg/mL Hydrocortisone	PromoCell	HCAECs culture
Lysis buffer	5 mL of 1M Tris-HCL (pH 7.4) 5 mL of 5M NaCl 1 mL of 0.5 EDTA 300 μL (0.3%) triton x-100 100 mL distilled water 1 tablet of protease inhibitor cocktail	In-house	Western blotting
Oil red O stain	50 mL of distilled water 30 mL of oil red O solution (1 mL of distilled water + 99 mL of Isopropanol [1:100] saturated in oil red O)	In-house	Plaque staining

Sample buffer	2.5 mL of 0.5 M Tris-HCL PH 6.8 4 mL of 10% SDS 0.5 mL of 0.1% bromophenol blue 3 mL of glycerol 2.5-5% B-mercaptoethanol	In-house	Western blotting
TO-PRO^{TM} -3 iodide (642/661)	Nucleic acid stain	Thermo Fisher	*en-face* staining

Table 2.8. List of buffers, media and stains. Abbreviations: tris-buffered saline (TBS); tris-buffered saline and tween 20 (TBST); sodium chloride (NaCl); potassium chloride (KCl); hydrochloric acid (HCl); sodium dodecyl sulphate (SDS); ethylenediaminetetraacetic acid (EDTA).

2.1.9. Equipment

The equipment used in this study are listed in Table 2.9.

Equipment (supplier)
10 µl, 20 µl, 100 µl, 200 µl and 1,000 µL volumetric pipettes
20 µL, 200 µL and 1,000 µL plastic tips
12-well plate
6-well plate
6-well glass coverslips
96-well plate
15 cm Petri dish
Bijoux tubes
Cell culture flasks (CELLSTAR): 75 cm^2, 250 mL, sterile
Cell scraper (Greiner Bio-One)
Coverslips, 22 x 22 mm (Scientific Laboratory Supplies)
Disposable serological pipets (Fisherbrand): 5 mL, 10 mL and 25 mL
Eppendorf 0.5 mL
Eppendorf 1.5 mL
Foil
Forceps
Glass slides
Magnetic separator
Pipetboy (ErgoOne FAST)
Scissors
Table 2.9. List of equipment.

2.1.10. Instruments

The instruments used in this study are listed in Table 2.10.

Instrument	Supplier	Application
37° C, 5% CO_2 incubator	Panasonic	Cell culture
Trans-Blot Turbo	BIO-RAD	Western blotting (Transfer system)
Canon A650 IS	Canon	Aorta images
CFX384™ Real-Time System	BIO-RAD	qPCR
Heat block	Techne	Western blotting and 3'UTR pulldown
Light microscopy	Nikon	Microdissection
Leica Thunder imager	Leica	Microscopy
LSM 510 META confocal microscope	ZEISS	*en-face* staining
Orbital shaker	Grant-bio	Shear stress application
T100™ Thermal Cycler	Bio-Rad	RT-PCR
Table 2.10. List of instruments.		

2.2. Methods

2.2.1. General systemic factor assessment in Ankhd1 mouse models

Ankhd1 mouse models had their weight and terminal blood glucose and cholesterol measured. Glucose and cholesterol measurements were performed by introducing a needle directly into the heart and blood was drawn. To measure blood glucose, a small spot of blood was ejected from the syringe onto a glucose reader strip, and the strip was then placed in a glucometer (freestyle optium). To measure cholesterol levels, 20 µl of blood from the draw was placed on a PTS cholesterol panel (BHR pharma) and inserted into a cardiocheck reader (BHR pharma). Systolic blood pressure was measured in conscious mice by placing the mouse tail in the cuff (CODA non-invasive system), increasing pressure around the tail (250 mm Hg) to stop blood flow then releasing it and recording reflow of the vessels. Heart rate was measured in mice under 2% isoflurane anaesthesia using echocardiography via the Vevo 3100 micro-ultrasound imaging system (VisualSonics, Toronto, Canada).

2.2.2. Aorta microdissection

Chest cavities of all mice were surgically opened to dissect aortas under a dissecting light microscope. This procedure starts by extracting vital organs, such as the liver and lungs, using micro-forceps. Aortas were held from its descending part and peeled up to remove them; keeping them attached to the heart. After that, Excess connective tissues were cleaned up and aortas were extracted from the hearts. Extracted aortas were then placed in clean Eppendorf tubes labelled with mouse numbers and filled with 1% TBS. Finally, all dissected aortas were kept at 4° C.

Dissected aortas were used for *en-face* staining and/or oil red O application. In *en-face* staining, as we are aiming to test the effect of shear stress on endothelial *Ankhd1*, we used primary aortic arches, also known as ascending aortas (Figure 2.1). This is because the inner

curvatures of primary arches experience LSS, whereas the outer ones experience a high magnitude of shear stress (Suo et al., 2007). Therefore, extracting the primary arches helps in studying the influence of different shear magnitudes on endothelial cell responses. It was also aimed to test the effect of ANKHD1 on some target molecules, such as eNOS and PTGIS, in HSS regions of aortas. To achieve that, about 1 mm of descending thoracic aortas of *Ankhd1*$^{+/+}$ and *Ankhd1*$^{-/-}$ were dissected (Figure 2.1).
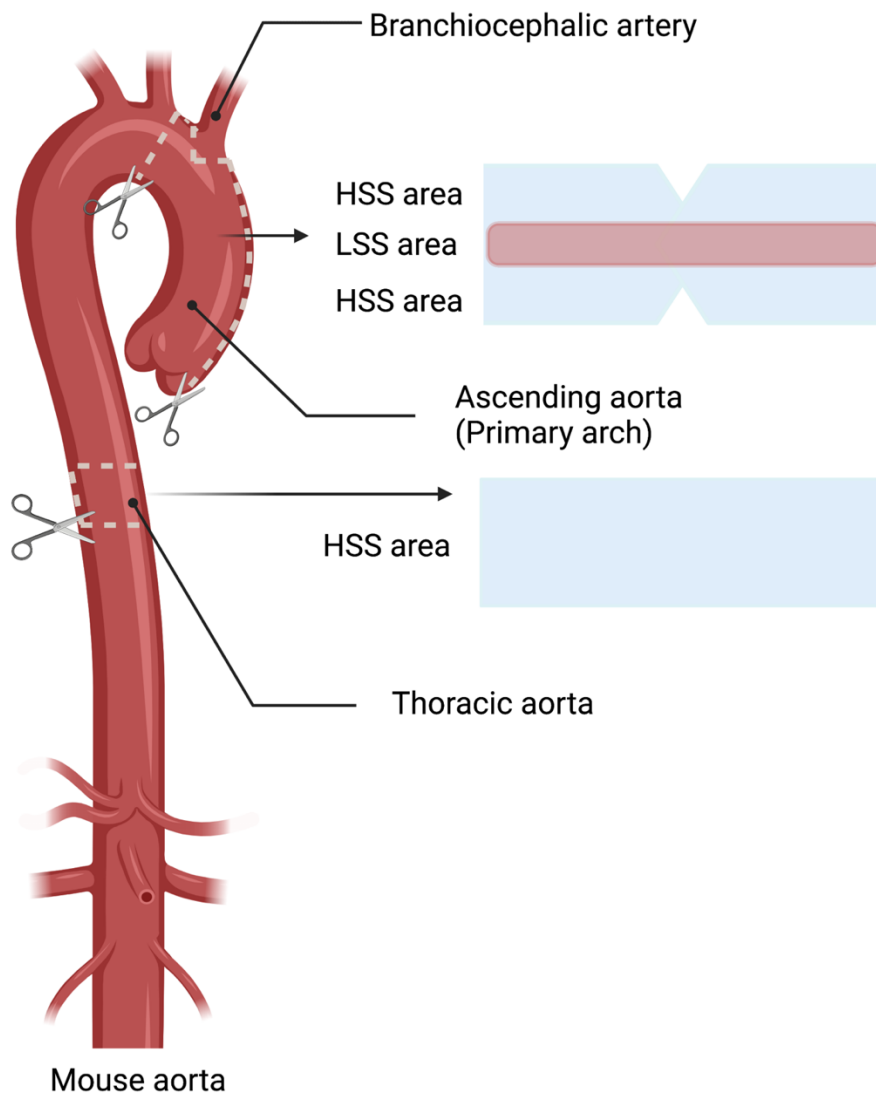
Figure 2.1. Aorta microdissection of Ankhd1 mouse models for en-face staining. The outer curvature of the ascending aorta and thoracic aorta expose to HSS, and the inner curvature of the ascending aorta exposes to LSS.

2.2.3. En-face staining

The protocol of *en-face* staining is the same for all aortic parts (descending aorta or aortic arch). Prelabelled 96-well plates with the relevant mouse number, corresponding aortic part (e.g., primary arch), and the primary antibody applied (e.g., anti-ANKHD1) were used to stain mouse tissues. Each dissected primary arch or thoracic aorta took one row in a 96-well plate. In the first column, 100 μL of the blocking buffer (3% BSA) was placed in which each tissue can be incubated for two hours at room temperature on the shaker. 100 μL of a diluted primary antibody in 3% BSA was then placed in the second column. After blocking with 3% BSA, tissues were transferred into the next wells containing primary antibodies. Primary antibodies' degrees of dilutions were 1:100 for ANKHD1, eNOS and CD62E and 1:200 for PTGIS. 96-well plate was then covered with foil and left overnight at 4°C. After that, tissues were washed three times in the next three wells containing 1% TBST. Tissues were then incubated in the secondary fluorescent antibody (568 gout anti-rabbit IgG: 1:150), covered with foil and left on the shaker for five hours at room temperature. Tissues were washed three times in the previous three columns containing 1% TBST and then transferred into 100 μL of (1:50) CD31. This 96-well plate was then covered with foil and left at 4°C for 4-5 days. After staining with CD31, all parts of the aortas were washed twice in 1% TBST, placed in To-opro (1:250) for 5 minutes and washed once in 1% TBST. To visualise the innermost layers containing endothelial cells, the tube was opened on a slide covered with 3 μL of mounting media making the innermost layer face the coverslip. Each slide was prelabelled with staining date, mouse number (ID), primary antibody and aortic part. Finally, the confocal microscope (LSM 510 META confocal microscope) was used to visualise the fluorescently stained endothelium.

Quantification. A minimum of three images were taken per each aortic part (inner primary arch, outer primary arch and descending aorta). I then used ImageJ software to quantify the mean fluorescence intensity from each image/tissue. The mean fluorescence intensity was

measured by subtracting the background florescence generated by the negative control, which is the isotype-matched IgG. The ImageJ Macro tool was used to calculate the nuclear-to-cytoplasmic ratio of ANKHD1 in endothelial cells of mouse descending aortas (Grune et al., 2018). Then, I used the software Prism 8 to plot the results from multiple animals as well as perform statistical analysis.

2.2.4. Oil Red O staining and haematoxylin and eosin staining

Aortic root preparation for haematoxylin and eosin staining. Aortic roots embedded in paraffin were deparaffinised and then rehydrated in a sequence of incubations. I started by placing the aortic root two times in xylene for 2 minutes each, followed by two times in 99% ethanol for 2 minutes each, one time in 95% ethanol for 2 minutes, one time in 70% ethanol for 2 minutes and finally in running water for 2 minutes.

haematoxylin and eosin staining for aortic roots. Tissue was stained with haematoxylin for 3 minutes, washed with running water for 5 minutes, immersed in 1% acetic acid for 30 seconds, washed with running water for 5 minutes, immersed in 95% ethanol for 30 seconds, counterstained with eosin staining for 30 seconds, washed with running water for 5 minutes and dehydrated in a sequence of incubations. It starts with 70% ethanol for 2 minutes, 95% ethanol two times for 2 minutes each, 99% ethanol for 2 minutes and in xylene two times for 2 minutes each.

To measure plaque sizes in aortic roots, aortic roots were mounted with DPX Mountant media under glass coverslips and then tailed images of stained aortic roots were taken via a 10x lens of Leica thunder microscope. Plaque measurements were performed to provide the relative lesion areas, which are in the aortic sinuses, to the total root area using ImageJ (Centa et al., 2019).

Oil red O staining for aortas of mice. Aortas of *Ankhd1*$^{+/+}$, *Ankhd1*$^{-/+}$ and *Ankhd1*$^{-/-}$ mice with atherosclerosis, PCSK9-AAV transduced mice, were used to quantify plaque burden. Staining has been performed by placing the aorta in 5 mL of 60% isopropanol for 2 minutes, followed by oil red O for 15 minutes, 60% of isopropanol for 2 minutes and in double distilled water.

To measure plaque sizes in aortas, stained aortas were cut through the inner curvature to open the vessel. The ascending primary arch was also cut from the outer curvature to make a 2D shape of the aorta (Figure 2.2). Images of the open aortas were taken via Canon A650 IS microscope and lesion sizes were measured via Nis-elements BR, which indicates the plaque areas per the total aortic area.
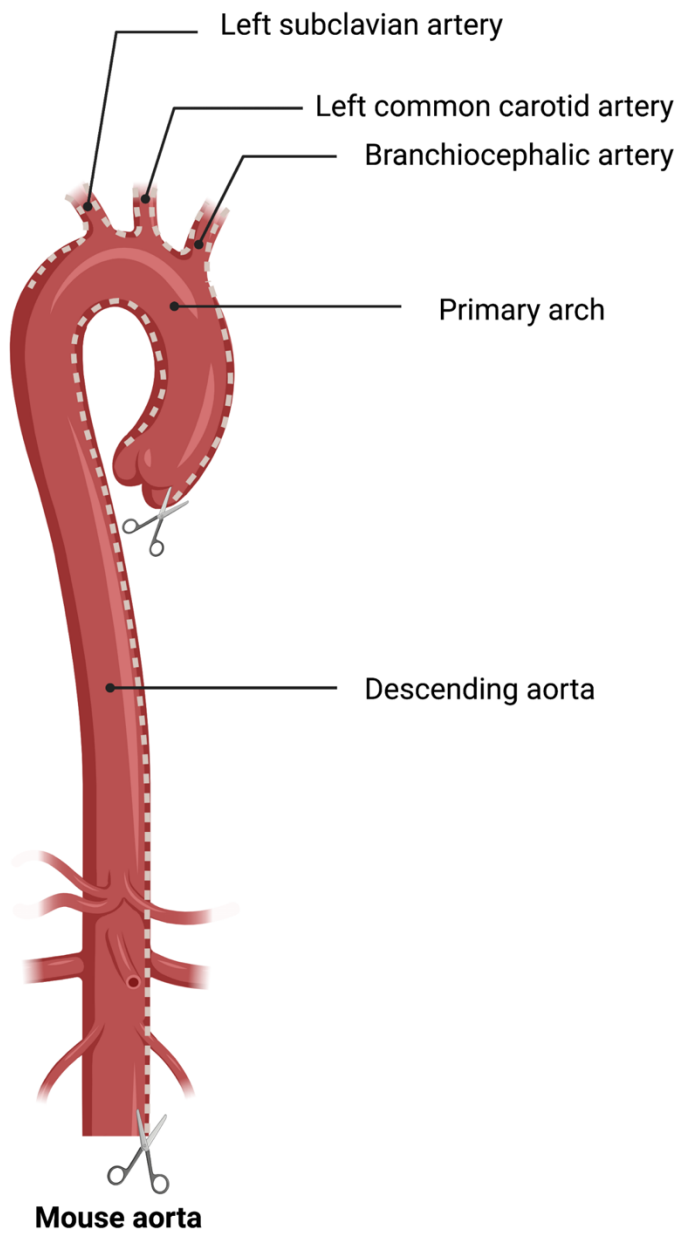
Figure 2.2. Aorta microdissection of Ankhd1 mouse models for Oil red O staining.

2.2.5. Primary cell culture

Primary HUVECs and HCAECs were received in frozen vials that were kept in liquid nitrogen. To culture HUVECs, a 75 mL flask was coated with 8 mL of 1% gelatine and left in the incubator ($37°$ C, 5% CO_2) for half an hour. Excess gelatine was then discarded, and the flask was filled with 15 mL of DMEM growth media and incubated at $37°$ C, 5% CO_2. After that, cells were thawed in the water bath ($37°$ C) for one minute. They were then transferred into the gelatine pre-coated flask containing warm growth media. HUVECs were kept in the incubator for 2-3 days to become highly confluent (95%-100%).

To grow HCAECs, 15 mL of MV growth media (C-22010) was pre-incubated in a 75 mL flask at $37°$ C 5% CO_2 for an hour. HCAECs in a frozen vial were defrosted in the water bath ($37°$ C) for one minute. This is to transfer them in a 75 mL flask containing warm growth media. HUVEC and HCAEC growth was observed daily, and their media was replaced regularly.

When cells grow and become highly confluent (95%-100%), they can be sub-cultured to increase their numbers and to use them in subsequent experiments, such as shear stress application and/or *ANKHD1* silencing.

To use cells for experiments, media was discarded, and the cells were washed twice with 10 mL of 1% TBS. Cells were then detached from 75 mL flasks by adding 3 mL of trypsin and incubating them for 2 minutes at $37°$ C, 5% CO_2. They were subsequently resuspended in growth media. The amount of the media depends on the number of new flasks and/or 6-well plates/12-well plates. Each flask needs 10 ml of the media whereas 12 mL was for a 6-well plate/12-well plate. Cells in flasks were kept in the incubator to grow and be used for further experiments. On the other hand, those cultured on a 6-well plate/12-well plate were stimulated with shear stress, *ANKHD1*siRNAs and/or actinomycin D.

2.2.6. Shear stress application

Orbital shaker system. To apply shear stress to endothelial cells, they were seeded on a 6-well plate and the plate was placed on the orbital shaker for 72 hours, set at 210 rotations per minute (rpm). Cells grown in the periphery of each well were exposed to HSS (13 dyne/cm^2); while cells in the centre were exposed to LSS (4 dyne/cm^2) (Warboys et al., 2014). After 72 hours, a template for the 6-well plate was used to extract cells from the periphery and centre via a cell scraper, while the middle portion was discarded (Figure 2.3). As a result, the expressions of different mRNAs and proteins in different levels of shear stress were quantified by qPCR and western blotting, respectively.

2.2.7. Endothelial cell extraction

Media was discarded and replaced by 1 mL/well of cold 1% TBS after 72 hours of shear stress stimulation. I used the template (Figure 2.3) to extract cells from centres or peripheries. Cells in centres were detached via a cell scraper to keep peripheral cells for RNA/protein extraction and vice versa. 1% TBS was discarded, and cells were washed one more with 1 mL/well cold 1% TBS. Then the RNA/protein was extracted, and gene expression was quantified via qPCR/western blotting (described in more detail below, in section 2.2.13 and section 2.2.14). To identify the responsiveness of a particular gene (e.g., ANKHD1) to shear stress, cells that were not stimulated with shear stress, in static conditions, were extracted from the whole well of the 6-well plate. This is to compare the levels of ANKHD1 protein between static, HSS (in the periphery) and LSS (in the centres) conditions.

Periphery (HSS)
Middle
Centre (LSS)
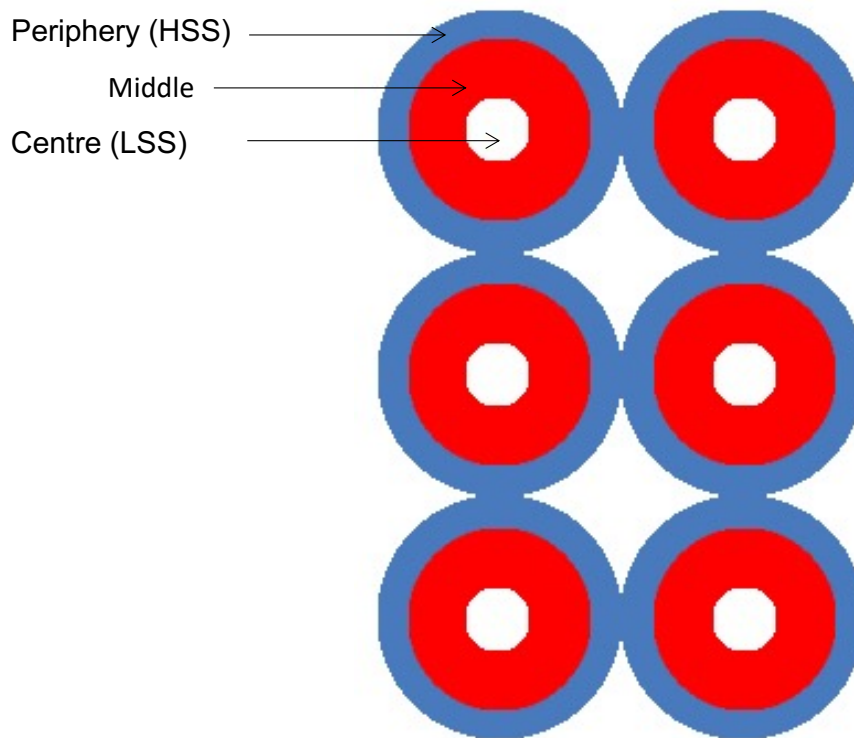
Figure 2.3. 6-well plate template used to extract cells stimulated with shear stress using the orbital shaker system. HSS-stimulated cells are in the periphery (blue) whereas LSS-stimulated cells are in the centre (white). Cells in the middle area (red) are discarded.

2.2.8. ANKHD1 silencing via siRNA-lipotransfection

For ANKHD1 silencing experiments, one control siRNA (non-target siRNA [NT-siRNA]), two different ANKHD1siRNAs, Optemim and RNAiMax (Lipo) were used. One of the *ANKHD1*siRNAs is *ANKHD1*siRNA-1, which is a pool of four *ANKHD1*siRNA sequences. The other one is *ANKHD1*siRNA-2, which contains one siRNA sequence.

siRNA-lipotransfection was applied directly after splitting primary cells into 6-well plates. For each well containing 2 ml of media, a mixture of 150 μL of optemim, 7 μL of RNAiMax (Lipo) and 20 μL of 2 μM of either control siRNA, *ANKHD1*siRNA-1 or *ANKHD1*siRNA-2 were prepared. After five minutes of incubating the mixture, it was added to the primary cell suspension in a growth media. Cells were left to attach into wells in an incubator for 5 hours at 37° C, 5% CO_2. The 6-well plate was then placed on the orbital shaker for 72 hours at 37° C, 5% CO_2.

2.2.9. RNA sequencing via NovoGene

Two HCAECs donors transfected with NT-siRNA or *ANKHD1*siRNA-2 were sent for sequencing and analysis to NovoGene. Figure 2.4. shows the workflow of the RNA sequencing approach used. The raw sequenced reads provided via Illumina platforms were having quality control assessment by determining error rates for each base, which equal 2-3% in all of my samples, and being filtered to remove any reads that contain adaptors, match with more than one gene, have uncertain nucleotides. Reads were then aligned and mapped with the hg38 human genome via HISAT2 to identify the expressed genes in each sample. This is followed by gene expression quantification via counting the sequenced reads of each mapped gene. The read count of each gene, which correlates with read depth, gene length and gene expression, is estimated by FPKM (Fragments Per Kilobase of transcript sequence per Million base pairs sequenced) (Mortazavi et al., 2008). This is followed by statistical analysis of the differentially

expressed genes via DESeq2 software, which is used for samples with biological replicates, to identify the *p*-value and adjusted *p*-value accounting for the multiple comparisons (Negative Binomial Distribution). The threshold for the differential gene analysis was log2 (FoldChange) = 0 and the *p*-value and adjusted *p*-value were ≤ 0.05. Finally, the differentially expressed genes, upregulated or downregulated, can undergo functional analysis (e.g., Kyoto Encyclopedia of Genes and Genomes [KEGG]) to identify the enriched pathways and diseases.

RNA Sequencing

① **Pure RNA samples**

② **Cut RNA into short sequences**

③ **Reverse transcription of RNA fragments into cDNA**

④ **Sequence ligation to adapters and amplification**

⑤ **Perform NGS sequencing (Illumina platform)**

⑥ **Data quality control and Map sequencing reads to the transcriptome/genome**

Exon   Exon
Intron
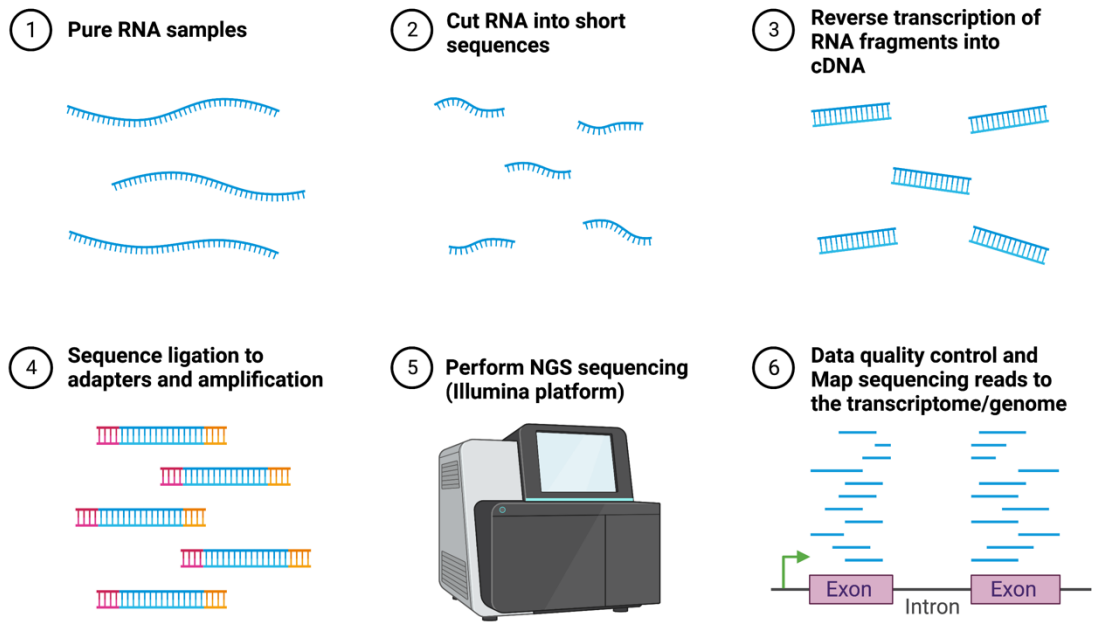
Figure 2.4. NovoGene RNA sequencing workflow. Abbreviation: Next generation sequencing (NGS).

2.2.10. RIP Assay

Magnetic beads preparation. Two 1.5 mL Eppendorf tubes were pre-labelled with either ANKHD1 antibody or rabbit IgG (negative control). 50 μL of magnetic beads were placed in each of the Eppendorf. To wash the beads, 500 μL of RIP washing buffer was also added to the Eppendorf containing the beads and the Eppendorf was then placed into the magnetic separator rack to discard the supernatant after bead aggregation. This washing step was repeated one more, and then, 5 μg of ANKHD1 antibody or IgG were added into their Eppendorfs. The beads-antibody mixture was incubated on the roller for 30 minutes at room temperature. After 30 minutes of incubation, tubes containing beads-antibody complex were spun down, placed on the magnetic rack, and washed with 500 μL of RIP washing buffer. This washing step was repeated twice.

Sample preparation. HUVECs were grown to confluency on a 15 cm petri dish. Proteins were extracted from HUVECs by adding 124 μL of RIP lysis buffer. A volume of 100 μL of protein lysates was used for each RIP (ANKHD1 or IgG). A volume of 24 μL of protein lysates was used for the 10% initial input of western blotting and qPCR.

RIP immunoprecipitation buffer preparation. For each RIP, a volume of 900 μL RIP immunoprecipitation buffer was prepared from 860 μL RIP wash buffer, 35 μL 0.5 M EDTA and 5 μL RNase inhibitor.

ANKHD1-RNA complex immunoprecipitation. A volume of 100 μL protein lysates was added into each of the beads-ANKHD1 antibody complex and the beads-IgG complex. 900 μL of RIP immunoprecipitation buffer was added to each sample. These were then incubated for 4 hours at 4° C on the roller. After that, all tubes were placed on the magnetic rack to discard the supernatant and wash the RIP complexes (beads-antibody-protein complex) four times with 500 μL RIP washing buffer. 500 μL RIP washing buffer was mixed with the RIP complex. Subsequently, 50 μL from the RIP complex was kept for western blotting to perform quality

control assurance. The tubes were then placed on the magnetic rack to discard the supernatant and extract the RNA via the Qiagen miRNeasy Micro kit. The 2.2.13 and 2.2.14 sections are going to explain the methods of RNA extraction and quantification and western blotting.

2.2.11. RNA stability assay

HUVECs in 12-well plates were transfected with either control siRNA or *ANKHD1*siRNA-1 (Figure 2.5). For each well, a mixture of 75 μL of optemim, 3.5 μL of RNAiMax (Lipo) and 10 μL of 2 μM of either control non-targeting siRNA or *ANKHD1*siRNA-1 was prepared. Then, the cells were placed in the incubator at 37° C, 5% CO_2 overnight. On the next day, the cells were treated with (1 μM) actinomycin D at different time points to inhibit RNA transcription over 0, 2, 4 and 16 hours. This would allow me to assess the stability of the pre-transcribed mRNA following transcription inhibition with and without *ANKHD1* silencing (Ratnadiwakara and Änkö, 2018). After completing the incubation hours with actinomycin D, HUVECs were washed twice with ice-cold 1% TBS and treated with Qiazol to extract RNA (miRNeasy Micro kit) at the same time. RNA was quantified by qPCR. The steps of RNA extraction and quantification are going to be explained later in this chapter (2.2.13 section).
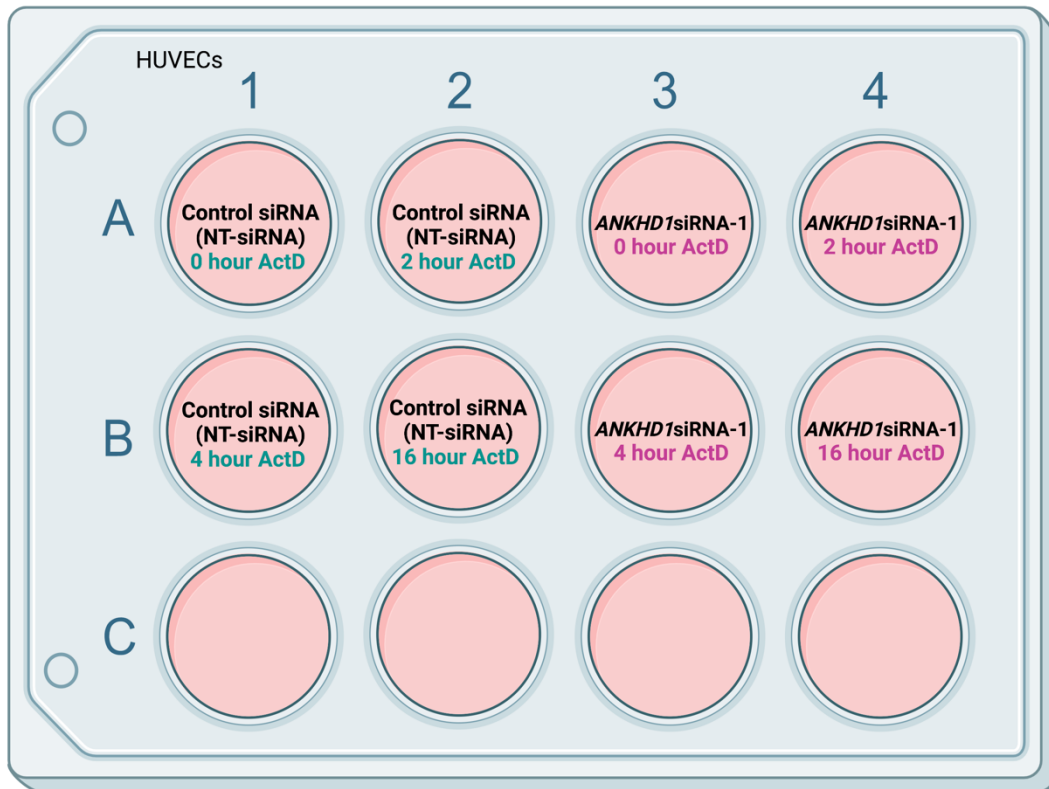
Figure 2.5. RNA stability assay applied on HUVECs in 12-well plate. Abbreviation: actinomycin D (ActD).

2.2.12. Biotinylated 3'UTR precipitation

Plasmid linearisation. 5 μg of each plasmid (WT *eNOS* 3'UTR or *eN*OS 3'UTR lacking AU-rich element [*eNOS* 3'UTRΔAUR]; Figure 2.6) was linearised via the restriction enzyme Xbal in two prelabelled Eppendorfs with the plasmid name. This was performed by mixing 5 μg of each plasmid with 2 μL of 1:10 BSA, 2 μL of restriction enzyme 10x buffer and 1 μL of the restriction enzyme Xbal. Then, the volume was made up to 20 μL with nuclease-free water. This mixture was then incubated at 37° C for two hours.

Ethanol precipitation. In the two DNA tubes, the volume was made up to 200 μL with nuclease-free water and 20 μL of 3 M sodium acetate and 500 μL of 100% ethanol were added to ethanol precipitate the DNA overnight at -80° C. On the next day, the two tubes of precipitated DNA (WT *eNOS* 3'UTR and *eNOS* 3'UTRΔAUR) were spun down at 16,000 g for 10 minutes. Then, the supernatant was discarded, and the pellet was left to dry. The dry pellet was resuspended with 20 μL of nuclease-free water and the DNA quality and quantity were measured via the nanodrop.

In vitro **transcription.** The RNA labelling mix was prepared by mixing 10 μL of each ATP, CTP and GTP, 6.5 μL of UTP and 3.5 μL of Biotin-16-UTP. For each linearised plasmid, a transcription reaction tube was prepared by mixing 8 μL of the RNA labelling mix and 2 μL of 10x transcription buffer, 1 μg of the DNA (either WT *eNOS* 3'UTR or *eNOS* 3'UTRΔAUR), 1μL of RNase inhibitor and 2 μL of Sp6 polymerase were added. The reaction tubes were mixed, briefly centrifuged, and placed in the heat block at 37° C for two hours. Then, to digest the DNA and have a pure biotinylated 3'UTR, 2 μL of DNase/tube was added into the transcription reaction tube, mixed and incubated at 37° C for 15 minutes. After that, 0.8 μL of 5M EDTA was added into each tube and mixed and the tube was then heated to 65° C for 10 minutes. The biotinylated 3'UTR was then ethanol precipitated overnight.

RNA pulldown. After ethanol precipitation, the biotinylated RNA of WT *eNOS* 3'UTR and *eNOS* 3'UTRΔAUR was measured via nanodrop. 2 μg of each 3'UTR (WT *eNOS* 3'UTR and *eNOS* 3'UTRΔAUR) was added into 200 μg of protein lysates (extracted from HUVECs). The negative control sample has 200 μg protein lysates with no 3'UTR (no RNA) while 20 μg of protein was kept as a positive control (10% input). The three samples, WT *eNOS* 3'UTR, *eNOS* 3'UTRΔAUR and no RNA samples, were incubated for 1 hour with the 200 μg of protein lysates at 4° C on the rotator and will be then used for the RNA pulldown.

20 μL of beads/sample were washed twice with 500 μL of lysis buffer, resuspended with 20 μL of lysis buffer, added into each of the three samples (WT *eNO*S 3'UTR, *eNOS* 3'UTRΔAUR and no RNA) and incubated for 1 hour in the rotator at 4° C. Then, beads of each sample were washed five times with 200 μL of lysis buffer, resuspended in 45 μL sample buffer, mixed with 1 μL benzonase and incubated in the rotator at 4° C for 30 minutes. The initial input sample was mixed with 45 μL of sample buffer. Finally, all four samples were boiled at 95° C for 5 minutes to perform western blotting to assess ANKHD1 binding to *eNOS* 3'UTR (Iqbal et al., 2014).
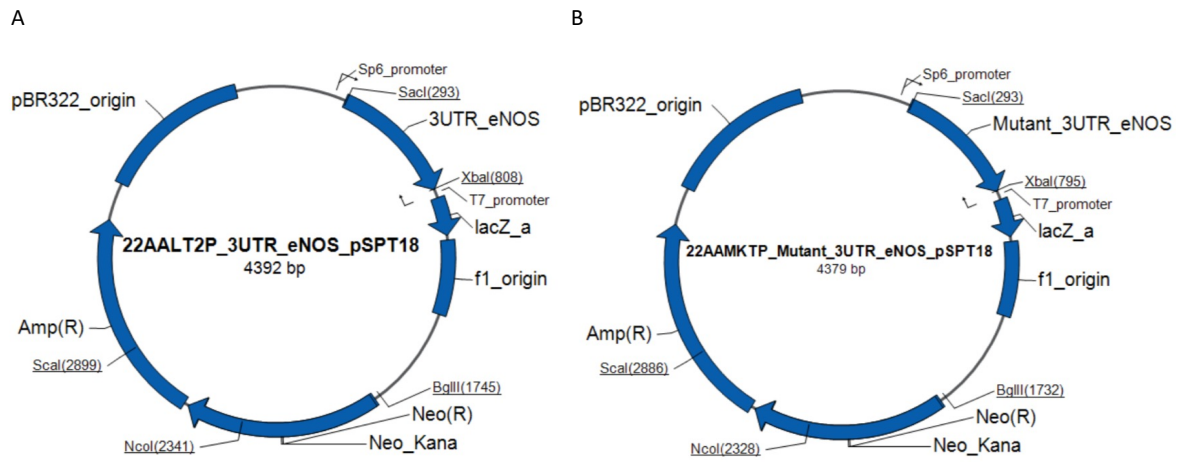
Figure 2.6. Plasmid maps used for in vitro 3'UTR transcription. WT eNOS 3'UTR (A) and

eNOS 3'UTRΔAUR (B) are shown.

2.2.13. Quantifying RNA levels via qRT-PCR

Total RNA extraction (miRNeasy Micro Kit). Primary cells extracted from HSS areas (peripheries) or LSS areas (centres) were dissolved in 280 μL of QIAzol lysis reagent in Eppendorfs for 5 minutes at room temperature. Then, these cell extracts were mixed with 56 μL of chloroform, vortexed vigorously for 15 seconds and incubated at room temperature for 2-3 minutes. These Eppendorfs containing cell extracts were then centrifuged at 12,000 g at 4° C for 15 minutes. After that, the upper aqueous phase, which contains the total RNA, was transferred into a new Eppendorf. Then, 165 μL of 100% ethanol was added and mixed thoroughly. This was transferred into an RNeasy MinElute spin column in a 2 mL collection tube, centrifuged at 8000 g for 15 seconds at room temperature and discarded its flow-through. 700 μL of RWT buffer was added to the column and centrifuged at 8000 g for 15 seconds at room temperature. The flow-through was discarded. 500 μL of RPE buffer was then added to the column and centrifuged at 8000 g for 15 seconds at room temperature. The flow-through was discarded. Next, 500 μL of 80% ethanol was added to the column and centrifuged at 8000 g for 2 minutes at room temperature and the flow-through and the collection tube were discarded. The RNeasy MinElute spin column with the lid open was then placed in a 2 mL collection tube and centrifuged at full speed for 5 minutes to dry the membrane. The 2 mL collection tube was replaced with a 1.5 mL collection tube. 14 μL of RNase-free water was added into the column and centrifuged at full speed for 1 minute to elute the RNA. The extracted RNA was stored in an ice box, and its concentration and purity were measured using the nanodrop.

RNA quantity and quality assessment. A NanoDrop 2000 spectrophotometer (Thermo Fisher) was used to measure the RNA concentration and purity in each sample. The RNA extract is considered highly pure when the ratio of absorbance (260/280) is 2, accepted values were a ratio equal to or greater than 1.8.

cDNA synthesis via RT-PCR. The RNA yield was normalised to 100 ng\μL, so the volume of RNA used to prepare the reverse transcription (RT) reaction mix is variable. The total volume of the RT mix is 20 μL; this includes 4 μL of 5x iScript RT Reaction Mix and variable amounts of RNA and nuclease-free water. This preparation was mixed in micro-Eppendorfs and incubated in a thermal cycler called T100^{TM} Thermal Cycler. The thermal cycler protocol for the iScript reaction is priming at 25° C for 5 minutes, RT at 46° C for 20 minutes and, finally, reverse transcriptase inactivation at 95° C for 1 minute. The synthesized cDNA was then measured by qPCR, which determined the RNA expression levels.

cDNA quantification via qPCR. I used primers targeting *ANKHD1* full length, *ANKHD1* transcript variants, *KLF2*, *KLF4*, *eNOS*, *PTGIS*, *F3*, *IL1β*, *GPC1*, *GSTP-1*, *GSTO-1* and *MCP1*. I also used primers for the housekeeping genes which are *HPRT* and *B-actin*. To quantify all of these transcripts, 8 μL PCR master mix was prepared from 5 μL/well of SsoAdvanced^{TM} Universal SYBR Green Supermix, 2 μL/well of 1 μM primers, forward and reverse, for the targeted gene and 1 μL/well of nuclease-free water. Then, a 96-well plate was pre-labelled with the target gene name(s) on each row. 2 μL of a cDNA sample (diluted at 1:100) generated from the extracted RNA was mixed with the 8 μL PCR master mix in each well. Each cDNA sample was tested twice, two technical replicates. For each target gene, there were two negative controls which are 8 μL of the PCR master mix/well. In the qPCR machine (CFX384^{TM} Real-Time System), the 96-well plate was placed to quantify the target transcripts. Each of the 40 cycles of qPCR started with denaturation for 0.25 minutes at 95°C, annealing for 0.45 minutes at 58°C and elongation for 0.05 minutes at 65°C.

Quantification of gene expression. each technical replicate (N= 2) has a Ct value, and these values were averaged. The housekeeping gene *HPRT*, expressed in the periphery or the NT-siRNA transfected cells, was used to normalise all target genes' expressions. To calculate the fold change of these genes, the normalised Ct values were quantified as 2^ΔΔCt (Schmittgen

and Livak, 2008). Finally, they were presented on graphs using Prism 8.1.2 software and the statistics were applied on ΔCt (paired analysis).

2.2.14. Western blotting

Protein extraction. Proteins were extracted by adding a hundred microliters of lysis buffer containing protease inhibitor cocktail onto the HUVECs or HCAECs attached to four centres or one periphery, parts of the well that were not needed were previously scraped and removed. The extracted proteins were then kept in -20° C in a pre-labelled Eppendorf tube.

Gel electrophoresis. For each 10 μL of protein lysates, 10 μL of the sample buffer was placed in a prelabelled clean Eppendorf. This mixture was placed in the heat block at 95° C for 5 minutes. Mini-Protean TGX Gels were placed vertically in the apparatus inside the tank, and then, the 1% running buffer was added into the tank. The comb for 12 wells was pulled out carefully from the gel to add 20 μL of the samples into each well. 3 μL of the Precision Plus Protein™ ladder was loaded. The loaded samples and ladders were then run at 200V for 30 minutes.

Protein transfer. The comb part that forms the wells of the gel and the bottom of the gel were cut and removed first. Next, the transfer membrane on the bottom ion reservoir stack was placed on the bottom anode (+) cassette. The gel was then placed on top of the transfer membrane. The roller was used to remove air bubbles between the gel and the transfer membrane. The top ion reservoir stack was placed on the gel. Finally, these were then locked by the top cathode (-) cassette and inserted into the transfer system (Trans-Blot Turbo). The proteins were transferred at 2.5 A constant, up to 25 V for 7 minutes.

Protein immunoblotting. The transfer membranes were then incubated in the 5% milk (blocking solution) for 30 minutes on the shaker at room temperature. In a 50 mL falcon tube, 3 μL of a primary antibody (e.g., anti-ANKHD1 antibody) were added to 3 mL of 3% BSA to

make a 1:1000 dilution. After blocking the transfer membrane, it was incubated in the falcon containing the primary antibody overnight on the roller at 4° C. On the next day, the transfer membranes were washed three times with 1% TBST for 5 minutes each.

To prepare the secondary antibody, 5 μL of the secondary antibody (e.g., polyclonal gout anti-rabbit immunoglobulins/HRP) was added to 50 mL of 5% milk buffer in a 50 mL Falcon tube. The transfer membrane was then incubated with the secondary antibody for 30 minutes on the shaker at room temperature. This was followed by washing the transfer membrane with 1%TBST five times each for 2 minutes on the shaker at room temperature. After that, a 1:1 ratio of A and B ECL western blotting detection reagents was prepared and added to the transfer membrane. ChemiDoc XRS+ System was used to detect the protein bands on the transfer membrane. Finally, protein levels of the target and the housekeeper genes were quantified using ImageJ.

2.2.15. Immunofluorescence staining

HUVECs with or without *ANKHD1*siRNA lipotransfection were grown on 1% gelatine pre-coated glass coverslip in a 6-well plate and stimulated with shear stress using the orbital shaker system. To stain these HUVECs with immunofluorescence staining, they were fixed first with ice-cold methanol, then blocked with 3% BSA for 2 hours and stained with ANKHD1 (1:100 in 3%BSA) or PTGIS primary antibody (1:200 in 3%BSA) overnight at 4° C. On the next day, HUVECs were washed twice with 1% TBST, stained with secondary antibody (568 gout anti-rabbit IgG: 1:150 in 3% BSA) for 3 hours, washed twice in 1% TBST, stained with VE-cadherin primary antibody (Mouse anti-human CD144: 1:100 in 3%BSA) for 1 hour and incubated with secondary antibody (Anti-mouse IgG Alexa Fluor 488: 1:100 in 3% BSA) for

1 hour. For nuclear staining, To-pro (1:250 3% BSA) was added for 5 minutes and washed once with 1% TBST. Cells on glass coverslips were then mounted on a glass slide via Diamond mounting media. Images of cells in the peripheries/centres and with/without *ANKHD1* silencing were taken via Leica microscope. The mean fluorescence intensity was quantified via ImageJ.

2.2.16. Quantification and Statistical analysis

The images and data from *in vivo* work were collected in a blinded fashion depending on mouse number/ID only. After quantification, the data were matched with mouse genotype to apply statistics. Both in vivo and in vitro findings are presented on graphs as mean ± standard error of the mean. The statistical analysis test used depends on the normality of the data, which was assessed using Graphpad. When the data were normally distributed, a parametric paired, unpaired t-test or multiple comparisons were conducted (paired for paired observations). If data were not normally distributed, non-parametric Wilcoxon Mann Whitney test or multiple comparison tests were performed. *p*-values smaller than 0.05 were considered statistically significant (Significance limit = 0.05).

Chapter 3: The effect of shear stress on ANKHD1 expression and function in endothelial cells

3.1. Outlines

3.2. ANKHD1 is highly expressed in endothelial cells

3.3. ANKHD1 regulates pathways involved in fluid shear stress and atherosclerosis

3.6. Assessing the effect of ANKHD1 on shear stress-responsive genes in endothelial cells

3.7. ANKHD1 responses to shear stress in human-derived endothelial cells

3.6. ANKHD1 levels in atheroprotective/atheroprone areas in murine aortas

3.7. Haemodynamic force upregulates ANKHD1 expression

3.8. Discussion

3.8.1. RNA-sequencing approach illustrated previously identified ANKHD1 functions

3.8.2. The novel ANKHD1 roles in regulating shear-responsive genes in healthy endothelium

3.8.3. ANKHD1 is a shear-stress regulated RNA-binding protein

3.8.4. ANKHD1 localisation in mouse aortic endothelial cells

3.1. Outlines

Since, single-cell RNA sequencing data showed ANKHD1 concentration was high in the endothelial cells compared to other cells derived from heart muscles (Gtexportal, 2021) and ANKHD1 function is currently unexplored in human endothelial cells, the major aim of my PhD studies is to study ANKHD1 functions in endothelial cells. Studying expression and loss-of-functions of ANKHD1 in endothelial cells accompanied by RNA sequencing approach and studying ANKHD1 under different shear stress conditions would allow me to infer a possible function/s of ANKHD1 in endothelial cells and its contribution to endothelial dysfunction and atherosclerosis.

Hypothesis: ANKHD1 is expressed in human and mouse endothelial cells and contributes to important endothelial cell functions.

To understand the functions of ANKHD1, I have decided to take a reductionist approach and I have used siRNA to lower *ANKHD1* expression. Endothelial cells from different donors were used to silence *ANKHD1*; and thus, to discover the genes that are under its control.

The specific aims of this chapter are:

1. To confirm the expression of ANKHD1 in human and mouse endothelial cells

2. To perform RNA sequencing to identify, in an unbiased way, the functions of ANKHD1 in human coronary artery endothelial cells.

3. To experimentally validate some of the top functions/genes associated with ANKHD1 in endothelial cells.

To find the answers, I combined the use of human cell models (*in vitro* models) and mouse models (*in vivo* models), I statistically analysed the data and discussed the potential importance of these findings in this chapter.

3.2. ANKHD1 is highly expressed in endothelial cells

To verify the expression of the ANKHD1 protein in endothelial cells, I experimentally tested its expression in cultured endothelial cells and mouse aortas. I extracted proteins from primary human endothelial cells (Human Umbilical Vein Endothelial Cells [HUVECs] and Human Coronary Artery Endothelial cells [HCAECs]). ANKHD1 was expressed in static (no flow) HUVECs and HCAECs (Figure 3.1: A and B). ANKHD1 appears as multiple bands, which may be the outcome of the different transcript variants that it is well-known to produce. All of these ANKHD1 bands had a very low intensity when *ANKHD1* was silenced using a specific *ANKHD1*siRNA compared to cells transfected with a non-targeting siRNA (negative control). This indicates the specificity of the ANKHD1 antibody (Figure 3.1: B), as all the bands appear to be reduced by silencing of *ANKHD1*.

I then assessed whether ANKHD1 is also expressed in mouse aortic endothelial cells by staining them with ANKHD1 antibody and the endothelial cell marker CD31, which allows me to identify the endothelial layer with the use of confocal microscopy. ANKHD1 was highly expressed in the mouse endothelium of the descending aorta. ANKHD1 does not appear to localise in a single organelle but instead, it is found in both the nucleus and the cytoplasm (Figure 3.1: C). Compared with $Ankhd1^{+/+}$ mice, ANKHD1 fluorescence intensity was markedly reduced in $Ankhd1^{-/-}$ mice (Figure 3.1: D). This also confirms the specificity of the ANKHD1 antibody with this staining technique.
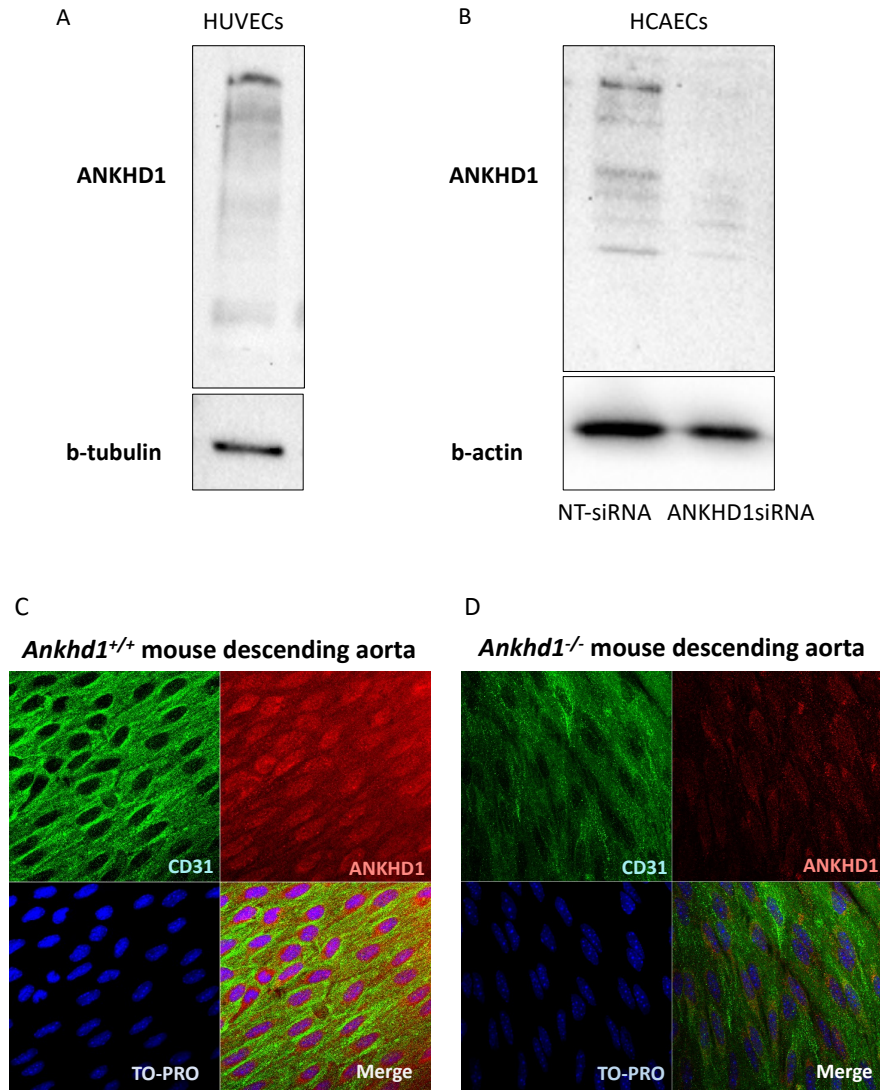
Figure 3.1. Primary human endothelial cells express ANKHD1. Immunoblotting of ANKHD1 protein from HUVECs (A) and HCAECs (B) are shown. The loading controls are b-tubulin and b-actin, respectively. ANKHD1 expression is shown in control HCAECs, transfected with non-targeting siRNA (NT-siRNA), and ANKHD1-deficient HCAECs, transfected with *ANKHD1*siRNA (B). *en-face* staining of ANKHD1 (in red) and CD31 (in green) was performed on the descending aortas (C and D). ANKHD1 expression is shown in *Ankhd1*^{+/+} mice (C) and *Ankhd1*^{-/-} mice (D).

3.3. ANKHD1 regulates pathways involved in fluid shear stress and atherosclerosis

I transfected two different HCAEC donors with either control siRNA (non-targeting siRNA [NT-siRNA]) or *ANKHD1*-targeting siRNA (*ANKHD1*siRNA-2). The cells were subsequently stimulated with HSS for 72 hours and RNA sequencing was performed by NovoGene. The purpose of this experiment was to identify, in an unbiased way, the roles of ANKHD1 in primary human endothelial cells under HSS conditions.

The results showed that, out of the 19614 co-expressed genes in NT-siRNA and *ANKHD1*siRNA-2 transfected cells, 949 genes were significantly upregulated, and 1058 genes were downregulated significantly (p <0.05) when *ANKHD1* was silenced. The distribution of these genes is shown in a volcano plot (Figure 3.2: A). Methionine adenosyltransferase 2A (*MAT2A*) mRNA was the most significantly upregulated mRNA (p= 2.32E-10) while ribosomal protein L13a pseudogene 25 (*RPL13AP25*) mRNA is the most significantly downregulated mRNA (p= 1.71E-09) in ANKHD1- deficient HCAECs. The level of ANKHD1 reduction in these cells was -1.2938806 log2 fold. The heat map provides a visual of how the differentially expressed genes (rows) that have a similar pattern of expression were clustered in the control cells (NT-siRNA) and ANKHD1-deficient cells (*ANKHD1*siRNA-2) (columns) (Figure 3.2: B). Gene ontology and pathway analysis revealed some of the functions of ANKHD1 in endothelial cells. KEGG pathway analysis showed the top 20 pathways that are under the control of ANKHD1 (Figure 3.2: C). The regulations of apoptosis, mitophagy, lysosome and microRNAs in cancer are known and published functions of ANKHD1 (Zhu, Li, Tian and Wu, 2015; Zhu, Zhang, Tian and Wu, 2017; Fragiadaki and Zeidler, 2018); thus, validating this RNA-sequencing approach. It is worthwhile also to note that functions previously not associated with ANKHD1 have also been identified, for example, IL17 signalling and adherens junctions (Figure 3.2: C).
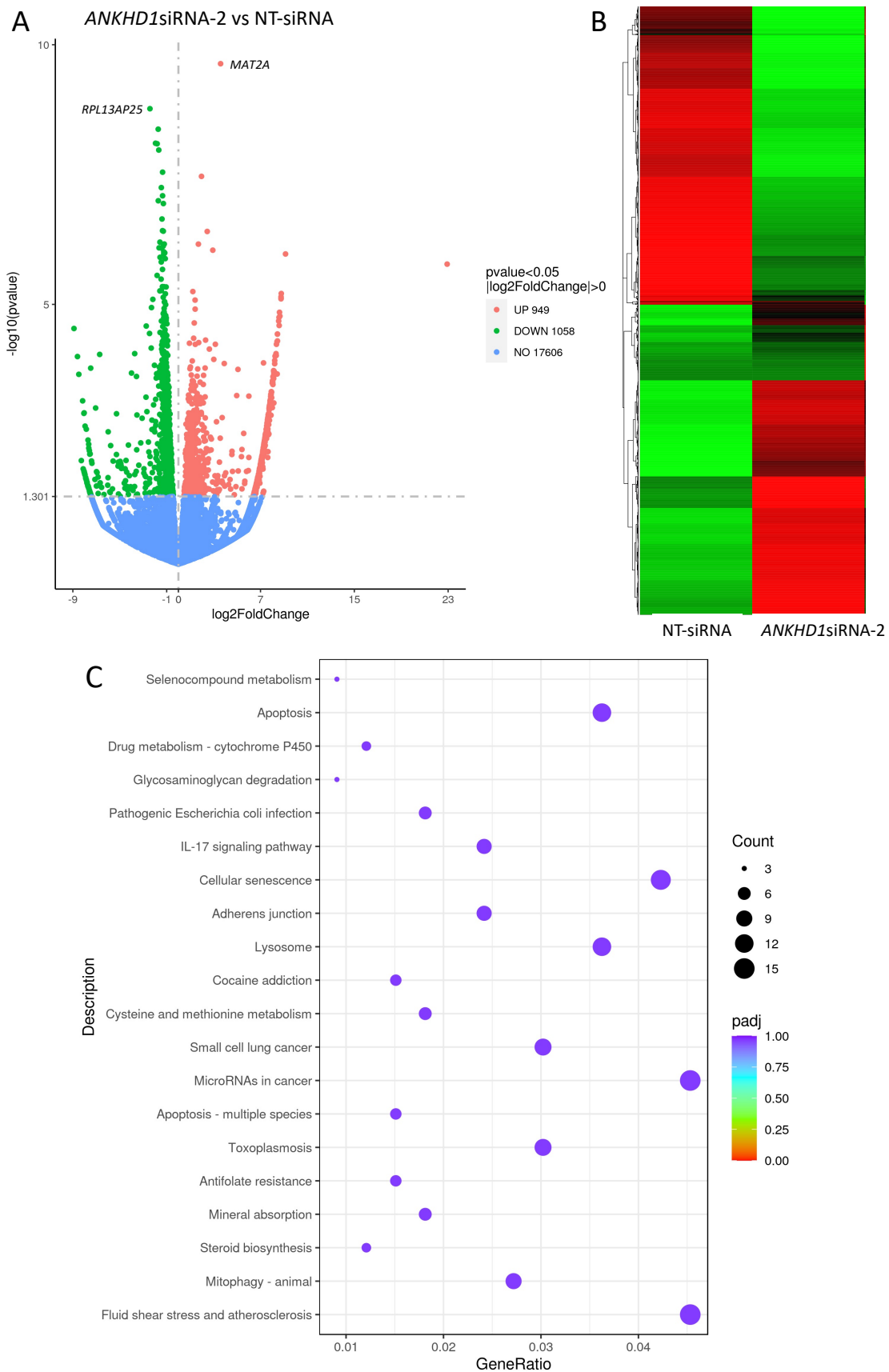
Figure 3.2. Differentially expressed genes and pathway analysis in ANKHD1-deficient HCAECs. The volcano plot shows the significantly upregulated (red dots) and

downregulated (green dots) genes in HSS-stimulated HCAECs transfected with *ANKHD1*siRNA-2 compared with control cells (N=2 different donors). The x-axis shows the fold change of each gene comparing with the threshold of log2 (FoldChange) = 0 while the y-axis shows the statistical significance (*p*<0.05) (A). The heatmap shows the differentially expressed genes with and without *ANKHD1* silencing. Column represents each treatment group (NT-siRNA and *ANKHD1*siRNA-2) including the two biological replicates while the rows represent the genes (B). KEGG pathway analysis showed the fluid shear stress and atherosclerosis as one of the top enriched pathways (C).

Interestingly, fluid shear stress and atherosclerosis were one of the top enriched pathways, suggesting the possible involvement of ANKHD1 in atherosclerosis downstream of shear stress sensation. The fact that ANKHD1 is linked to atherosclerosis and fluid shear stress has encouraged me to study this further, as shear stress has been shown to be a major contributor to the focal nature of plaque development. Table 3.1 displays the upregulated and downregulated genes in the pathways regulated under shear stress and atherosclerosis conditions via ANKHD1. ANKHD1 controls 7 genes that are involved in inflammation in the context of shear stress, including the pro-inflammatory and pro-atherogenic interleukin 1 β (*IL1β*) and its receptor *IL1R1*. Silencing of *ANKHD1* causes a 2.261 of *IL1β* and a 1.136 log2 fold increase of its receptor. Additionally, ANKHD1 negatively regulates *IKBKB* (*IKKβ*). *IKKβ* is a gene that phosphorylates the inhibitor of the pro-inflammatory NF-κB complex, I kappa B (IκB), thus causing activation of NF-κB (Karin and Ben-Neriah, 2000). Moreover, ANKHD1 also negatively regulates *ICAM-1*, which is an NF-κB target gene with a role in the recruitment of inflammatory cells into the intima. In addition to its potential role in inflammation suppression, ANKHD1 appears to also be responsible for regulating a number of mechanosensors, including *glypican 1*, *VE-cadherin* and *VEGFR2*.

Taken together, based on the strong expression of ANKHD1 in human and mouse endothelial cells and its identified roles in the suppression of inflammation and sensing of mechanical forces, I hypothesised that ANKHD1 has major roles in endothelial cells, which are going to be investigated in the next chapters.

ID	Gene Name	Log2 Fold change	Function
ENSG00000177606	Jun proto-oncogene, AP-1 transcription factor subunit (*JUN*)	0.727328871	Inflammation
ENSG00000120129	dual specificity phosphatase 1 (*DUSP1*)	0.687318794	
ENSG00000161011	sequestosome 1 (*SQSTM1*)	1.100343423	
ENSG00000104365	inhibitor of nuclear factor kappa B kinase subunit beta (*IKBKB*)	0.658823191	
ENSG00000090339	intercellular adhesion molecule 1 (*ICAM-1*)	1.690778348	
ENSG00000125538	interleukin 1 beta (*IL1β*)	2.261884581	
ENSG00000115594	interleukin 1 receptor type 1 (*IL1R1*)	1.136089697	
ENSG00000128340	Rac family small GTPase 2 (*RAC2*)	0.831520028	Proliferation and migration
ENSG00000117020	AKT serine/threonine kinase 3 (*AKT3*)	0.852559613	
ENSG00000128052	kinase insert domain receptor (*KDR* or *VEGFR2*)	0.843280787	
ENSG00000168036	catenin beta 1 (*CTNNB1*, beta-cateinin)	0.986079613	
ENSG00000169750	Rac family small GTPase 3 (*RAC3*)	-1.412512086	
ENSG00000185386	mitogen-activated protein kinase 11 (*MAPK11*)	-0.813476956	
ENSG00000188130	mitogen-activated protein kinase 12 (*MAPK12*)	-0.756087905	
ENSG00000179776	cadherin 5 (*CDH5*, VE-cadherin)	0.822632867	Cell adhesion

ENSG00000116044	NFE2 like bZIP transcription factor 2 (*NRF2*)	3.79594256	Oxidative stress
ENSG00000148834	glutathione S-transferase omega 1 (*GSTO-1*)	-0.689968279	
ENSG00000084207	glutathione S-transferase pi 1 (*GSTP-1*)	-0.819984755	
ENSG00000166484	mitogen-activated protein kinase 7 (*MAPK7*, *ERK5*)	1.107514205	Vascular tone
ENSG00000117020	AKT serine/threonine kinase 3 (*AKT3*)	0.852559613	
ENSG00000063660	glypican 1 (*GPC1*)	-0.503566349	
ENSG00000179776	cadherin 5 (*CDH5*)	0.822632867	Mechanosensor
ENSG00000063660	glypican 1 (*GPC1*)	-0.503566349	
ENSG00000128052	kinase insert domain receptor (*KDR* or *VEGFR2*)	0.843280787	
ENSG00000178726	Thrombomodulin (*THBD*, *TM*)	0.798533437	Thrombosis

Table 3.1. Differentially regulated genes in the shear stress and atherosclerosis pathway in HSS-stimulated HCAECs (NTsiRNA [control] vs ANKHD1siRNA-2). The log2 fold change represents the level of each gene in ANKHD1 deficient cells when compared to control cells. The functional annotation of these genes was identified in the bioinformatic tool (KEGG).

3.4. Assessing the effect of ANKHD1 on shear stress-responsive genes in endothelial cells

To further validate the RNA sequencing approach, I assessed using qPCR the effect of *ANKHD1* inhibition on the expression of the major mechanosensor *GPC1* mRNA, which promotes vasorelaxation and vasoprotection, and mechanosensing genes including pro-inflammatory molecules, *IL1β* and *ICAM-1* mRNAs, and antioxidant enzymes, *GSTP-1* and *GSTO-1* mRNAs, in HSS-stimulated HCAECs via the orbital shaker. All primer pairs used for qPCR in this study show single peaks in their melting curves; thus, indicating target specificity (Appendix 7.1). *ANKHD1* inhibition via *ANKHD1*siRNA-2 showed a significant increase in *IL1β* and *ICAM-1* whereas a significant reduction was seen in *glypican 1* and *GSTP-1* (Figure 3.3: A-D). *ANKHD1* inhibition did not reduce *GSTO-1* significantly, however, there is a trend toward reduction in ANKHD1-deficient cells (Figure 3.3: E). This might be overcome by increasing the biological replicates. Taken together these results validate the RNA sequencing data and indicate that ANKHD1 is important to mediate atheroprotective shear stress responses in endothelial cells, particularly, vasorelaxation, inflammation and oxidative stress.
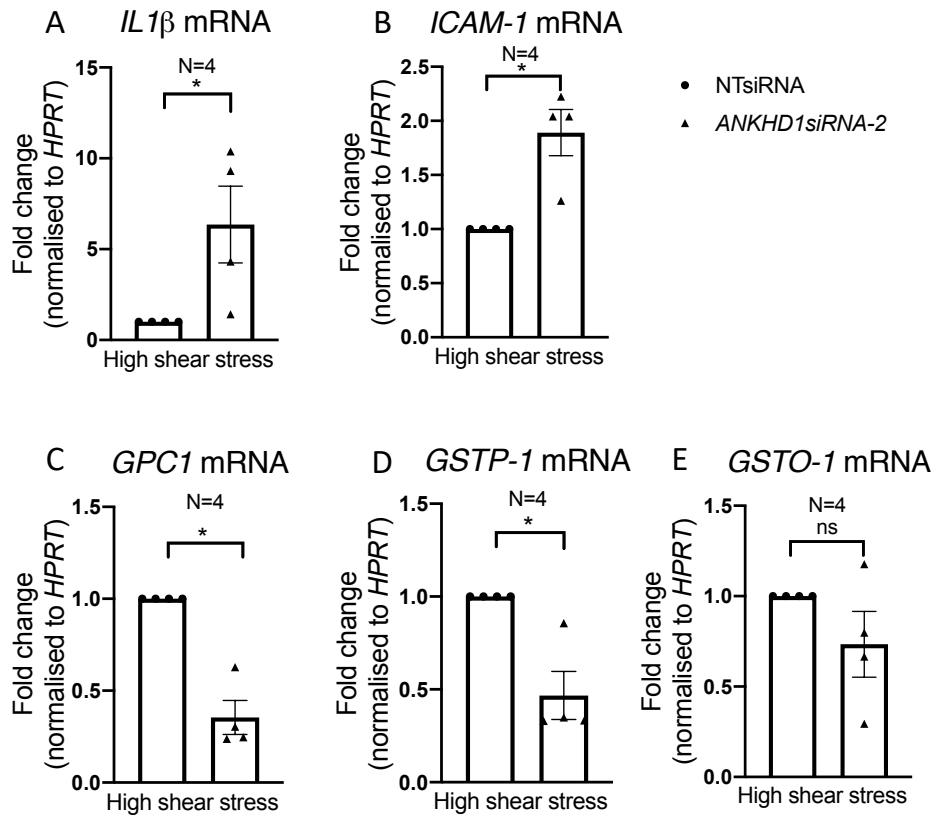
Figure 3.3. IL1β, ICAM-1, GPC1, GSTP-1 and GSTO-1 mRNA expression in HSS-stimulated HCAECs with and without ANKHD1-deficiency. Quantification of *IL1β* mRNA (A), *ICAM-1* mRNA (B), *GPC1* mRNA (C), *GSTP-1* mRNA (D) and *GSTO-1* mRNA (E) in non-targeting siRNA (control) and *ANKHD1*siRNA-2 transfected cells showed that *ANKHD1* silencing significantly increased *IL1β* and *ICAM-1* (Two-tailed paired t-test: *IL1β: p*= 0.0399; *ICAM-1: p*= 0.0175), while significantly reduced *GPC1* and *GSTP-1* (Two-tailed paired t-test: *GPC1: p*= 0.0156; *GSTP-1: p*= 0.0352). All mRNAs were normalised to the housekeeping gene *HPRT*, and all dots represent different biological donors and error bars show the standard error of the mean.

3.5. ANKHD1 responses to shear stress in human-derived endothelial cells

The data from the unbiased RNA-sequencing approach shows that ANKHD1 controls shear-responsive pathways. Therefore, it is important to identify whether ANKHD1 may also be regulated by shear stress conditions at mRNA or protein levels. HCAECs and HUVECs were stimulated with shear stress using the orbital shaker system. Then, mRNA and protein expression of ANKHD1 were quantified by qPCR and western blotting/immunofluorescence staining, respectively. In agreement with previous work in the lab, *HPRT* was not changed in response to flow compared to static conditions (Figure 3.4). Therefore, I used *HPRT* as a housekeeping gene to normalise the expression of *ANKHD1* from high and low shear stress stimulated HCAECs and HUVECs.
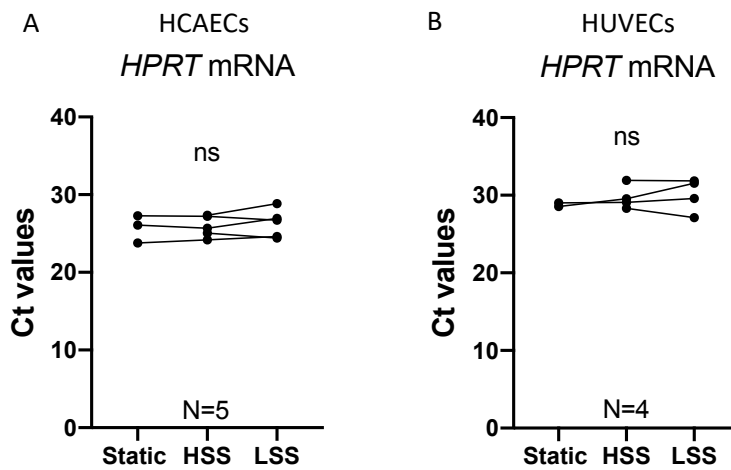
Figure 3.4. HPRT mRNA expression in HCAECs and HUVECs with and without flow stimulation. There were no changes in *HPRT* mRNA levels in both endothelial cells after exposure to flow (One-way ANOVA, Dunnett's multiple comparisons test: $p>0.05$), paired samples are indicated.

Next, I wished to verify whether the cells have indeed experienced HSS and LSS generated via the orbital shaker system. To achieve this, I used a number of genes that are shear responsive as quality control transcripts. *KLF4* and *eNOS* are well-known HSS markers whereas *MCP1* is a proinflammatory gene induced by LSS conditions (McCormick et al., 2001; Zhou et al., 2012; Zhang et al., 2016). In addition to positive and negative controls, I also investigated the expression of the target transcript *ANKHD1*. My qPCR results showed single melting curve peaks for all genes used in my study including *ANKHD1, KLF4, eNOS, MCP1 and HPRT*, thereby showing target-specificity (Appendix 7.1).

When cells are exposed to shear stress, there are morphological changes that take place, including alignment of the cells with the flow in the area of uniform flow, and misalignment and gaps in areas exposed to low and oscillatory shear stress. As expected, when using materials from different human donors, I observed heterogeneity in the response from the different HCAEC and HUVEC donors in terms of alignment with the flow and activation of shear-responsive genes. Hence, to overcome this inherent problem, only cells that passed quality assurance, defined as expressing high levels of *KLF4* and *eNOS* mRNAs in HSS-stimulated cells and high levels of *MCP1* mRNA in LSS-stimulated cells, were used for subsequent experiments and the study of target genes (Figure 3.5). *KLF4* and *eNOS* mRNAs were significantly upregulated in HSS-stimulated HCAECs and HUVECs whereas *MCP1* mRNA was elevated in LSS-stimulated cells, achieving statistical significance in HCAECs (N=5). The full-length *ANKHD1* transcript exhibited significantly elevated expression in HSS in HCAECs and HUVECs compared to LSS conditions at mRNA levels (Figure 3.6: A and C).

Because *ANKHD1* has different transcript variants, the expression of these transcript variants under different shear stress conditions was also assessed via qPCR using primer pairs that pick three transcript variants of *ANKHD1*, *ANKHD1-203* (full-length ANKHD1), *ANKHD1-204* and *ANKHD1-205*. There was a clear trend toward an increase of *ANKHD1*

113

transcripts in HSS-stimulated HCAECs and HUVECs (Figure 3.6: B and D). This increase was statistically significant in HUVECs.

The effect of shear stress generated via the orbital shaker system on ANKHD1 was also assessed at protein levels in HCAECs and HUVECs using western blotting and immunofluorescence staining, respectively (Figure 3.6: E-H). ANKHD1 protein was upregulated in HSS-stimulated HCAECs and HUVECs. These data together suggest that ANKHD1 may be a HSS-regulated gene in human endothelial cells and validate the RNA sequencing approach showing that ANKHD1 is involved in shear stress-mediated endothelial cell responses.
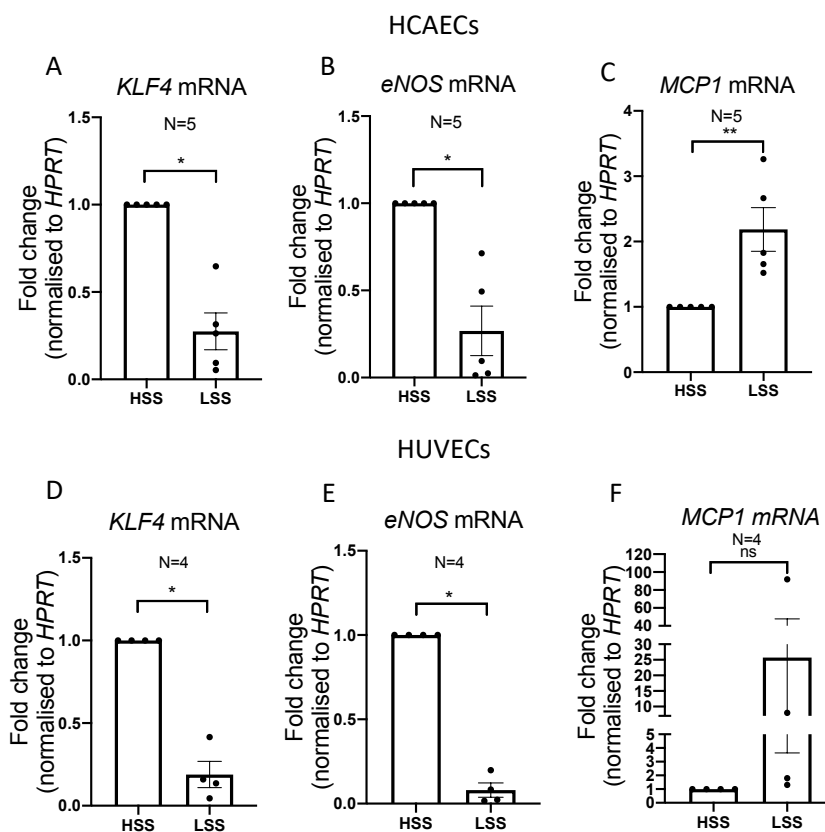
Figure 3.5. HCAECs and HUVECs respond to flow generated via the orbital shaker. The expression of quality control genes (*KLF4, eNOS* and *MCP1*) was quantified in HSS and LSS stimulated HCAECs (A-C) and in HSS and LSS stimulated HUVECs (D-F). These experiments passed the quality control assessment as the expression of *KLF4* and *eNOS* mRNAs were significantly high in HSS conditions (Two-tailed paired t-test: *KLF4*: HCAECs: *p*= 0.0353; HUVECs: *p*= 0.0324); (Two-tailed paired t-test: *eNOS*: HCAECs: *p*= 0.0312; HUVECs: *p*= 0.0138) while the expression of *MCP1* mRNA was very low; however, that was statistically significant in HCAECs (Two-tailed paired t-test: *p*= 0.0082). All mRNAs were normalised to the housekeeper gene *HPRT* and all dots represent different biological donors and error bars show the standard error of the mean.
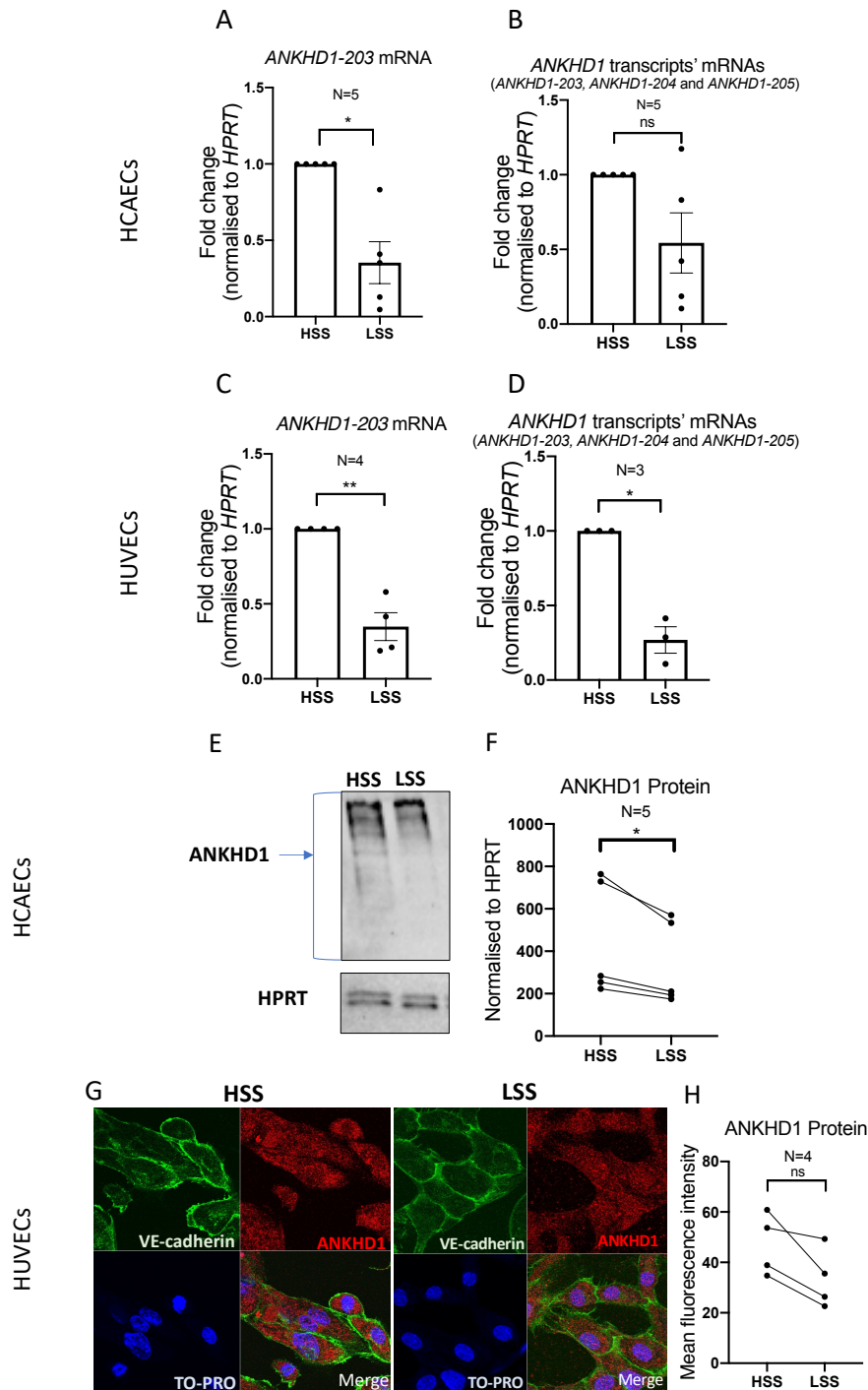
Figure 3.6. ANKHD1 responses to shear stress generated via the orbital shaker in HCAECs and HUVECs. *ANKHD1-203* mRNA quantification in HSS and LSS stimulated HCAECs (A) and HUVECs (C) showed that it was significantly high in HSS conditions (Two-tailed paired t-test: HCAECs: *p*= 0.0475; HUVECs: *p*= 0.0043). *ANKHD1* transcript variants' mRNA quantification showed an increase in *ANKHD1* isoforms in HSS-stimulated

HCAECs (B) and HUVECs (D) when compared to LSS-stimulated endothelial cells. This increase was statistically significant in HUVECs (Two-tailed paired t-test: p= 0.0447) (D). ANKHD1 protein quantification, using western blotting, showed that it was significantly elevated in HCAECs in response to HSS compared to LSS (p= 0.0137) (E and F). Images of the immunoblotting were taken from five biological replicates (F). ANKHD1 expression was also estimated via immunofluorescence staining in HUVECs in HSS and LSS conditions (G and H). Images of the immunofluorescence staining were taken from four biological replicates (G). ANKHD1 levels, in qPCR and immunoblotting, were normalised to the housekeeper gene *HPRT*. All dots represent different biological donors and error bars in mRNA graphs show the standard error of the mean.

3.6. ANKHD1 levels in atheroprotective/atheroprone areas in murine aortas

Next, ANKHD1 protein levels were assessed in mouse endothelial cells exposed to different shear stress conditions. Inner curvatures of primary aortic arches experience LSS conditions, which are atheroprone, while outer curvatures experience HSS conditions, which are atheroprotective (Suo et al., 2007; Winter et al., 2019), (Figure 3.7: A). Using this, I was able to compare ANKHD1 levels in these two areas in mice with *Ankhd1$^{+/+}$*. The endothelial cell layer in the aorta was identified by staining with a specific endothelial cell marker (namely PECAM-1 or CD31). ANKHD1 expression was significantly higher in endothelial cells in atheroprotective areas of the aorta, (outer curvature) when compared with atheroprone areas (inner curvature) (N= 6; Figure 3.7: B and C).

In these mice, ANKHD1 appears to localise differently in different areas of primary arches. In the inner curvature, its localisation is more pronounced in the nucleus when compared to the outer curvature (Figure 3.7: B). Therefore, I assessed the ANKHD1 intensity and distribution in the inner and outer curvature of *Ankhd1$^{+/+}$* mice by measuring the nuclear-to-cytoplasmic ratio using ImageJ. In both inner and outer curvature, *Ankhd1* significantly colocalises with the nucleus when compared to the cytoplasm (N= 6: Figure 3.7: D). Interestingly, looking at the overall distribution of ANKHD1, ANKHD1 was preferentially located in the nucleus in the inner curvature compared to the outer curvature. In the outer curvature, it was more in the cytoplasm when compared to the inner curvature (Appendix 7.2). Although there were no significant differences, increasing the biological replicates is needed for statistical support of these findings.

The current findings raised the question of whether there is a link between different haemodynamic forces and ANKHD1 functions which in turn controls endothelial cell behaviours.
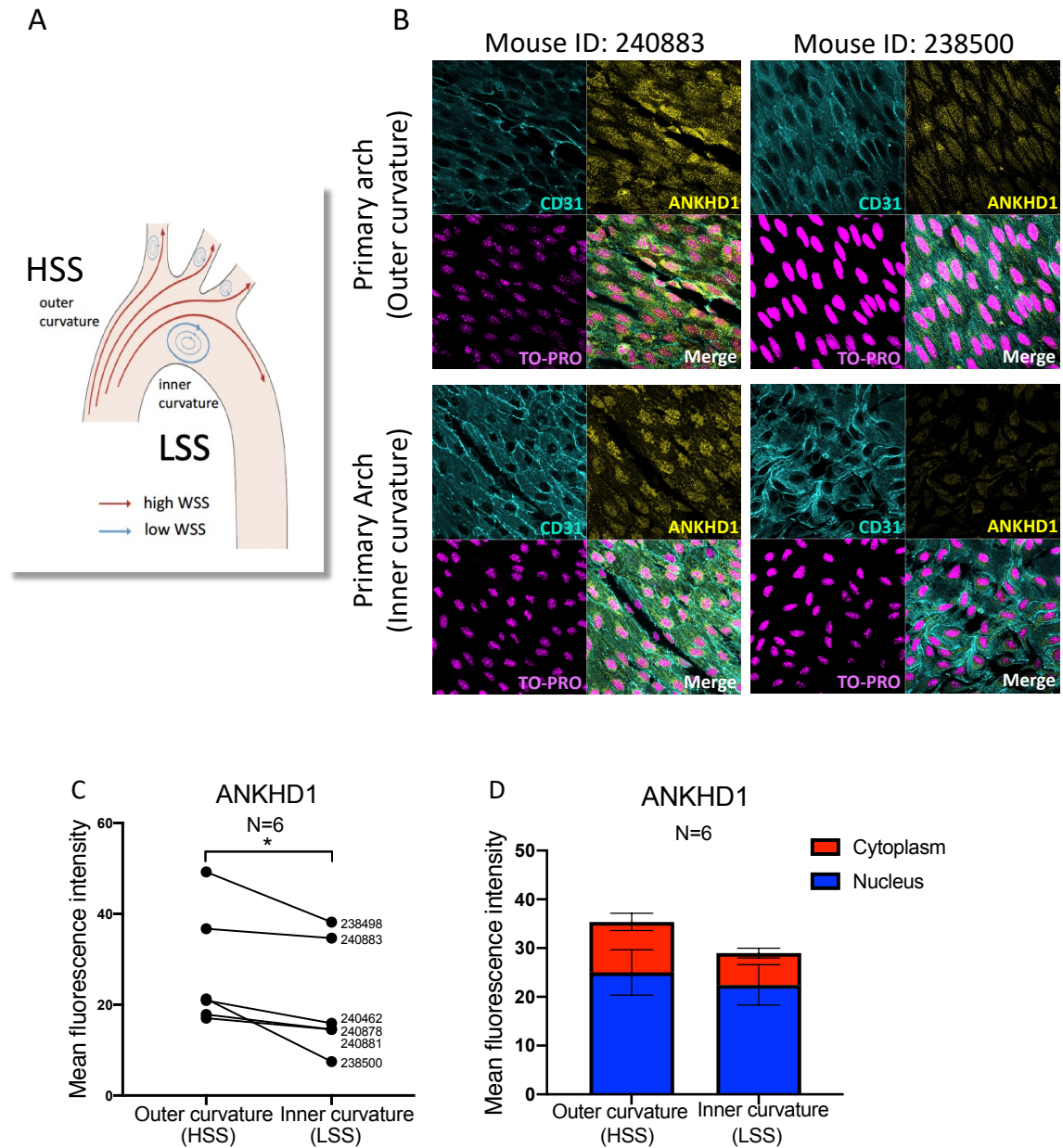
Figure 3.7. ANKHD1 responses to shear stress in vivo. A Schematic diagram of the arch indicates the HSS areas and the LSS areas in the outer and the inner curvature, respectively (A). Endothelial cells were stained with ANKHD1 (yellow) and CD31 (cyan) in the outer curvature (HSS regions) of $Ankhd1^{+/+}$ primary arches and the inner curvature (LSS regions) of $Ankhd1^{+/+}$ primary arches (B). Images of the *en-face* staining were taken from six biological replicates (B). The mean fluorescence intensity of ANKHD1 in different shear regions in the aortas of mice with $Ankhd1^{+/+}$ showed that ANKHD1 was significantly higher

in the outer curvature when compared to the inner curvature of *Ankhd1*$^{+/+}$ mice (Two-tailed paired t-test: *p*= 0.0266) (C). The nuclear-to-cytoplasmic ratio of ANKHD1 in the *Ankhd1*$^{+/+}$ primary arch showed that ANKHD1 was significantly more in the nucleus when compared to the cytoplasm in the inner and the outer curvature of the primary arch (Two-tailed two-way ANOVA, Sidak's multiple comparisons test: Outer curvature: adjusted *p*= 0.0002; inner curvature: adjusted *p*= 0.0001). ANKHD1 was more in the nucleus and less in the cytoplasm in the inner curvature compared to the outer curvature, however, this did not result in any statistical significance (Two-tailed two-way ANOVA, Sidak's multiple comparisons test: *p*>0.05) (D).

3.7. Haemodynamic force upregulates ANKHD1 expression

Previous results (section 3.5) highlighted that the message and protein of ANKHD1 are elevated in endothelial cells exposed to HSS. However, it is not clear whether it is the HSS that upregulates ANKHD1 or whether it is LSS that suppresses it. To address this, I compared the levels of ANKHD1 in cells exposed to flow (orbital system) or cells that were cultured in static conditions and had no consistent flow with (static cells). I hypothesised that this comparison would allow me to find the effect of flow on ANKHD1 expression and which shear stress condition/s controls ANKHD1 expression. ANKHD1 protein was elevated in HCAECs and HUVECs in response to HSS when compared to static cells (HCAECs: Figure 3.8: A; HUVECs: Figure 3.8: B). This increase of ANKHD1 protein in HSS was statistically significant in HUVECs. The fact that HSS induces ANKHD1 suggests that ANKHD1 may be transcriptionally activated by HSS or alternatively, its message and/or protein becomes stabilised during HSS conditions. Taking these data together, it is the HSS that upregulates ANKHD1 expression, the mechanism employed by HSS to stabilise ANKHD1 is currently unknown.

A HCAECs

Static | HSS | LSS

ANKHD1

B-actin

ANKHD1 Protein

ns
ns
N=3

MCP1 mRNA
N=3
ns

B HUVECs

Static | HSS | LSS

ANKHD1

B-tubulin

ANKHD1 Protein

ns
*
N=3
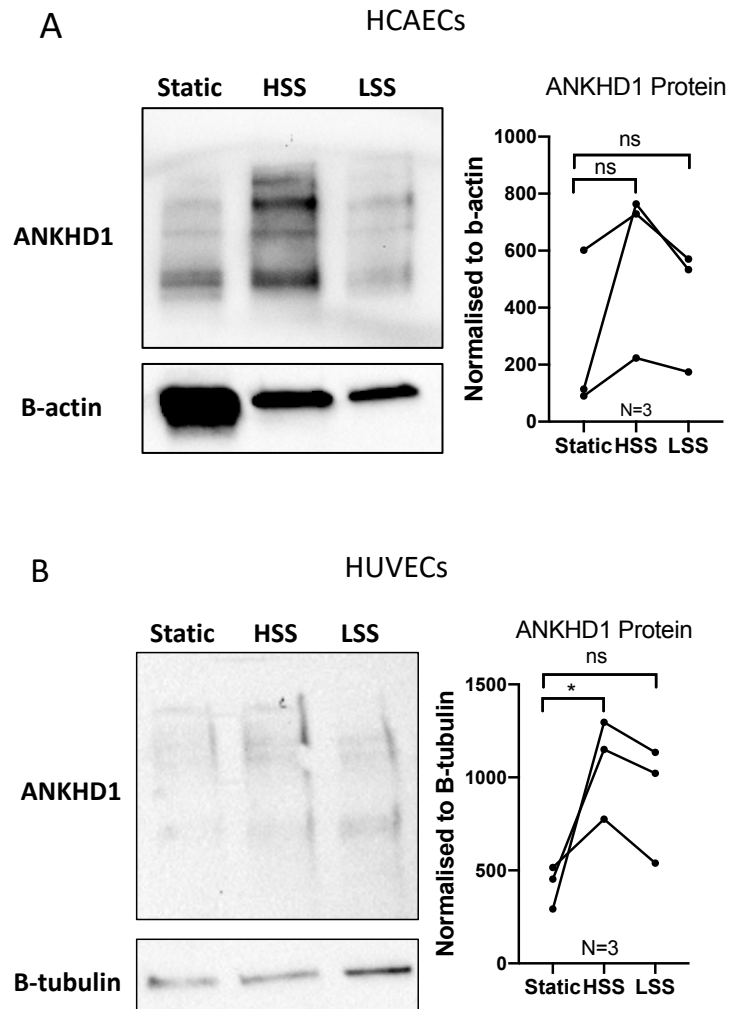
Figure 3.8. HSS generated by the orbital shaker upregulates ANKHD1 in HCAECs and HUVECs. ANKHD1 protein quantification, using western blotting, in HCAECs (A) and HUVECs (B) is shown. Although there was no statistical significance (Two-tailed one-way ANOVA, Dunnett's multiple comparisons test: adjusted $p>0.05$), there was a trend toward an increase in ANKHD1 protein expression in HSS-stimulated HCAECs. In HUVECs, ANKHD1 protein was significantly elevated in response to HSS compared to static cells (Two-tailed one-way ANOVA, Dunnett's multiple comparisons test: adjusted $p= 0.0278$). Images of the immunoblotting were taken from three biological replicates from HCAECs and HUVECs. All proteins were normalised to the housekeeper gene b-actin/b-tubulin and all lines represent different biological donors.

3.8. Discussion

In summary, this part of the work has provided orthogonal evidence that ANKHD1 protein and mRNA are expressed highly in both human endothelial cells (HUVECs and HCAECs) *in vitro* and in mouse endothelial cells *in vivo*. Given the fact that ANKHD1 has not been studied in normal endothelial cells previously, RNA-sequencing was employed to begin to understand some of its new functions in HCAECs. ANKHD1 showed to control important mechanosensors, such as glypican 1, and mechanoresponsive pathways, such as NFκB signalling. Then, I decided to focus my efforts on examining whether ANKHD1 was shear responsive. The fact that HSS significantly induces the expression of ANKHD1 in human cellular models was also verified *in vivo*, using *en-face* staining of mouse aortas, these combined approaches provided strong evidence that: (1) ANKHD1 is highly expressed in endothelial cells and (2) ANKHD1 responds to shear stress *in vitro* and *in vivo*.

3.8.1. RNA-sequencing approach illustrated previously identified ANKHD1 functions

It is already known in the literature that ANKHD1 interacts with PINK1 and PARKIN, proteins responsible for the control of dysfunctional mitochondrial degradation, by regulating mitophagy in drosophila (Zhu et al., 2015). ANKHD1 also promotes dysfunctional macromolecule degradation in the autophagy/lysosomal pathway (Zhu et al., 2017). It also acts as an RNA-binding protein and regulates microRNAs in renal cancer (Fragiadaki and Zeidler, 2018). These functions (microRNAs in cancer/mitophagy and macromolecule degradation) of ANKHD1 were also identified in this study, using the endothelial cell RNA-sequencing approach. The fact that RNA-sequencing has identified previously observed functions of ANKHD1 validates the RNA-sequencing approach. More widely, it further provides evidence of the potential involvement of ANKHD1 in controlling these functions in additional tissues (arteries). In future work, it would be interesting to validate the role of ANKHD1 in mitochondria and lysosome control and try to understand how ANKHD1 exerts these

functions, potentially via altering the microRNA subset to control atherothrombosis. Mitochondria are the energy powerhouse of cells, and therefore, important for all processes, especially in atherogenesis where mitochondria dysfunction has been reported to be an important contributor to pathogenesis (Ballinger et al., 2000).

3.8.2. The novel ANKHD1 roles in regulating shear-responsive genes in healthy endothelium

Results from the RNA-sequencing approach have also unveiled that ANKHD1 controls shear stress and atherosclerosis pathways, which have not been identified before. The precise mechanism utilised by ANKHD1 to regulate major mechanosensors and cellular behaviours is currently unknown, however, a large body of evidence suggests that ANKHD1 is required for cells to be able to sense and respond to shear stress. It is well-documented that endothelial cells respond to flow via mechanosensors. These usually are membrane-bound proteins decorating the surface of cells. Their role is to recognise and transduce the physical and mechanical forces into chemical signals to drive an appropriate cellular response (e.g., inflammation, migration). Some of these mechanosensors have been extensively studied (Li et al., 2022). The endothelial glycocalyx is a prime example. It is a sugar coat made up of polysaccharides and proteins which line the vascular endothelium. Glypican 1 is a major protein component of the glycocalyx that is under the control of ANKHD1. Mechanosensing also takes place at junctional complexes. These are protein complexes between endothelial cells. VEGF2R, VE-cadherin and PECAM-1 (CD31), which form a protein heterotrimeric complex, are well-known to sense and respond to mechanical stimuli (Tzima et al., 2005). My study identified ANKHD1 as a protein capable of regulating two out of the three mechanosensors (specifically, VE-cadherin and VEGF2R). It is interesting to note that lowering ANKHD1 results in an upregulation of these two receptors under atheroprotective shear stress. Further evidence that ANKHD1 may be capable of controlling endothelial mechanosensing comes from analysing all the genes known to

participate or respond to shear stress (N= 21 regulated by ANKHD1). These include core genes involved in NFκB signalling (*IKKβ* and *ICAM-1*), AP-1/Jun signalling (*JUN*, *DUSP1*, *SQSTM1*) and interleukin 1 (*IL-1β* and *IL1R1*). In addition to inflammatory genes, ANKHD1 also regulates oxidative stress genes (*RAC2*, *NRF2*, *GSTO-1* and *GSTP-1*). Taken together this unbiased study into the potential functions of ANKHD1 in endothelial cells revealed a previously unknown major role for this RNA-binding protein in controlling key pathways integral in mechanical response.

ANKHD1 roles in mechenosensors affecting NO and PGI$_2$ production

Most of the shear stress and atherosclerosis pathway genes that are under the control of ANKHD1 are involved in either NO/PGI$_2$ production and/or inflammation (Figures 3.9 and 3.10). The intercellular adhesion complex, VE-cadherin, VEGF2R and PECAM-1 sense the haemodynamic HSS flow and activates PI3K- AKT3 pathway and c-Src pathway which in turn enhances eNOS mRNA and protein expression/activation and NO production (Davis et al., 2001; Tzima et al., 2005; Iring et al., 2019; Bartosch et al., 2021); thus, enhancing vasoactivity and vasoprotection. HSS upregulates *VEGFR2*, *VE-cadherin* and *AKT3* expression (Dimmeler et al., 1999; Chen et al., 2001; de Bruin et al., 2016). RNA-sequencing data showed that ANKHD1 in HSS promotes the reduction of *VE-cadherin* and *VEGF2R* as well as the mechanoresponsive *AKT3* expression, without affecting the expression of *PECAM-1*. *Beta-catenin*, *ERK5*, *TM* and *NRF2* were also found to be highly upregulated by HSS (Dekker et al., 2002; Parmar et al., 2006; de Bruin et al., 2016; Psefteli et al., 2021). Interestingly, ANKHD1 reduced their expression in HSS conditions. It is unknown the mechanism by which ANKHD1 controls the expression of these mechanoresponsive genes, but it is hypothesized that the intracellular signalling genes are affected as a result of altering the expression of mechanoreceptors. It is also unknown whether limiting the inducible nature of these genes

under protective shear stress will result in any changes in the activity of the downstream pathway.

On the other hand, glypican 1 promotes functional endothelial cells by upregulating NO and PGI_2 release via PECAM-1 phosphorylation ultimately leading to vasodilation and inhibition of inflammation (Russell-Puleri et al., 2017; Ebong et al., 2014; Bartosch et al., 2021). My study showed that ANKHD1 upregulates *glypican 1*. Given the link between ANKHD1/Glypican 1/NO/PGI_2, it would be of interest to study whether ANKHD1 also controls the production of NO/PGI_2. eNOS is a major intracellular producer of NO, while PTGIS produces PGI_2. At this stage of the project, a number of questions remain unanswered: (1) Does ANKHD1 control *eNOS*/*PTGIS* expression as well as NO/PGI_2 release? 2) Does ANKHD1 enhances *glypican 1*/*eNOS*/*PTGIS* mRNA by promoting their expression and/or stability? And finally (3) would *Ankhd1* deletion lead to aging-related stiffness-induced endothelial dysfunction and vasoconstriction via glypican 1? Interestingly, the most significantly reduced mRNA in ANKHD1-deficient HCAECs, *RPL13AP25*, is significantly reduced in the serum of older individuals (80–85-years) when compared with younger individuals (30–32-year-old) (Dluzen et al., 2018). These data together suggest that ANKHD1 deficiency might contribute to age-related endothelial cell changes and vascular diseases.
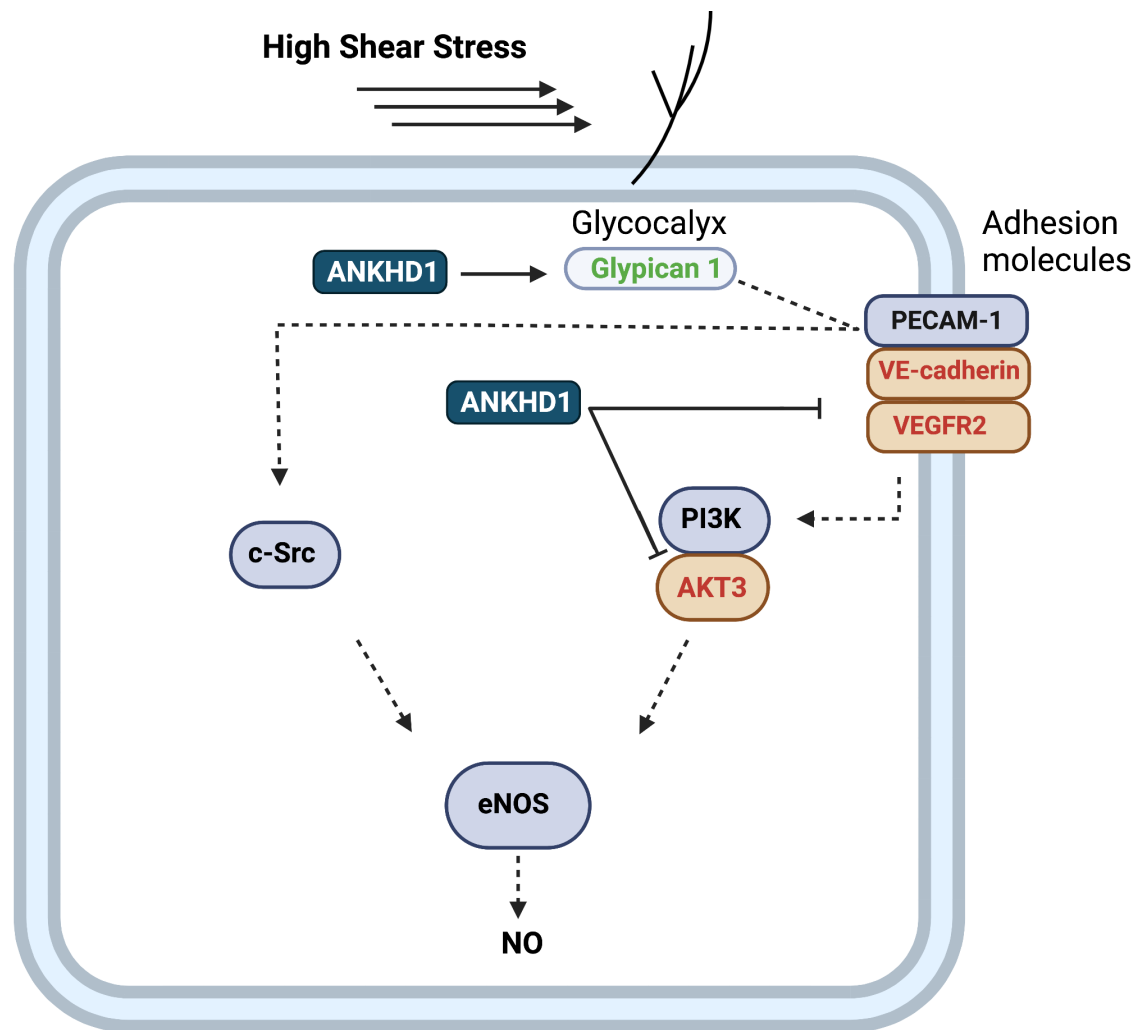
Figure 3.9. Potential roles of ANKHD1 in NO production in HSS-stimulated HCAECs.

This diagram shows the contributions of the upregulated genes (green) and the downregulated genes (red), which have been shown to be under the control of ANKHD1. In HSS conditions, ANKHD1 regulates the expressions of mechanosensors (glypican 1, VE-cadherin and VEGFR2). ANKHD1 might induce NO production via the glypican 1/PECAM-1/c-Src pathway but not via VEGFR2/VE-cadherin/PI3K-AKT3 pathway.

ANKHD1 roles in inflammation and oxidative stress

Endothelial dysfunction has been linked with high levels of inflammation and oxidative stress. ANKHD1 inhibited the major proinflammatory pathways, NFκB signalling, AP-1 signalling and IL1β, that promote endothelial dysfunction, leukocyte infiltration and atherogenesis. Mice lacking endothelial NFκB were shown to develop smaller atherosclerotic plaques and exhibited reduced inflammation when compared to the control group (Gareus et al., 2008). Elevated levels of the Jun subunit of the AP-1 transcription factor family can also result in activated NFκB signalling (Wang et al., 2011), providing two distinct mechanisms by which ANKHD1 can employ to suppress the inflammatory profile of endothelial cells. The contribution of ANKHD1 in these major pathways (Figure 3.10) has generated the question of whether ANKHD1 protects from atherosclerosis and inflammation by acting as an anti-inflammatory gene.

It is known in the literature that HSS or ROS upregulates the transcription factor *NRF2* levels (Hosoya et al., 2005; TakabeWarabi and Noguchi, 2011; Psefteli et al., 2021), here we report that HSS induces ANKHD1 which negatively controls *NRF2* levels. This is interesting because it implicates that ANKHD1 controls cellular redox independently of the NRF2-mediated antioxidant effects. On the other hand, Glutathione S-transferases are regulated by shear stress (Chen et al., 2001) and are cytoprotective and antioxidant enzymes that attenuate elevated ROS formation (Yan, F. et al., 2008), ANKHD1 was shown to positively regulate *GSTP-1*, hence shedding light into the potential mechanism of the antioxidant actions of ANKHD1. Likewise, it has been reported that RAC2 can produce high levels of ROS (Ambruso et al., 2000; Nieborowska-Skorska et al., 2012) and this study identifies ANKHD1 as a negative regulator of *RAC2*. Taken together, ANKHD1 appears to have a novel role in controlling the levels of oxidants in endothelial cells. It is unknown whether the increase of *NRF2* in ANKHD1-deficient cells exposed to HSS is a result of increased ROS levels via other

pathways regulated by ANKHD1 (e.g., glutathione-s-transferase) (Figure 3.10). Moreover, elevated ROS, as expected in cells lacking ANKHD1, can also attenuate the vasorelaxant NO levels (Beckman et al., 1990) and upregulates inflammatory pathways, AP-1/Jun pathway and NFκB pathway (József and Filep, 2003; TakabeWarabi and Noguchi, 2011). It is unknown whether ANKHD1 controls these pathways directly and/or indirectly via elevated ROS.

In HUVECs, *GSTP-1* was shown to inhibit endothelial cell permeability by attenuating tumour necrosis factor alpha (TNF-α)-mediated cytoskeletal remodelling via myosin light chain kinase (MLCK) independent pathway. In this pathway, TNF-a induces the phosphorylation of p38, MK2 and heat shock protein 27. This results in conformational changes of F-actin, which result in enhanced endothelial permeability (Yang et al., 2018). Hence, ANKHD1 enhances *GSTP-1* mRNA in healthy HCAECs suggesting it may also contribute to maintaining endothelial cell barrier via controlling endothelial contractile forces.
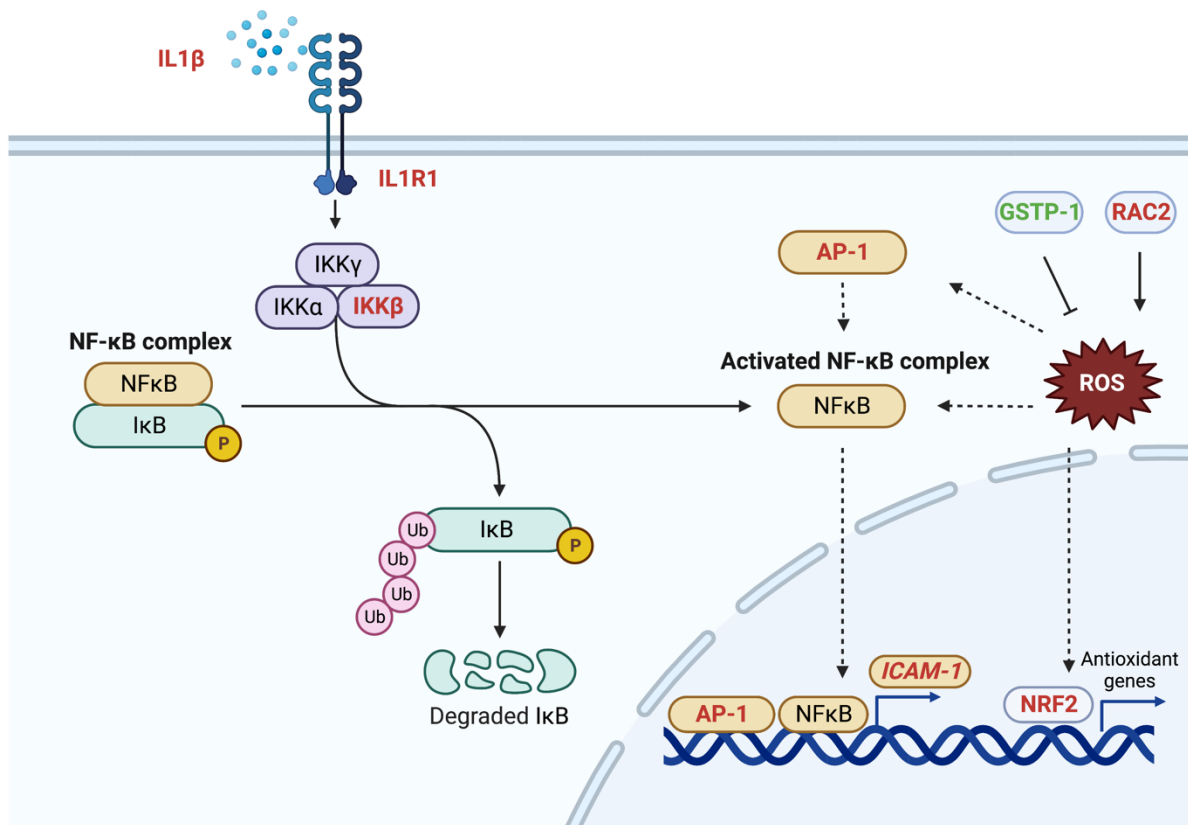
Figure 3.10. Potential roles of ANKHD1 in regulating inflammation and oxidative stress in HSS-stimulated HCAECs. This diagram shows the contribution of the upregulated genes (green) and downregulated genes (red), which are under the control of ANKHD1. ANKHD1 via IL1β, IL1R1 and IKKβ inhibition can reduce NFκB activation and inflammatory gene expression, particularly *ICAM-1*. ANKHD1 inhibits the proinflammatory transcription factor AP-1, which can further activate NFκB. The inhibition of the pro-oxidant RAC2 accompanied by the increase of the antioxidant GSTP-1 suggest the involvement of ANKHD1 in regulating ROS-mediated NFκB, AP-1 and NRF2 activation.

Does ANKHD1 control angiogenesis?

Proliferation and migration of endothelial cells are the initial processes of vascular angiogenesis that are activated via the vascular endothelial growth factor (VEGF) pathway signalling (Rousseau et al., 1997). EGFL7 is an endothelial-cell specific proangiogenic molecule. It enhances the VEGF pathway, and as such, new tube formation (Takeuchi et al., 2014). In glioma angiogenesis, ANKHD1 enhanced proliferation, migration, and thus, angiogenesis via upregulating EGFL7 (Yang, C. et al., 2020), yet in my study using non-cancer healthy endothelial cells, EGFL7 was unaltered upon *ANKHD1* silencing. Instead, I identified that ANKHD1 regulates a number of VEGF pathway genes. Specifically, it negatively regulates *VEGFR2*, *AKT3*, and *RAC2*, while it positively regulates *MAPK11*, *MAPK12*, and *RAC3* in HSS-stimulated HCAECs. I also found that ANKHD1 significantly reduced the expression of the *MAT2A* gene (the most significantly reduced gene). Previous studies showed that MAT2A promotes vascular angiogenesis in obese mice (Chen et al., 2021), thus providing more evidence for the potential involvement of ANKHD1 in the control of angiogenesis. The significance of the potential contribution of ANKHD1 to angiogenesis in normal endothelial cells has not been studied yet and can be assessed in the future.

3.8.3. ANKHD1 is a shear stress-regulated RNA-binding protein

The application of shear stress acts on primary endothelial cells was performed using the 6-well plate method, which was described by the Evans group and Warboys et al. (2014). The orbital shaker system generates a complex flow pattern that is closer to the physiological flow pattern (Dardik et al., 2005). My orbital shaker experiment provided strong evidence that ANKHD1 is under the control of HSS.

Previous studies have used microarrays applied on HSS-stimulated HUVECs and HCAECs and have found a significant enrichment in pathways linked to atherosclerosis,

specifically inflammation, redox system, thrombosis, vascular tone, junctional adhesion, and signal transduction (Chen et al., 2001; McCormick et al., 2001). Although ANKHD1 did not appear in these microarrays, probably because of the different experimental settings in which primary human endothelial cells were exposed to shear stress for ≤24 hours or the fact that it is a gene made up of many different transcript variants. My study clearly demonstrates that it is indeed induced by HSS. Specifically, ANKHD1 is upregulated by chronic stimulation with shear stress (72 hours), which is going to be further studied in chapter 4 (Figure 4.7).

Multiple bands of ANKHD1 in western blotting can be different transcript variants, protein degradation, processing and/or ubiquitination. ANKHD1 has 21 transcript variants with variable molecular weights that correspond to the identified bands (269-60 kDa); thus, suggesting that they are different transcripts of ANKHD1. A number of questions remain unanswered: (1) how is *ANKHD1* upregulated in HSS conditions, (2) which mechanosensor controls *ANKHD1* levels and (3) is ANKHD1 controlled at transcription levels and/or at mRNA/protein stability levels? Using an online genome database tool (Genecards, 2022), a putative nuclear receptor subfamily 2 group F member 2 (NR2F2) binding site was found on the enhancer regions of *ANKHD1*. NR2F2 is of interest to endothelial biology and atherosclerosis, as it has been shown to be an anti-inflammatory and anti-atherogenic transcription factor (Cui et al., 2015). Chromatin immunoprecipitation and deep sequencing (ChIP-Seq) showed that the active *ANKHD1* enhancer in endothelial cells has two NR2F2 binding sites. Knockdown of *NR2F2* downregulated *ANKHD1* significantly in primary human endothelial cells (Sissaoui et al., 2020). However, it is unknown whether NR2F2 promotes HSS-stimulated *ANKHD1* expression. The time course experiment is a simple experiment to assess the effect of shear stress on NR2F2 and ANKHD1 levels and to identify whether NR2F2 is upregulated by flow before ANKHD1. Also, ChIP assay can be applied to precipitate the

DNA-protein complex of the *ANKHD1* enhancer sequence and the bound transcription factor/s in HSS-stimulated endothelial cells.

3.8.4. ANKHD1 localisation in mouse aortic endothelial cells

ANKHD1 is found to be in the cytoplasm and nucleus. In the cytoplasm, it can bind to non-coding RNAs via its KH domain to regulate post-transcription gene expression (Yang, C. et al., 2020; Yao et al., 2022). Via its Ankyrin repeats, ANKHD1 can bind to YAP1 protein and bring YAP1 into the nucleus to activate cellular growth in different types of cancer (Yao et al., 2022). In my study, ANKHD1 is localised in both the cytoplasm and in the nucleus in endothelial cells of the normal mouse primary arch. It is more in the nucleus than in the cytoplasm. In the atheroprone regions of the primary arch, ANKHD1 was slightly more in the nucleus and less in the cytoplasm when compared to the atheroprotective regions. The most obvious difference, however, was the levels of ANKHD1 which were significantly lower in areas prone to the disease development. It currently remains unknown whether (1) ANKHD1 has different functions under different shear stress conditions; (2) the availability of ANKHD1 in the cytoplasm contributes to the stability of atheroprotective gene expression in the outer curvature compared to the inner curvature; (3) ANKHD1 promotes YAP1 activation and translocation into the nucleus under disturbed flow conditions. Disturbed flow has been linked with YAP1 activation and translocation into the nucleus (Lv and Ai, 2022). Moreover, the YAP pathway was identified as a major mechanotransducer that senses mechanical stimuli to control transcriptional programmes relating to a number of functions, including proliferation and differentiation (Dupont et al., 2011). It would be of interest to study whether ANKHD1 actively controls YAP/TAZ or whether YAP controls the activity of ANKHD1 in endothelial cells and how these interactions impact the physiological functions of endothelial cells.

This study focuses on exploring ANKHD1 functions under atheroprotective conditions, therefore, studying whether ANKHD1 contributes to atheroprotection via regulating some of the critical endothelial cell functions is my major research aim.

Summary

ANKHD1 is a novel protein upregulated by HSS in human and mouse endothelial cells. It is linked with the atheroprotective microenvironment and controls the endothelial cell responses to protective signals (atheroprotective shear stress) by potentially regulating important mechanosensors and by suppressing inflammation. Thus, if ANKHD1 protects the endothelial cells from sustained inflammation and atherosclerosis by sensing and responding to flow signals, it follows to focus on the study of the molecular mechanism whereby ANKHD1 promotes anti-inflammatory and endothelial cell protective molecules expression and stability.

Chapter 4: ANKHD1 controls major vasoprotective molecules in murine and human endothelial cells

4.1. Outlines

4.2. The influence of ANKHD1 loss-of-function on vasoprotective modulators in aortas of mice

4.3. The influence of ANKHD1 loss-of-function on vasoprotective modulators in primary human endothelial cells

4.3.1.   eNOS and PTGIS responses to shear stress

4.3.2. The effect of ANKHD1 on the vasoprotective eNOS and PTGIS in primary human cells

4.4. ANKHD1 binds to *eNOS* mRNA and *PTGIS* mRNA in HUVECs

4.5. ANKHD1 controls *eNOS* mRNA stability in HUVECs

4.6. Does ANKHD1 control *eNOS* and *PTGIS* transcription via KLF2?

4.7. Discussion

4.7.1. ANKHD1 controls the major vasoprotective modulators – eNOS / PTGIS

4.7.2. Potential mechanisms for eNOS mRNA stability

4.7.3. Potential roles of ANKHD1 in regulating KLF2 in healthy endothelium

4.1. Outlines

The previous chapter discussed the expression of ANKHD1, which is high in healthy endothelial cells. I validated that protective HSS consistently upregulated ANKHD1 expression (protein and mRNA) in primary human endothelial cells. RNA-sequencing revealed a role for ANKHD1 in shear-stress-controlled atherosclerosis pathways. Specifically, ANKHD1 was found to positively regulate vasoprotective pathways involved in NO and PGI_2 production. NO and PGI_2 are strong vasodilators, antithrombotic and anti-inflammatory molecules and are produced by the enzymes eNOS and PTGIS, respectively. In this chapter, I aimed to assess whether ANKHD1 loss-of-function affects the expression of the major vasorelaxants, anti-thrombotic, anti-inflammatory and vasoprotective modulators, which are *eNOS* and *PTGIS*, and then, I went on to begin to provide a mechanistic understanding of the functions of ANKHD1.

Hypothesis: ANKHD1 directly controls major vasoprotective pathways, including *eNOS* and *PTGIS*, by utilising its RNA-binding domain.

The specific aims of this chapter are:

1. To investigate the effect of ANKHD1 loss-of-function on eNOS and PTGIS expression *in vivo* in the murine aortas

2. To assess the effect of ANKHD1 inhibition on eNOS and PTGIS expression *in vitro* in primary human endothelial cells

3. To identify the underlying molecular mechanisms that are responsible for *eNOS* stability, focusing on the ability of ANKHD1 to bind RNA.

To begin to provide some answers, I used ANKHD1 loss-of-function human cell models (*in vitro* models) and mouse models (*in vivo* models) to assess the target genes (*eNOS*, *PTGIS*, *KLF4 and KLF2*), I statistically analysed the data and discussed the potential importance of these findings in this chapter.

4.2. The influence of ANKHD1 loss-of-function on vasoprotective modulators in aortas of mice

Endothelial cells in the descending aortas of mice were used, as the descending aorta is exposed to high and protective shear stress (Suo et al., 2007) and also express high levels of ANKHD1. *Ankhd1*$^{+/+}$ and *Ankhd1*$^{-/-}$ descending aortas were immunostained using the *en-face* staining method. To confirm that the cells that were imaged were indeed endothelial cells, aortas were stained with CD31, which is a well-validated endothelial cell marker. Endothelial cells expressed CD31 highly in endothelial junctions as anticipated, which confirmed that they were endothelial cells (Figure 4.1, cyan top panel and green in lower panel). Aortas of *Ankhd1*$^{+/+}$ and *Ankhd1*$^{-/-}$ mice were also stained with either eNOS or PTGIS specific antibodies. The negative control was isotype-matched IgG, which produced very little signal (Figure 4.1: A and D), confirming that the staining of eNOS and PTGIS is specific. Next, I studied the localisation and the expression of eNOS and PTGIS. eNOS expression was mainly localised in the Golgi and plasma membrane, which are known sites of eNOS (Fulton et al., 2002) (Figure 4.1: B, yellow panel). PTGIS expression is predicted to be nuclear, perinuclear and in the plasma membrane (Uniprot, 2022), which matched the observed expression in my analysis (Figure 4.1: E, red panel), where PTGIS expression is mainly perinuclear and cytoplasmic.

Interestingly, in all animals studied, *Ankhd1*$^{-/-}$ led to a marked decrease in the expression of both eNOS and PTGIS at protein levels (Figure 4.1: C and F). The quantification of the mean fluorescence intensity of eNOS and PTGIS revealed that ANKHD1-deficient mice had significantly lower levels of eNOS and PTGIS in endothelial cells when compared to wild-type littermate control mice (eNOS: Figure 4.1: G; PTGIS: Figure 4.1: H). Since ANKHD1 controls the protein levels of eNOS and PTGIS *in vivo* and given that disruption of either of these genes leads to impaired vascular functions and accelerated atherosclerosis, I hypothesize that

ANKHD1 may control vasoprotection and atherogenesis via eNOS and PTGIS, which is going to be studied in the next chapter.
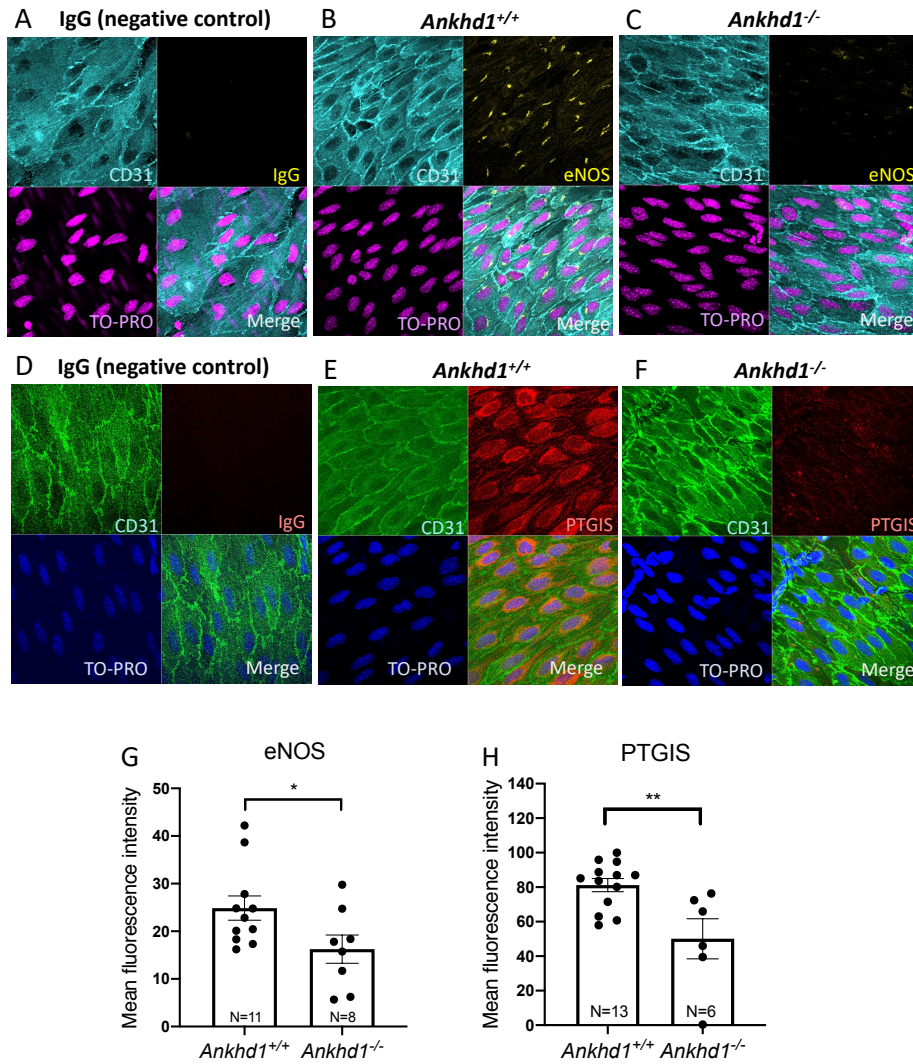
Figure 4.1. eNOS and PTGIS expression in endothelial cells of Ankhd1^{+/+} and Ankhd1^{-/-} *descending aortas of mice.* Endothelial cells were distinguished from other vascular cells using the endothelial marker CD31 (cyan top panel and green lower panel). They were co-stained with isotype-matched IgG in yellow or red (A and D), eNOS staining in yellow (B and C) or PTGIS staining in red (E and F). Multiple images of the *en face* staining were taken (eNOS: *Ankhd1^{+/+}*: N=11, *Ankhd1^{-/-}*: N=8; PTGIS: *Ankhd1^{+/+}*: N=13, *Ankhd1^{-/-}*: N=6) Quantification of multiple animals expressed as mean fluorescence intensity showed a significant reduction in eNOS and PTGIS *in Ankhd1^{-/-}* when compared to the control group (Two-tailed unpaired t-test: eNOS: *p*= 0.0425; PTGIS: *p*= 0.0045) (G and H). All dots represent different animals and error bars show the standard error of the mean.

4.3. The influence of ANKHD1 loss-of-function on vasoprotective modulators in primary human endothelial cells

Given that murine ANKHD1 positively regulates eNOS and PTGIS in mouse vessels exposed to physiological HSS, I wished to assess whether the human ANKHD1 can also regulate eNOS and PTGIS. To test this, I used primary human endothelial cells from a number of different donors. The use of different donors allows me to assess the robustness of the observations. I applied shear stress chronically (72 hours) to the cells to mimic the *in vivo* system, which is constantly experiencing shear stress, and quantified eNOS and PTGIS expression with and without *ANKHD1* silencing.

4.3.1. *eNOS and PTGIS responses to shear stress*

To assess the levels of mRNA and protein expression of the human *eNOS* and *PTGIS* genes in response to shear stress, I started by stimulating HUVECs as well as HCAECs with shear stress via the orbital shaker system. While *eNOS* is a well-known HSS gene, whether *PTGIS* responds to shear is less well-known. eNOS and PTGIS levels were quantified from orbited cells in the LSS (centre) and HSS (periphery) conditions using qPCR and western blotting.

As expected eNOS mRNA (Figure 4.2: A and B) and protein (Figure 4.2: C and D) were upregulated by HSS in both HUVECs and HCAECs. This confirms previously published work in which eNOS was demonstrated to be positively regulated by HSS (SenBanerjee et al., 2004; Parmar et al., 2006; Iring et al., 2019). It also confirms that the cells responded adequately to HSS generated from the orbital shaker system.
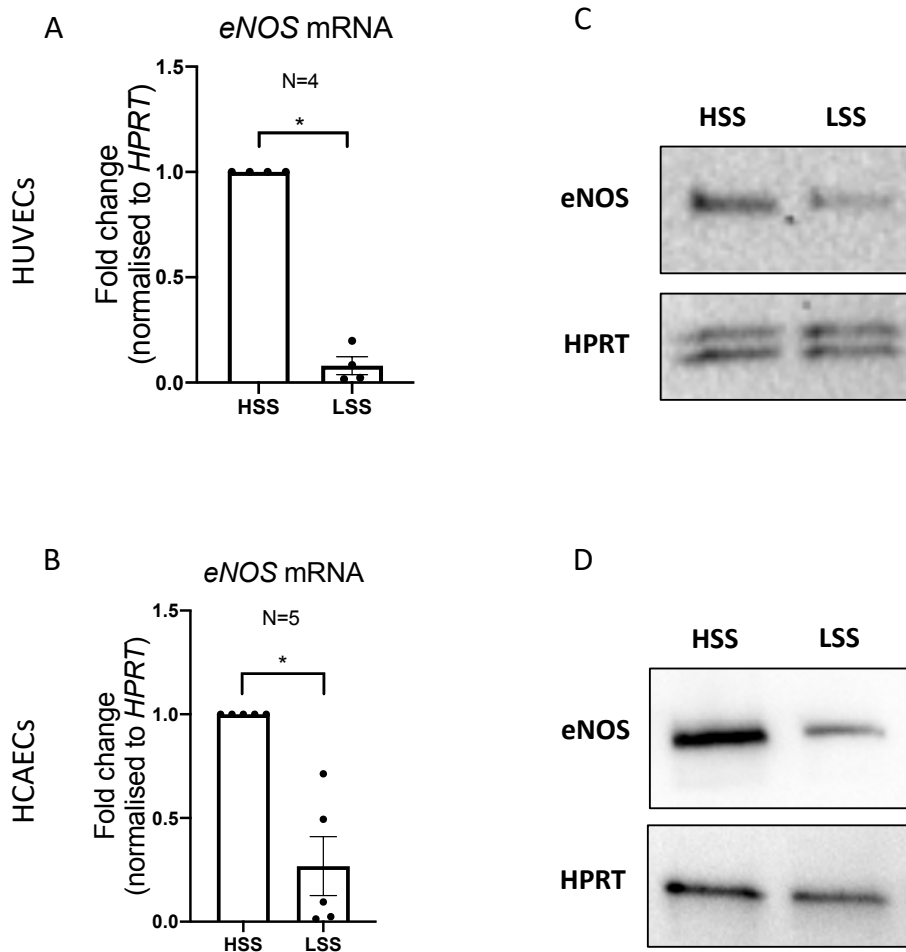
Figure 4.2. eNOS responds to flow generated by the orbital shaker in HUVECs and HCAECs. Quantification of *eNOS* mRNA levels in shear stress stimulated HUVECs (A) and HCAECs (B) are shown. The expression of *eNOS* was significantly high in HSS conditions (Two-tailed paired t-test: HUVECs: *p*= 0.0138; HCAECs: *p*= 0.0312). All data were normalised to the housekeeper *HPRT* and all dots represent different biological donors and error bars show the standard error of the mean (A and B). Immunoblottings from one biological replicate present eNOS protein levels in HSS and LSS stimulated HUVECs (C) and HCAECs (D). There is an increase in eNOS protein levels in HSS-stimulated cells. HPRT could appear as a single or double bands in (C and D immunoblottings). The double band can be attributed to protein modification (i.e., glycosylation) (GlyGen, 2022) or protein cleavage.

Next, I examined the mRNA and protein expression of *PTGIS*, a vasorelaxant and anti-thrombotic gene. My data shows for the first time that the *PTGIS* gene is strongly upregulated by HSS conditions at mRNA levels in HUVECs (Figure 4.3: A) and in HCAECs (Figure 4.3: B). Next, to confirm this finding and further assess the expression levels of *PTGIS*, I studied protein levels. HUVECs stimulated with shear stress were stained with PTGIS and VE-cadherin antibodies. VE-cadherin is a marker of endothelial cell junctions. The result showed that HUVECs had significantly higher PTGIS concentrations in HSS conditions when compared to LSS conditions (Figure 4.3: C). To further validate this result, I performed immunoblotting on HCAECs stimulated with shear stress. PTGIS protein was significantly elevated by HSS when compared to LSS conditions (Figure 4.3: D). In summary, my results show that in addition to eNOS, PTGIS levels are also enhanced by atheroprotective HSS, hence identifying *PTGIS* as a novel HSS-induced gene.
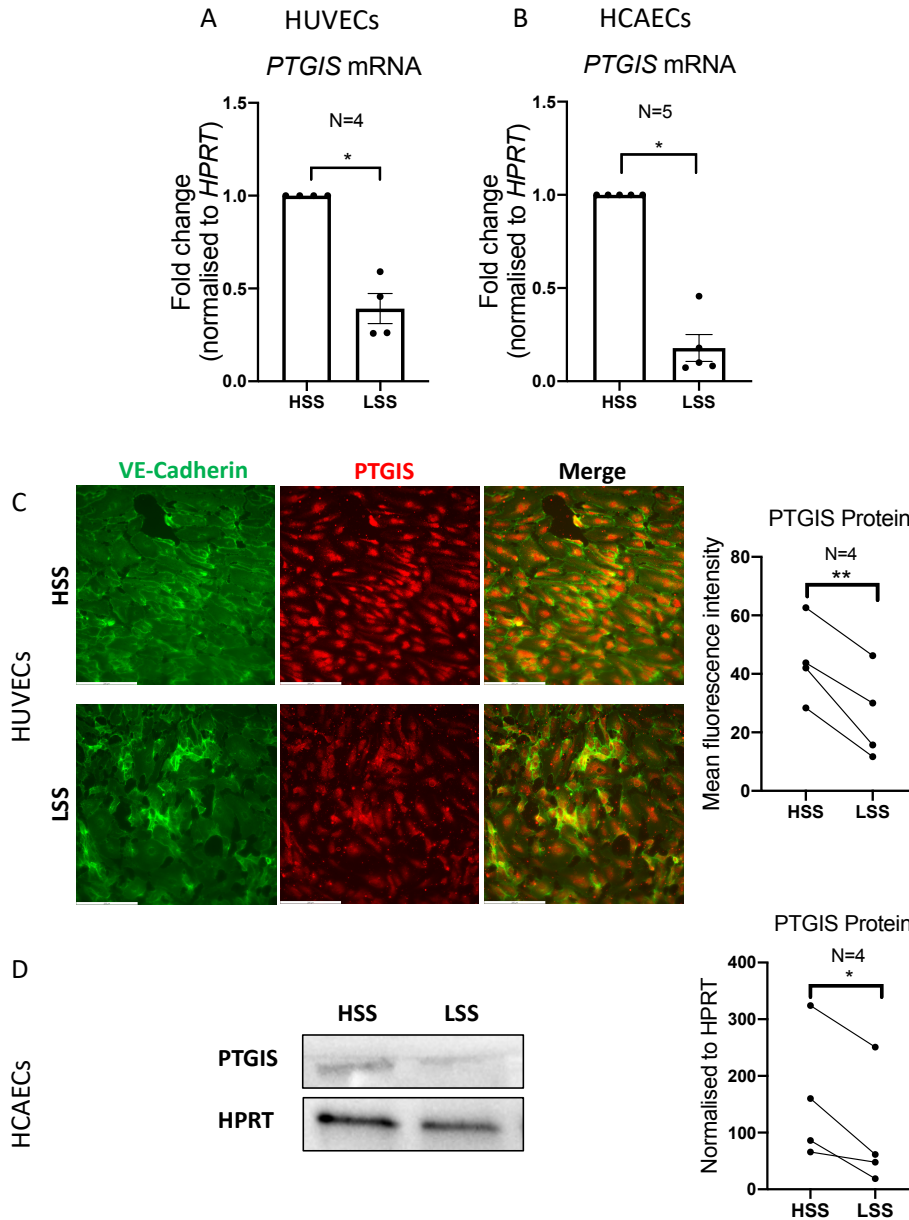
Figure 4.3. PTGIS responds to flow in HUVECs and HCAECs. Graphs showing *PTGIS*

mRNA levels in HUVECs (A) and in HCAECs (B) that are stimulated with shear stress. The

expression of *PTGIS* was significantly high in HSS conditions (Two-tailed paired t-test:

HUVECs: *p*= 0.0365; HCAECs: *p*= 0.0254). Immunofluorescence staining of PTGIS from

one biological replicate shows significantly higher protein levels in HSS when compared

with LSS-stimulated HUVECs (Two-tailed paired t-test: *p*= 0.0070) (C). Immunoblotting of

PTGIS from one biological replicate shows significantly elevated protein levels in HSS when

compared with LSS-stimulated HCAECs (Two-tailed paired t-test: p=0.0320) (D). All the results of qPCR and immunoblotting were normalised to the housekeeper HPRT, all dots represent different biological donors and error bars show the standard error of the mean.

4.3.2. The effect of ANKHD1 on the vasoprotective eNOS and PTGIS in primary human cells

Next, I investigated the effect of ANKHD1 inhibition in HCAECs in atheroprotective conditions. Either non-targeting siRNA (control) or two different siRNAs against *ANKHD1* (*ANKHD1*siRNA-1 and *ANKHD1*siRNA-2) were transfected into HCAECs. *ANKHD1*siRNA-1 lipotransfection resulted in a significant reduction in the full-length *ANKHD1-203* mRNA (1.88 to 24.21-fold inhibition; Figure 4.4: A) and in the *ANKHD1* transcript variants, which are *ANKHD1-203* transcript variant 1, *ANKHD1-204* transcript variant 2 and *ANKHD1-205* transcript variant 3 (1.87 to 11.76-fold inhibition; Figure 4.4: B) compared to the control group. Transfection with *ANKHD1*siRNA-2 also resulted in significant inhibition of *ANKHD1-203* (1.58 to 20.68-fold inhibition; Figure 4.4: A) and *ANKHD1* transcript variants (1.15 to 10.78-fold inhibition; Figure 4.4: B) compared to the control group.

In line with previous *in vivo* experiments on mouse endothelial cells, human *ANKHD1* knockdown via *ANKHD1*siRNA-1 or *ANKHD1*siRNA-2 in HSS-stimulated HCAECs also resulted in a significant reduction in *eNOS* and *PTGIS* mRNA expression (*eNOS*: 1.54 to 17.24-fold of inhibition; *PTGIS*: 1.69 to 149.61-fold of inhibition) compared to the control group (Figure 4.4: C and D). This has been studied further at the protein level via immunoblotting of eNOS and PTGIS applied on HCAECs and via immunofluorescence staining of HUVECs with PTGIS and VE-cadherin, with and without *ANKHD1* inhibition via siRNAs. The results showed that inhibition of ANKHD1 attenuated the effect of HSS on eNOS and PTGIS in HCAECs (Figure 4.4: E) and PTGIS in HUVECs markedly (Figure 4.4: F). Taken together the mouse and human work indicate that ANKHD1 is a regulator of eNOS and PTGIS expression in endothelial cells exposed to HSS conditions, whether ANKHD1 induces vasodilation through controlling eNOS and PTGIS remains unclear.
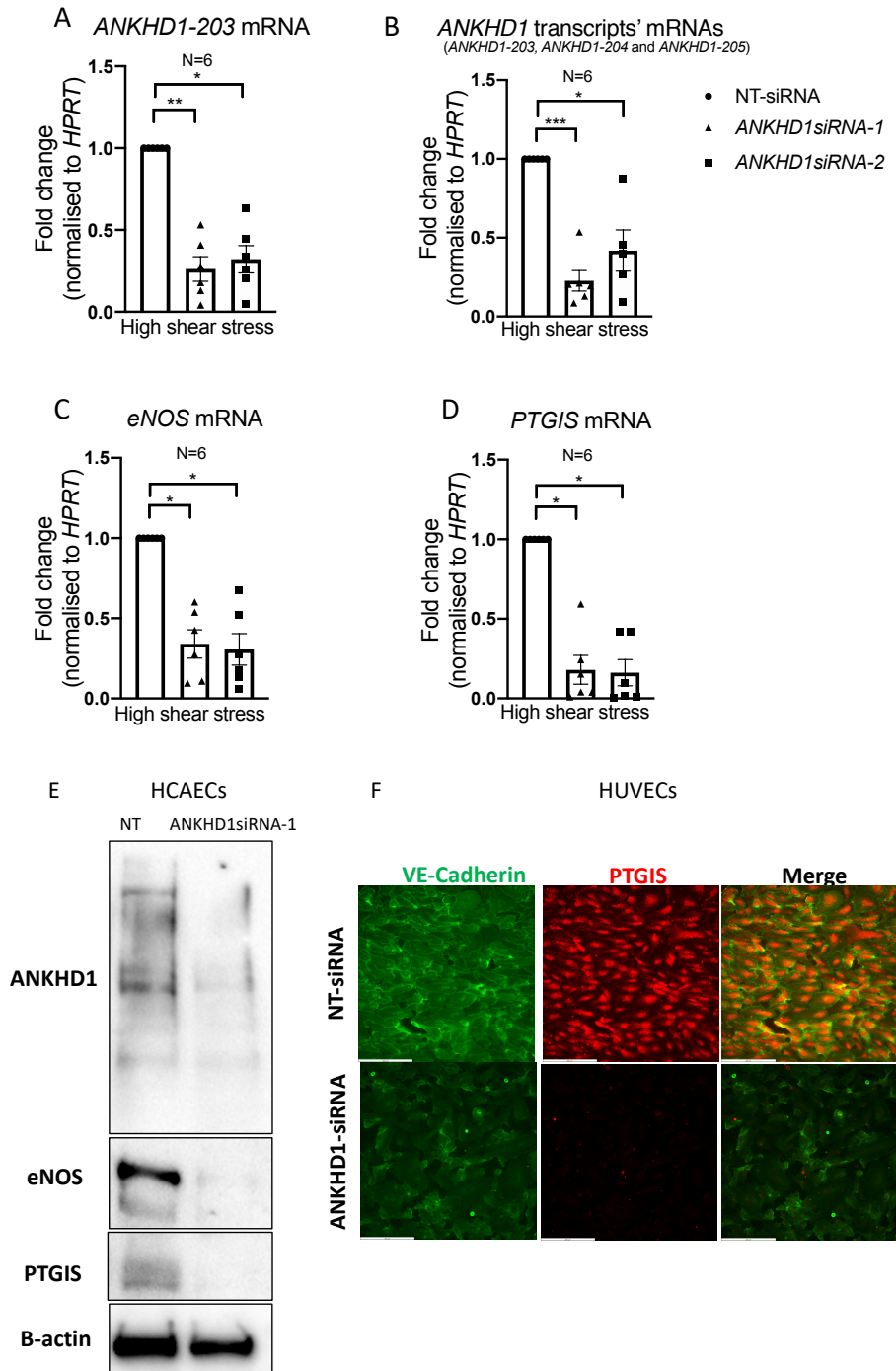
Figure 4.4. HCAECs responses to ANKHD1 absence in HSS conditions generated via the orbital shaker. mRNA Graphs show the quantification of the full-length *ANKHD1-203* mRNA (A), *ANKHD1* transcript variant mRNAs (B), *eNOS* mRNA (C) and *PTGIS* mRNA (D) in control HCAECs (non-targeting siRNA transfected cells) and ANKHD1-deficient HCAECs (*ANKHD1*siRNA-1 or *ANKHD1*siRNA-2 transfected cells) treated with HSS. I

applied a two-tailed one-way-ANOVA test (Dunnett's multiple comparisons test). Cells treated with *ANKHD1*siRNA-1 inhibited *ANKHD1-203* mRNA expression (A) and the transcript variants (B) significantly (*ANKHD1-203:* adjusted $p= 0.0096$; transcript variants: adjusted $p = 0.0010$). Inhibition with *ANKHD1*siRNA-2 was also significant (*ANKHD1-203:* adjusted $p= 0.0321$; transcript variants: adjusted $p= 0.0430$). *eNOS* mRNA (C) and *PTGIS* mRNA (D) were significantly inhibited in cells transfected with *ANKHD1*siRNA-1 (*eNOS*: adjusted $p= 0.0247$; *PTGIS*: adjusted $p= 0.0227$) and *ANKHD1*siRNA-2 (*eNOS*: adjusted $p= 0.0209$; *PTGIS*: adjusted $p= 0.0271$). All the results were normalised to the housekeeper *HPRT*, all dots represent different biological donors and error bars show the standard error of the mean (A-D). Immunoblotting of ANKHD1, eNOS, PTGIS and the housekeeper B-actin (E) and immunofluorescence staining with PTGIS and VE-cadherin (F) in HSS-stimulated endothelial cells with and without *ANKHD1* silencing from one biological replicate.

4.4. ANKHD1 binds to *eNOS* mRNA and *PTGIS* mRNA in HUVECs

Our lab identified that ANKHD1 acts as an RNA-binding protein that requires its KH-domain for association with RNA, as the ANKHD1 mutant that lacked a functional KH domain was unable to associate with its target RNA (Fragiadaki and Zeidler, 2018). Whether ANKHD1 interacts with *eNOS* and *PTGIS* mRNA via mRNA binding is currently unknown and is analysed here using a well-established technique in our lab, namely RNA-immunoprecipitation assay (RIP assay; Figure 4.5: A). In RIP assays, the protein of interest (i.e., ANKHD1) was pulled down from HUVEC lysates via a specific and RIP-validated anti-ANKHD1 antibody. An isotype-matched rabbit IgG antibody was used as a negative control. This assay allows the detection of interactions between ANKHD1 and its target RNAs, focusing on mRNA for this study. I used western blotting to confirm the efficiency and specificity of the pull-down performed in the RIP assay by showing that the ANKHD1 protein was successfully precipitated with the ANKHD1 antibody (Figure 4.5: B). The levels of the precipitated ANKHD1 are comparable to the 10% of the initial input sample. The negative control IgG did not precipitate ANKHD1 protein. Therefore, I proceeded with total RNA extraction (which was of high quality). I then quantified *eNOS* and *PTGIS* mRNA in the ANKHD1 RIP and compared this with the background interactions of these messages with the non-specific portion of the IgG (negative control). The results showed that ANKHD1 is capable of capturing *eNOS* mRNA on average at 500-fold and *PTGIS* at 12-fold greater than IgG (Figure 4.5: C and D). This indicates that ANKHD1 binds to these vasoprotective molecules at the level of mRNA.
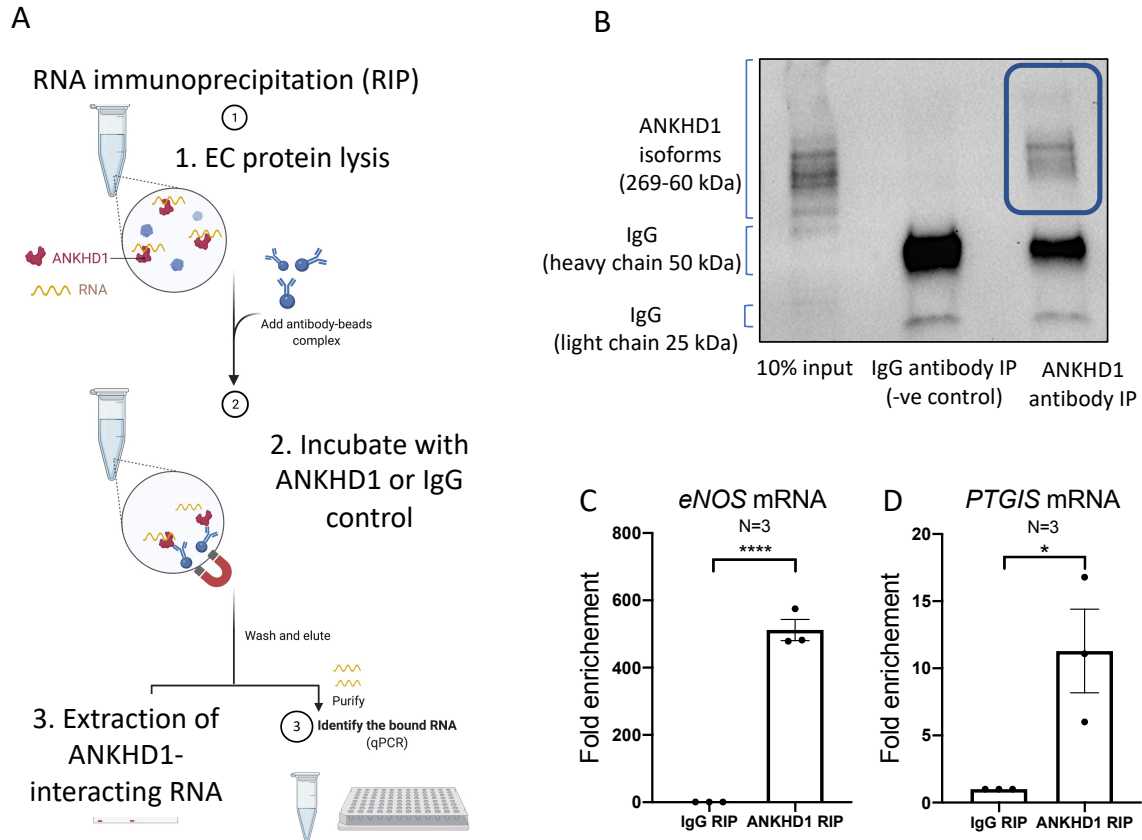
Figure 4.5. Quantification of eNOS and PTGIS mRNA-binding to ANKHD1 via RNA-immunoprecipitation assay in HUVECs. Workflow presents the RNA-immunoprecipitation via either the ANKHD1 antibody or the isotype negative control (IgG) (A). Immunoblotting of the 10% input, immunoprecipitated IgG and ANKHD1 showed that the precipitation passed the quality control assurance (B). This has been applied on three biological replicates. Quantification of *eNOS* mRNA (C) and *PTGIS* mRNA (D) levels via qPCR in the immunoprecipitated IgG and ANKHD1. *eNOS* and *PTGIS* mRNAs were significantly enriched in the immunoprecipitated ANKHD1 when compared to the negative control IgG (Two-tailed paired t-test: *eNOS*: $p < 0.0001$; *PTGIS*: $p = 0.0172$). All dots represent different biological donors and error bars show the standard error of the mean.

4.5. ANKHD1 controls *eNOS* mRNA stability in HUVECs

Given that ANKHD1 loss-of-function results in significantly lower levels of eNOS and PTGIS mRNA and protein in both mouse and human models; and ANKHD1 binds to *eNOS* and *PTGIS* mRNAs, I wished to investigate whether ANKHD1 controls *eNOS* and *PTGIS* at either the level of mRNA stability and/or transcription. Understanding how ANKHD1 controls mRNA levels is important as it will allow me to decipher the molecular mechanism responsible for regulating eNOS/PTGIS in the vasculature.

To start finding the mechanism, I performed a time course experiment in which I stimulated different HCAEC donors with shear stress for 4, 24 and 72 hours using the orbital shaker system. 4-24 hours of shear represents a model of acute induction of fluid flow while 72 hours represents a model of more chronic fluid flow. The results showed that *KLF2* and *KLF4* mRNAs were upregulated by acute shear stress, and their expression was already high by 4 hours when compared to static cells that did not experience fluid flow. *eNOS* mRNA was upregulated by 24 hours (acute induction) and *ANKHD1* and *PTGIS* mRNAs were induced by 72 hours, suggesting that *ANKHD1* and *PTGIS* require prolonged shear stress for their induction. All genes, including *ANKHD1* and *PTGIS*, were significantly upregulated by shear stress at 72 hours when compared with the static cells (Figure 4.6: A and B). These results demonstrate that the *KLFs* and *eNOS* are induced by shear stress before the induction of *ANKHD1*, and as such, the acute induction of *eNOS* mRNA expression is not primarily dependent on the fluid flow-induced ANKHD1, which is upregulated at a later time point. Taken together, this experiment highlights that the kinetics of responding to flow is different for each gene studied and suggests that *ANKHD1* and *PTGIS* require a chronic fluid flow to be fully induced, while *KLFs* and *eNOS* can respond to flow much more acutely.
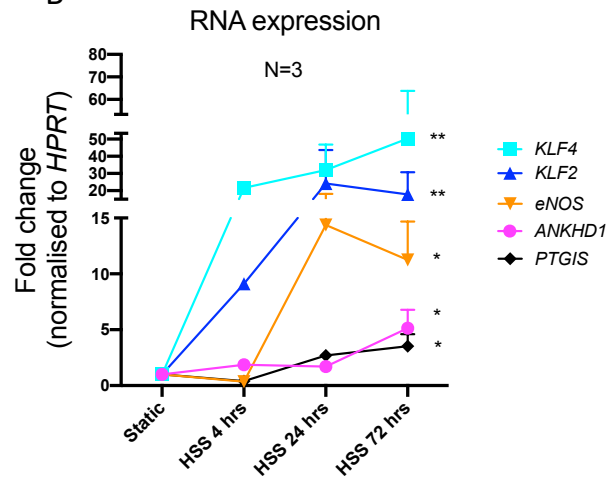
Figure 4.6. HSS induces KLFs, ANKHD1, eNOS and PTGIS at different time points. A time course experiment was applied on primary HCAECs (A). Quantification of *KLF4*, *KLF2*, *eNOS*, *ANKHD1* and *PTGIS* mRNAs was performed in HCAECs that had experienced either static (no flow) or HSS for the indicated time points (B). At 72 hours, all mRNAs were increased significantly when compared with the static cells (Two-tailed one-way ANOVA, Dunnett's multiple comparisons test: *KLF4*: adjusted p= 0.0070; *KLF2*: adjusted p= 0.0087; *eNOS*: adjusted p= 0.0324; *ANKHD1*: adjusted p= 0.0431; *PTGIS*: adjusted p= 0.0491). All the results were normalised to the housekeeper *HPRT*.

To further investigate the mechanism of the mRNA control that ANKHD1 exerts on *eNOS*, I performed actinomycin D assays. Actinomycin D was used because it inhibits RNA transcription and allows to study the pre-transcribed mRNA over time (Ratnadiwakara and Änkö, 2018). HUVECs with or without *ANKHD1* silencing were treated with 1 μM of actinomycin D for 0, 2, 4 or 16 hours.

I have used a number of housekeeping genes as markers of activity of the actinomycin D treatment. *HPRT* and *B-actin* both reduced their expression by 5.6 hours and 8.3 hours, respectively, after treatment, which agrees with previously published work (SteenSahlén and Lambert, 1991; Dormoy-Raclet et al., 2007); suggesting that the treatment effectively blocked transcription (Figure 4.7: A and D). Next, I investigated the mRNA levels of *ANKHD1* (gene of interest) and *eNOS* (target gene). The results showed that the *ANKHD1* mRNA is under the control of mRNA degradation, which by 8 hours becomes massively reduced in actinomycin D-treated cells. The curve of *ANKHD1* mRNA expression tends toward reduction in treated cells and this is not affected by the silencing status. With *ANKHD1* silencing, *ANKHD1* mRNA half-life was reduced to 3 hours; indicating that as expected the siRNA results in degradation of the pre-transcribed *ANKHD1* mRNA (Figure 4.7: B and D). Taken together, these results indicate that *ANKHD1* mRNA is downregulated by actinomycin D, while the reduction in *HPRT* and *B-actin* mRNA confirms that the treatment worked efficiently.

Next, I examined the effect of actinomycin D on mRNA levels of *eNOS* (target gene). The results showed that *eNOS* mRNA is relatively long-lived in the presence of ANKHD1. The half-life of *eNOS* mRNA equals 32.32 hours (blue line: Figure 4.7: C) which agrees with previously published work that reports *eNOS* mRNA half-life >24 hours (Ho et al., 2013). As soon as *ANKHD1* is silenced, however, *eNOS* mRNA becomes short-lived as indicated by the rapid turnover of the mRNA. Specifically, endothelial cells that have lower ANKHD1 expression (*ANKHD1* silencing) result in a greater than 50% reduction of *eNOS* mRNA as

early as 1.41 hours after treatment (magenta line: Figure 4.7: C). This time-course experiment suggests that ANKHD1 is required for the well-documented long-lived stability of *eNOS* mRNA. Since actinomycin D, at the dosage used, inhibits *de novo* transcription, it follows that the turnover of *eNOS* mRNA in ANKHD1-deficient cells is due to a rapid reduction of the pre-synthesized mRNA. How ANKHD1 may control the stability of *eNOS* mRNA at the post-transcriptional level is currently unknown.

A RNA expression

B *ANKHD1* mRNA

C *eNOS* mRNA

D

	B-actin	**HPRT**
K	0.08264	0.1236
Half Life	8.387	5.610
R squared	0.3653	0.3924
ANKHD1 mRNA	**NTsiRNA**	**ANKHD1siRNA-1**
K	0.08676	0.2248
Half Life	7.990	3.084
R squared	0.5178	0.4549
eNOS mRNA	**NTsiRNA**	**ANKHD1siRNA-1**
K	0.02145	0.4920
Half Life	32.32	1.409
R squared	0.01419	0.6726
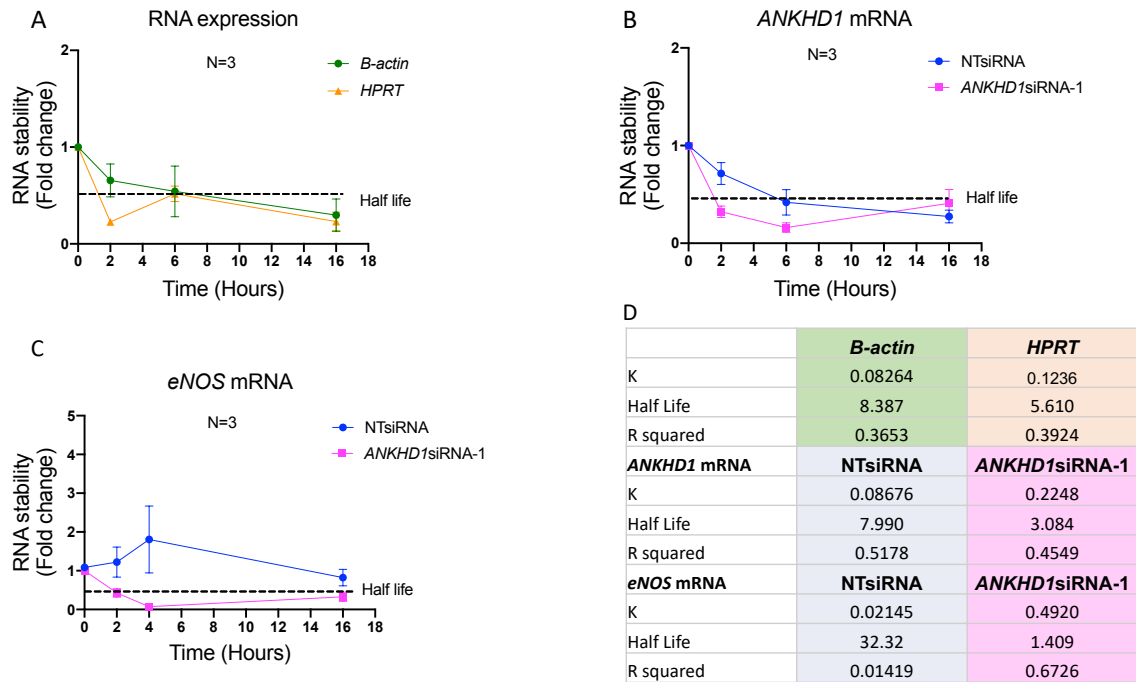
Figure 4.7. Quantification of RNA stability of eNOS mRNA in HUVECs. B-actin and *HPRT* mRNA decay in HUVECs treated with ActD is shown (A). Graphs present *ANKHD1* mRNA (B) and *eNOS* mRNA (C) levels in HUVECs transfected with either NTsiRNA (in blue) or *ANKHD1*siRNA-1 (in magenta) and treated with actinomycin D. One-phase decay analysis (D) revealed that the K values (represents the rate of mRNA decay overtime) of *B-actin* and *HPRT* in HUVECs treated with actinomycin D and *ANKHD1* and *eNOS* mRNA in HUVECs treated with NTsiRNA+ActD and *ANKHD1*siRNA+ActD. The half-life was measured by this equation In(2)/K and the R square represents the goodness of decay.

ANKHD1 binds to the 3'UTR of eNOS mRNA

The reduction of *eNOS* mRNA after only approximately 2 hours in ANKHD1-deficient cells suggested that *eNOS* mRNA has the capacity to rapidly turnover in cells that do not express high levels of ANKHD1. This suggests that either ANKHD1 confers direct protection of *eNOS* mRNA or alternatively ANKHD1 inhibits a protein that is involved in the active degradation of the *eNOS* mRNA. To begin to shed light on this, I decided to study whether the 3'UTR of *eNOS* contains any canonical AU-rich (AUR) elements. AU-rich elements are regions in the regulatory sequence of mRNAs that have a sequence rich in uridine (U) and adenosine (A) nucleotides. This specific sequence motif can be targeted by a few RNA-binding proteins to either confer protection or facilitate RNA degradation. For example, the mRNA-degrading protein tristetraprolin (TTP) can bind to AUR elements and result in quick mRNA decay (Lai et al., 1999), while ELAV-like RNA-binding protein 1 binds to AUR elements and protect their target mRNAs from degradation (Bakheet et al., 2018). While CU-rich stability elements within the *eNOS* 3'UTR have been studied (Ho et al., 2013), the role of AU-rich elements is currently unknown.

The 3'UTR of *eNOS* mRNA is made out of 419 bases and contains a canonical AUR element. This AUR element was identified using the online software (AREsite2) and then manually assessed for the motif UAUUUAU (Figure 4.8: A). Then, I compared *eNOS* 3'UTR identities between humans and different species. The flanking region shares an evolutionary conservation that is 22.46% for *Canis lupus*, 33.89% for *Bos taurus* and 32.45% for *Sus scrofa*. Although there are high dissimilarities in overall *eNOS* 3'UTR between humans and these species, the AUR element is 100% conserved (Figure 4.8: B). The presence of a canonical AUR element on *eNOS* mRNA generated the question of whether ANKHD1 may bind around the AUR area to protect the mRNA from rapid turnover, or alternatively bind the mRNA to

transport it away from active mRNA degradation sites (such as the processing bodies) and/or by inhibiting interactions with decay proteins.

Ray et al. (2013) identified the agacgww motif, which is the evolutionarily conserved binding motif for ANKHD1. I used RBPMap to identify the predicted ANKHD1 binding site via its agacgww motif on *eNOS* 3'UTR. RBPMap shows AGAUGUU or GGAAGUU in the 3'UTR of *eNOS* as predicted binding sites for ANKHD1 (AGAUGUU: Z-score=2.348, *p*= 0.00944; GGAAGUU: Z-score= 2.116, *p*= 0.0172; Figure 4.8: B). These sequences are located downstream and close to the AUR element (344-351 base), but they are not overlapping it, suggesting that ANKHD1 does not require interactions with the AU-rich element.

A

Chromosome 7

ENST00000297494   NOS3 3'UTR

WWTTTWW

AU-rich element
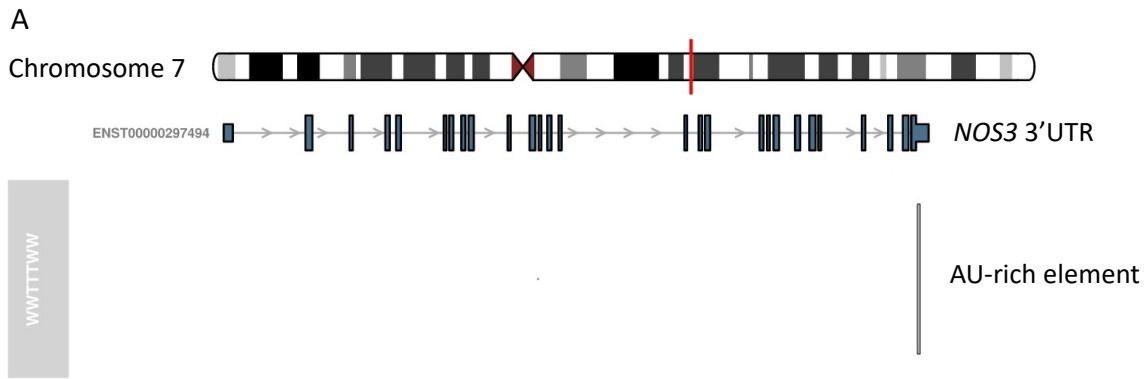
(RNA sequence: *eNOS* 3'UTR):
GAGCCGCCUGGCUUUCCCUUCCAGUUCCGGGAGAGCGGCUGCCCGACUCAGGUCCGCCCGACCAGGAUCAGCCCCGCUCCUCCC
CUCUUGAGGUGGUGCCUUCUCACAUCUGUCCAGAGGCUGCAAGGAUUCAGCAUUAUUCCUCCAGGAAGGAGCAAAACGCCUCUU
UUCCCUCUCUAGGCCUGUUGCCUCGGGCCUGGGUCCGCCUUAAUCUGGAAGGCCCCUCCCAGCAGCGGUACCCCAGGGCCUACU
GCCACCCGCUUCCUGUUUCUUAGUCGAAUGUUAGAUUCCCUCUUGCCUCUCUCAGGAGUAUCUUACCUGUAAAGUCUAAUCUCUA
AAUCAAG<mark>UAUUUAU</mark>UAUUGAAGAUUUACCAUAAGGGACUGUGCCAGAUGUUAGGAGAACUACUAAAGUGCCUACCCCAGCUCA

Chromosome	Start	End	Motif	Motif-family	Strand	Gene	Transcript	Annotation
chr7	151014512	151014519	TATTTAT	WWTTTWW	+	*NOS3*	ENST00000297494	Exon^3UTR

B

```
                    AUR-element                                ANKHD1 binding site
Canis lupus    TTCCAAGTATTTATTATTGAAGATTCACCATAAGAGACTGGACCAGATGTTATGAGAGCT
Homo sapiens   AATCAAGTATTTATTATTGAAGATTTACCATAAGGGACTGTGCCAGATGTTAGGAGAACT
Bos taurus     ATTTAAATATTTATTACTGGAGATTCACCGTAATAGACTGGACCGGAAGTTACCAGAGCT
Sus scrofa     ATTTAAATATTTATTACTGGAGATTCACCGTAATAGACTGGACCGGAAGTTACCAGAGCT
               **  ********* **  ***** *** ***   *****  ** ** ****  *** **
```

Figure 4.8. Identification of AU-rich element and ANKHD1 binding site in the 3'UTR of eNOS mRNA via AURsite2 and RBPmap. The AUR element of *NOS3* (eNOS coding gene) TATTTAT (RNA sequence: UAUUUAU) was found in human genome chromosome 7 (151014512-151014519) and located in the 3'UTR of *NOS3* exon (A). Evolutionary *eNOS* 3'UTR cDNA comparison by Clustal Omega shows highly conserved TATTTAT sequence (yellow) and predicted ANKHD1 binding sites (green: AGATGTT and GGAAGTT) (B).

Therefore, I experimentally tested whether ANKHD1 binds to the 3'UTR of *eNOS* mRNA and whether this interaction does not require the AUR element, I constructed plasmids that contain either the full-length wild-type 3'UTR of *eNOS* (419 bp) or *eNOS* 3'UTR lacking the AUR element, which I called delta AUR (ΔAUR) plasmid. These two 3'UTRs were *in vitro* transcribed and labelled using RNA polymerase and biotinylated Uracil bases, respectively. This generated biotinylated sequences that were then used to precipitate interacting protein from lysates using streptavidin magnetic beads (Figure 4.9: A). The results showed that ANKHD1 can bind to *in vitro* transcribed *eNOS* 3'UTR. The binding of ANKHD1 was not affected negatively by the deletion of the AUR element when using the RNA transcribed from the **ΔAUR** plasmid. This was compared with no RNA precipitation sample, which has beads and protein only, and 10% initial input. There were no bands detected in the immunoblotting from no RNA precipitation sample. In addition, the 10% initial input contains all protein lysates and showed ANKHD1 and B-actin bands. B-actin was used as a non-binder, and therefore, acts as a negative control. B-actin was not found significantly precipitated with the *eNOS* 3'UTR biotinylated RNA and no RNA sample (Figure 4.9: B); indicating that the biotinylated RNA pulldown exhibited specificity. This *in vitro* experiment revealed that ANKHD1 can bind to *eNOS* by engaging with its 3'UTR and the deletion of the canonical AUR element did not negatively impact the ability of ANKHD1 to engage with the *eNOS* mRNA. Taken together, these results identify ANKHD1 as an RNA-binding protein with a canonical binding site within the *eNOS* 3'UTR.
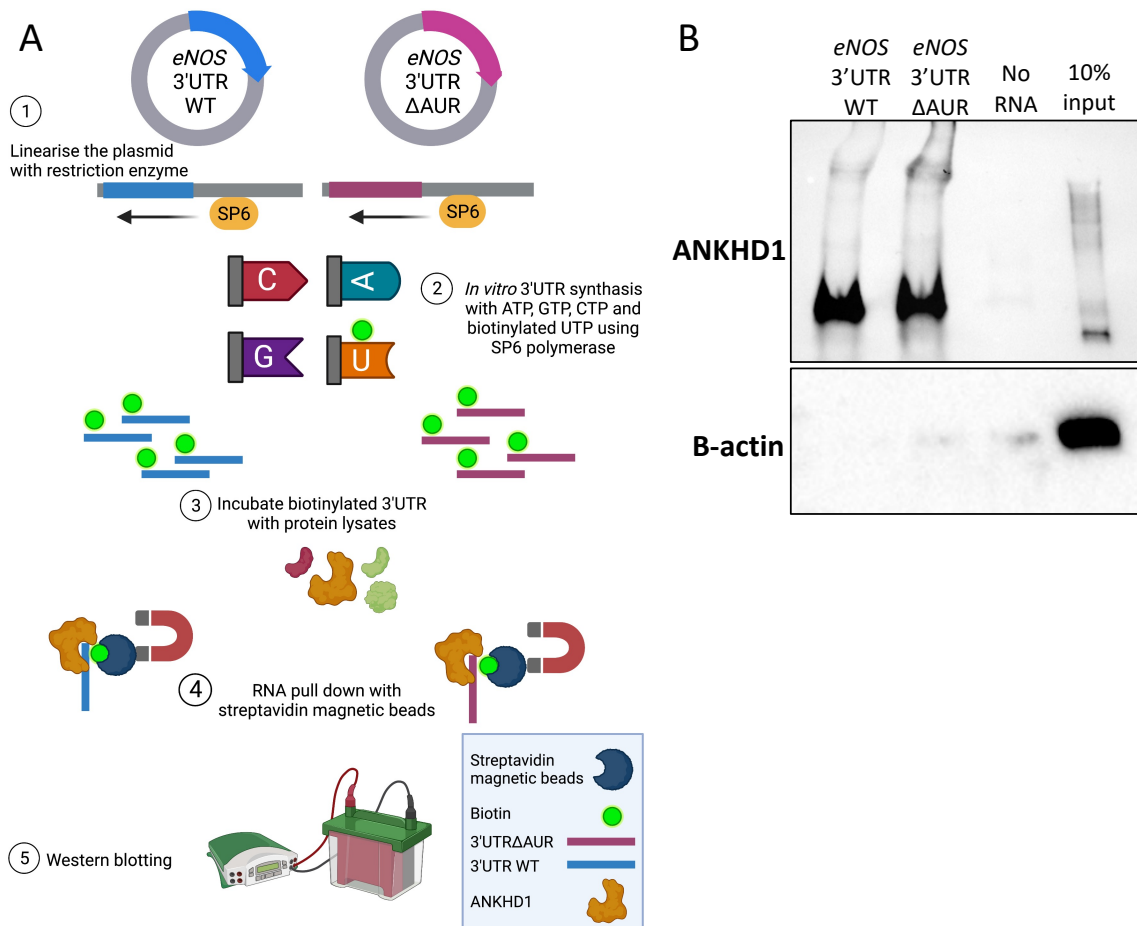
Figure 4.9. ANKHD1 binding to 3'UTR of eNOS mRNA. A schematic representation of the biotinylated 3'UTR of *eNOS* mRNA pulldown assay is shown (A). Immunoblotting of ANKHD1 and B-actin, which has been applied once, shows that ANKHD1 was precipitated with both *eNOS* 3'UTR and *eNOS* 3'UTRΔAUR, whereas B-actin was only in the initial 10% lysates (B).

4.6. Does ANKHD1 control *eNOS* and *PTGIS* transcription via KLF2?

Previous sections showed that ANKHD1 controls *eNOS* mRNA stability, via interacting with the *eNOS* 3'UTR and promoting mRNA stability. Whether ANKHD1 can additionally control the transcription of *eNOS* and *PTGIS*, especially during chronic shear stress, has not been formally tested. KLF2, which is an early HSS-induced transcription factor, is known to transcriptionally activate both *eNOS* and *PTGIS* in primary endothelial cells (Dekker et al., 2006). KLF4 is an additional transcription factor that has been shown to enhance *eNOS* expression (Zhou et al., 2012; Lu et al., 2019). Therefore, I assessed the levels of *KLF2* and *KLF4* mRNAs in ANKHD1-deficient HCAECs, to identify whether ANKHD1 can potentially control transcription of *eNOS*/*PTGIS* by altering the levels of their known transcriptional regulators, KLF2/KLF4. Compared to the control group, ANKHD1 inhibition abrogated the effects of shear stress on *KLF2* but not *KLF4* expression, suggesting that *KLF2* is under the control of ANKHD1 in different HCAEC donors (Figure 4.10: A and B). In the RNA-immunoprecipitation assay, *KLF2* mRNA was enriched in the immunoprecipitated ANKHD1 (Figure 4:10: C). These results raised the hypothesis that ANKHD1 may additionally induce *eNOS* and *PTGIS* at the level of transcription via KLF2. To examine this hypothesis, I transfected HCAECs with either non-targeting siRNA (the control siRNA), *ANKHD1*siRNA-1 or *KLF2*siRNA. The results showed that both *ANKHD1* and *KLF2* silencing were successful as it resulted in a significant reduction of *ANKHD1* mRNA (Figure 4.11: A and B) and *KLF2* mRNA (Figure 4.11: C), respectively. ANKHD1 inhibition downregulated *KLF2* mRNA, *eNOS* mRNA and *PTGIS* mRNA. Interestingly, *KLF2* inhibition has no effect on *eNOS* or *PTGIS* mRNA in HSS-stimulated HCAECs (Figure 4.11: D and E). This indicates that the positive effect of ANKHD1 on eNOS and PTGIS is KLF2-independent in chronic stimulation with HSS. This also agrees with the fact that *eNOS* mRNA is relatively stable and long-lived in ANKHD1-expressing cells. Taken together, ANKHD1 positively controls mRNA

expression of protective genes by binding to mRNA, in an AUR-independent and KLF2/KLF4-independent fashion.
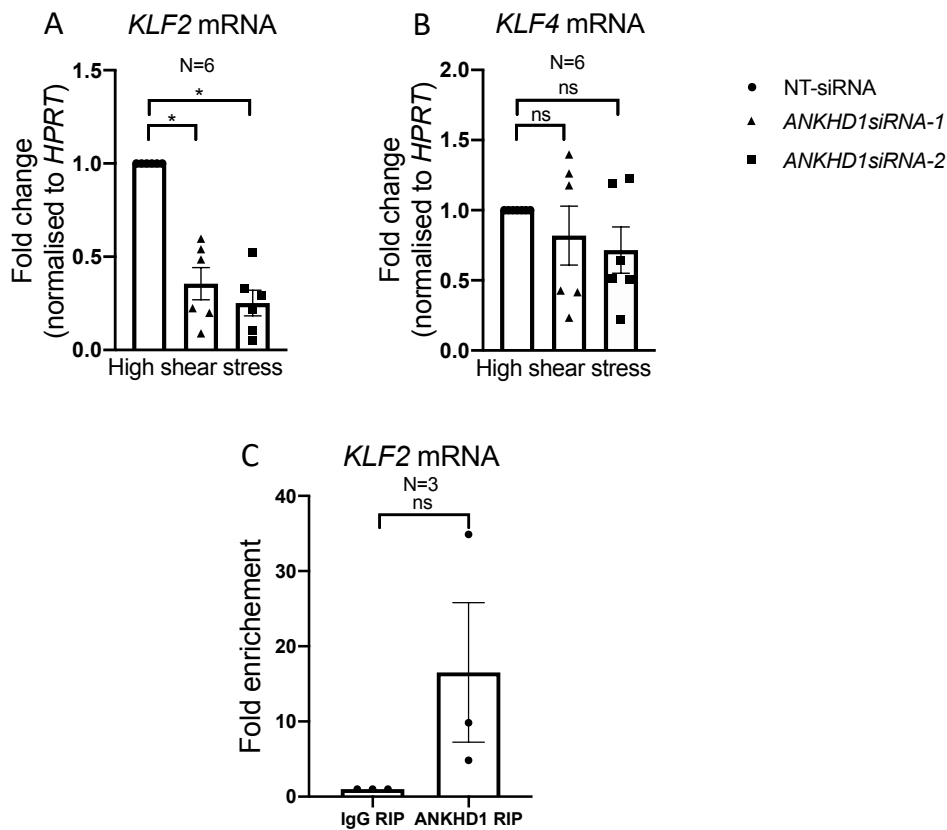
Figure 4.10. KLF2 and KLF4 mRNA expression in ANKHD1siRNA-transfected

HCAECs. Graphs show the quantification of *KLF2* mRNA (A) and *KLF4* mRNA (B) levels

in ANKHD1-deficient HCAECs stimulated with HSS using the orbital shaker system. *KLF2*

mRNA was significantly downregulated in ANKHD1-deficient cells (One-way-ANOVA

test, Dunnett's multiple comparisons test: *ANKHD1*siRNA-1: adjusted p= 0.0133 and

*ANKHD1*siRNA-2: adjusted p= 0.0130). Quantification of *KLF2* mRNA (C) fold change in

the immunoprecipitated ANKHD1 and IgG is shown. Although there was no statistical

significance in *KLF2* enrichment (Two-tailed paired t-test, p= 0.0504), an average of 16.52-

fold increase of *KLF2* mRNA binding to ANKHD1 was found when compared to IgG

control. All dots represent different biological donors and error bars show the standard error

of the mean.
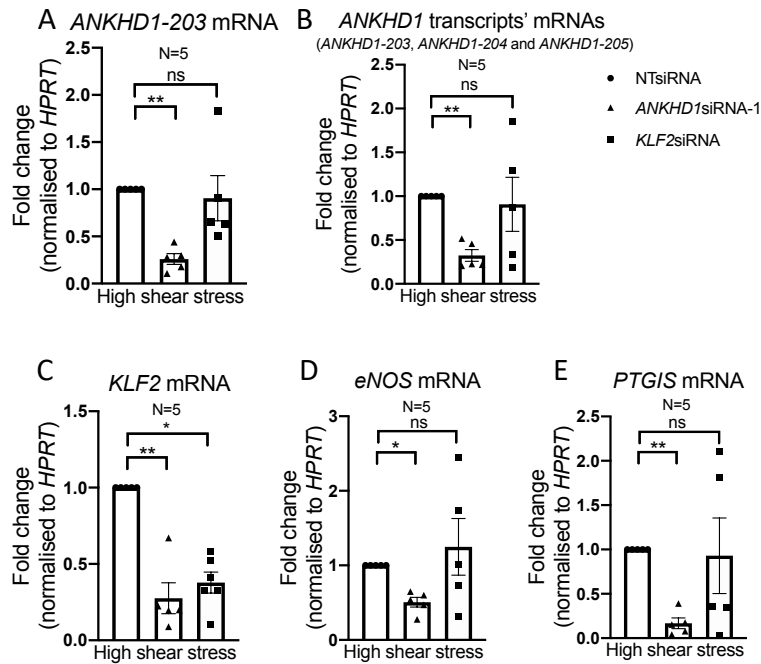
Figure 4.11. The effect of ANKHD1 and KLF2 on eNOS mRNA and PTGIS mRNA in orbited HCAECs. Quantification of the full-length and the transcript variants of *ANKHD1* mRNAs (A and B), *KLF2* mRNA (C), *eNOS* mRNA (D) and *PTGIS* mRNA (E) in control, ANKHD1-deficient or KLF2-deficient HCAECs is shown. One-way ANOVA, Dunnett's multiple comparisons test showed that: (A and B) ANKHD1 was significantly downregulated with *ANKHD1*siRNA-1 (*ANKHD1-203*: adjusted p= 0.0037; *ANKHD1* transcript variants: adjusted p= 0.0078), however, *KLF2*siRNA does not control *ANKHD1* mRNA levels. (C) *KLF2* mRNA was significantly inhibited in ANKHD1-deficient or *KLF2*-deficient HCAECs (adjusted p= 0.0094 or adjusted p= 0.0312, respectively). (D and E) *eNOS* mRNA and *PTGIS* mRNA were significantly downregulated via *ANKHD1*siRNA-1 (adjusted p= 0.0231 and adjusted p= 0.0088, respectively). However, *KLF2*siRNA did not inhibit *eNOS* and *PTGIS* expression significantly in HSS-stimulated HCAECs. All mRNAs were normalised to the housekeeper *HPRT*. All dots represent different biological donors and error bars show the standard error of the mean.

4.7. Discussion

This chapter provides strong mechanistic evidence that ANKHD1 provides vasoprotection at the cellular level via controlling three significant downstream effectors of protective shear stress, namely the vasoprotective molecules eNOS, KLF2 and PTGIS. ANKHD1 controlled the vasorelaxant and vasoprotective *eNOS* and *PTGIS* at the mRNA level leading to an accumulation of eNOS/PTGIS protein, which is the functional unit of these genes, under atheroprotective shear stress in primary human endothelial cells and mouse descending aortas. eNOS protein level was reduced in endothelial cells with low ANKHD1 levels, for example, when *ANKHD1* was silenced with siRNA or when ANKHD1 is naturally low (i.e., cells exposed to low shear stress conditions). Mechanistically, ANKHD1 stabilises *eNOS* mRNA and binds to an *in vitro* transcribed 3'UTR of *eNOS* without requiring the AUR element, suggesting that its interaction with *eNOS* may not require facilitation by AUR element binding proteins.

4.7.1. ANKHD1 controls the major vasoprotective modulators – eNOS / PTGIS

In this chapter, I have examined the role of ANKHD1 in positively controlling the vasoprotective eNOS expression and activation. The pathway by which NO is produced is controlled by the mechanosensor glycocalyx (Ebong et al., 2014; Zeng and Liu, 2016; Mahmoud et al., 2021; Bartosch et al., 2021). As mentioned, a major protein of the glycocalyx, which is glypican 1, promotes functional endothelial cells by enhancing NO and PGI_2 release via PECAM-1 phosphorylation; leading to vasodilation and inhibition of inflammation (Russell-Puleri et al., 2017; Ebong et al., 2014; Bartosch et al., 2021). Moreover, *glypican 1* knockout mice were found to be unable to produce NO under physiological HSS (Bartosch et al., 2021). In addition, glypican 1 was found to be needed to maintain vascular elasticity and avoid stiffness in older cells (Mahmoud et al., 2021). Previously published work, therefore,

highlights the critical importance of glypican-1, a protein regulated by ANKHD1, in maintaining vascular protection. It remains to be studied whether the effect of ANKHD1 on *eNOS* mRNA protection is dependent on an intact glycocalyx possibly via glycocalyx/glypican 1 communicating intracellularly to activate c-Src/AKT to maintain NO production. However, it is reported that the glycocalyx morphology and thickness are negatively impacted in cultured endothelial cells in static conditions (Chappell et al., 2009). Given the fact that I have performed the RIP assays (interactions between ANKHD1 and eNOS/PTGIS/KLF2) in cells in static conditions it is more likely that any effects of ANKHD1 are likely to be direct but interactions with glypican 1 cannot be formally excluded.

In addition, VE-cadherin, a junctional adhesion molecule transducing shear stress signal to enhance NO production, has been shown to be negatively regulated by ANKHD1 in HSS-stimulated HCAECs (RNA sequencing). However, in HUVECs stimulated with HSS, ANKHD1 showed to positively regulates VE-cadherin (Figure 5.6: F). This discrepancy can be attributed to different cellular origins (artery/vein) or different genetic backgrounds.

Russell-Puleri et al. (2017) identified that HSS upregulates PGI_2 production. According to Yokoyama et al. (1996), the *PTGIS* gene sequence has a shear stress responsive sequence (GAGACC), but whether it can directly respond to different shear stress magnitudes (low vs high shear stress) and also respond to chronic flow has not been examined. This chapter shows that chronic HSS (72 hours) positively controls *PTGIS* expression. Moreover, in this chapter, I identify an increase of PTGIS under the HSS condition, which is one of the mechanisms employed by ANKHD1 to protect primary human endothelial cells. The requirement of ANKHD1 for *PTGIS* expression suggests that ANKHD1 is needed for the production of the vasorelaxant PGI_2. Since PTGIS is a required enzyme in the conversion of lipid membrane-derived arachidonic acid into the vasoprotective mediator PGI_2, it follows that in the absence of ANKHD1, PGI_2 production is defective.

4.7.2. Potential mechanisms for eNOS mRNA stability

Research has shown that *eNOS* mRNA can be maintained by the binding of proteins into the CU-rich stability element of *eNOS* which is present in its 3'UTR (Ho et al., 2013). Yet how shear stress controls the stability of *eNOS* is largely unknown, despite its important role. Here I find that (1) inhibition of ANKHD1 in human endothelial cells reduces *eNOS* mRNA stability (2) ANKHD1 can bind to the 3' UTR of *eNOS* mRNA and finally (3) the positive regulation of ANKHD1 on *eNOS* is KLF2 independent.

The presence of the highly conserved AUR element in the 3'UTR of *eNOS* suggests that *eNOS* could be under the control of AUR element-mediated decay, yet *eNOS* mRNA is long-lived, suggesting the presence of a protective protein/factor. It has been identified by Lai et al. (1999) that the AUR element is recognised by the RNA-degrading protein TTP and results in mRNA degradation. ANKHD1 binds to *eNOS* 3'UTR at a region close to the AUR element but it does not overlap with the AUR element. This suggests that ANKHD1 does not directly interact with the AUR element-binding proteins. However, this does not exclude the possibility of inhibiting AUR element-mediated decay indirectly. ANKHD1 might bind to *eNOS* mRNA and mask the nearby AUR element or alternatively move the mRNA away from active sites of RNA degradation.

Two bands of ANKHD1 appeared at the biotinylated 3'UTR pull-down assay, one was above the 250 kDa and the other was around 60 kDa (Figure 5.13: B). The 60 kDa ANKHD1 could be due to alternative splice forms and/or proteolytic processing of the ANKHD1 protein. Interestingly, ANKHD1 was precipitated more with *eNOS*-3'UTRΔAUR when compared with the *eNOS*-3'UTR-WT. *eNOS*-3'UTRΔAUR could be more stable as it lacks the AUR element when compared to the WT and hence the increased binding could be due to more available RNA. This model would support the hypothesis that *eNOS* mRNA is usually under the control of AUR element-mediated decay, but this decay might be blocked in high shear by the actions

of ANKHD1. Furthermore, the RNA-sequencing approach in the healthy endothelium showed that ANKHD1 upregulates p38/MAPK via regulating *MAPK11* and *MAPK12* genes. Mahtani et al. (2001) identified that phosphorylation of TTP via p38 resulted in TTP inactivation; thus, enhancing mRNA stability. Inactivation of TTP indirectly could provide another protective mechanism utilised by ANKHD1 to confer vascular protection and enhance eNOS activity. Taking together, the findings of this chapter support the hypothesis that ANKHD1 promotes *eNOS* mRNA stability in healthy endothelium by binding to its 3'UTR but without excluding the possibility of additional protective pathways.

4.7.3. Potential roles of ANKHD1 in regulating KLF2 in healthy endothelium

SenBanerjee et al. (2004) overexpressed KLF2 in static-HUVECs and identified that KLF2 upregulates *eNOS* expression. Dekker et al. (2006) overexpressed KLF2 in static HUVECs and showed that KLF2 upregulates *eNOS* and *PTGIS* mRNAs. Because silencing of *ANKHD1* in HSS-stimulated HCAECs downregulated *KLF2*, *eNOS* and *PTGIS* mRNAs significantly, the possibility of whether ANKHD1 controls *eNOS* and *PTGIS* via KLF2-mediated transcription had to be examined. However, in contrast with previously published work, *KLF2* silencing in HSS-stimulated cells did not cause the expected reduction of *eNOS* and *PTGIS* mRNAs. These data suggest that the effect of ANKHD1 on *eNOS* and *PTGIS* is KLF2-independent in the HSS conditions.

ANKHD1 could control *KLF2* at mRNA levels possibly by binding, this was confirmed in my work using the RIP assay. KLF2 is an antithrombotic and anti-inflammatory transcription factor. Its upregulation increased the clotting time whereas KLF2 inhibition induces a prothrombotic phenotype by accelerating clotting at a short time and elevating *F3* expression (Lin et al., 2005). KLF2 inhibits the activation of the proinflammatory adhesion molecules CD62E and VCAM-1 via inhibiting NFκB. This has been associated with a reduction of the

inflammatory T-cells adhesion and rolling (SenBanerjee et al., 2004; Lin et al., 2005; Parmar et al., 2006). Therefore, KLF2 has been studied in the context of atherosclerosis, where Atkins et al. (2008) identified that *Klf2*-deficient mice with *ApoE*$^{-/-}$ background had accelerated foam cell formation and inflammatory cell infiltration into the vessel wall, and as such, increased atherosclerotic lesion sizes when compared to *Klf2*$^{+/+}$ *ApoE*$^{-/-}$ mice. It is currently unknown whether ANKHD1 attenuates inflammation, thrombosis and atherosclerosis via KLF2 and/or redox system regulation or whether additional mechanisms are at play. The mechanism by which ANKHD1 controls inflammation has not yet been explored, but I hypothesize that ANKHD1-mediated KLF2 expression may be an important driver.

Summary

This chapter describes some of the mechanisms utilised by ANKHD1 to exert its cytoprotective functions. Using an advanced mechanistic approach, ANKHD1 promotes *eNOS, PTGIS* and *KLF2* levels which raised the question of whether ANKHD1 contributes to vasoprotection and atheroprotection. This is going to be investigated in the next chapter. In the future, it would be valuable to study further the anti-inflammatory effects, for example, of ANKHD1 and the possible involvement of KLF2.

Chapter 5: Identification of ANKHD1 functions in murine aortas

5.1. Outlines

5.2. *Ankhd1* mouse models

5.3. The influence of ANKHD1 on murine aortas

5.3.1.   ANKHD1 controls aortic diameters

5.3.2.   The influence of ANKHD1 on thrombosis

5.3.3.   ANKHD1 role in inflammation

5.3.4.   ANKHD1 controls endothelial cell numbers

5.4. ANKHD1 role in atherosclerosis

5.5. Discussion

5.5.1.   Evaluation of systemic risk factor for atherosclerosis in Ankhd1 mouse models

5.5.2.   The influence of ANKHD1 on aortic diameter

5.5.3.   ANKHD1 protects from thrombosis

5.5.4.   ANKHD1 might prevent leukocyte adhesion and infiltration

5.5.5.   ANKHD1 controls endothelial cell number

5.5.6.   ANKHD1 provides atheroprotection

5.1. Outlines

Results presented in the previous two chapters show that ANKHD1 is highly expressed in vascular endothelial cells in mouse aortas and primary human endothelial cells. ANKHD1 was upregulated in the HSS condition, and it was predicted to be a regulator of major shear stress and atherosclerosis pathways including NO and PGI_2. ANKHD1 showed to regulate the vasoprotective *eNOS*, *PTGIS* and *KLF2* in endothelial cells. Previous studies showed that inhibition of these vasoprotective molecules resulted in inflammation, thrombosis and accelerated atherosclerosis (RadomskiPalmer and Moncada, 1987; Yokoyama et al., 2002; Lin et al., 2005; Atkins et al., 2008; Ponnuswamy et al., 2012). These observations raised the question of whether ANKHD1 promotes endothelial-dependent vasoprotection. Specifically, I decided to examine vasoactivity, inflammation and thrombosis. It is important to assess the potential role of ANKHD1 in vasoprotection and atheroprotection *in vivo* using mouse aortas as simpler cellular-based models do not fully recapitulate the complexity of the disease. As such, in this chapter, I present my analysis showing the role of ANKHD1 in ANKHD1 loss-of-function mouse models with and without atherosclerosis.

Hypothesis: Since ANKHD1 is capable of suppressing inflammatory genes and activating antioxidant and vasoprotective ones, I hypothesize that ANKHD1 is a vasoprotective RNA-binding protein, and as such, its inhibition is predicted to result in endothelial dysfunction and atherosclerosis.

The specific aims of this chapter are:

Considering that endothelial cells can control vascular functions, the main aims of this chapter are to study ANKHD1 functions in the mouse vasculature by:

1. Assessing whether *Ankhd1* deletion alters the levels of systemic risk factors of cardiovascular dysfunction (e.g., body weight, hypertension, hypercholesterolemia, and hyperglycaemia).

2. Characterising the effect of *Ankhd1* deletion in mouse aortas (macroscopically).

3. Assessing whether *Ankhd1* deletion results in endothelial dysfunction (microscopically – markers of the disease).

4. Studying whether *Ankhd1* deletion accelerates atherosclerosis development.

To find the answers I used *Ankhd1$^{+/+}$, Ankhd1$^{+/-}$* and *Ankhd1$^{-/-}$* mouse models (*in vivo* models), I statically analysed the data, and discussed the potential importance of these findings in this chapter.

5.2. *Ankhd1* mouse models

In this study, I used c57bl6N mice that were either wild-type for *Ankhd1* (*Ankhd1$^{+/+}$*), heterozygotes or homozygote knockouts (*Ankhd1$^{+/-}$* or *Ankhd1$^{-/-}$*). All these mice underwent genotyping with gene-specific primers in our lab. The expression of ANKHD1 was confirmed by *en-face* staining of the endothelial cells of the descending aortas using an anti-ANKHD1 primary antibody, which was previously verified in western blotting with siRNA and in *en-face* staining (Chapter 3: Figure 3.1: B and D). The endothelial cell layer was identified by staining the aorta with a specific marker expressed highly in endothelial cells, PECAM-1, also known as CD31. CD31 is a cell-cell adhesion protein that responds to the shear stress and transduces signals to the endothelial cells (Tzima et al., 2005) and here it is used as a marker of endothelial cells within the aorta, while TO-PRO was used as a nuclear counterstain.

Quantification of the *en-face* staining revealed that the highest concentration of ANKHD1 was found in the endothelial cells of *Ankhd1$^{+/+}$* mice (N= 17), with little expression seen in the endothelium of mice with *Ankhd1$^{+/-}$* (N= 4) or *Ankhd1$^{-/-}$* (N= 14) (Figure 5.1). This verified firstly the genotyping approach, secondly, ANKHD1 is highly expressed in murine aortas and thirdly the antibody I used to detect ANKHD1 is specific in this assay, as the knockouts show significantly reduced ANKHD1 expression.
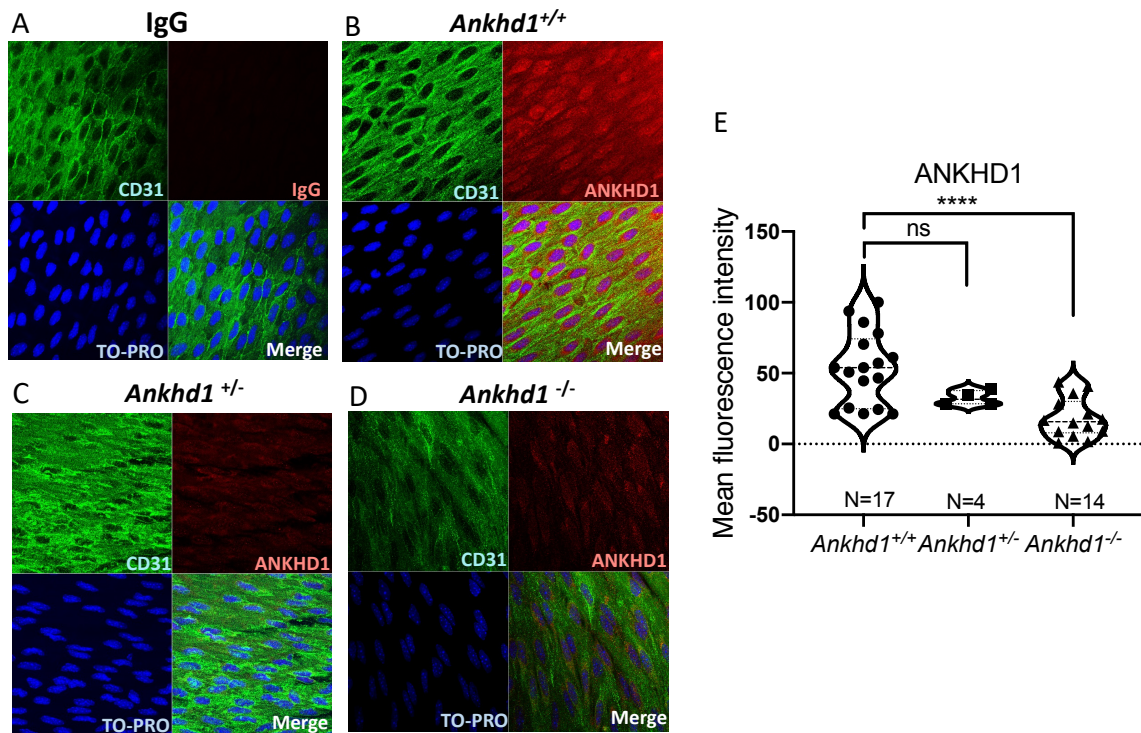
Figure 5.1. ANKHD1 levels in endothelial cells of Ankhd1$^{+/+}$, Ankhd1$^{+/-}$ and Ankhd1$^{-/-}$ mouse descending aortas. A representative image (negative control) of murine aortic endothelial cells of *Ankhd1$^{+/+}$* mice stained with isotype control rabbit IgG (red), and counterstained with the endothelial marker CD31 (green) and the nuclear dye TO-PRO (blue) is shown (A). Representative images of endothelial cells stained with ANKHD1 antibodies (red), CD31 (green) and TO-PRO (blue) in *Ankhd1$^{+/+}$*, *Ankhd1$^{+/-}$* and *Ankhd1$^{-/-}$* are shown (B–D). The *en-face* staining images were taken from all mice (three images/mouse) in this study to quantify the mean fluorescence intensity (The biological replicates used for IgG were N=4, *Ankhd1$^{+/+}$* were N=17, *Ankhd1$^{+/-}$* were N=4 and *Ankhd1$^{-/-}$* were N=14). The mean fluorescence intensity was determined for all groups (*Ankhd1$^{+/+}$, Ankhd1$^{+/-}$* or *Ankhd1$^{-/-}$*) and is shown as a violin chart (E). Mice with *Ankhd1$^{-/-}$* had significantly lower ANKHD1 concentrations than mice with *Ankhd1$^{+/+}$* (Two-tailed one-way ANOVA test, Dunnett's multiple comparisons test: adjusted *p<0.0001*).

None of the mice analysed (N= 35) show any severe illnesses. To better understand their phenotype, I examined a number of blood parameters. They did not show any differences in their blood glucose levels (Figure 5.2: A). Blood pressure tends to increase in $Ankhd1^{+/-}$ mice when compared to $Ankhd1^{+/+}$ mice, however, that increase is not statistically significant. Measuring blood pressure in more $Ankhd1$ mice will give a clear insight into whether ANKHD1 affects blood pressure (Figure 5.2: B). Additionally, $Ankhd1^{+/+}$ and $Ankhd1^{-/-}$ mice did not exhibit a statistically significant change in heart rate (Figure 5.2: C), body weight (Figure 5.3: C) and their cholesterol levels were below the detection threshold (less than 2.59 mmol/L). This means that the deletion of $Ankhd1$ does not greatly alter the risk factors associated with accelerated atherosclerosis, such as diabetes, hypertension, obesity and hypercholesterolemia. It is, therefore, deduced that any effects that the deletion of $Ankhd1$ may have on the vascular function would be due to the alterations of the function of the vasculature and not due to systemic changes.
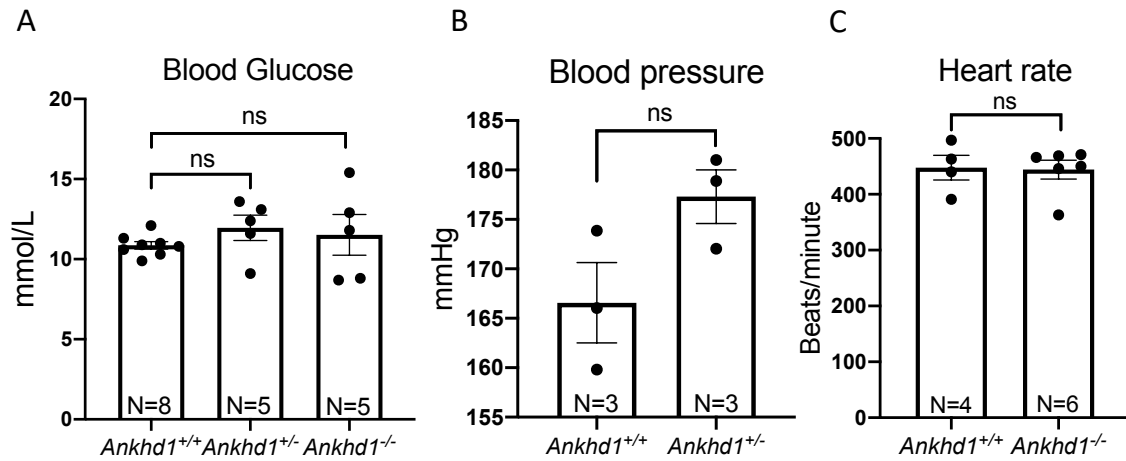
Figure 5.2. Blood glucose levels, blood pressure and heart rate measurements in Ankhd1^{+/+}, Ankhd1^{+/-} and Ankhd1^{-/-} mice. The glucose level was measured from mouse blood using a glucometer and it was found to be relatively similar between the different groups of mice (two-tailed one-way ANOVA, Dunnett's multiple comparisons test: $p>0.05$) (A). Blood pressure (B) and heart rate (C) were measured by non-invasive tail cuff and echocardiography, respectively. There were no significant differences in blood pressure and heart rate between the mouse groups (two-tailed unpaired t-test: $p>0.05$). All dots represent different animals and error bars show the standard error of the mean.

5.3. The influence of ANKHD1 on murine aortas

Since ANKHD1 controls *eNOS*, *PTGIS* and *KLF2* which modulate vascular tone, inflammation and thrombosis, and the RNA sequencing suggested that ANKHD1 can control these important functions in primary human endothelial cells, the aim of this section is to identify whether the deletion of *Ankhd1* may affect any of these vascular phenotypes in aortas of mice with ANKHD1-deficiency (*Ankhd1*$^{-/-}$) when compared with wild-type littermate control mice. Mice were divided into four groups based on age: adult [5 months old] and young [4–5 weeks old], and on genotype: *Ankhd1* wild-type [*Ankhd1*$^{+/+}$; control group] and *Ankhd1* knockout [*Ankhd1*$^{-/-}$; experimental group].

5.3.1. ANKHD1 *controls aortic diameters*

Extracted aortas were macroscopically inspected, a narrower appearance was noted in *Ankhd1*$^{-/-}$ mice when compared with aortas from wild-type littermate controls (Figure 5.3: A). This visual difference was quantified by ImageJ using 20 regions throughout the aortas and it was found that aortas from *Ankhd1*$^{-/-}$ 5-month-old mice (older) were on average 0.8343 mm in diameter while aortas from age-matched *Ankhd1*$^{+/+}$ mice were on average 0.9318 mm in diameter (Figure 5.3: B). This difference in aortic diameter conferred by the genotype (due to the deletion of *Ankhd1*) was statistically significant. Next, I compared body weights to determine whether (1) they differed between the experimental and the control groups and (2) whether they were responsible for the varying aortic diameters. However, there was no significant difference between the experimental and the control groups in body weights that could account for the differences in aortic diameters (Figure 5.3: C), suggesting that ANKHD1 does not control vessel diameters by influencing body weights. Moreover, the fact that the wild-type and the knockout mice are of similar weights excludes obesity as a driver of disease, which is a systemic risk factor for atherosclerosis progression. An alternative hypothesis is that

ANKHD1 may be directly influencing vasoactivity. Given that increased age can also drive endothelial dysfunction (Mahmoud et al., 2021), I also studied young mice, at the time of weaning (4 weeks of age), to examine the potential contribution of aging. While I only have two *Ankhd1*^{-/-} mice, there is a clear trend towards reduced vessel diameters in *Ankhd1*^{-/-} mice when compared with age-matched young wild-type littermate controls (Figure 5.3: D). These data together identify for the first time that ANKHD1 positively controls the diameter of the aorta in both young and older mice, while knocking out this gene results in the narrowing of the large blood vessel from a younger age. Since the narrowing of blood vessels could lead to a number of events this is an interesting observation that I decided to follow up.
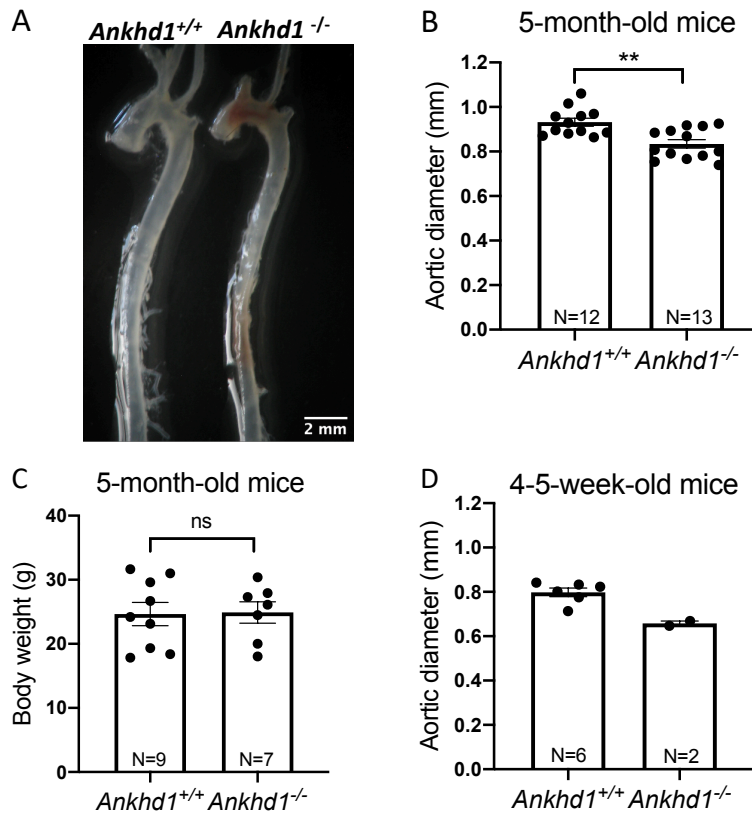
Figure 5.3. Aortic diameter and body weight measurements in young and adult Ankhd1 mouse models. A comparison of dissected aortas from 5-month-old mice in the control and the experimental groups is shown (A). The effects of ANKHD1 on the aortas of adult mice (5-month-old) were quantified. Mice with *Ankhd1*$^{+/+}$ (control group) had significantly wider aortas than those with *Ankhd1*$^{-/-}$ (experimental group), (two-tailed unpaired t-test: *p*= 0.0011), (B). The body weights (in grams) of 5-month-old mice were not statistically significant (two-tailed unpaired t-test: *p*> 0.05) (C). The effects of ANKHD1 on the aortas of young mice (4-5-week-old) were quantified. The control group tended to have wider aortas than the experimental group (D). All dots represent different animals and error bars show the standard error of the mean.

5.3.2. The influence of ANKHD1 on thrombosis

Macroscopic inspection of the extracted aortas was performed in *Ankhd1* mouse models. Thrombosis has been recognised consistently in the aortas of *Ankhd1$^{-/-}$* mice, mainly in the aortic arch, which colocalises with LSS areas that are more prone to disease development. Figure 5.4: A and B, show *Ankhd1$^{+/+}$* and *Ankhd1$^{-/-}$* aortas dissected at different times from different batches of mice. *Ankhd1$^{-/-}$* aortas exhibited signs that were consistent with blood clotting. The area of clotting was noted both within the arch and the descending aortas. Clotting was not observed in any wild-type age- and gender-matched littermate controls studied here. This raises the interest to further investigate the role of ANKHD1 in haemostasis. Previous work in our lab (RNA sequencing of epithelial cells) identified that ANKHD1 controls the coagulation factor *F3* mRNA expression and ANKHD1 inhibition enhanced pro-inflammatory pathways, including NFκB activation and the transcription factor AP-1, which were also identified in RNA-sequencing data from HCAECs. Parry and Mackman (1995) identified that NFκB and AP-1 are transcription factors that enhance *F3* expression. In addition, KLF2 has been shown to downregulate *F3* expression (Lin et al., 2005). Therefore, I examined variant 1 (NM_001993.5, the full-length transcript) of *F3* mRNA expression in HSS-induced HCAECs transfected with either non-targeting siRNA (NT-siRNA) or *ANKHD1*siRNA-1 via qPCR. The qPCR results showed that there was a clear trend toward increased expression of *F3* mRNA in *ANKHD1*-silenced HCAECs stimulated with HSS (Figure 5.4: C). This increase was statistically significant; indicating that ANKHD1 controls the full-length *F3* expression in HCAECs. However, a high level of variability was noted, which may be explained by differences due to donor variability (e.g., different genetics). Single nucleotide polymorphisms in *F3* have been reported to lead to altered *F3* mRNA expression (Mälarstig et al., 2005). Moreover, *F3* is upregulated by inflammation, and therefore, it is expected to have variable expression given the level of inflammatory activation present within each different experiment

(Parry and Mackman, 1995). Taken together, ANKHD1 loss-of-function leads to enhanced

blood clotting and elevated *F3* mRNA expression.

A *Ankhd1+/+* aorta **B** *Ankhd1-/-* aortas

5-month-old mice

Body weight (g)

C *F3* mRNA

- ● NT-siRNA HSS
- ▲ ANKHD1siRNA-1 HSS
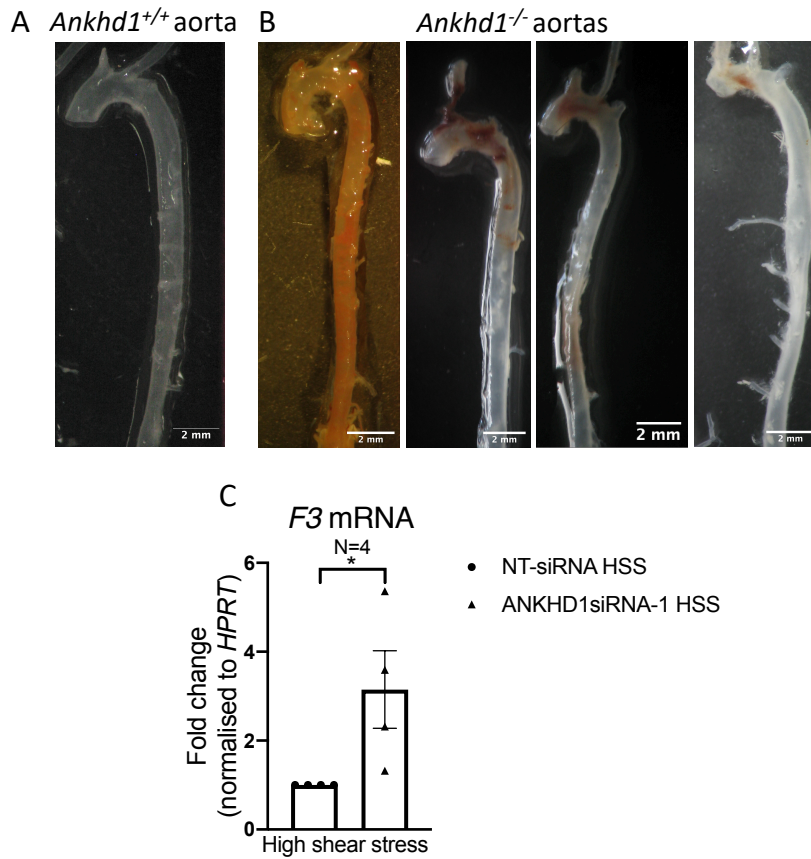
Figure 5.4. Thrombosis studies in Ankhd1-/- aortas and ANKHD1-deficient HCAECs.
Microscopic images of *Ankhd1+/+* (A) and *Ankhd1-/-* (B) aortas show blood clots in the
aortas of mice with *Ankhd1-/-* only. Quantification of *F3* mRNA transcript variant 1 (C) in
NT-siRNA and *ANKHD1*siRNA-1 transfected-HCAECs under HSS condition showed
that *F3* is significantly increased in ANKHD1-deficient cells (two-tailed paired t-test: *p =*
0.0425). mRNA was normalised to the housekeeper *HPRT*. All dots represent different
biological donors and error bars show the standard error of the mean.

5.3.3. ANKHD1 role in inflammation

Inflammation was one of the highly enriched pathways revealed by RNA-sequencing of *ANKHD1*-silenced HCAECs in HSS conditions. Specifically, I validated that endothelial cells with ANKHD1 loss-of-function have elevated *IL1β* and *ICAM-1* mRNA production. NFκB signalling is not only responsible for elevated IL1 β/ICAM-1 but also results in *CD62E* upregulation and protein activation; in turn, leading to leukocyte adhesion and infiltration (Hiscott et al., 1993; Collins et al., 1995; Kiely et al., 2003). Therefore, I assessed the levels and localisation of CD62E in endothelial cells of *Ankhd1*$^{+/+}$ and *Ankhd1*$^{-/-}$ mouse descending aortas. Two validated antibodies were used to stain for CD62E*:* i) CD62E (ab18981 from Abcam) (Figure 5.5.: A-C) and ii) CD62E (NBP1-45545 from Novus) (Figure 5.5: D-F). Staining with either antibody shows that, in *Ankhd1*$^{+/+}$ endothelial cells, there are low levels of CD62E, which is predominantly perinuclear (Figure 5.5: A and D), whereas *Ankhd1*$^{-/-}$ cells have redistributed CD62E into large puncta accompanied with intercellular gaps (Figure 5.5: B and E). It has been reported by Kiely (2003) that when CD62E is activated, it is redistributed into large puncta; suggesting that ANKHD1 has a role in CD62E activity and vascular permeability, and thus, validating the anti-inflammatory phenotype identified by the unbiased RNA-sequencing. Apart from CD62E activation, CD62E protein level was elevated in *Ankhd1*$^{-/-}$ mice when compared to *Ankhd1*$^{+/+}$ (Figure 5.5: C and F), quantified by mean fluorescence intensity. This increase was statistically significant in tissues stained with the CD62E antibody from Abcam as the numbers of animals were sufficient to show the difference. Taken together, these data show that ANKHD1 controls CD62E activation and localisation/distribution within the mouse vasculature, suggesting an anti-inflammatory role for ANKHD1 that is likely to involve IL1β/NFκB and a number of adhesion molecules, including CD62E that was analysed here.
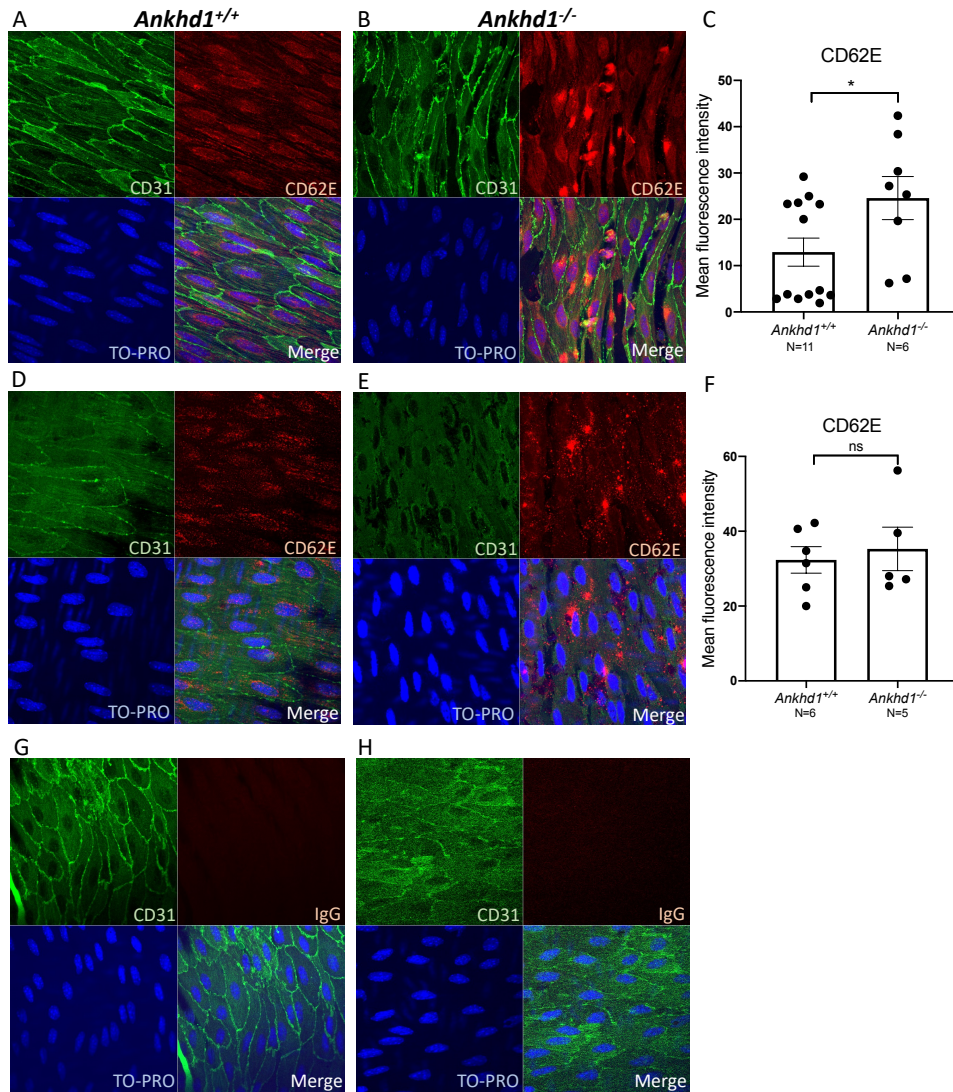
Figure 5.5. CD62E expression and distribution in endothelial cells of Ankhd1$^{+/+}$ and Ankhd1$^{-/-}$ mouse descending aortas. CD62E staining and mean fluorescence intensity quantification from either Abcam antibody (A-C) or Novus antibody (D-F) stained tissues are shown. IgG isotype staining in Ankhd1$^{+/+}$ (G) and Ankhd1$^{-/-}$ (H) tissues showed the specificity of both CD62E antibodies. The *en-face* staining images were taken from Ankhd1$^{+/+}$ and Ankhd1$^{-/-}$ mice (three images/mouse) to quantify the mean fluorescence intensity (The biological replicates used for IgG were N=4, Ankhd1$^{+/+}$ were N=11 (Abcam) and N=6 (Novus), and Ankhd1$^{-/-}$ were N=6 (Abcam) and N=5 (Novus). The data quantified in (C) showed that there was a significant increase in CD62E expression in Ankhd1$^{-/-}$

endothelial cells (two-tailed unpaired t-test: p= 0.0193). However, the differences in CD62E expression in (F) were not statistically significant (p>0.05). All dots represent different animals and error bars show standard error of the mean.

5.3.4. *ANKHD1 controls endothelial cell numbers*

One of the key drivers of thrombus formation and atherogenesis is endothelial cell loss, which can be triggered by tissue damage leading to endothelial cell apoptosis and denudation (CaroFitz-Gerald and Schroter, 1971; Durand et al., 2004). I have observed large gaps in the endothelium in knockout animals. To examine whether ANKHD1-deficiency alters the endothelial cell coverage, extracted aortas were microscopically inspected at the endothelial cell level. It was consistently recognised that, in *Ankhd1$^{-/-}$* aortas, there were significantly lower numbers of endothelial cells. Therefore, I quantified the numbers of endothelial cells per field of view using ImageJ. I took the average of at least five images of endothelial cell numbers per animal using the descending aorta, as this is a region of HSS with high expression of ANKHD1 and generally protected from endothelial cell loss. The results showed that *Ankhd1$^{-/-}$* mice have on average 19 cells per field of view whereeases *Ankhd1$^{+/+}$* mice have on average 25 cells per field of view. This difference in the endothelial cell numbers was statistically significant (Figure 5.6: A and B); indicating that ANKHD1-deficiency results in reduced endothelial cell numbers. It is unknown how ANKHD1 controls endothelial cell numbers. Apart from endothelial cell numbers, I examined the cell junctions of endothelial cells. I found that there was a tendency towards uneven and undefined endothelial cell junction and perhaps endothelial cell loss in *Ankhd1$^{-/-}$* mice when compared to *Ankhd1$^{+/+}$* (Figure 5.6: A and C).
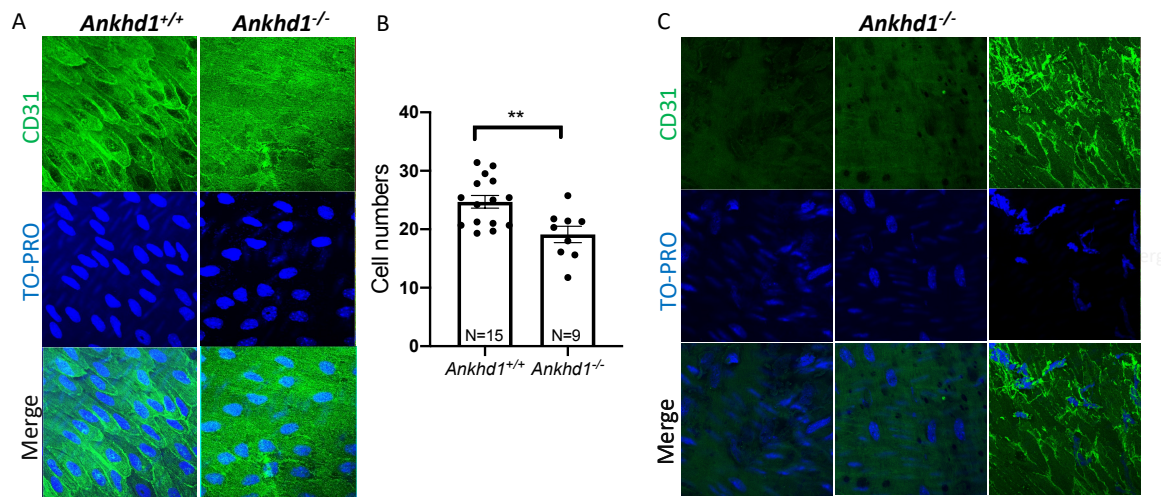
Figure 5.6. ANKHD1 affects endothelial cell numbers. Endothelial cells in the descending aortas of *Ankhd1*$^{+/+}$ and *Ankhd1*$^{-/-}$ were stained with CD31 antibody and TO-PRO (A). The *en-face* staining images were taken from all mice (three images/mouse) in this study to quantify cell numbers (The biological replicates used for *Ankhd1*$^{+/+}$ were N=15 and *Ankhd1*$^{-/-}$ were N=9). The difference in endothelial cell number in *Ankhd1* mouse was statistically significant (two-tailed unpaired t-test: *p*= 0.0044) (B). Signs of endothelial cell loss and uneven junctions in the descending aortas of *Ankhd1*$^{-/-}$ mice, images were taken from three biological replicates (C). All dots represent different animals and error bars show standard error of the mean.

5.4. ANKHD1 role in atherosclerosis

Finally, given that endothelial ANKHD1 is highly expressed in areas protected from atherosclerosis (Section 3.6; Figure 3.7), controls shear stress protective pathways in primary human coronary artery endothelial cells, and limits inflammation *in vivo* (Section 5.3.3; Figure 5.5), I wished to study whether lowering ANKHD1 may promote accelerated progression of atherosclerosis. Atherosclerosis develops as a chronic progressive plaque comprising accumulated lipids and different inflammatory cells in the arterial walls.

Mice with *Ankhd1$^{+/+}$*, *Ankhd1$^{+/-}$* and *Ankhd1$^{-/-}$* were virally transduced with a single tail-vain injection of PCSK9-AAV and administered a high-fat diet for 12 weeks to induce atherosclerosis. After aorta microdissection, Oil red O staining was used to stain lesions/lipid content in the three groups of mice with atherosclerosis (PCSK9-AAV). Then, the lesion size was quantified using the software Nis-elements BR. There was a significant increase in plaque size in *Ankhd1$^{+/-}$* mice when compared with *Ankhd1$^{+/+}$* (Figure 5.7: A-D). Although the N numbers of these animals are insufficient, *Ankhd1$^{+/+}$* mice (N = 5) had the smallest lesion sizes compared to *Ankhd1$^{-/-}$* mice (N = 7), but this was not statistically significant. Quantification of lesion sizes in the aortic roots also showed larger plaques in *Ankhd1$^{+/-}$* (N=3) compared to the *Ankhd1$^{+/+}$* (N=3) (Figure 5.7: E-G).

Taken together, the data presented here clearly indicate that ANKHD1 can protect from high fat and high cholesterol driven atherosclerosis development while lowering ANKHD1 expression is sufficient to promote increased atherogenesis (i.e., *Ankhd1$^{+/-}$*). This can be attributed to the anti-thrombotic and anti-inflammatory phenotype of ANKHD1.
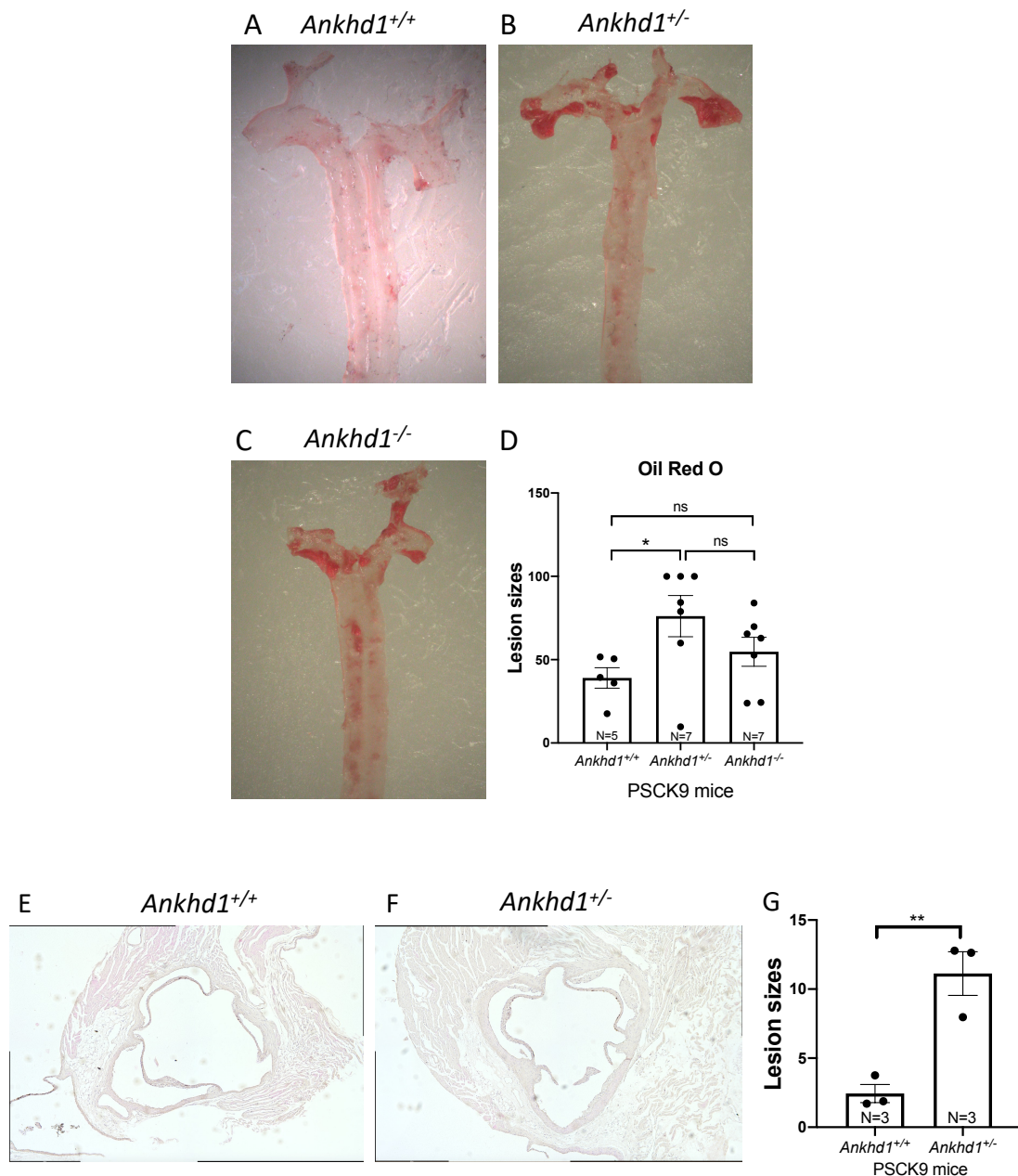
Figure 5.7. Oil red O and haematoxylin and eosin staining of plaques in Ankhd1 mice with atherosclerosis. Representative images of oil red O (red) lesions in the aortas of *Ankhd1*$^{+/+}$ (A), *Ankhd1*$^{+/-}$ (B) and *Ankhd1*$^{-/-}$ mice (C) are shown. Plaque sizes quantification in *Ankhd1* murine aortas showed that the differences were statistically significant between *Ankhd1*$^{+/+}$ and *Ankhd1*$^{+/}$ (two-tailed one-way ANOVA, Dunn's multiple comparisons test: adjusted *p*= 0.0307) (D). Images of haematoxylin and eosin-stained aortic roots from *Ankhd1*$^{+/+}$ (E) and *Ankhd1*$^{+/-}$ (F) mice are shown. Quantification of plaque areas in the aortic

roots of three mice per group showed a significant increase in *Ankhd1$^{+/-}$* (two-tailed unpaired t-test: *p*= 0.0071) (G). All dots represent different animals and error bars show the standard error of the mean.

5.5. Discussion

Ankhd1 knockout mouse models had a distinct vascular phenotype with a significant effect on aortic diameter, thrombosis, inflammation and endothelial cell numbers together leading to accelerated atherosclerosis development. ANKHD1-deficient mice had narrower aortas, observable blood clots, intercellular gaps, reduced endothelial cell numbers and accelerated atherosclerosis. Together these phenotypes indicate that the presence of ANKHD1 is cytoprotective in the vasculature, while lowering ANKHD1 is sufficient to drive increased plaque formation.

5.5.1. *Evaluation of systemic risk factor for atherosclerosis in Ankhd1 mouse models*

Sowers et al. (1993) illustrated a positive correlation between diabetes, hypertension, obesity and hypercholesterolemia with endothelial cell injury and atherogenesis. My current data showed that there was no major effect of ANKHD1-deficiency on these systemic risk factors. While there was a trend toward an increase in blood pressure, this was not sufficient to achieve statistical significance, due to the low number of animals studied. More animals are needed to verify this finding, therefore currently we cannot officially exclude the possibility of an effect of ANKHD1 on blood pressure. In addition to hypertension, hypercholesterolemia and hyperglycaemia have also been linked with vessel constriction (McCalden and Nath, 1989; Xiang et al., 2007). My current findings in my experimental model suggest that ANKHD1 does not control body weight or cholesterol or glucose levels, which promote atherosclerosis and vasoconstriction; indicating the roles of ANKHD1 in vascular biology are independent of glucose, cholesterol and body weight and are therefore likely to be mediated at the cellular level, with a major effect on endothelial physiology.

5.5.2. The influence of ANKHD1 on aortic diameter

A narrower aortic diameter can increase the wall shear stress magnitude, and as such, contribute to endothelial dysfunction and injury (CaroFitz-Gerald and Schroter, 1971). It is unknown whether the shear stress magnitude has changed in the constricted $Ankhd1^{-/-}$ aorta. However, there is a positive correlation between heart rate and shear stress magnitude (LaosiripisanParkhurst and Tanaka, 2017) and my data showed that ANKHD1 does not change heart rate. On the grounds of that, it can be predicted that there is no significant change in shear stress magnitude, yet to confirm this finding additional experiments are required.

It is of interest to discuss the contribution of endothelial cells in controlling blood pressure. Specifically, endothelial denudation is known to lead to vessel constriction. A large body of evidence from human and mouse studies has shown a major effect of the endothelial cell in vasorelaxation and as such, blood pressure. The underlying mechanism is endothelial cell production of NO and PGI_2 (Adelstein et al., 1978; Ignarro et al., 1981; AdelsteinConti and Hathaway, 1978; LawlerMiggin and Kinsella, 2001; Coletta et al., 2012; Russell-Puleri et al., 2017; ChengVanhoutte and Leung, 2018; Iring et al., 2019), factors that modify blood pressure. These factors have been shown to be regulated by ANKHD1 *in vivo* and *in vitro*. On the grounds of these previous findings together with my findings of the dependency on ANKHD1 for vessel diameter, I raised the question of whether there is a link between ANKHD1 and endothelial-dependent vasorelaxation via NO and PGI_2, resulting in aortic diameter changes. Given the importance of maintaining tight control of vascular tone, it becomes important to understand the contribution of ANKHD1 in controlling vasorelaxation. As such, this can be studied further in the future.

5.5.3. ANKHD1 protects from thrombosis

It was consistently recognised that the aortic arch of ANKHD1-deficient mice had thrombi. In some of the mice, the phenotype was more severe where the clots have been seen to cover the entire aorta, whereas in other cases the thrombi were mainly seen in the aortic arch. It is currently unknown how ANKHD1 protects from thrombosis, and likewise how deletion of *Ankhd1* promotes thrombus formation. In my thesis, I have uncovered that *Ankhd1*$^{-/-}$ mice exhibit endothelial cell loss, which is known to cause thrombus generation as shown by Durand et al. (2004). Yet the specific steps and mechanisms that govern endothelial loss and thrombus formation remain elusive. ANKHD1 positively controlled the anti-thrombotic *eNOS* and *PTGIS*, while it negatively controlled *F3*. PTGIS and eNOS release PGI$_2$ and NO, respectively, and inhibit platelet adhesion and aggregation (TatesonMoncada and Vane, 1977; Mellion et al., 1981; RadomskiPalmer and Moncada, 1987). Given that ANKHD1 regulates the levels of *eNOS* and *PTGIS*, and consequently, could exert its antithrombotic effects via NO and PGI$_2$, and *F3* is elevated when *ANKHD1* is silenced, I hypothesized that the prothrombotic phenotype could be due to a dual mechanism involving not only NO/PGI$_2$ but also *F3* expression (Figure 5.8). Yet the full extent of the contribution of ANKHD1 in protection from endothelial injury could be broader than its effects on *eNOS, PTGIS* and *F3*. In addition, it is unknown whether (1) the observed *F3* modulation is NFκB and/or KLF2 mediated, as it is known that *F3* is under the control of NFκB and KLF2; and (2) what is the functional significance of thrombosis on the atherosclerosis phenotype. Studies by Fuster et al. (1978), Methia et al. (2001), Pratico et al. (2001), and Doddapattar et al. (2018) indicate the involvement of platelets in atherogenesis. Activated platelets contribute to early lesion formation via platelet adhesion and activation; thus, larger plaques in ANKHD1-deficient PCSK9 mice could be the results of these aggregated thrombocytes since *Ankhd1*$^{-/-}$ mice had an evident thrombosis phenotype.
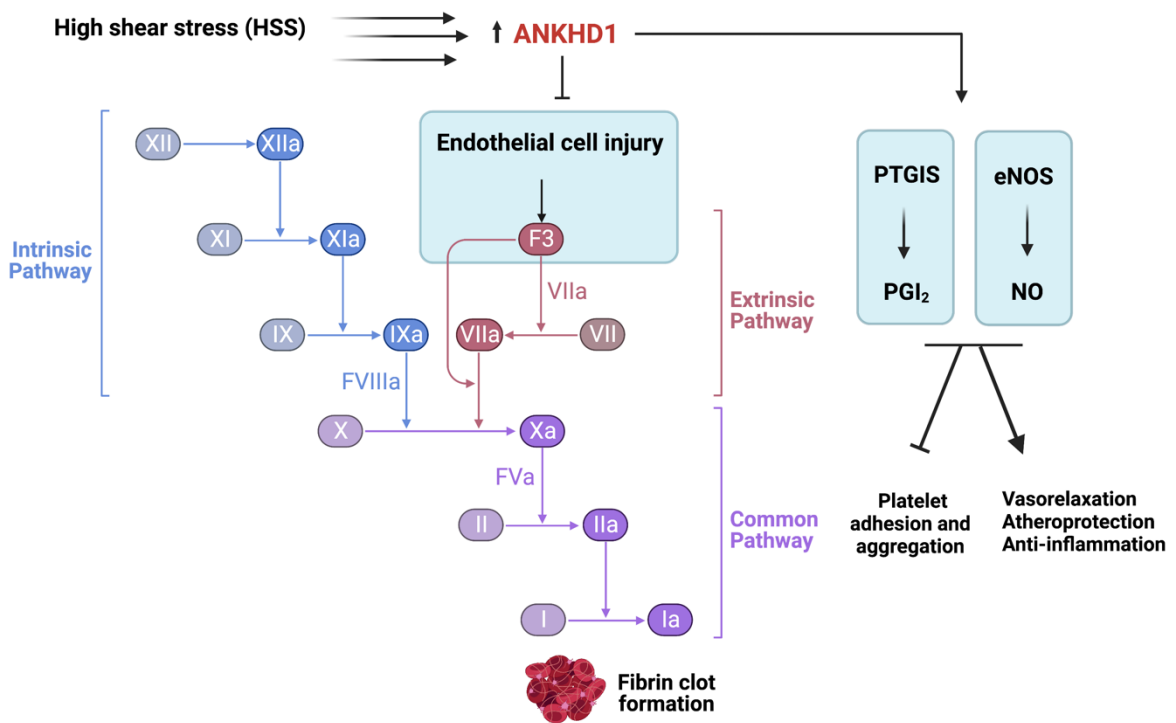
Figure 5.8. Proposed model of how ANKHD1 prevents from thrombosis and provides vasoprotection. HSS enhances the cytoprotective ANKHD1 production which in turn maintains intact endothelial cell layer, promotes vasorelaxation and prevents coagulation cascade initiation, platelet adhesion and aggregation and atherogenesis.

5.5.4. *ANKHD1 might prevent leukocyte adhesion and infiltration*

Inflammation has been associated with inter-endothelial cell gaps. During leukocyte-endothelial cell adhesion and IL1β activation, endothelial CD62E is redistributed into lipid-rich rafts or macrodomains within endothelial cells. These lipid rafts facilitate the interaction between activated CD62E and phospholipase C gamma (PLCγ). Activated PLCγ can increase intracellular calcium levels, and as such, enhances MLCK phosphorylation and endothelial permeability (Kiely et al., 2003). Interestingly, the endothelium exposed to atheroprotective shear stress in *Ankhd1$^{-/-}$* mouse aortas had a marked redistribution of CD62E into large puncta, whether these structures are lipid rafts is currently unknown. The large CD62E positive puncta were accompanied by an uneven and discontinuous distribution at inter-endothelial cell junctions that form gaps between cells; suggesting that these endothelial cells are inflamed and possibly bound to circulating inflammatory cells; leading to leukocyte infiltration through the gaps into the sub-endothelium.

RNA-sequencing data coupled with qPCR validation showed that ANKHD1 regulates inflammation and endothelial cell permeability via controlling NFκB activation and GSTP-1 expression. ANKHD1 showed to positively regulate KLF2, which is also an anti-inflammatory transcription factor that inhibits the activation of CD62E. The findings of inter-endothelial cell gaps accompanied by CD62E activation in mouse aortas further support the vasoprotective role of ANKHD1 that was proposed by the RNA-sequencing approach and KLF2 regulation.

CD62E expression and subsequent leukocyte infiltration have been linked with accelerated atherosclerosis (van der Wal et al., 1992; Collins et al., 2000); this also provides mechanistic evidence of why *Ankhd1*-deficient mice develop larger plaque sizes.

5.5.5. *Ankhd1 controls endothelial cell number*

Inhibition of *Ankhd1* in mice resulted in a reduction in endothelial cell numbers. It is unknown whether these endothelial cells become more apoptotic. This can be identified by assessing the markers of apoptosis, such as cleaved caspase 3. Apoptosis was one of the enriched functions controlled by ANKHD1 according to the RNA-sequencing applied on HSS-stimulated HCAECs. It is also unknown whether some endothelial cells are less proliferative, thus less likely to be able to divide to fill the gaps. This work could be followed up in the future, as it will allow us to gain a mechanistic understanding of the observed phenotype of altered cell numbers.

ANKHD1 was identified as a regulator of the major pathways that control cellular growth. Müller et al. (2005) and Fisher et al. (2018) found that ANKHD1 controls JAK/STAT pathway activity. Moreover, Sidor, Brain and Thompson (2013) identified that ANKHD1 controls the Hippo pathway. Given that both the JAK/STAT and Hippo pathways are major regulators of cellular growth and survival, we could speculate that ANKHD1 may have a role in controlling cell growth and survival, via its JAK/STAT and HIPPO actions. After that, Yao et al. (2018) determined that human ANKHD1 enhances Akt activity via YAP1 activation, a transcription regulator that is controlled by the Hippo pathway, resulting in tissue growth and confirming the Drosophila findings in human cells. Most recently, Yao et al. (2022) reported that *ANKHD1* silencing inhibited YAP1 transcription, activation and translocation of the transcription activator YAP-1 into the nucleus in cancer cells. Whether ANKHD1 controls normal (i.e., not in the context of cancer) endothelial cell proliferation via JAK/STAT and/or Hippo pathway has not yet been studied. In addition, ANKHD1 via YAP1 activation prevents DNA damage via inhibiting ROS formation and promotes ATM phosphorylation to enhance DNA repair pathways (Yao et al., 2022); thus ANKHD1 was found to prevent apoptosis of cancer cells. The potential regulation of the JAK/STAT and/or Hippo pathway components

could explain the differences in cell numbers implying a difference in proliferative potential observed in endothelial cells lacking ANKHD1 and may further explain the tendency towards increased cell death in *Ankhd1* knockout mice.

My observation of endothelial cell loss (Section 5.3.4: Figure 5.6) could also be a result of NO deficiency. NO generated via eNOS protects the endothelial cell microenvironment from vasoconstriction, inflammation and oxidative stress that can cause endothelial cell loss (CaroFitz-Gerald and Schroter, 1971; Ponnuswamy et al., 2012; SiuGao and Cai, 2016; Iring et al., 2019). It is currently unknown what causes endothelial cell loss in ANKHD1-deficient mice, specifically whether it is because of high levels of oxidative stress generated by NO reduction and/or ROS formation. Previous work on cancer cells showed that ANKHD1 inhibition exacerbated oxidative stress levels within cells via increasing ROS formation. High levels of ROS resulted in cellular apoptosis (Yao et al., 2022), however, the mechanism by which ANKHD1 regulates oxidative stress has not been unveiled. As mentioned in chapter 3, ANKHD1 inhibits the pro-oxidant *RAC2* that generates ROS; suggesting at least one potential mechanism of antioxidant function of ANKHD1 that could protect from endothelial cell loss.

5.5.6. *ANKHD1 provides atheroprotection*

The ANKHD1-deficient mouse model, with global deletion of the *Ankhd1* gene, showed accelerated atherosclerosis development compared to the control group (*Ankhd1$^{+/+}$* mice). Interestingly, *Ankhd1$^{+/-}$* mice appeared to have a trend towards larger plaque sizes compared to *Ankhd1$^{-/-}$*, however, that increase did not reach statistical significance. ANKHD1 is ubiquitously expressed by a variety of cell types, it is an evolutionarily conserved gene and hence is predicted to have evolutionarily conserved and important functions. Therefore, total body knockout might have a compensatory mechanism that provides some protection from accelerated atherosclerosis development when *Ankhd1* is globally deleted. Although it is also not clear which cell type(s) regulates vasoprotection/atherogenesis, conditional *Ankhd1* inhibition in a single cell type (e.g., endothelial cells) could identify the contribution of endothelial ANKHD1 in vasodilation and atheroprotection. Yet the major vasoprotective molecules, NO and PGI$_2$, that have been studied profoundly, are expressed mainly in the endothelial cells where ANKHD1 is highly expressed. Therefore, I hypothesise that ANKHD1 has a role to play in endothelial cells, however, my studies cannot exclude the contributions of many other cell types, including smooth muscle cells, pericytes, stem cells, and immune cells.

It is well-known that disruption of some of the high shear regulated and protective genes can lead to increased lesions in models of atherosclerosis. The prime examples of these are *eNOS* (*NOS3*), *PTGIS* and *KLF2*, HSS-regulated protective genes. Inhibition of eNOS activity leads to a pro-inflammatory, prothrombotic and atherogenic phenotype. This results in accelerated atherosclerosis development (Mellion et al., 1981; Ozaki et al., 2002; Ponnuswamy et al., 2012; Douglas et al., 2018). Genetic deletion of *PTGIS* enhanced atherosclerosis development in mice (Yokoyama et al., 2002). PGI$_2$ was found to decrease in mice after four months of administering a high-fat diet (CyrusDing and Praticò, 2010). Inhibited PGI$_2$ activity resulted in inflammatory cell accumulation and larger plaque sizes in mice (Kobayashi et al.,

2004). Mutation of *PTGIS* has been associated with adverse cardiovascular events in humans (Nakayama et al., 2002; Yamada et al., 2006). KLF2 is also an anti-inflammatory, anti-thrombotic and atheroprotective transcription factor. Its inhibition resulted in accelerated inflammation and atherogenesis (Atkins et al., 2008). These findings together highlight the importance of NO, PGI$_2$ and KLF2, which are under the control of ANKHD1, in promoting functional vasoactivity and atheroprotection. They also give a possible answer to the observed phenotypes in ANKHD-deficient endothelium from humans and mice, which are (i) changes in endothelial cells numbers, (ii) inflammation, (iii) vasorelaxation, (iv) oxidative stress and (iv) thrombosis, thus providing a unifying proposed mechanism of ANKHD1-driven vasoprotection and atheroprotection.

Summary

This chapter discussed the function of ANKHD1 in an experimental model of atherosclerosis and vessels of mice without the disease. The findings of this chapter support this chapter's hypothesis by providing clear evidence that ANKHD1 is a cytoprotective protein that controls major vascular functions (dilation/constriction, inflammation, thrombosis, cell quantity and ultimately atherogenesis).

Chapter 6: General discussion

The roles of ANKHD1 in the healthy endothelium and in the context of atherosclerosis had not been studied before. This study identifies novel functions of the RNA-binding protein ANKHD1 in the vasculature by RNA-sequencing of HSS-stimulated HCAECs and by ANKHD1 loss-of-function in mice and cellular models. Shear stress and atherosclerosis pathways were highly enriched as one of the major functions of ANKHD1 in the vascular endothelial cells. Atheroprotective forces enhance ANKHD1 expression at mRNA and protein levels in HUVECs and HCAECs. ANKHD1 was also upregulated in areas of mouse aortas exposed to HSS. Consequently, it contributes to vasoprotection by promoting the major vasoprotective molecules eNOS, PTGIS and KLF2 in healthy endothelial cells (Figure 6.1: proposed model). Its inhibition resulted in vasoconstriction and pro-inflammatory, pro-thrombotic and proatherogenic endothelium leading to endothelial dysfunction and atherosclerosis.

6.1. ANKHD1 protects from endothelial dysfunction

I showed here that ANKHD1 controls *eNOS* mRNA stability and eNOS protein activity. I demonstrated that ANKHD1 employs two potential mechanisms to potentiate the activity of eNOS. The first mechanism is direct and involves the physical binding of ANKHD1 to the 3' UTR of *eNOS*, leading to message stability. The second, less well-studied and indirect mechanism, involved the positive control of a major glycocalyx component protein, glypican 1. Glypican-1 promotes eNOS activity and is significantly associated with the healthy endothelium, and as such, the vasculature. While not directly assessed in my studies, it is expected that with the right co-factors eNOS can produce the antioxidant, anti-inflammatory and anti-thrombotic NO; thus, preventing endothelial dysfunction and atherosclerosis (TatesonMoncada and Vane, 1977; Mellion et al., 1981; RadomskiPalmer and Moncada, 1987;

Ponnuswamy et al., 2012; Douglas et al., 2018). It, therefore, follows that ANKHD1 may control NO by regulating *eNOS* levels. Moreover, Mahmoud et al. (2021) and Bartosch et al., (2021) showed that *glypican 1* inhibition has been associated with endothelial dysfunction and generates a proatherogenic microenvironment by upregulation of the proinflammatory molecules ICAM-1 and VCAM-1 and downregulation of NO production. In vascular aging, glypican 1 and eNOS expression and activation were reduced while proinflammatory molecules ICAM-1 and VECAM-1 and leukocyte adhesion have the opposite trend. However, the mechanism by which the process of ageing causes *glypican 1* and *eNOS* reduction and pro-inflammatory molecule production has not yet been studied. In addition, because ANKHD1 induced the endothelial cell protective transcription factor KLF2 production, the prothrombotic and proinflammatory vascular and endothelial cell phenotype of *Ankhd1$^{-/-}$* mice and ANKHD1-deficient cells can also be attributed, at least partly, to the reduction in KLF2. My study supports that ANKHD1 plays a significant role by preventing endothelial dysfunction and endothelial cell loss in young and healthy endothelial cells possibly via enhancing KLF2 and glypican 1/eNOS and inhibiting NFκB/ICAM-1/CD62E.

6.2. Possible consequences of ANKHD1/PTGIS regulation

It has been identified by Cheng et al. (2002) that the PGI$_2$, which is produced by PTGIS, attenuates the effect of the prothrombotic and the atherogenic thromboxane A$_2$ (TXA$_2$). TXA$_2$, which is produced by platelets and is elevated in mice during the development of atherosclerosis. TXA$_2$ further enhances platelet activation and aggregation and thrombus formation while TXA$_2$ inhibition attenuates atherosclerosis development in mice (Praticò et al., 2001). In addition, a high TXA$_2$-to-PGI$_2$ ratio has been associated with vasoconstriction (Xiang et al., 2007). My work shows that ANKHD1 can positively regulate *PTGIS* in HSS conditions. It is unknown whether ANKHD1 (1) influences TXA$_2$-to-PGI$_2$ ratio; (2) regulates TXA$_2$

production and (3) further contributes to vasoconstriction, thrombosis and/or atherosclerosis via TXA$_2$.

The mechanism by which *PTGIS* is upregulated in HSS via ANKHD1 has not yet been elucidated. My work showed that ANKHD1 can physically interact with the mRNA of *PTGIS* in HUVECs. But unlike the eNOS interaction, this interaction is enriched by 12-fold (whereas eNOS is more than 500-fold), as such the relevance of this interaction remains unclear. I have also shown that the regulation exerted by ANKHD1 on *PTGIS* is KLF2 independent, this has allowed me to exclude the possibility of ANKHD1 regulating *PTGIS* indirectly via its effects on KLF2. There are a number of potential mechanisms that ANKHD1 can employ to positively regulate *PTGIS*. ANKHD1 is an RNA-binding protein, and it interacts with *PTGIS*, so it may promote its mRNA stability or promote its translation. Additionally, ANKHD1 has been reported by others to act as a transcriptional co-activator (Sidor et al., 2019). Therefore, it remains possible that ANKHD1 may interact with the promoter of *PTGIS* and enhance its expression transcriptionally. In fact, my time-course experiment shows that *ANKHD1* and *PTGIS* have a very similar profile of activation by shear (fully induced by chronic shear after 72 hours). Whether ANKHD1 controls *PTGIS* transcriptionally and which canonical transcription factor may be its partner are currently unknown. Lastly, a single nucleotide polymorphism in the *PTGIS* gene (1117C>A: in exon 8) has been significantly associated with hypertension and myocardial infarction in humans; thus, indicating the critical involvement of PTGIS in cardiovascular health (Nakayama et al., 2002; Yamada et al., 2006). As such, by association, ANKHD1 may protect from cardiovascular diseases via controlling *PTGIS* production.

6.3. ANKHD1 regulates vasoactivity and thrombosis

ANKHD1 inhibition was accompanied by vasoconstriction, and it has been reported by Malmsjö et al. (1998), Wihlborg et al. (2003), Guns et al. (2005) and Cheng, Vanhoutte and Leung (2018) that endothelial cells are key regulators of vasoactivity as endothelial denudation resulted in vasoconstriction. This is because endothelial cells produce potent vasorelaxant molecules, NO and PGI_2. My study suggests that the reduction of these endothelial vasorelaxants via *eNOS* and *PTGIS* inhibition can be possible evidence for the narrower *Ankhd1*$^{-/-}$ aortas. However, we are not excluding any possibility of the involvement of vasoconstrictors (e.g., thromboxane A_2 [TXA_2])) and/or smooth muscle cell (SMC) density or activity. Further research can characterise the SMC-dependent vasoactivity in ANKHD1 cellular/animal models.

It is known that both NO produced by eNOS and PGI_2 produced by PTGIS inhibit platelet adhesion and aggregation (TatesonMoncada and Vane, 1977; Mellion et al., 1981; RadomskiPalmer and Moncada, 1987). and KLF2 prolongs clotting time while endothelial cell injury results in thrombus formation (Lin et al., 2005; Kumar et al., 2013). *Ankhd1*$^{-/-}$ mice showed signs consistent with thrombosis in the aortas, these included low levels of eNOS and PTGIS which was accompanied by endothelial cell loss. Additionally, ANKHD1-deficient HCAECs exhibited a pro-thrombotic phenotype with reduced *KLF2* and enhanced expression of the coagulation factor *F3*. These findings together identify ANKHD1 as an anti-thrombotic factor.
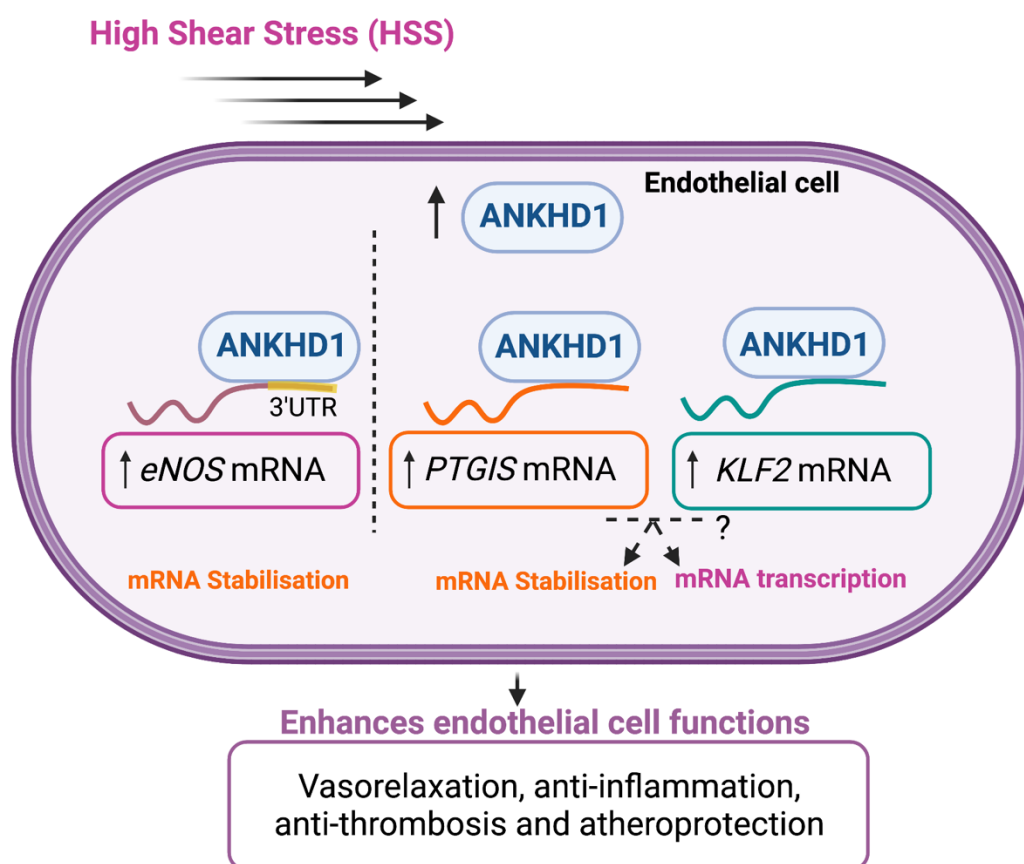
Figure 6.1. ANKHD1 promotes eNOS, PTGIS and KLF2 mRNA levels in HSS-stimulated endothelial cells to induce functional vasculature. HSS upregulates *ANKHD1*, *eNOS*, *PTGIS* and *KLF2* mRNA expression in healthy endothelial cells. ANKHD1 can bind to *eNOS* 3'UTR and enhance *eNOS* mRNA stability. It can also bind to *PTGIS* and *KLF2* mRNAs, however, the molecular mechanism of *PTGIS* and *KLF2* mRNA regulation exerted by ANKHD1 has not yet been unveiled. These data together suggest the ability of ANKHD1 in enhancing major endothelial cell functions (i.e., vasorelaxation, anti-inflammation, anti-thrombosis and atheroprotection) via regulating key vasoprotective molecules, eNOS, PTGIS and KLF2.

6.4. A possible therapeutic strategy to increase ANKHD1 levels in atheroprone areas

This study together with previous studies in cancer identify ANKHD1 as a cytoprotective molecule that maintains healthy endothelial cells and cancerous cells. In cancer cells, it results in radioresistance as it inhibits ROS-mediated DNA damage and enhances cellular growth (Fragiadaki and Zeidler, 2018; Yao et al., 2022). Therefore, when thinking of the potential therapeutic implications of my findings, it is important to enhance the cytoprotective/atheroprotective function of ANKHD1 in atheroprone areas only, to limit any potential of carcinogenesis. Nanoparticle-targeted therapy to the dysfunctional endothelium could be a possible way of enhancing ANKHD1 levels, and thus, providing protection. Kheirolomoom et al. (2015) generated nanoparticles carrying anti-miRNA (anti-miR712) coated with VCAM-1 ligands, thus binding specifically to endothelial cells expressing VCAM-1 in atheroprone areas to deliver the miRNA-712 inhibitor. This was shown to attenuate the progression of atherosclerosis in mice. Although it is currently unknown which the activators/inhibitors of *ANKHD1* expression are, miRTarBase, an online bioinformatic tool, has provided several inhibitory miRNAs that are predicted to downregulate *ANKHD1* expression. Thus, *ANKHD1* might be under the regulation of miRNA-mediated RNA degradation. This can be confirmed by (i) assessing the levels of these miRNAs in primary human endothelial cells exposed to flow (HSS/LSS) and (ii) quantifying ANKHD1 levels in cells lacking/overexpressing a targeting miRNA. Chung et al. (2022) showed differentially expressed miRNAs from extracellular microvesicles released from endothelial cells in response to unidirectional HSS or disturbed LSS. miR-320a, which is a predicted inhibitor of *ANKHD1*, was one of the significantly upregulated miRNAs from endothelial cells exposed to disturbed LSS. Whether miR-320a inhibits *ANKHD1* in athero-indusive conditions *in vitro* and *in vivo* is currently unidentified. Once identifying the miRNA targeting *ANKHD1* mRNA,

nanoparticles carrying the miRNA inhibitor (miRNA antagomir) to specifically target plaque-prone areas might be a possible 'on-target' future treatment.

6.5. Study limitations

A potential limitation of the study is the heavy reliance on gene loss-of-function studies. Currently, I have used mouse knockouts of ANKHD1, which have generated ANKHD1 loss-of-function and siRNA to reduce the levels of ANKHD1 in human cellular models. It would be of interest to complement these studies with overexpression experiments, where I overexpress ANKHD1 in human cellular models, to avoid relying on siRNA. To minimise the inherent problem with reliance on siRNA, I have used two siRNAs to minimise the possibility of picking up non-specific effects. I have also complemented *in vitro* with *in vivo* studies. The use of *in vivo* studies is a good complementary experiment as the loss-of-function of ANKHD1 in the mice is not mediated by siRNA and is more likely to be an 'on-target' effect. The use of siRNAs is also potentially concerning, as siRNAs are known to activate the immune system. However, in HUVEC and HCAEC cultures, the ability to overexpress genes with plasmid DNA especially genes like ANKHD1 (280kDa), is technically difficult (involving electroporation, which damages the cells), as primary endothelial cells are known to be hard to transfect cells.

An additional inherent limitation of this study is the use of animal models to study a human disease, atherosclerosis. It is well known that there are a number of differences between human and murine atherosclerosis. Yet this limitation is partially mitigated with the use of human cellular models. It should be noted, however, that cellular models also carry their own inherent limitations, such as genetic heterogeneity (limiting experimental control) and the fact that cells are not in their *in vivo* 3D environment, instead they are grown on plates, which generated an unnatural system and is likely to change their responses. With these caveats in mind and using *in vivo* models as much as possible, I draw conclusions by comparing the two

systems. Ideally, in the future, I would like to complement my studies with studies of human coronary atheromas, where I can stain for ANKHD1 and its partners. ANKHD1 is a rather stably and ubiquitously expressed gene, and therefore I have not been able to find people with altered ANKHD1 expression in large datasets.

Another limitation of the study is the use of global *Ankhd1* deletion in mice. These mice have provided strong evidence that *Ankhd1* controls murine vascular biology, yet it is still unclear what the contribution of *Ankhd1* in single-cell types may be. Inhibition of *Ankhd1* in single-cell types (e.g., only in endothelial cells or smooth muscle cells) *in vivo* is needed to know the cell-specific contribution of *Ankhd1* in vascular function.

6.6. Future plans

It is of interest to have the entire perspective of how ANKHD1 is regulated and what is the role of ANKHD1 in the healthy vasculature and atherosclerosis. While there are plenty of future experiments that can be done, I have prioritised these four main experiments, described below.

6.6.1. How is ANKHD1 upregulated in the HSS conditions?

My study shows that the ANKHD1 level in endothelial cells is consistently upregulated under the HSS condition. However, it is currently unknown (1) what upregulates the transcription and/or stability of ANKHD1 at mRNA and protein levels in endothelial cells exposed to HSS and (2) which is the mechanosensor/s and the transcription factor/s that enhance ANKHD1 expression. To find out whether it is the transcription or the stability that controls ANKHD1 expression in HSS-stimulated cells, an actinomycin D experiment can be applied on static and HSS and LSS stimulated endothelial cells. This can provide the half-life of ANKHD1 mRNA in each condition and allow me to answer the question. ChIP-seq of activated enhancers and promoters in cells with shear stress when compared with static would probably suggest the activated sequence/s and the transcription factor that enhances ANKHD1 expression. Assessing the contribution of mechanosensors on ANKHD1 expression can be achieved by inhibitors or siRNA lipotransfection followed by shear stress stimulation of endothelial cells.

6.6.2. How does ANKHD1 controls eNOS and PTGIS expression?

My work showed that ANKHD1 promotes eNOS mRNA stability via direct binding to 3'UTR. The RNBmap showed a predicted binding site in the 3'UTR that I found to be highly conserved cross-species. This needs to be confirmed by constructing a plasmid expressing

eNOS 3'UTR lacking the ANKHD1 binding site, flowed by *in vitro* biotinylated 3'UTR transcription, pulling down, and western blotting of ANKHD1.

ANKHD1 inhibition attenuates the effect of HSS on PTGIS expression by massively reducing its level. ANKHD1 can directly bind to PTGIS mRNA. However, it is still unclear how ANKHD1 protects PTGIS expression in HSS conditions. Whether it is at mRNA stability levels and/or mRNA transcription levels.

The possibility of micro-RNA mediated-mRNA degradation of eNOS and PTGIS has not been excluded. Whether the binding of ANKHD1 to eNOS and/or PTGIS mRNA protects them from miRNA degradation. This can be assessed by inhibiting the dicer enzyme, which is an endonuclease that can promote miRNA maturation in the cells and by assessing the microRNAs that are predicted to target PTGIS/eNOS. microRNA mimics or inhibitors can be used to allow the study of the effects of a specific miRNA on eNOS/PTGIS mRNA levels in cells transfected with either NT-siRNA or *ANKHD1*siRNA with and without dicer.

6.6.3. Does ANKHD1 controls endothelial- and/or SMC- dependent vasorelaxation?

Ankhd1$^{-/-}$ mice had narrower aortic diameters when compared to *Ankhd1$^{+/+}$* mice. To confirm whether the reduction of eNOS and PTGIS results in constricted aortas, this can be assessed by conditional inhibition of *Ankhd1* in mouse endothelial cells. One way to assess the contribution of endothelial cells is to measure aortic diameters and vasoactivity of live vessels via myography and compare it with the *Ankhd1$^{+/+}$* aortas. As it is possible that ANKHD1 in SMCs contributes to vasoactivity, conditional inhibition of *Ankhd1* in SMCs in mouse aortas followed by quantifying vasoactivity and aortic diameter quantification can be used to assess SMC-related contribution.

Because endothelial NO and PGI$_2$ impair MLCK phosphorylation in SMCs, and subsequently, result in vasorelaxation (LeeLi and Kitazawa, 1997; LawlerMiggin and Kinsella,

2001; ChengVanhoutte and Leung, 2018). MLCK phosphorylation can be assessed in ANKHD1-deficient SMCs *in vitro* and mice with conditional inhibition of *Ankhd1* in endothelial cells or SMCs. Also, it is unknown whether ANKHD1 controls SMC density, therefore, SMC proliferation can be assessed with and without *ANKHD1* silencing.

6.6.4. What is the function of ANKHD1 in atherosclerosis?

My research unveils that ANKHD1 exhibits a number of protective functions collectively promoting vascular health. *Ankhd1* deficiency leads to accelerated atherosclerosis. *Ankhd1*-deficient mice have larger plaque sizes when compared with the littermate wild-type control group. In endothelial cells, ANKHD1 promotes the expression of the atheroprotective molecules *eNOS*, *PTGIS* and *KLF2* while it inhibits NFκB pathway activity and suppresses subsequent CD62E activation. Therefore, studying whether conditional inhibition of ANKHD1 in mouse endothelial cells leads to accelerated leukocyte infiltration, atherosclerosis and thrombosis is required to uncouple some of the protective mechanisms.

It is also important to study where about, which cells and at which stage of atherosclerotic lesions ANKHD1 is expressed in human plaques. This might provide an insight into whether (1) ANKHD1 is expressed in single/multiple cell type in plaques, (2) ANKHD1 levels change in stable/vulnerable plaque, and as such, this might suggest possible functions of ANKHD1 in atherosclerosis.

6.7. Summary

Endothelial cells in HSS condition have been consistently identified as healthy cells that prevent atherosclerosis development. ANKHD1 is a gene that has not previously been studied in the normal vasculature or in atherosclerosis. This research identifies ANKHD1 as a highly upregulated RNA-binding protein in atheroprotective conditions that enhances well-known vasoprotective molecules, such as eNOS, PTGIS and KLF2. Its inhibition results in impaired endothelial cell functions, inflammation and accelerated atherosclerosis. The general discussion presented herein outlined some important future plans that I am hoping to find the answers in the coming years.

7. Appendix

Appendix 7.1.
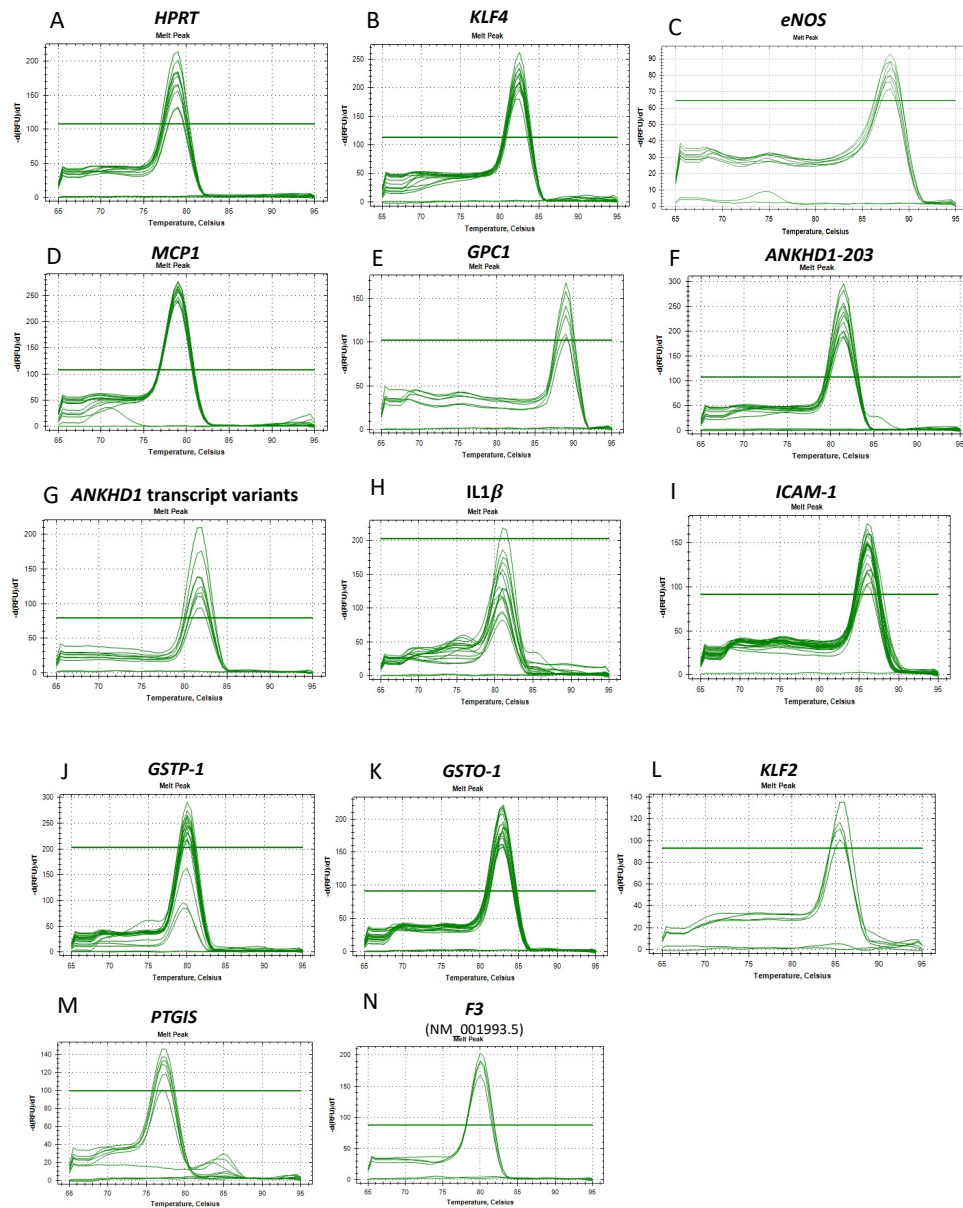
Figure 7.1. Melting curves of qPCR products. Graphs show melting curves of the housekeeping gene *HPRT* (A), quality control genes: *KLF4*, *eNOS* and *MCP1* (B-D) and the target transcripts *GPC1*, *ANKHD1-203* (full-length *ANKHD1*) (F) and *ANKHD1-203*, *ANKHD1-204* and *ANKHD1-205* (*ANKHD1* transcript variants) (G), *IL1β* (H), *ICAM-1* (I), *GSTP-1* (J), *GSTO-1* (K), *KLF2* (L), *PTGIS* (M) and *F3* (NM_001993.5) (N).

Appendix 7.2.
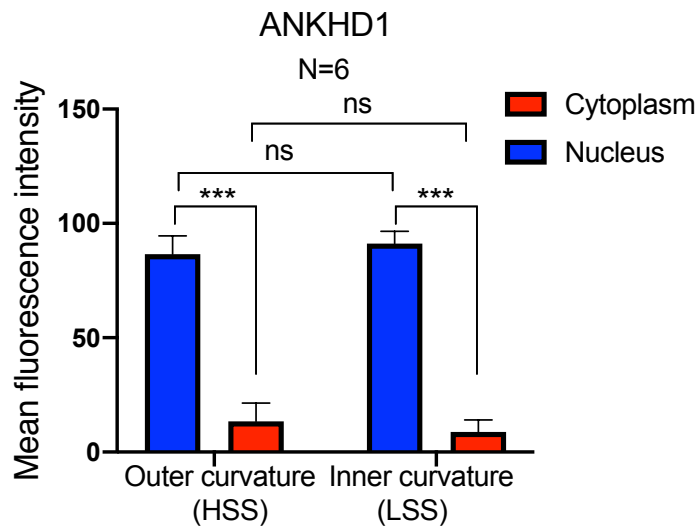
Figure 7.2. The overall ANKHD1 distribution (in %) in the inner and outer curvature in

Ankhd1^{+/+} mouse primary aortas. ANKHD1 was significantly higher in the nucleus than in

the cytoplasm in the outer and inner curvatures (two-tailed two-way ANOVA, Sidak's

multiple comparisons test: outer curvature adjusted *p*= 0.0002; inner curvature adjusted *p*=

0.0001). ANKHD1 was slightly more in the nucleus (mean= 91.25%) and less in the

cytoplasm (mean= 8.751%) in the inner curvature when compared to the outer curvature

(nucleus: mean= 86.55%; cytoplasm: mean= 13.45%).

8. References

Adelstein, R., Conti, M. and Hathaway, D. (1978). Phosphorylation of Smooth Muscle Myosin Light Chain Kinase by the Catalytic Subunit of Adenosine 3': 5'-Monophosphate-dependent Protein Kinase. *The journal of biological chemistry.* **253**(23), pp.8347-8350.

Adelstein, R.S., Conti, M.A., Hathaway, D.R. and Klee, C.B. (1978). Phosphorylation of smooth muscle myosin light chain kinase by the catalytic subunit of adenosine 3': 5'-monophosphate-dependent protein kinase. *J Biol Chem.* **253**(23), pp.8347-8350.

Ambruso, D.R., Knall, C., Abell, A.N., Panepinto, J., Kurkchubasche, A., Thurman, G., Gonzalez-Aller, C., Hiester, A., deBoer, M., Harbeck, R.J., Oyer, R., Johnson, G.L. and Roos, D. (2000). Human neutrophil immunodeficiency syndrome is associated with an inhibitory Rac2 mutation. *Proc Natl Acad Sci U S A.* **97**(9), pp.4654-4659.

Armstrong, M.L., Warner, E.D. and Connor, W.E. (1970). Regression of coronary atheromatosis in rhesus monkeys. *Circ Res.* **27**(1), pp.59-67.

Atkins, G.B., Wang, Y., Mahabeleshwar, G.H., Shi, H., Gao, H., Kawanami, D., Natesan, V., Lin, Z., Simon, D.I. and Jain, M.K. (2008). Hemizygous deficiency of Krüppel-like factor 2 augments experimental atherosclerosis. *Circ Res.* **103**(7), pp.690-693.

Bakheet, T., Hitti, E., Al-Saif, M., Moghrabi, W.N. and Khabar, K.S.A. (2018). The AU-rich element landscape across human transcriptome reveals a large proportion in introns and regulation by ELAVL1/HuR. *Biochim Biophys Acta Gene Regul Mech.* **1861**(2), pp.167-177.

Ballinger, S.W., Patterson, C., Yan, C.N., Doan, R., Burow, D.L., Young, C.G., Yakes, F.M., Van Houten, B., Ballinger, C.A., Freeman, B.A. and Runge, M.S. (2000). Hydrogen peroxide- and peroxynitrite-induced mitochondrial DNA damage and dysfunction in vascular endothelial and smooth muscle cells. *Circ Res.* **86**(9), pp.960-966.

Bartosch, A.M.W., Mathews, R., Mahmoud, M.M., Cancel, L.M., Haq, Z.S. and Tarbell, J.M. (2021). Heparan sulfate proteoglycan glypican-1 and PECAM-1 cooperate in shear-induced endothelial nitric oxide production. *Sci Rep.* **11**(1), p11386.

Beckman, J.S., Beckman, T.W., Chen, J., Marshall, P.A. and Freeman, B.A. (1990). Apparent hydroxyl radical production by peroxynitrite: implications for endothelial injury from nitric oxide and superoxide. *Proc Natl Acad Sci U S A.* **87**(4), pp.1620-1624.

Bertani, F., Di Francesco, D., Corrado, M.D., Talmon, M., Fresu, L.G. and Boccafoschi, F. (2021). Paracrine Shear-Stress-Dependent Signaling from Endothelial Cells Affects Downstream Endothelial Function and Inflammation. *Int J Mol Sci.* **22**(24).

Bjørklund, M.M., Hollensen, A.K., Hagensen, M.K., Dagnaes-Hansen, F., Christoffersen, C., Mikkelsen, J.G. and Bentzon, J.F. (2014). Induction of atherosclerosis in mice and hamsters without germline genetic engineering. *Circ Res.* **114**(11), pp.1684-1689.

Cadroy, Y., Diquélou, A., Dupouy, D., Bossavy, J.P., Sakariassen, K.S., Sié, P. and Boneu, B. (1997). The thrombomodulin/protein C/protein S anticoagulant pathway modulates the thrombogenic properties of the normal resting and stimulated endothelium. *Arterioscler Thromb Vasc Biol.* **17**(3), pp.520-527.

Caro, C.G., Fitz-Gerald, J.M. and Schroter, R.C. (1969). Arterial wall shear and distribution of early atheroma in man. *Nature.* **223**(5211), pp.1159-1160.

Caro, C.G., Fitz-Gerald, J.M. and Schroter, R.C. (1971). Atheroma and arterial wall shear. Observation, correlation and proposal of a shear dependent mass transfer mechanism for atherogenesis. *Proc R Soc Lond B Biol Sci.* **177**(1046), pp.109-159.

Centa, M., Ketelhuth, D.F.J., Malin, S. and Gisterå, A. (2019). Quantification of Atherosclerosis in Mice. *J Vis Exp.* (148).

Chao, Y., Ye, P., Zhu, L., Kong, X., Qu, X., Zhang, J., Luo, J., Yang, H. and Chen, S. (2018). Low shear stress induces endothelial reactive oxygen species via the AT1R/eNOS/NO pathway. *J Cell Physiol.* **233**(2), pp.1384-1395.

Chappell, D., Jacob, M., Paul, O., Rehm, M., Welsch, U., Stoeckelhuber, M., Conzen, P. and Becker, B.F. (2009). The glycocalyx of the human umbilical vein endothelial cell: an impressive structure ex vivo but not in culture. *Circ Res.* **104**(11), pp.1313-1317.

Chen, B.P., Li, Y.S., Zhao, Y., Chen, K.D., Li, S., Lao, J., Yuan, S., Shyy, J.Y. and Chien, S. (2001). DNA microarray analysis of gene expression in endothelial cells in response to 24-h shear stress. *Physiol Genomics.* **7**(1), pp.55-63.

Chen, L., Liu, X., Zhou, H., Li, G., Huang, F., Zhang, J., Xia, T., Lei, W., Zhao, J., Li, C. and Chen, M. (2021). Activating transcription factor 4 regulates angiogenesis under lipid overload via methionine adenosyltransferase 2A-mediated endothelial epigenetic alteration. *FASEB J.* **35**(6), pe21612.

Cheng, C., Tempel, D., van Haperen, R., van der Baan, A., Grosveld, F., Daemen, M.J., Krams, R. and de Crom, R. (2006). Atherosclerotic lesion size and vulnerability are determined by patterns of fluid shear stress. *Circulation.* **113**(23), pp.2744-2753.

Cheng, Y., Austin, S.C., Rocca, B., Koller, B.H., Coffman, T.M., Grosser, T., Lawson, J.A. and FitzGerald, G.A. (2002). Role of prostacyclin in the cardiovascular response to thromboxane A2. *Science.* **296**(5567), pp.539-541.

Cheng, Y., Vanhoutte, P.M. and Leung, S.W.S. (2018). Apolipoprotein E favours the blunting by high-fat diet of prostacyclin receptor activation in the mouse aorta. *Br J Pharmacol.* **175**(17), pp.3453-3469.

Chung, J., Kim, K.H., Yu, N., An, S.H., Lee, S. and Kwon, K. (2022). Fluid Shear Stress Regulates the Landscape of microRNAs in Endothelial Cell-Derived Small Extracellular Vesicles and Modulates the Function of Endothelial Cells. *Int J Mol Sci.* **23**(3).

Clark, P.R., Jensen, T.J., Kluger, M.S., Morelock, M., Hanidu, A., Qi, Z., Tatake, R.J. and Pober, J.S. (2011). MEK5 is activated by shear stress, activates ERK5 and induces KLF4 to modulate TNF responses in human dermal microvascular endothelial cells. *Microcirculation.* **18**(2), pp.102-117.

Coletta, C., Papapetropoulos, A., Erdelyi, K., Olah, G., Modis, K., Panopoulos, P., Asimakopoulou, A., Gero, D., Sharina, I., Martin, E. and Szabo, C. (2012). Hydrogen sulfide and nitric oxide are mutually dependent in the regulation of angiogenesis and endothelium-dependent vasorelaxation. *Proceedings of the National Academy of Sciences.* **109**(23), pp.9161-9166.

Collins, R.G., Velji, R., Guevara, N.V., Hicks, M.J., Chan, L. and Beaudet, A.L. (2000). P-Selectin or intercellular adhesion molecule (ICAM)-1 deficiency substantially protects against atherosclerosis in apolipoprotein E-deficient mice. *J Exp Med.* **191**(1), pp.189-194.

Collins, T., Read, M.A., Neish, A.S., Whitley, M.Z., Thanos, D. and Maniatis, T. (1995). Transcriptional regulation of endothelial cell adhesion molecules: NF-kappa B and cytokine-inducible enhancers. *FASEB J.* **9**(10), pp.899-909.

Conklin, B.S., Vito, R.P. and Chen, C. (2007). Effect of low shear stress on permeability and occludin expression in porcine artery endothelial cells. *World J Surg.* **31**(4), pp.733-743.

Cui, X., Lu, Y.W., Lee, V., Kim, D., Dorsey, T., Wang, Q., Lee, Y., Vincent, P., Schwarz, J. and Dai, G. (2015). Venous Endothelial Marker COUP-TFII Regulates the Distinct Pathologic Potentials of Adult Arteries and Veins. *Sci Rep.* **5**, p16193.

Cyrus, T., Ding, T. and Praticò, D. (2010). Expression of thromboxane synthase, prostacyclin synthase and thromboxane receptor in atherosclerotic lesions: Correlation with plaque composition. *Atherosclerosis.* **208**(2), pp.376-381.

da Silva, J.F., Bolsoni, J.A., da Costa, R.M., Alves, J.V., Bressan, A.F.M., Silva, L.E.V., Costa, T.J., Oliveira, A.E.R., Manzato, C.P., Aguiar, C.A., Fazan, R., Cunha, F.Q., Nakaya, H.I., Carneiro, F.S. and Tostes, R.C. (2022). Aryl hydrocarbon receptor (AhR) activation contributes to high-fat diet-induced vascular dysfunction. *Br J Pharmacol.* **179**(12), pp.2938-2952.

Dardik, A., Chen, L., Frattini, J., Asada, H., Aziz, F., Kudo, F.A. and Sumpio, B.E. (2005). Differential effects of orbital and laminar shear stress on endothelial cells. *J Vasc Surg.* **41**(5), pp.869-880.

Davis, M., Cai, H., Drummond, G. and Harrison, D. (2001). Shear Stress Regulates Endothelial Nitric Oxide Synthase Expression Through c-Src by Divergent Signaling Pathways. *Circulation Research.* **89**(11), pp.1073-1080.

de Bruin, R.G., van der Veer, E.P., Prins, J., Lee, D.H., Dane, M.J., Zhang, H., Roeten, M.K., Bijkerk, R., de Boer, H.C., Rabelink, T.J., van Zonneveld, A.J. and van Gils, J.M. (2016). The RNA-binding protein quaking maintains endothelial barrier function and affects VE-cadherin and β-catenin protein expression. *Sci Rep.* **6**, p21643.

Dekker, R.J., Boon, R.A., Rondaij, M.G., Kragt, A., Volger, O.L., Elderkamp, Y.W., Meijers, J.C., Voorberg, J., Pannekoek, H. and Horrevoets, A.J. (2006). KLF2 provokes a gene expression pattern that establishes functional quiescent differentiation of the endothelium. *Blood.* **107**(11), pp.4354-4363.

Dekker, R.J., van Soest, S., Fontijn, R.D., Salamanca, S., de Groot, P.G., VanBavel, E., Pannekoek, H. and Horrevoets, A.J. (2002). Prolonged fluid shear stress induces a distinct set of endothelial cell genes, most specifically lung Krüppel-like factor (KLF2). *Blood.* **100**(5), pp.1689-1698.

Dekker, R.J., van Thienen, J.V., Rohlena, J., de Jager, S.C., Elderkamp, Y.W., Seppen, J., de Vries, C.J., Biessen, E.A., van Berkel, T.J., Pannekoek, H. and Horrevoets, A.J. (2005). Endothelial KLF2 links local arterial shear stress levels to the expression of vascular tone-regulating genes. *Am J Pathol.* **167**(2), pp.609-618.

DeMaio, L., Rouhanizadeh, M., Reddy, S., Sevanian, A., Hwang, J. and Hsiai, T.K. (2006). Oxidized phospholipids mediate occludin expression and phosphorylation in vascular endothelial cells. *Am J Physiol Heart Circ Physiol.* **290**(2), pp.H674-683.

Dimmeler, S., Fleming, I., Fisslthaler, B., Hermann, C., Busse, R. and Zeiher, A.M. (1999). Activation of nitric oxide synthase in endothelial cells by Akt-dependent phosphorylation. *Nature.* **399**(6736), pp.601-605.

Dixit, M., Loot, A.E., Mohamed, A., Fisslthaler, B., Boulanger, C.M., Ceacareanu, B., Hassid, A., Busse, R. and Fleming, I. (2005). Gab1, SHP2, and protein kinase A are crucial for the activation of the endothelial NO synthase by fluid shear stress. *Circ Res.* **97**(12), pp.1236-1244.

Dluzen, D.F., Noren Hooten, N., De, S., Wood, W.H., Zhang, Y., Becker, K.G., Zonderman, A.B., Tanaka, T., Ferrucci, L. and Evans, M.K. (2018). Extracellular RNA profiles with human age. *Aging Cell.* **17**(4), pe12785.

Doddapattar, P., Dhanesha, N., Chorawala, M.R., Tinsman, C., Jain, M., Nayak, M.K., Staber, J.M. and Chauhan, A.K. (2018). Endothelial Cell-Derived Von Willebrand Factor, But Not Platelet-Derived, Promotes Atherosclerosis in Apolipoprotein E-Deficient Mice. *Arterioscler Thromb Vasc Biol.* **38**(3), pp.520-528.

Dormoy-Raclet, V., Ménard, I., Clair, E., Kurban, G., Mazroui, R., Di Marco, S., von Roretz, C., Pause, A. and Gallouzi, I.E. (2007). The RNA-binding protein HuR promotes cell migration and cell invasion by stabilizing the beta-actin mRNA in a U-rich-element-dependent manner. *Mol Cell Biol.* **27**(15), pp.5365-5380.

Douglas, G., Hale, A.B., Patel, J., Chuaiphichai, S., Al Haj Zen, A., Rashbrook, V.S., Trelfa, L., Crabtree, M.J., McNeill, E. and Channon, K.M. (2018). Roles for endothelial cell and macrophage Gch1 and tetrahydrobiopterin in atherosclerosis progression. *Cardiovasc Res.* **114**(10), pp.1385-1399.

Drake, T.A., Hannani, K., Fei, H.H., Lavi, S. and Berliner, J.A. (1991). Minimally oxidized low-density lipoprotein induces tissue factor expression in cultured human endothelial cells. *Am J Pathol.* **138**(3), pp.601-607.

Dupont, S., Morsut, L., Aragona, M., Enzo, E., Giulitti, S., Cordenonsi, M., Zanconato, F., Le Digabel, J., Forcato, M., Bicciato, S., Elvassore, N. and Piccolo, S. (2011). Role of YAP/TAZ in mechanotransduction. *Nature.* **474**(7350), pp.179-183.

Durand, E., Scoazec, A., Lafont, A., Boddaert, J., Al Hajzen, A., Addad, F., Mirshahi, M., Desnos, M., Tedgui, A. and Mallat, Z. (2004). In vivo induction of endothelial apoptosis leads to vessel thrombosis and endothelial denudation: a clue to the understanding of the mechanisms of thrombotic plaque erosion. *Circulation.* **109**(21), pp.2503-2506.

Ebong, E.E., Lopez-Quintero, S.V., Rizzo, V., Spray, D.C. and Tarbell, J.M. (2014). Shear-induced endothelial NOS activation and remodeling via heparan sulfate, glypican-1, and syndecan-1. *Integr Biol (Camb).* **6**(3), pp.338-347.

Fisher, K.H., Fragiadaki, M., Pugazhendhi, D., Bausek, N., Arredondo, M.A., Thomas, S.J., Brown, S. and Zeidler, M.P. (2018). A genome-wide RNAi screen identifies MASK as a positive regulator of cytokine receptor stability. *J Cell Sci.* **131**(13).

Fragiadaki, M. and Zeidler, M.P. (2018). Ankyrin repeat and single KH domain 1 (ANKHD1) drives renal cancer cell proliferation via binding to and altering a subset of miRNAs. *J Biol Chem.* **293**(25), pp.9570-9579.

Friedman, M.H., Deters, O.J., Mark, F.F., Bargeron, C.B. and Hutchins, G.M. (1983). Arterial geometry affects hemodynamics. A potential risk factor for athersoclerosis. *Atherosclerosis.* **46**(2), pp.225-231.

Fulton, D., Fontana, J., Sowa, G., Gratton, J.P., Lin, M., Li, K.X., Michell, B., Kemp, B.E., Rodman, D. and Sessa, W.C. (2002). Localization of endothelial nitric-oxide synthase phosphorylated on serine 1179 and nitric oxide in Golgi and plasma membrane defines the existence of two pools of active enzyme. *J Biol Chem.* **277**(6), pp.4277-4284.

Fuster, W., Bowie, E.J., Lewis, J.C., Fass, D.N., Owen, C.A. and Brown, A.L. (1978). Resistance to arteriosclerosis in pigs with von Willebrand's disease. Spontaneous and high cholesterol diet-induced arteriosclerosis. *J Clin Invest.* **61**(3), pp.722-730.

Galbusera, M., Zoja, C., Donadelli, R., Paris, S., Morigi, M., Benigni, A., Figliuzzi, M., Remuzzi, G. and Remuzzi, A. (1997). Fluid shear stress modulates von Willebrand factor release from human vascular endothelium. *Blood.* **90**(4), pp.1558-1564.

Gareus, R., Kotsaki, E., Xanthoulea, S., van der Made, I., Gijbels, M.J., Kardakaris, R., Polykratis, A., Kollias, G., de Winther, M.P. and Pasparakis, M. (2008). Endothelial cell-specific NF-kappaB inhibition protects mice from atherosclerosis. *Cell Metab.* **8**(5), pp.372-383.

Gebuhrer, V., Murphy, J.F., Bordet, J.C., Reck, M.P. and McGregor, J.L. (1995). Oxidized low-density lipoprotein induces the expression of P-selectin (GMP140/PADGEM/CD62) on human endothelial cells. *Biochem J.* **306 (Pt 1)**, pp.293-298.

Genecards. (2022). *Subcellular locations from UniProtKB/Swiss-Prot for PTGIS Gene.* [online]. Available from: https://www.genecards.org/cgi-bin/carddisp.pl?gene=PTGIS

Ghosh, S. and Hayden, M.S. (2008). New regulators of NF-kappaB in inflammation. *Nat Rev Immunol.* **8**(11), pp.837-848.

Grune, T., Kehm, R., Höhn, A. and Jung, T. (2018). "Cyt/Nuc," a Customizable and Documenting ImageJ Macro for Evaluation of Protein Distributions Between Cytosol and Nucleus. *Biotechnol J.* **13**(5), pe1700652.

Gryglewski, R.J., Dembińska-Kièć, A., Zmuda, A. and Gryglewska, T. (1978). Prostacyclin and thromboxane A2 biosynthesis capacities of heart, arteries and platelets at various stages of experimental atherosclerosis in rabbits. *Atherosclerosis.* **31**(4), pp.385-394.

Gtexportal. (2021). *Single tissue expression for ANKHD1 (ENSG00000131503.20).* [online]. Available from: https://www.gtexportal.org/home/gene/ENSG00000131503

Guns, P.J., Korda, A., Crauwels, H.M., Van Assche, T., Robaye, B., Boeynaems, J.M. and Bult, H. (2005). Pharmacological characterization of nucleotide P2Y receptors on endothelial cells of the mouse aorta. *Br J Pharmacol.* **146**(2), pp.288-295.

Hanna, R.N., Shaked, I., Hubbeling, H.G., Punt, J.A., Wu, R., Herrley, E., Zaugg, C., Pei, H., Geissmann, F., Ley, K. and Hedrick, C.C. (2012). NR4A1 (Nur77) deletion polarizes macrophages toward an inflammatory phenotype and increases atherosclerosis. *Circ Res.* **110**(3), pp.416-427.

Harry, B.L., Sanders, J.M., Feaver, R.E., Lansey, M., Deem, T.L., Zarbock, A., Bruce, A.C., Pryor, A.W., Gelfand, B.D., Blackman, B.R., Schwartz, M.A. and Ley, K. (2008). Endothelial cell PECAM-1 promotes atherosclerotic lesions in areas of disturbed flow in ApoE-deficient mice. *Arterioscler Thromb Vasc Biol.* **28**(11), pp.2003-2008.

Herrmann, R.A., Malinauskas, R.A. and Truskey, G.A. (1994). Characterization of sites with elevated LDL permeability at intercostal, celiac, and iliac branches of the normal rabbit aorta. *Arterioscler Thromb.* **14**(2), pp.313-323.

Hiscott, J., Marois, J., Garoufalis, J., D'Addario, M., Roulston, A., Kwan, I., Pepin, N., Lacoste, J., Nguyen, H. and Bensi, G. (1993). Characterization of a functional NF-kappa B site in the human interleukin 1 beta promoter: evidence for a positive autoregulatory loop. *Mol Cell Biol.* **13**(10), pp.6231-6240.

Ho, J.J., Robb, G.B., Tai, S.C., Turgeon, P.J., Mawji, I.A., Man, H.S. and Marsden, P.A. (2013). Active stabilization of human endothelial nitric oxide synthase mRNA by hnRNP E1 protects against antisense RNA and microRNAs. *Mol Cell Biol.* **33**(10), pp.2029-2046.

Hosoya, T., Maruyama, A., Kang, M.I., Kawatani, Y., Shibata, T., Uchida, K., Warabi, E., Noguchi, N., Itoh, K. and Yamamoto, M. (2005). Differential responses of the Nrf2-Keap1 system to laminar and oscillatory shear stresses in endothelial cells. *J Biol Chem.* **280**(29), pp.27244-27250.

Howard, G., Wagenknecht, L.E., Burke, G.L., Diez-Roux, A., Evans, G.W., McGovern, P., Nieto, F.J. and Tell, G.S. (1998). Cigarette smoking and progression of atherosclerosis: The Atherosclerosis Risk in Communities (ARIC) Study. *JAMA.* **279**(2), pp.119-124.

Huang, H.Y., Lin, Y.C., Cui, S., Huang, Y., Tang, Y., Xu, J., Bao, J., Li, Y., Wen, J., Zuo, H., Wang, W., Li, J., Ni, J., Ruan, Y., Li, L., Chen, Y., Xie, Y., Zhu, Z., Cai, X., Chen, X., Yao, L., Luo, Y., LuXu, S., Luo, M., Chiu, C.M., Ma, K., Zhu, L., Cheng, G.J., Bai, C., Chiang, Y.C., Wang, L., Wei, F., Lee, T.Y. and Huang, H.D. (2022). miRTarBase update 2022: an informative resource for experimentally validated miRNA-target interactions. *Nucleic Acids Res.* **50**(D1), pp.D222-D230.

Hwang, J., Ing, M.H., Salazar, A., Lassègue, B., Griendling, K., Navab, M., Sevanian, A. and Hsiai, T.K. (2003). Pulsatile versus oscillatory shear stress regulates NADPH oxidase subunit expression: implication for native LDL oxidation. *Circ Res.* **93**(12), pp.1225-1232.

Ichinose, A., Kisiel, W. and Fujikawa, K. (1984). Proteolytic activation of tissue plasminogen activator by plasma and tissue enzymes. *FEBS Lett.* **175**(2), pp.412-418.

Ignarro, L.J., Buga, G.M., Wood, K.S., Byrns, R.E. and Chaudhuri, G. (1987). Endothelium-derived relaxing factor produced and released from artery and vein is nitric oxide. *Proc Natl Acad Sci U S A.* **84**(24), pp.9265-9269.

Ignarro, L.J., Lippton, H., Edwards, J.C., Baricos, W.H., Hyman, A.L., Kadowitz, P.J. and Gruetter, C.A. (1981). Mechanism of vascular smooth muscle relaxation by organic nitrates, nitrites, nitroprusside and nitric oxide: evidence for the involvement of S-nitrosothiols as active intermediates. *J Pharmacol Exp Ther.* **218**(3), pp.739-749.

Iqbal, M.B., Johns, M., Cao, J., Liu, Y., Yu, S.C., Hyde, G.D., Laffan, M.A., Marchese, F.P., Cho, S.H., Clark, A.R., Gavins, F.N., Woollard, K.J., Blackshear, P.J., Mackman, N., Dean, J.L., Boothby, M. and Haskard, D.O. (2014). PARP-14 combines with tristetraprolin in the

selective posttranscriptional control of macrophage tissue factor expression. *Blood.* **124**(24), pp.3646-3655.

Iring, A., Jin, Y.J., Albarrán-Juárez, J., Siragusa, M., Wang, S., Dancs, P.T., Nakayama, A., Tonack, S., Chen, M., Künne, C., Sokol, A.M., Günther, S., Martínez, A., Fleming, I., Wettschureck, N., Graumann, J., Weinstein, L.S. and Offermanns, S. (2019). Shear stress-induced endothelial adrenomedullin signaling regulates vascular tone and blood pressure. *J Clin Invest.* **129**(7), pp.2775-2791.

Jin, Z.G., Wong, C., Wu, J. and Berk, B.C. (2005). Flow shear stress stimulates Gab1 tyrosine phosphorylation to mediate protein kinase B and endothelial nitric-oxide synthase activation in endothelial cells. *J Biol Chem.* **280**(13), pp.12305-12309.

József, L. and Filep, J.G. (2003). Selenium-containing compounds attenuate peroxynitrite-mediated NF-kappaB and AP-1 activation and interleukin-8 gene and protein expression in human leukocytes. *Free Radic Biol Med.* **35**(9), pp.1018-1027.

Kao, C.H., Chen, J.K., Kuo, J.S. and Yang, V.C. (1995). Visualization of the transport pathways of low density lipoproteins across the endothelial cells in the branched regions of rat arteries. *Atherosclerosis.* **116**(1), pp.27-41.

Karin, M. and Ben-Neriah, Y. (2000). Phosphorylation meets ubiquitination: the control of NF-[kappa]B activity. *Annu Rev Immunol.* **18**, pp.621-663.

Khan, B.V., Parthasarathy, S.S., Alexander, R.W. and Medford, R.M. (1995). Modified low density lipoprotein and its constituents augment cytokine-activated vascular cell adhesion molecule-1 gene expression in human vascular endothelial cells. *J Clin Invest.* **95**(3), pp.1262-1270.

Kheirolomoom, A., Kim, C.W., Seo, J.W., Kumar, S., Son, D.J., Gagnon, M.K., Ingham, E.S., Ferrara, K.W. and Jo, H. (2015). Multifunctional Nanoparticles Facilitate Molecular Targeting and miRNA Delivery to Inhibit Atherosclerosis in ApoE(-/-) Mice. *ACS Nano.* **9**(9), pp.8885-8897.

Khera, A.V., Won, H.H., Peloso, G.M., Lawson, K.S., Bartz, T.M., Deng, X., van Leeuwen, E.M., Natarajan, P., Emdin, C.A., Bick, A.G., Morrison, A.C., Brody, J.A., Gupta, N., Nomura, A., Kessler, T., Duga, S., Bis, J.C., van Duijn, C.M., Cupples, L.A., Psaty, B., Rader, D.J., Danesh, J., Schunkert, H., McPherson, R., Farrall, M., Watkins, H., Lander, E., Wilson, J.G., Correa, A., Boerwinkle, E., Merlini, P.A., Ardissino, D., Saleheen, D., Gabriel, S. and Kathiresan, S. (2016). Diagnostic Yield and Clinical Utility of Sequencing Familial Hypercholesterolemia Genes in Patients With Severe Hypercholesterolemia. *J Am Coll Cardiol.* **67**(22), pp.2578-2589.

Kiely, J.M., Hu, Y., García-Cardeña, G. and Gimbrone, M.A. (2003). Lipid raft localization of cell surface E-selectin is required for ligation-induced activation of phospholipase C gamma. *J Immunol.* **171**(6), pp.3216-3224.

Kisiel, W., Canfield, W.M., Ericsson, L.H. and Davie, E.W. (1977). Anticoagulant properties of bovine plasma protein C following activation by thrombin. *Biochemistry.* **16**(26), pp.5824-5831.

Knowles, J.W., Reddick, R.L., Jennette, J.C., Shesely, E.G., Smithies, O. and Maeda, N. (2000). Enhanced atherosclerosis and kidney dysfunction in eNOS(-/-)Apoe(-/-) mice are ameliorated by enalapril treatment. *J Clin Invest.* **105**(4), pp.451-458.

Kobayashi, T., Tahara, Y., Matsumoto, M., Iguchi, M., Sano, H., Murayama, T., Arai, H., Oida, H., Yurugi-Kobayashi, T., Yamashita, J.K., Katagiri, H., Majima, M., Yokode, M., Kita, T. and Narumiya, S. (2004). Roles of thromboxane A(2) and prostacyclin in the development of atherosclerosis in apoE-deficient mice. *J Clin Invest.* **114**(6), pp.784-794.

Kumar, A., Kim, C.S., Hoffman, T.A., Naqvi, A., Dericco, J., Jung, S.B., Lin, Z., Jain, M.K. and Irani, K. (2011). p53 impairs endothelial function by transcriptionally repressing Kruppel-Like Factor 2. *Arterioscler Thromb Vasc Biol.* **31**(1), pp.133-141.

Kumar, A., Kumar, S., Vikram, A., Hoffman, T.A., Naqvi, A., Lewarchik, C.M., Kim, Y.R. and Irani, K. (2013). Histone and DNA methylation-mediated epigenetic downregulation of endothelial Kruppel-like factor 2 by low-density lipoprotein cholesterol. *Arterioscler Thromb Vasc Biol.* **33**(8), pp.1936-1942.

Kuzkaya, N., Weissmann, N., Harrison, D.G. and Dikalov, S. (2003). Interactions of peroxynitrite, tetrahydrobiopterin, ascorbic acid, and thiols: implications for uncoupling endothelial nitric-oxide synthase. *J Biol Chem.* **278**(25), pp.22546-22554.

Lai, W.S., Carballo, E., Strum, J.R., Kennington, E.A., Phillips, R.S. and Blackshear, P.J. (1999). Evidence that tristetraprolin binds to AU-rich elements and promotes the deadenylation and destabilization of tumor necrosis factor alpha mRNA. *Mol Cell Biol.* **19**(6), pp.4311-4323.

Laosiripisan, J., Parkhurst, K.L. and Tanaka, H. (2017). Associations of resting heart rate with endothelium-dependent vasodilation and shear rate. *Clin Exp Hypertens.* **39**(2), pp.150-154.

Lawler, O.A., Miggin, S.M. and Kinsella, B.T. (2001). Protein kinase A-mediated phosphorylation of serine 357 of the mouse prostacyclin receptor regulates its coupling to G(s)-, to G(i)-, and to G(q)-coupled effector signaling. *J Biol Chem.* **276**(36), pp.33596-33607.

Lee, M.R., Li, L. and Kitazawa, T. (1997). Cyclic GMP causes Ca2+ desensitization in vascular smooth muscle by activating the myosin light chain phosphatase. *J Biol Chem.* **272**(8), pp.5063-5068.

Li, H., Zhou, W.Y., Xia, Y.Y. and Zhang, J.X. (2022). Endothelial Mechanosensors for Atheroprone and Atheroprotective Shear Stress Signals. *J Inflamm Res.* **15**, pp.1771-1783.

Libby, P. (2017). Interleukin-1 Beta as a Target for Atherosclerosis Therapy: Biological Basis of CANTOS and Beyond. *J Am Coll Cardiol.* **70**(18), pp.2278-2289.

Lin, Z., Kumar, A., SenBanerjee, S., Staniszewski, K., Parmar, K., Vaughan, D.E., Gimbrone, M.A., Balasubramanian, V., García-Cardeña, G. and Jain, M.K. (2005). Kruppel-like factor 2 (KLF2) regulates endothelial thrombotic function. *Circ Res.* **96**(5), pp.e48-57.

Lu, Q., Meng, Q., Qi, M., Li, F. and Liu, B. (2019). Shear-Sensitive lncRNA AF131217.1 Inhibits Inflammation in HUVECs via Regulation of KLF4. *Hypertension.* **73**(5), pp.e25-e34.

Luo, J.Y., Cheng, C.K., He, L., Pu, Y., Zhang, Y., Lin, X., Xu, A., Lau, C.W., Tian, X.Y., Ma, R.C.W., Jo, H. and Huang, Y. (2022). Endothelial UCP2 Is a Mechanosensitive Suppressor of Atherosclerosis. *Circ Res.* **131**(5), pp.424-441.

Lv, H. and Ai, D. (2022). Hippo/yes-associated protein signaling functions as a mechanotransducer in regulating vascular homeostasis. *J Mol Cell Cardiol.* **162**, pp.158-165.

Mahe, G., Carsin, M., Zeeny, M. and De Bosschere, J.P. (2011). Dietary pattern, a modifiable risk factor that can be easily assessed for atherosclerosis vascular disease prevention in clinical practice. *Public Health Nutr.* **14**(2), pp.319-326.

Mahmoud, M., Mayer, M., Cancel, L.M., Bartosch, A.M., Mathews, R. and Tarbell, J.M. (2021). The glycocalyx core protein Glypican 1 protects vessel wall endothelial cells from stiffness-mediated dysfunction and disease. *Cardiovasc Res.* **117**(6), pp.1592-1605.

Mahtani, K.R., Brook, M., Dean, J.L., Sully, G., Saklatvala, J. and Clark, A.R. (2001). Mitogen-activated protein kinase p38 controls the expression and posttranslational modification of tristetraprolin, a regulator of tumor necrosis factor alpha mRNA stability. *Mol Cell Biol.* **21**(19), pp.6461-6469.

Malek, A.M., Alper, S.L. and Izumo, S. (1999). Hemodynamic shear stress and its role in atherosclerosis. *JAMA.* **282**(21), pp.2035-2042.

Malmsjö, M., Edvinsson, L. and Erlinge, D. (1998). P2U-receptor mediated endothelium-dependent but nitric oxide-independent vascular relaxation. *Br J Pharmacol.* **123**(4), pp.719-729.

Maroney, S.A., Ellery, P.E., Wood, J.P., Ferrel, J.P., Martinez, N.D. and Mast, A.E. (2013). Comparison of the inhibitory activities of human tissue factor pathway inhibitor (TFPI)α and TFPIβ. *J Thromb Haemost.* **11**(5), pp.911-918.

Martin, T., Cardarelli, P.M., Parry, G.C., Felts, K.A. and Cobb, R.R. (1997). Cytokine induction of monocyte chemoattractant protein-1 gene expression in human endothelial cells depends on the cooperative action of NF-kappa B and AP-1. *Eur J Immunol.* **27**(5), pp.1091-1097.

McCalden, T.A. and Nath, R.G. (1989). Mechanisms of vascular supersensitivity in hypercholesterolemia. *Stroke.* **20**(2), pp.238-241.

McCormick, S.M., Eskin, S.G., McIntire, L.V., Teng, C.L., Lu, C.M., Russell, C.G. and Chittur, K.K. (2001). DNA microarray reveals changes in gene expression of shear stressed human umbilical vein endothelial cells. *Proc Natl Acad Sci U S A.* **98**(16), pp.8955-8960.

McGill, H.C., McMahan, C.A., Herderick, E.E., Zieske, A.W., Malcom, G.T., Tracy, R.E., Strong, J.P. and Group, P.D.o.A.i.Y.P.R. (2002). Obesity accelerates the progression of coronary atherosclerosis in young men. *Circulation.* **105**(23), pp.2712-2718.

Mellion, B.T., Ignarro, L.J., Ohlstein, E.H., Pontecorvo, E.G., Hyman, A.L. and Kadowitz, P.J. (1981). Evidence for the inhibitory role of guanosine 3', 5'-monophosphate in ADP-induced human platelet aggregation in the presence of nitric oxide and related vasodilators. *Blood.* **57**(5), pp.946-955.

Meng, F.C., HongQian, JiayiDai, XinyuanHuang, YanFan, Yubo. (2022). In vitro fluidic systems: Applying shear stress on endothelial cells. *Medicine in Novel Technology and Devices.* **15**, p100143.

Methia, N., André, P., Denis, C.V., Economopoulos, M. and Wagner, D.D. (2001). Localized reduction of atherosclerosis in von Willebrand factor-deficient mice. *Blood.* **98**(5), pp.1424-1428.

Milner, P., Kirkpatrick, K.A., Ralevic, V., Toothill, V., Pearson, J. and Burnstock, G. (1990). Endothelial cells cultured from human umbilical vein release ATP, substance P and acetylcholine in response to increased flow. *Proc Biol Sci.* **241**(1302), pp.245-248.

Mohan, S., Mohan, N. and Sprague, E.A. (1997). Differential activation of NF-kappa B in human aortic endothelial cells conditioned to specific flow environments. *Am J Physiol.* **273**(2 Pt 1), pp.C572-578.

Moncada, S., Grylewski, R., Bunting, S. and Vane, J. (1976). ChemInform Abstract: An Enzyme Isolated from Arteries Transforms Prostaglandin Endoperoxides to an Unstable Substance that Inhibits Platelet Aggregation. *Nature.* **263**, pp.663-665.

Moore, S. (1979). Endothelial injury and atherosclerosis. *Exp Mol Pathol.* **31**(1), pp.182-190.

Mortazavi, A., Williams, B.A., McCue, K., Schaeffer, L. and Wold, B. (2008). Mapping and quantifying mammalian transcriptomes by RNA-Seq. *Nat Methods.* **5**(7), pp.621-628.

Murata, T., Ushikubi, F., Matsuoka, T., Hirata, M., Yamasaki, A., Sugimoto, Y., Ichikawa, A., Aze, Y., Tanaka, T., Yoshida, N., Ueno, A., Oh-ishi, S. and Narumiya, S. (1997). Altered pain perception and inflammatory response in mice lacking prostacyclin receptor. *Nature.* **388**(6643), pp.678-682.

Mälarstig, A., Tenno, T., Johnston, N., Lagerqvist, B., Axelsson, T., Syvänen, A.C., Wallentin, L. and Siegbahn, A. (2005). Genetic variations in the tissue factor gene are associated with clinical outcome in acute coronary syndrome and expression levels in human monocytes. *Arterioscler Thromb Vasc Biol.* **25**(12), pp.2667-2672.

Müller, P., Kuttenkeuler, D., Gesellchen, V., Zeidler, M.P. and Boutros, M. (2005). Identification of JAK/STAT signalling components by genome-wide RNA interference. *Nature.* **436**(7052), pp.871-875.

Nagel, T., Resnick, N., Dewey, C.F. and Gimbrone, M.A. (1999). Vascular endothelial cells respond to spatial gradients in fluid shear stress by enhanced activation of transcription factors. *Arterioscler Thromb Vasc Biol.* **19**(8), pp.1825-1834.

Nakashima, Y., Raines, E.W., Plump, A.S., Breslow, J.L. and Ross, R. (1998). Upregulation of VCAM-1 and ICAM-1 at atherosclerosis-prone sites on the endothelium in the ApoE-deficient mouse. *Arterioscler Thromb Vasc Biol.* **18**(5), pp.842-851.

Nakayama, T., Soma, M., Saito, S., Honye, J., Yajima, J., Rahmutula, D., Kaneko, Y., Sato, M., Uwabo, J., Aoi, N., Kosuge, K., Kunimoto, M., Kanmatsuse, K. and Kokubun, S. (2002). Association of a novel single nucleotide polymorphism of the prostacyclin synthase gene with myocardial infarction. *Am Heart J.* **143**(5), pp.797-801.

Nam, D., Ni, C.W., Rezvan, A., Suo, J., Budzyn, K., Llanos, A., Harrison, D., Giddens, D. and Jo, H. (2009). Partial carotid ligation is a model of acutely induced disturbed flow, leading to rapid endothelial dysfunction and atherosclerosis. *Am J Physiol Heart Circ Physiol.* **297**(4), pp.H1535-1543.

Nieborowska-Skorska, M., Kopinski, P.K., Ray, R., Hoser, G., Ngaba, D., Flis, S., Cramer, K., Reddy, M.M., Koptyra, M., Penserga, T., Glodkowska-Mrowka, E., Bolton, E., Holyoake, T.L., Eaves, C.J., Cerny-Reiterer, S., Valent, P., Hochhaus, A., Hughes, T.P., van der Kuip, H., Sattler, M., Wiktor-Jedrzejczak, W., Richardson, C., Dorrance, A., Stoklosa, T., Williams, D.A. and Skorski, T. (2012). Rac2-MRC-cIII-generated ROS cause genomic instability in chronic myeloid leukemia stem cells and primitive progenitors. *Blood.* **119**(18), pp.4253-4263.

Nieuwenhuis, H.K., Akkerman, J.W., Houdijk, W.P. and Sixma, J.J. (1985). Human blood platelets showing no response to collagen fail to express surface glycoprotein Ia. *Nature.* **318**(6045), pp.470-472.

Owen, W.G. and Esmon, C.T. (1981). Functional properties of an endothelial cell cofactor for thrombin-catalyzed activation of protein C. *J Biol Chem.* **256**(11), pp.5532-5535.

Ozaki, M., Kawashima, S., Yamashita, T., Hirase, T., Namiki, M., Inoue, N., Hirata, K., Yasui, H., Sakurai, H., Yoshida, Y., Masada, M. and Yokoyama, M. (2002). Overexpression of endothelial nitric oxide synthase accelerates atherosclerotic lesion formation in apoE-deficient mice. *J Clin Invest.* **110**(3), pp.331-340.

Parmar, K.M., Larman, H.B., Dai, G., Zhang, Y., Wang, E.T., Moorthy, S.N., Kratz, J.R., Lin, Z., Jain, M.K., Gimbrone, M.A. and García-Cardeña, G. (2006). Integration of flow-dependent endothelial phenotypes by Kruppel-like factor 2. *J Clin Invest.* **116**(1), pp.49-58.

Parry, G.C. and Mackman, N. (1995). Transcriptional regulation of tissue factor expression in human endothelial cells. *Arterioscler Thromb Vasc Biol.* **15**(5), pp.612-621.

Patel, R., Varghese, J.F., Singh, R.P. and Yadav, U.C.S. (2019). Induction of endothelial dysfunction by oxidized low-density lipoproteins via downregulation of Erk-5/Mef2c/KLF2 signaling: Amelioration by fisetin. *Biochimie.* **163**, pp.152-162.

Pedersen, E.M., Oyre, S., Agerbaek, M., Kristensen, I.B., Ringgaard, S., Boesiger, P. and Paaske, W.P. (1999). Distribution of early atherosclerotic lesions in the human abdominal aorta correlates with wall shear stresses measured in vivo. *Eur J Vasc Endovasc Surg.* **18**(4), pp.328-333.

Piao, J., Hong, H.S. and Son, Y. (2018). Substance P ameliorates tumor necrosis factor-alpha-induced endothelial cell dysfunction by regulating eNOS expression in vitro. *Microcirculation.* **25**(3), pe12443.

Ponnuswamy, P., Schröttle, A., Ostermeier, E., Grüner, S., Huang, P.L., Ertl, G., Hoffmann, U., Nieswandt, B. and Kuhlencordt, P.J. (2012). eNOS protects from atherosclerosis despite relevant superoxide production by the enzyme in apoE mice. *PLoS One.* **7**(1), pe30193.

Praticò, D., Tillmann, C., Zhang, Z.B., Li, H. and FitzGerald, G.A. (2001). Acceleration of atherogenesis by COX-1-dependent prostanoid formation in low density lipoprotein receptor knockout mice. *Proc Natl Acad Sci U S A.* **98**(6), pp.3358-3363.

Psefteli, P.M., Kitscha, P., Vizcay, G., Fleck, R., Chapple, S.J., Mann, G.E., Fowler, M. and Siow, R.C. (2021). Glycocalyx sialic acids regulate Nrf2-mediated signaling by fluid shear stress in human endothelial cells. *Redox Biol.* **38**, p101816.

Radomski, M.W., Palmer, R.M. and Moncada, S. (1987). The role of nitric oxide and cGMP in platelet adhesion to vascular endothelium. *Biochem Biophys Res Commun.* **148**(3), pp.1482-1489.

Ranade, S.S., Qiu, Z., Woo, S.H., Hur, S.S., Murthy, S.E., Cahalan, S.M., Xu, J., Mathur, J., Bandell, M., Coste, B., Li, Y.S., Chien, S. and Patapoutian, A. (2014). Piezo1, a mechanically activated ion channel, is required for vascular development in mice. *Proc Natl Acad Sci U S A.* **111**(28), pp.10347-10352.

Ratnadiwakara, M. and Änkö, M.L. (2018). mRNA Stability Assay Using transcription inhibition by Actinomycin D in Mouse Pluripotent Stem Cells. *Bio Protoc.* **8**(21), pe3072.

Ray, D., Kazan, H., Cook, K.B., Weirauch, M.T., Najafabadi, H.S., Li, X., Gueroussov, S., Albu, M., Zheng, H., Yang, A., Na, H., Irimia, M., Matzat, L.H., Dale, R.K., Smith, S.A., Yarosh, C.A., Kelly, S.M., Nabet, B., Mecenas, D., Li, W., Laishram, R.S., Qiao, M., Lipshitz, H.D., Piano, F., Corbett, A.H., Carstens, R.P., Frey, B.J., Anderson, R.A., Lynch, K.W., Penalva, L.O., Lei, E.P., Fraser, A.G., Blencowe, B.J., Morris, Q.D. and Hughes, T.R. (2013). A compendium of RNA-binding motifs for decoding gene regulation. *Nature.* **499**(7457), pp.172-177.

Reidy, M.A. and Langille, B.L. (1980). The effect of local blood flow patterns on endothelial cell morphology. *Exp Mol Pathol.* **32**(3), pp.276-289.

Rousseau, S., Houle, F., Landry, J. and Huot, J. (1997). p38 MAP kinase activation by vascular endothelial growth factor mediates actin reorganization and cell migration in human endothelial cells. *Oncogene.* **15**(18), pp.2169-2177.

Russell-Puleri, S., Dela Paz, N.G., Adams, D., Chattopadhyay, M., Cancel, L., Ebong, E., Orr, A.W., Frangos, J.A. and Tarbell, J.M. (2017). Fluid shear stress induces upregulation of COX-2 and PGI. *Am J Physiol Heart Circ Physiol.* **312**(3), pp.H485-H500.

Saiag, B., Bodin, P., Shacoori, V., Catheline, M., Rault, B. and Burnstock, G. (2009). Uptake and Flow-induced Release of Uridine Nucleotides from Isolated Vascular Endothelial Cells. **2**, pp.279-285.

Savage, B., Sixma, J.J. and Ruggeri, Z.M. (2002). Functional self-association of von Willebrand factor during platelet adhesion under flow. *Proc Natl Acad Sci U S A.* **99**(1), pp.425-430.

Schmittgen, T.D. and Livak, K.J. (2008). Analyzing real-time PCR data by the comparative C(T) method. *Nat Protoc.* **3**(6), pp.1101-1108.

Searles, C.D., Miwa, Y., Harrison, D.G. and Ramasamy, S. (1999). Posttranscriptional regulation of endothelial nitric oxide synthase during cell growth. *Circ Res.* **85**(7), pp.588-595.

SenBanerjee, S., Lin, Z., Atkins, G.B., Greif, D.M., Rao, R.M., Kumar, A., Feinberg, M.W., Chen, Z., Simon, D.I., Luscinskas, F.W., Michel, T.M., Gimbrone, M.A., García-Cardeña, G. and Jain, M.K. (2004). KLF2 Is a novel transcriptional regulator of endothelial proinflammatory activation. *J Exp Med.* **199**(10), pp.1305-1315.

Sidor, C., Borreguero-Munoz, N., Fletcher, G.C., Elbediwy, A., Guillermin, O. and Thompson, B.J. (2019). Mask family proteins ANKHD1 and ANKRD17 regulate YAP nuclear import and stability. *Elife.* **8**.

Sidor, C.M., Brain, R. and Thompson, B.J. (2013). Mask proteins are cofactors of Yorkie/YAP in the Hippo pathway. *Curr Biol.* **23**(3), pp.223-228.

Sissaoui, S., Yu, J., Yan, A., Li, R., Yukselen, O., Kucukural, A., Zhu, L.J. and Lawson, N.D. (2020). Genomic Characterization of Endothelial Enhancers Reveals a Multifunctional Role for NR2F2 in Regulation of Arteriovenous Gene Expression. *Circ Res.* **126**(7), pp.875-888.

Siu, K.L., Gao, L. and Cai, H. (2016). Differential Roles of Protein Complexes NOX1-NOXO1 and NOX2-p47phox in Mediating Endothelial Redox Responses to Oscillatory and Unidirectional Laminar Shear Stress. *J Biol Chem.* **291**(16), pp.8653-8662.

Sowers, J.R., Standley, P.R., Ram, J.L., Jacober, S., Simpson, L. and Rose, K. (1993). Hyperinsulinemia, insulin resistance, and hyperglycemia: contributing factors in the pathogenesis of hypertension and atherosclerosis. *Am J Hypertens.* **6**(7 Pt 2), pp.260S-270S.

Stearns-Kurosawa, D.J., Kurosawa, S., Mollica, J.S., Ferrell, G.L. and Esmon, C.T. (1996). The endothelial cell protein C receptor augments protein C activation by the thrombin-thrombomodulin complex. *Proc Natl Acad Sci U S A.* **93**(19), pp.10212-10216.

Steen, A.M., Sahlén, S. and Lambert, B. (1991). Expression of the hypoxanthine phosphoribosyl transferase gene in resting and growth-stimulated human lymphocytes. *Biochim Biophys Acta.* **1088**(1), pp.77-85.

Sun, Z., Ou, C., Liu, J., Chen, C., Zhou, Q., Yang, S., Li, G., Wang, G., Song, J., Li, Z., Zhang, Z., Yuan, W. and Li, X. (2019). YAP1-induced MALAT1 promotes epithelial-mesenchymal transition and angiogenesis by sponging miR-126-5p in colorectal cancer. *Oncogene.* **38**(14), pp.2627-2644.

Suo, J., Ferrara, D.E., Sorescu, D., Guldberg, R.E., Taylor, W.R. and Giddens, D.P. (2007). Hemodynamic shear stresses in mouse aortas: implications for atherogenesis. *Arterioscler Thromb Vasc Biol.* **27**(2), pp.346-351.

Takabe, W., Warabi, E. and Noguchi, N. (2011). Anti-atherogenic effect of laminar shear stress via Nrf2 activation. *Antioxid Redox Signal.* **15**(5), pp.1415-1426.

Takeuchi, K., Yanai, R., Kumase, F., Morizane, Y., Suzuki, J., Kayama, M., Brodowska, K., Nakazawa, M., Miller, J.W., Connor, K.M. and Vavvas, D.G. (2014). EGF-like-domain-7 is required for VEGF-induced Akt/ERK activation and vascular tube formation in an ex vivo angiogenesis assay. *PLoS One.* **9**(3), pe91849.

Tao, X., Qiu, C., Feng, X. and Wang, L. (2022). Predictive Analysis of Serum NO, PGI2, and Ox-LDL Levels on Disease Progression in Patients with Lacunar Cerebral Infarction. *Comput Math Methods Med.* **2022**, p1221810.

Tarbell, J.M. (2003). Mass transport in arteries and the localization of atherosclerosis. *Annu Rev Biomed Eng.* **5**, pp.79-118.

Tateson, J.E., Moncada, S. and Vane, J.R. (1977). Effects of prostacyclin (PGX) on cyclic AMP concentrations in human platelets. *Prostaglandins.* **13**(3), pp.389-397.

Thorsen, S. and Philips, M. (1984). Isolation of tissue-type plasminogen activator-inhibitor complexes from human plasma. Evidence for a rapid plasminogen activator inhibitor. *Biochim Biophys Acta.* **802**(1), pp.111-118.

Tzima, E., Irani-Tehrani, M., Kiosses, W.B., Dejana, E., Schultz, D.A., Engelhardt, B., Cao, G., DeLisser, H. and Schwartz, M.A. (2005). A mechanosensory complex that mediates the endothelial cell response to fluid shear stress. *Nature.* **437**(7057), pp.426-431.

Uniprot. (2022). *Go annotations: localization for PTGIS.* [online]. Available from: https://www.uniprot.org/uniprotkb/Q16647/entry

van den Berg, B.M., Spaan, J.A. and Vink, H. (2009). Impaired glycocalyx barrier properties contribute to enhanced intimal low-density lipoprotein accumulation at the carotid artery bifurcation in mice. *Pflugers Arch.* **457**(6), pp.1199-1206.

van der Wal, A.C., Das, P.K., Tigges, A.J. and Becker, A.E. (1992). Adhesion molecules on the endothelium and mononuclear cells in human atherosclerotic lesions. *Am J Pathol.* **141**(6), pp.1427-1433.

van Nieuw Amerongen, G.P., van Delft, S., Vermeer, M.A., Collard, J.G. and van Hinsbergh, V.W. (2000). Activation of RhoA by thrombin in endothelial hyperpermeability: role of Rho kinase and protein tyrosine kinases. *Circ Res.* **87**(4), pp.335-340.

Vehar, G.A. and Davie, E.W. (1980). Preparation and properties of bovine factor VIII (antihemophilic factor). *Biochemistry.* **19**(3), pp.401-410.

Villarreal, G., Zhang, Y., Larman, H.B., Gracia-Sancho, J., Koo, A. and García-Cardeña, G. (2010). Defining the regulation of KLF4 expression and its downstream transcriptional targets in vascular endothelial cells. *Biochem Biophys Res Commun.* **391**(1), pp.984-989.

Virmani, R., Kolodgie, F.D., Burke, A.P., Farb, A. and Schwartz, S.M. (2000). Lessons from sudden coronary death: a comprehensive morphological classification scheme for atherosclerotic lesions. *Arterioscler Thromb Vasc Biol.* **20**(5), pp.1262-1275.

Wang, J., An, F.S., Zhang, W., Gong, L., Wei, S.J., Qin, W.D., Wang, X.P., Zhao, Y.X., Zhang, Y., Zhang, C. and Zhang, M.X. (2011). Inhibition of c-Jun N-terminal kinase attenuates low shear stress-induced atherogenesis in apolipoprotein E-deficient mice. *Mol Med.* **17**(9-10), pp.990-999.

Wang, S., Iring, A., Strilic, B., Albarrán Juárez, J., Kaur, H., Troidl, K., Tonack, S., Burbiel, J.C., Müller, C.E., Fleming, I., Lundberg, J.O., Wettschureck, N. and Offermanns, S. (2015). $P2Y_2$ and Gq/G_{11} control blood pressure by mediating endothelial mechanotransduction. *J Clin Invest.* **125**(8), pp.3077-3086.

Warboys, C.M., de Luca, A., Amini, N., Luong, L., Duckles, H., Hsiao, S., White, A., Biswas, S., Khamis, R., Chong, C.K., Cheung, W.M., Sherwin, S.J., Bennett, M.R., Gil, J., Mason, J.C., Haskard, D.O. and Evans, P.C. (2014). Disturbed flow promotes endothelial senescence via a p53-dependent pathway. *Arterioscler Thromb Vasc Biol.* **34**(5), pp.985-995.

Weber, M., Hagedorn, C.H., Harrison, D.G. and Searles, C.D. (2005). Laminar shear stress and 3' polyadenylation of eNOS mRNA. *Circ Res.* **96**(11), pp.1161-1168.

Weber, M., Kim, S., Patterson, N., Rooney, K. and Searles, C.D. (2014). MiRNA-155 targets myosin light chain kinase and modulates actin cytoskeleton organization in endothelial cells. *Am J Physiol Heart Circ Physiol.* **306**(8), pp.H1192-1203.

Weiss, H.J., Sussman, I.I. and Hoyer, L.W. (1977). Stabilization of factor VIII in plasma by the von Willebrand factor. Studies on posttransfusion and dissociated factor VIII and in patients with von Willebrand's disease. *J Clin Invest.* **60**(2), pp.390-404.

Weiss, H.J., Tschopp, T.B., Baumgartner, H.R., Sussman, I.I., Johnson, M.M. and Egan, J.J. (1974). Decreased adhesion of giant (Bernard-Soulier) platelets to subendothelium. Further implications on the role of the von Willebrand factor in hemostasis. *Am J Med.* **57**(6), pp.920-925.

WHO. (2019). *The top 10 causes of death.* [online]. [Viewed 10 July].

Wihlborg, A.K., Malmsjö, M., Eyjolfsson, A., Gustafsson, R., Jacobson, K. and Erlinge, D. (2003). Extracellular nucleotides induce vasodilatation in human arteries via prostaglandins, nitric oxide and endothelium-derived hyperpolarising factor. *Br J Pharmacol.* **138**(8), pp.1451-1458.

Winter, P., Andelovic, K., Kampf, T., Gutjahr, F.T., Heidenreich, J., Zernecke, A., Bauer, W.R., Jakob, P.M. and Herold, V. (2019). Fast self-navigated wall shear stress measurements in the murine aortic arch using radial 4D-phase contrast cardiovascular magnetic resonance at 17.6 T. *J Cardiovasc Magn Reson.* **21**(1), p64.

Xiang, L., Naik, J.S., Abram, S.R. and Hester, R.L. (2007). Chronic hyperglycemia impairs functional vasodilation via increasing thromboxane-receptor-mediated vasoconstriction. *Am J Physiol Heart Circ Physiol.* **292**(1), pp.H231-236.

Yamada, Y., Matsuo, H., Segawa, T., Watanabe, S., Kato, K., Hibino, T., Yokoi, K., Ichihara, S., Metoki, N., Yoshida, H., Satoh, K. and Nozawa, Y. (2006). Assessment of the genetic component of hypertension. *Am J Hypertens.* **19**(11), pp.1158-1165.

Yamamoto, K., Sokabe, T., Matsumoto, T., Yoshimura, K., Shibata, M., Ohura, N., Fukuda, T., Sato, T., Sekine, K., Kato, S., Isshiki, M., Fujita, T., Kobayashi, M., Kawamura, K., Masuda, H., Kamiya, A. and Ando, J. (2006). Impaired flow-dependent control of vascular tone and remodeling in P2X4-deficient mice. *Nat Med.* **12**(1), pp.133-137.

Yamamoto, K., Sokabe, T., Ohura, N., Nakatsuka, H., Kamiya, A. and Ando, J. (2003). Endogenously released ATP mediates shear stress-induced Ca2+ influx into pulmonary artery endothelial cells. *Am J Physiol Heart Circ Physiol.* **285**(2), pp.H793-803.

Yan, F., Yang, W.K., Li, X.Y., Lin, T.T., Lun, Y.N., Lin, F., Lv, S.W., Yan, G.L., Liu, J.Q., Shen, J.C., Mu, Y. and Luo, G.M. (2008). A trifunctional enzyme with glutathione S-transferase, glutathione peroxidase and superoxide dismutase activity. *Biochim Biophys Acta.* **1780**(6), pp.869-872.

Yan, G., You, B., Chen, S.P., Liao, J.K. and Sun, J. (2008). Tumor necrosis factor-alpha downregulates endothelial nitric oxide synthase mRNA stability via translation elongation factor 1-alpha 1. *Circ Res.* **103**(6), pp.591-597.

Yan, S., Chai, H., Wang, H., Yang, H., Nan, B., Yao, Q. and Chen, C. (2005). Effects of lysophosphatidylcholine on monolayer cell permeability of human coronary artery endothelial cells. *Surgery.* **138**(3), pp.464-473.

Yang, C., Zheng, J., Liu, X., Xue, Y., He, Q., Dong, Y., Wang, D., Li, Z., Liu, L., Ma, J., Cai, H. and Liu, Y. (2020). Role of ANKHD1/LINC00346/ZNF655 Feedback Loop in Regulating the Glioma Angiogenesis via Staufen1-Mediated mRNA Decay. *Mol Ther Nucleic Acids.* **20**, pp.866-878.

Yang, F., Zhang, Y., Zhu, J., Wang, J., Jiang, Z., Zhao, C., Yang, Q., Huang, Y., Yao, W., Pang, W., Han, L. and Zhou, J. (2020). Laminar Flow Protects Vascular Endothelial Tight Junctions and Barrier Function via Maintaining the Expression of Long Non-coding RNA MALAT1. *Front Bioeng Biotechnol.* **8**, p647.

Yang, Y., Yin, F., Hang, Q., Dong, X., Chen, J., Li, L., Cao, P., Yin, Z. and Luo, L. (2018). Regulation of Endothelial Permeability by Glutathione S-Transferase Pi Against Actin Polymerization. *Cell Physiol Biochem.* **45**(1), pp.406-418.

Yao, P., Li, Y., Shen, W., Xu, X., Zhu, W., Yang, X., Cao, J. and Xing, C. (2018). ANKHD1 silencing suppresses the proliferation, migration and invasion of CRC cells by inhibiting YAP1-induced activation of EMT. *Am J Cancer Res.* **8**(11), pp.2311-2324.

Yao, P.A., Wu, Y., Zhao, K., Li, Y., Cao, J. and Xing, C. (2022). The feedback loop of ANKHD1/lncRNA MALAT1/YAP1 strengthens the radioresistance of CRC by activating YAP1/AKT signaling. *Cell Death Dis.* **13**(2), p103.

Yokoyama, C., Yabuki, T., Inoue, H., Tone, Y., Hara, S., Hatae, T., Nagata, M., Takahashi, E.I. and Tanabe, T. (1996). Human gene encoding prostacyclin synthase (PTGIS): genomic organization, chromosomal localization, and promoter activity. *Genomics.* **36**(2), pp.296-304.

Yokoyama, C., Yabuki, T., Shimonishi, M., Wada, M., Hatae, T., Ohkawara, S., Takeda, J., Kinoshita, T., Okabe, M. and Tanabe, T. (2002). Prostacyclin-deficient mice develop ischemic renal disorders, including nephrosclerosis and renal infarction. *Circulation.* **106**(18), pp.2397-2403.

Yu, H., Zeng, Y., Hu, J. and Li, C. (2002). Fluid shear stress induces the secretion of monocyte chemoattractant protein-1 in cultured human umbilical vein endothelial cells. *Clin Hemorheol Microcirc.* **26**(3), pp.199-207.

Zakkar, M., Van der Heiden, K., Luong, l.A., Chaudhury, H., Cuhlmann, S., Hamdulay, S.S., Krams, R., Edirisinghe, I., Rahman, I., Carlsen, H., Haskard, D.O., Mason, J.C. and Evans, P.C. (2009). Activation of Nrf2 in endothelial cells protects arteries from exhibiting a proinflammatory state. *Arterioscler Thromb Vasc Biol.* **29**(11), pp.1851-1857.

Zamarron, C., Lijnen, H.R. and Collen, D. (1984). Kinetics of the activation of plasminogen by natural and recombinant tissue-type plasminogen activator. *J Biol Chem.* **259**(4), pp.2080-2083.

Zeng, Y. and Liu, J. (2016). Role of glypican-1 in endothelial NOS activation under various steady shear stress magnitudes. *Exp Cell Res.* **348**(2), pp.184-189.

Zhang, J., Wang, Z., Zuo, G., Li, B., Tian, N. and Chen, S. (2013). Low shear stress induces human vascular endothelial cell apoptosis by activating Akt signal and increasing reactive oxygen species. *Nan Fang Yi Ke Da Xue Xue Bao.* **33**(3), pp.313-317.

Zhang, S.H., Reddick, R.L., Piedrahita, J.A. and Maeda, N. (1992). Spontaneous hypercholesterolemia and arterial lesions in mice lacking apolipoprotein E. *Science.* **258**(5081), pp.468-471.

Zhang, Y., Liao, B., Li, M., Cheng, M., Fu, Y., Liu, Q., Chen, Q., Liu, H., Fang, Y., Zhang, G. and Yu, F. (2016). Shear stress regulates endothelial cell function through SRB1-eNOS signaling pathway. *Cardiovasc Ther.* **34**(5), pp.308-313.

Zhou, G., Hamik, A., Nayak, L., Tian, H., Shi, H., Lu, Y., Sharma, N., Liao, X., Hale, A., Boerboom, L., Feaver, R.E., Gao, H., Desai, A., Schmaier, A., Gerson, S.L., Wang, Y., Atkins, G.B., Blackman, B.R., Simon, D.I. and Jain, M.K. (2012). Endothelial Kruppel-like factor 4 protects against atherothrombosis in mice. *J Clin Invest.* **122**(12), pp.4727-4731.

Zhu, M., Li, X., Tian, X. and Wu, C. (2015). Mask loss-of-function rescues mitochondrial impairment and muscle degeneration of Drosophila pink1 and parkin mutants. *Hum Mol Genet.* **24**(11), pp.3272-3285.

Zhu, M., Zhang, S., Tian, X. and Wu, C. (2017). Mask mitigates MAPT- and FUS-induced degeneration by enhancing autophagy through lysosomal acidification. *Autophagy.* **13**(11), pp.1924-1938.